

Evaluation of two prototype three phase photovoltaic water pumping systems

Axel Scholle *B.Sc (Eng) UCT*

Submitted to the University of Cape Town in partial fulfilment for the degree of
Master of Science In Engineering

Energy for Development Research Centre
Energy Research Institute, University of Cape Town

May 1994

The University of Cape Town has been given
the right to reproduce this thesis in whole
or in part. Copyright is held by the author.

The copyright of this thesis vests in the author. No quotation from it or information derived from it is to be published without full acknowledgement of the source. The thesis is to be used for private study or non-commercial research purposes only.

Published by the University of Cape Town (UCT) in terms of the non-exclusive license granted to UCT by the author.

ABSTRACT

Two prototype three phase AC photovoltaic pump systems (Solvo, MLT) and a DC PV pump (Miltek) were tested on a farm borehole in Namibia (latitude 21°6', longitude 17°6'). The PV array consisted of twelve modules (636W_{peak}) mounted on a single-axis passive tracker. The depth of the water was 75m and a progressive cavity pump with a self-compensating stator was used in all the tests. Customised data acquisition was designed to measure performance characteristics through a range of operating conditions (mainly steady state); a secondary data acquisition system was used to capture samples of high frequency signals. The data allowed detailed analysis of system, subsystem and component performance, as well as performance evaluation over Standard Solar Days.

The focus of the investigation was evaluation of the AC prototypes, in terms of performance, other technical factors, reliability and economic criteria. The analog-based DC system served as a basis for comparison.

Both AC systems employed microprocessor control and PWM variable-frequency variable-voltage inversion. Efficiencies, optimality, stability, start-up behaviour, non-productive operating modes and protection were examined. A number of recommendations were proposed for improvements in the basic control algorithms, monitoring and managing non-productive modes, improved protection, layout and user diagnostic features.

AC PV pumping systems are less common than DC counterparts, in the application and power range investigated. AC systems are potentially cheaper, and the inverters and motors can be manufactured locally. The tested prototypes did not attain subsystem or system efficiencies equal to the DC PV pump, but with optimisation could still provide an attractive alternative. Simulations were conducted (using typical meteorological year data, for two sites) for the tested systems, and additionally for a proven Grundfos AC system with centrifugal pump. The results indicated lowest unit pumped water costs for the DC system, followed by the prototype AC systems, for pumping at a 75m head in the sub-kW power range.

ACKNOWLEDGEMENTS

It has been some time now and it was not without help. I am thanking - -

Bill Cowan, my supervisor, for excellent and sensitive supervision - I enjoyed our interaction;

John Greene, my co-supervisor for his guidance in design of the measurement electronics;

Conrad Roedern, who financed this project; Herzlichen Dank Conrad, für Zeit, Führung, Gedanken und Geduld; Thank you Solar Age Namibia;

Glynn Morris for his efforts to arrange this project with Conrad and help me on my way towards monitoring;

Mark Davis for software support. And thanks especially for that help in those last hours;

Jochen Roeber for the time taken to explain things about power measurement;

Helmut Geiger, Rudi Wortmann and Erwin Trossbach von Elwiwa für Hilfsbereitschaft Eberhart Fischer and Peter Toll von Edelstahlbau für eine nette Anzahl Metalstrukturen

Andreas and Mandy Brückner for making a room available to me for such a really long time - I felt comfortable with you;

Marco und Wiltrud Simoni für Unterhaltung, Hilfe, schönes Essen und enorme Pilze - herzlichen Dank, daß Ihr mich so lange untergebracht habt;

Rudi und Giesel Allers für den Gebrauch Eures Wohnwagens - dies hat das Dasein auf der Farm praxtsich, genial und romantisch gemacht;

Gero Diekmann, hab' Dank Gero, mein Freund, dafür daß Du mir das Auto zur Verfügung gestellt hast;

Pari Callias for organising things at EDRC while I was in Namibia;

Chris Purcell for advice on measurements;

Peter Beckedahl für daß beistehen in manch einem Test;

Stephanie Hardy for giving me lots of time and taking care of Pascoe - it was not always easy but we did okay, for the rest lets not rely on words;

Marlies Scholle, Du standest voll dahinter und hast dabei sicher auch gelitten - daß ist jetzt vorbei - vielen Dank für Deine Unterstützung;

Renate Scholle, als Retter in jeder Not - Brüderchen bedankt sich.

TABLE OF CONTENTS

<i>Abstract</i>	i
<i>Acknowledgements</i>	iii
<i>List of Figures</i>	xiii
<i>List of Tables</i>	xix
<i>Abbreviations</i>	xxi
<i>List of symbols</i>	xxiii
Chapter One: Introduction	1
1.1 Conventions for this dissertation	1
1.2 Objectives	2
1.3 Scope	2
1.4 Structure	3
1.5 The evaluation criteria	3
Chapter Two: Photovoltaic water pumping	5
2.1 Advantages and disadvantages of PV pumping	5
2.2 PV pumping configurations	6
2.3 Classifying the systems under test	9
2.4 Three phase PVP's versus DC PVP's	11
2.5 Analog versus digital controller implementation	11
2.6 Introduction to three phase PV pumps	13
2.6.1 AC technical developments	13
2.6.2 Switch-mode inverters	13
2.6.3 The induction motors	21
2.6.4 Torque pulsations	25
2.6.5 The function of DC input capacitance	26
2.7 Efficiency considerations in PV pump systems	26
2.7.1 PV pump component efficiencies	26
2.7.2 The impact of component interaction on the overall efficiency	32

Chapter Three: System description	35
3.1 Details of the site	35
3.2 The array	36
3.2.1 Specifications	36
3.2.2 Configurations used	37
3.2.3 Tracking array mechanism	37
3.3 The pump	38
3.3.1 Specifications	38
3.3.2 Installation	38
3.3.3 Transmission	38
3.4 The Miltek DC to DC converter	39
3.4.1 Specifications	39
3.4.2 Configuration of the converter in the PVP test system	39
3.4.3 Control algorithm	40
3.4.4 Hardware	40
3.4.5 Signal profile	42
3.5 The Solvo three phase inverter	43
3.5.1 Specifications	43
3.5.2 Configuration of the inverter in the PVP test system	43
3.5.3 Hardware	44
3.5.4 Software	47
3.5.5 Signal profile	49
3.5.6 Future developments	40
3.6 The MLT three phase inverter	51
3.6.1 Specifications	51
3.6.2 Configuration of the inverter in the PVP test system	51
3.6.3 Hardware	51
3.6.4 Software	54
3.6.5 Signal profile	55
3.7 The motors	57
3.7.1 Specifications of the Baldor DC motor	57
3.7.2 Specifications of the GEC three phase induction motor	57
Chapter Four: Research questions and test methodology	59
4.1 Research questions	59
4.2 Choice of parameters	61
4.2.1 Equations	61
4.2.2 Parameters	63
4.3 Test methodology	64

Chapter Five: Data acquisition systems	67
5.1 Description of the primary data acquisition system	67
5.1.1 Transducers	69
5.1.2 Data logger	72
5.1.3 Signal interface	73
5.1.4 Power meter	73
5.1.5 Design procedure for the signal processing units	75
5.1.6 Layout of the primary data acquisition system	75
5.1.7 Limitations of the signal processing unit	76
5.1.8 Problems encountered	77
5.2 Calibration	79
5.3 Uncertainty in the measured data	81
5.4 The secondary data acquisition unit	82
Chapter Six: Array, pump and Miltek system performance	83
6.1 Array performance evaluation	83
6.1.1 Array characteristics	83
6.1.2 Array efficiency compared to the specifications	85
6.1.3 Fixed voltage operation in relation to the MPP	87
6.1.4 The effect of shading on the IV curve	89
6.1.5 Tracking versus fixed array	90
6.2 Pump performance evaluation	93
6.2.1 Flowrate and drawdown correlations to pump speed	94
6.2.2 Torque characteristics of the pump	96
6.2.3 Characteristics of the pumping set at different heads	101
6.2.4 Pumping set losses	102
6.2.5 Comparison to pump specifications	103
6.2.6 Conclusion on the type of pump used	106
6.3 Miltek system performance analysis	107
6.3.1 Converter and motor performance	108
6.3.2 Array operating point characteristics	111
6.3.3 General observations	113
6.3.4 System performance	114

Chapter Seven: Solvo system performance analysis	119
7.1 Inverter and motor performance	121
7.1.1 Efficiency at standard head	121
7.1.2 Efficiency at higher heads	124
7.1.3 Characteristic inverter and motor curves	125
7.2 Steady state array operating point characteristics	126
7.3 Dynamic array operating point characteristics	126
7.3.1 Shape of oscillation waveform	127
7.3.2 Array power losses	127
7.3.3 PWM envelope	130
7.3.4 Effects of increased input capacitance	130
7.4 Voltage to hertz relation	131
7.5 Observed control algorithm characteristics	133
7.6 General observations	135
7.7 System performance	138
7.7.1 Instantaneous performance	138
7.7.2 Daily energy efficiency performance	139
Chapter Eight: MLT system performance analysis	143
8.1 Inverter and motor performance	144
8.1.1 Efficiency at standard head	144
8.1.2 Efficiency at higher head	148
8.1.3 Characteristic inverter and motor curves	149
8.2 Steady state array operating point characteristics	150
8.3 Dynamic array operating point characteristics	152
8.3.1 Shapes of oscillation waveform	152
8.3.2 Array power losses	153
8.3.3 PWM envelope	154
8.3.4 Effects of increased input capacitance	155
8.4 Voltage to hertz relation	157
8.5 Observed control algorithm characteristics	158
8.5.1 Basic control algorithm implementation	158
8.5.2 Fixed voltage operation	158
8.5.3 Maximum speed tracking	159
8.6 General observations	161
8.7 System performance	163
8.7.1 Instantaneous performance	163
8.7.2 Daily energy efficiency performance	165

Chapter Nine: Proposed improvements for the prototype inverters	171
9.1 Control algorithm evaluation	171
9.1.1 Problem analysis	172
9.1.2 Suggestions towards the design of a suitable controller	174
9.2 Monitoring of undesired states of operation	179
9.2.1 Incorrect array operating point	179
9.2.2 Minimum power threshold	180
9.2.3 Monitoring overvoltage	181
9.3 Voltage to hertz relation	182
9.4 Solvo inverter switching frequency	183
9.5 Peculiarities of the MLT inverter	184
9.6 Inverter protection	185
9.7 General design considerations	189
Chapter Ten: Comparative evaluation and simulation	191
10.1 Performance of the Miltek, Solvo and MLT PVP systems	191
10.1.1 Instantaneous performance	191
10.1.2 Daily energy efficiency performance	195
10.2 Simulated comparison with a Grundfos PVP system	199
10.3 Other technical aspects of the PVP systems	204
10.3.1 System requirements	204
10.3.2 System attributes	206
10.4 Cost analysis	208
Chapter Eleven: Conclusions	213
Chapter Twelve: References	221
APPENDIX A1: PV pump component specification sheets	227
A1.1 Siemens M55S module	227
A1.2 Zomeworks TRPM12/AR passive solar tracker	228
A1.3 Mono S2M borehole pump	230
A1.4 Solvo circuit breaker and power module	231
A1.4.1 Thermal three phase circuit breaker Mbs 25	231
A1.4.2 IGBT module BSM 15 GD 100 D	232
A1.5 GEC 70W DZ90L three phase motor	233

APPENDIX A2: Test methodology details	235
A2.1 The array	235
A2.1.1 IV curves	236
A2.1.2 Tracking versus fixed array	237
A2.2 The pump	238
A2.2.1 Correlations	238
A2.2.2 Torque and efficiency characteristics	239
A2.2.3 Pump characteristics at higher heads	239
A2.3 The Miltek DC system	240
A2.3.1 The main system and component performance tests	240
A2.3.2 Dynamic array operating point with the Miltek converter	241
A2.3.3 Dynamic conditions	241
A2.4 The Solvo and MLT three phase systems	242
A2.4.1 The main system and component performance tests	242
A2.4.2 Dynamic array operating point tests	243
A2.4.3 Dynamic operating conditions test	244
APPENDIX A3: Specifications for the data acquisition systems	245
A3.1 Transducers and data logger specification sheets	245
A3.1.1 LI-COR pyranometer LI-200SZ	245
A3.1.2 Temperature sensor LM35D	246
A3.1.3 LEM current probe LA 50-P	247
A3.1.4 Loadcell UBG 10	248
A3.1.5 Optical switch TCST 2000	249
A3.1.6 Flow-captor Type 4113.30	250
A3.1.7 PSM water meter size 3	251
A3.1.8 Pressure transmitter model 891.14.525	252
A3.1.9 Data logger MS-256	253
A3.2 Interface circuits and description	254
A3.2.1 Irradiance	255
A3.2.2 Temperature	256
A3.2.3 Array voltage	256
A3.2.4 Array current	257
A3.2.5 Converter voltage	258
A3.2.6 Converter current	258
A3.2.7 Motor torque	259
A3.2.8 Motor speed	260
A3.2.9 Flowrate	260
A3.2.10 Static and pressure head	260
A3.2.11 Power supply	261
A3.3 Power meter circuits and description	262
A3.3.1 Inverter current	263
A3.3.2 Inverter frequency	265
A3.3.3 Inverter voltage	265
A3.3.4 Inverter active power	268

A3.3.5 Power supply	270
A3.4 Data sheets for electronic components	271
A3.5 Specifications of calibration devices	277
A3.5.1 LI-COR calibration certificate	277
A3.5.2 Fluke 83 DVM	277
A3.5.3 Soar DVM	278
A3.6 Uncertainty analysis of acquired data	279
A3.6.1 Plane of array irradiance data	282
A3.6.2 Ambient and module temperature	282
A3.6.3 Array voltage	283
A3.6.4 Array current	283
A3.6.5 Converter voltage	284
A3.6.6 Converter current	284
A3.6.7 Motor torque	285
A3.6.8 Motor speed	285
A3.6.9 Flowrate	286
A3.6.10 Static head	286
A3.6.11 Inverter current	287
A3.6.12 Inverter frequency	287
A3.6.13 Inverter voltage	288
A3.6.14 Inverter power	288
A3.7 Calculation of the uncertainty in the efficiency data	289
A3.8 Specifications of the secondary data acquisition system	290
 APPENDIX A4: Processing method of module specifications	 293
 APPENDIX A5: Calculation of daily energy efficiency	 295
A5.1 Definitions	295
A5.2 Method of calculation	297
A5.3 List of fitted curves	299
 APPENDIX A6: Calculation of array losses due to array voltage oscillations	 303
 APPENDIX A7: Solvo inverter improvements	 307
A7.1 Controller with regions and deadband	287
A7.2 Incorrect array operating point	310
A7.3 Minimum power threshold	311
A7.4 Higher resolution voltage to hertz relation	313
A7.5 Solvo inverter switching frequency	315
 APPENDIX A8: Simulation conditions	 317
 APPENDIX A9: Costing equations	 321

LIST OF FIGURES

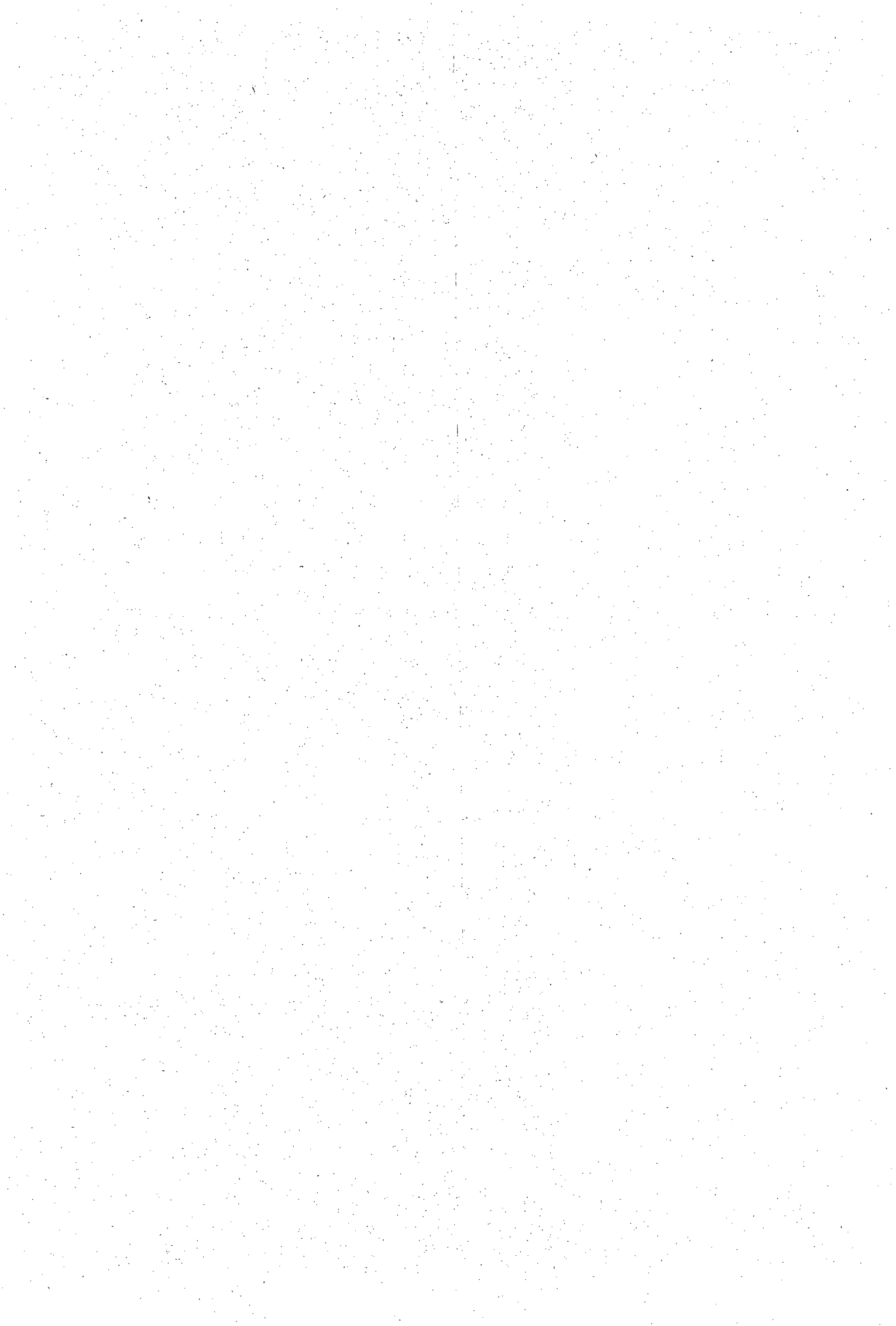
2.1:	Possible components in a PVP system	6
2.2:	Basic circuit diagram of a three phase inverter power module	14
2.3:	A PWM signal - half a cycle	15
2.4:	Sinusoidal PWM waveform	16
2.5:	Frequency spectrum of a sinusoidal PWM signal	17
2.6:	Harmonic elimination PWM waveform	18
2.7:	Frequency spectrum of a harmonic elimination PWM signal	19
2.8:	Delta and star induction motor configuration	21
2.9:	The ripple on the line current: (a) Square wave and (b) PWM	22
2.10:	Induction motor torque versus speed characteristics for fixed voltage and fixed frequency operation	23
2.11:	Induction motor variable voltage and frequency operation	24
2.12:	Matching of two non-identical cells in series	27
3.1:	Supplied data for S2M pump: (a) Flowrate and efficiency of the pump at 75m; (b) Rising main losses	38
3.2:	Basic block-diagram of the Miltek converter	40
3.3:	Characteristic converter output signal	42
3.4:	Basic block-diagram of the Solvo inverter	44
3.5:	Some Solvo inverter characteristics	49
3.6:	Current and voltage of the Solvo inverter	50
3.7:	MLT inverter block-diagram	52
3.8:	Sinusoidal and harmonic elimination PWM techniques used in the MLT inverter	55
3.9:	MLT inverter current and voltage	56
5.1:	Block-diagram of the PVP and the primary data acquisition system	67
5.2:	Torque measurement arrangement	70
5.3:	Block-diagram of the power meter circuitry	74
6.1:	Array characteristics as a function of irradiance: (a) IV curves; (b) power curves	84
6.2:	IV and power curves for the series and parallel configured array	84
6.3:	Array temperature characteristics: (a) IV curves; (b) power curves	85
6.4:	(a) Measured array characteristics; (b) Specifications	86
6.5:	The measured results as a percentage of the specifications	86
6.6:	Array peak power as a function of the array voltage for different levels and module temperature	88
6.7:	Percentage decrease in array output power relative to the MPP as a function of irradiance	88

6.8:	Percentage decrease in array output power relative to the MPP as a function of module temperature	89
6.9:	Effects of shading on the characteristic array curves	90
6.10:	Fixed versus tracking array for a particular day	91
6.11:	Cumulated solar irradiance and accumulated flow for a fixed and two types of tracking arrays	91
6.12:	Block-diagram of the pumping set	93
6.13:	Flowrate to pump speed correlation: (a) at 75m and (b) at 82m	94
6.14:	Drawdown to pump speed correlation: (a) 75m and (b) 82m	96
6.15:	Typical torque versus speed characteristics of the pump	97
6.16:	Diagram of a self-compensating stator, progressive cavity pump	97
6.17:	Two distinct torque versus speed profiles	99
6.18:	Torque at the start-up of the pump	100
6.19:	Pumping set efficiency and flowrate characteristics versus motor shaft power	101
6.20:	(a) Pump efficiency over a range of heads; (b) head variations (key to Graph a)	102
6.21:	Measured torque and flowrate compared to specifications	104
6.22:	Measured pump efficiency and output power characteristics compared to the specifications	104
6.23:	Measured efficiency compared to specifications over a range of heads	105
6.24:	Efficiency of the Mono S2M and the Orbit 0101 & 0102 pump	106
6.25:	Array voltage as a function of irradiance for different pulley diameters	108
6.26:	Miltek converter, motor and subset efficiency versus array power	109
6.27:	(a) Converter efficiency and (b) motor efficiency over a range of heads	110
6.28:	Characteristic converter and motor (referred to pump) curves	111
6.29:	Miltek converter fixed voltage operation (with direct mode)	112
6.30:	Ripple on the array voltage due to converter switching scheme	112
6.31:	Response of the subsystem to an array-current step input	113
6.32:	System status prior to start-up	114
6.33:	(a) Miltek system performance and (b) subsystem performance	115
6.34:	Miltek system daily energy efficiency of (a) system components and (b) subset and subsystem	116
6.35:	Miltek system daily energy efficiency and daily volume flow	117
6.36:	Tracking solar day and standard solar day for Miltek system DEE and volume flow: (a) performance and (b) percentage of TSD over SSD	118
6.37:	Average noon peak irradiance on a tilted surface at Windhoek	118

7.1:	Linear and logarithmic voltage to hertz relation	120
7.2:	Solvo inverter, motor and subset efficiency versus input power	121
7.3:	Solvo inverter losses	122
7.4:	Solvo subset efficiency at one higher simulated head	124
7.5:	Characteristic subsystem curves: (a) Phase current and pump torque (b) frequency, slip and pump speed	125
7.6:	Fixed voltage operation of Solvo inverter	126
7.7:	A typical array voltage oscillation waveform riding on $182V_{arr}$	127
7.8:	Percentage of remaining array power versus a range of oscillation waveform amplitudes while operating (on average) at MPP	128
7.9:	Percentage of remaining array power versus a range of array voltage oscillation amplitudes while operating (on average) 5V to the right of MPP	128
7.10:	Percentage of remaining array power versus the same array oscillation waveform but oscillating around different operating points	129
7.11:	PWM envelope curve of the Solvo inverter	130
7.12:	Effects of larger DC input capacitance: (a) array oscillation waveform; (b) percentage remaining array power	131
7.13:	Programmed voltage to hertz relation: (a) logarithmic relation; (b) linear relation	135
7.14:	Solvo system response under dynamic conditions: (a) Array voltage and current; (b) array current, phase current, line voltage and torque; (c) array current and speed	135
7.15:	Array voltage at start-up: (a) Start failure; (b) start success	136
7.16:	(a) Solvo system performance and (b) subsystem performance	138
7.17:	Solvo system daily energy efficiency: (a) components and (b) subset and subsystem	140
7.18:	Solvo system daily energy efficiency and daily volume flow	140
7.19:	Tracking solar day and standard solar day for the Solvo system DEE and volume flow: (a) performance and (b) percentage of TSD over SSD	141
8.1:	MLT inverter, GEC motor and subset efficiency versus input power: Fixed voltage operation	145
8.2:	MLT inverter, GEC motor and subset efficiency versus input power: Maximum speed tracking	145
8.3:	MLT inverter losses: Maximum speed tracking	146
8.4:	MLT subset efficiency at two static heads	148
8.5:	MLT characteristic subsystem curves: (a) phase current & pump torque; (b) frequency, slip and pump speed	149
8.6:	Fixed voltage operation of the MLT inverter	150
8.7:	MLT inverter-control of the array operating point while in maximum speed tracking mode	151
8.8:	Typical array voltage oscillation waveforms riding on $90V_{arr}$	152

8.9:	Percentage of remaining array power versus a range of oscillation waveform amplitudes while operating (on average) at MPP	153
8.10:	Percentage of remaining array power versus a range of array voltage oscillation amplitudes while operating (on average) 4V to the right of MPP	154
8.11:	PWM envelope curve of the MLT inverter	155
8.12:	Effects of a larger DC input capacitance on the oscillation waveform	155
8.13:	Percentage remaining array power with larger DC input capacitance	156
8.14:	PWM envelope curve with a larger DC input capacitance	157
8.15:	Programmed voltage to hertz relation of the MLT inverter	157
8.16:	MLT system response under dynamic conditions: (a) array voltage and current; (b) phase current and pump torque; (c) line-to-line voltage and pump speed	161
8.17:	FVO operating mode: (a) MLT system performance; (b) MLT subsystem performance	164
8.18:	MST operating mode: (a) MLT system performance; (b) MLT subsystem performance	164
8.19:	MLT system in FVO mode: (a) DEE of components and (b) DEE of subset and subsystem components	165
8.20:	MLT system in FVO mode: system DEE and daily volume flow	166
8.21:	Tracking solar day and standard solar day for the MLT system DEE and volume flow in FVO mode: (a) performance and (b) percentage of TSD over SSD performance	167
8.22:	MLT system in MST mode: (a) DEE of components and (b) DEE of subset and subsystem components	167
8.23:	MLT system in MST mode: system DEE and daily volume flow	168
8.24:	Tracking solar day and standard solar day for the MLT system DEE and volume flow in MST mode: (a) performance and (b) percentage of TSD over SSD performance	169
9.1:	The basic control algorithm as currently implemented in the prototype inverter	172
9.2:	Signal shape and relation to currently implemented control algorithm	173
9.3:	Control diagram of a PVP system with fixed voltage operation	174
9.4:	Graphical representation of a controller with regions and a deadband	178
9.5:	Flowchart for the monitoring of a low array voltage operating point	179
9.6:	Flowchart for the detection of a minimum power threshold	180
9.7:	Proposed hardware protection features in an inverter	186
10.1:	Efficiency of (a) the controllers and (b) the motors	191
10.2:	Subset efficiency of the PVP systems	193
10.3:	Performance of the PVP systems: (a) system efficiency and (b) subsystem efficiency	194
10.4:	Performance of the PVP systems at a static head of 75m: (a) flowrate versus incident irradiance; (b) flowrate versus array power	195

10.5:	DEE of the PVP systems versus the standard solar day	195
10.6:	Daily volume flow of the PVP systems versus the standard solar day	196
10.7:	Percentage TSD over SSD PVP system performance versus the noon peak irradiance	197
10.8:	Percentage higher volume flow of TSD over SSD versus the noon peak irradiance	198
10.9:	Flowrate of the PVP system over a particular day	200
10.10:	Monthly simulation results for the PVP's at 76m: Windhoek: (a) Daily irradiation, (b) daily volume flow, (c) Percentage difference in volume flow compared to the Solvo PVP system	202
10.11:	Monthly simulation results for the PVP's at 76m: Durban: (a) Daily irradiation, (b) daily volume flow, (c) Percentage difference in volume flow compared to the Solvo PVP system	203
A3.1:	Circuit diagram of the irradiance and temperature parameters	255
A3.2:	Circuit diagram of array voltage and array current parameter	257
A3.3:	Circuit diagram for the converter voltage and current parameter	258
A3.4:	Circuit diagram for the motor torque and motor speed parameters	259
A3.5:	Circuit diagram for the flowrate, pressure and static head parameter	261
A3.6:	Circuit diagram of the interface power supply	261
A3.7:	Block-diagram of the PCB layout of the power meter	262
A3.8:	Circuit diagram of the inverter current and the frequency parameter	264
A3.9:	Circuit diagram of the floating inverter voltage and floating active power parameters	266
A3.10:	Circuit diagram of the inverter voltage and active power parameters referenced to signal ground	267
A3.11:	Circuit diagram of the power meter power supply	270
A4.1:	Logarithmic increase of array voltage as a function of irradiance	293
A5.1:	Standard solar day and tracking solar day irradiance profile	296
A5.2:	Acquired and fitted data for the GEC motor (driven by MLT inverter)	301
A6.1:	Array oscillation voltage superimposed on steady state array power versus voltage characteristics	303
A6.2:	Fitted power curve with (a) actual data and (b) confirmation of fitted curve on a different data set	304
A7.1:	Flowchart for the regions-and-deadband algorithm	307
A7.2:	Flowchart for avoiding incorrect array operating points	310
A7.3:	Flowchart for the detection of a minimum power threshold	312
A7.4:	Flowchart for keeping track of the minor gear	313
A7.5:	Flowchart for the assigning of a higher resolution voltage to hertz relation	314



LIST OF TABLES

2.1:	Available PV pump configurations in southern Africa (60m to 150m)	9
2.2:	Characteristics of the prototype PVP systems and the Grundfos system under deep well conditions	10
2.3:	Comparison of AC and DC controller and motor characteristics	11
2.4:	Areas of optimisation in a PV pump	32
3.1:	Details of the site at which all the tests were conducted	35
3.2:	Specifications of a Siemens M55S module	36
3.3:	Possible array output for series and parallel configuration	37
3.4:	Specifications of the Miltek converter	39
3.5:	Solvo inverter specifications	43
3.6:	Specifications of the MLT inverter	51
3.7:	Specifications for the Baldor DC motor	57
3.8:	Specifications of GEC three phase induction motor	57
4.1:	The parameters of the PVP system which were measured	63
5.1:	Parameters logged by the primary data acquisition system	68
5.2:	Calibration of parameters	79
5.3:	The absolute and relative uncertainty in the logged parameters	81
9.1:	Solvo frequency range per major gear	183
10.1:	Relative uncertainty in the controller and motor efficiency data	192
10.2:	Relative uncertainty in the subset efficiency data	193
10.3:	Daily energy efficiency at 5kWh/m ² /day	197
10.4:	Costs of components in each PVP system	208
10.5:	Initial installation costs for all four PVP systems	209
10.6:	Maintenance and replacement costs for all four PVP systems	209
10.7:	Life cycle cost of the four PVP systems with a project life of 20 years	210
10.8:	Unit water cost for all four PVP systems	211
10.9:	Hydraulic unit water cost for all four PVP systems at 76m static head	211

A2.1:	Test methodology for IV curves	236
A2.2:	Test methodology for tracking and fixed array	237
A2.3:	Test methodology for the main pump characteristics	239
A2.4:	Test methodology for the main Miltek DC PVP system characteristics	240
A2.5:	Test methodology for testing dynamic conditions	241
A2.6:	Test methodology for the prototype system performance tests	242
A2.7:	Methodology for testing dynamic conditions	244
A3.1:	Uncertainty in the irradiance measurement	282
A3.2:	Uncertainty in the temperature measurement	282
A3.3:	Uncertainty in the array voltage measurement	283
A3.4:	Uncertainty in the array current measurement	283
A3.5:	Uncertainty in the converter voltage measurement	284
A3.6:	Uncertainty in the converter current measurement	284
A3.7:	Uncertainty in the motor torque measurement	285
A3.8:	Uncertainty in the flowrate measurement	286
A3.9:	Uncertainty in the inverter current measurement	287
A3.10:	Uncertainty in the inverter voltage measurement	288
A3.11:	Uncertainty in the inverter power measurement	288
A5.1:	Energy content of a SSD and a TSD for different peak irradiance levels	297
A5.2:	Fitted equations for the array and the pump	299
A5.3:	Fitted equations for the Miltek subset components	299
A5.4:	Fitted equations for the Solvo subset components	299
A5.5:	Fitted equations for the MLT subset components: MST	300
A5.6:	Fitted equations for the MLT subset components: FVO	300
A7.1:	Program values for a lower switching frequency	315

ABBREVIATIONS

General abbreviations

cubm	cubic meter
DAS	data acquisition system
DEE	daily energy efficiency
DVM	digital volt-meter
FSR	full scale reading
min	minutes
msec	milli-seconds
MTBF	mean time between failures
OD	outer diameter
op	operating point
PV	photovoltaic
PCD	pitch centre diameter
pp	peak-to-peak
PVP	photovoltaic water pumping
RAPS	remote area power supply
sqm	square meter (used in Figures)
W_{peak}	watt peak

Photovoltaic related abbreviations

FV	fixed voltage
FVP	fixed voltage point
IV	current voltage
MPP	maximum power point
NOCT	normal operating cell temperature
POA	plane of array
SSD	standard solar day
STC	standard test conditions
TSD	tracking solar day

Controller operating modes related abbreviations

FVO	fixed voltage operation
MPPT	maximum power point track-ing/er
MST	maximum speed tracking
OVPT	optimum voltage point tracking

Electronics related abbreviations

ADC	analog to digital converter
CMRR	common mode rejection ratio
EPROM	erasable programmable read only memory
HF	high frequency
IC	integrated circuit
IGBT	insulated gate bipolar transistor
LED	light emitting diode
LPF	low pass filter
MOSFET	metal oxide silicon field effect transistor
MOV	metal oxide varistor
op-amp	operational amplifier
PCB	printed circuit board
PNP	positive-negative-positive (transistor related)
PSRR	power supply rejection ratio
PWM	pulse width modulation
quant	quantization error
RC	resistor and capacitor combination (usually a lowpass filter)
rms	root-mean-square
SCR	silicon controlled rectifier
SF	switching frequency
SQW	square-wave
TTL	transistor-transistor logic
V/Hz	voltage to hertz relation
VSI	voltage-source inverter
τ	time-constant

LIST OF SYMBOLS

Photovoltaic array related symbols

E_{incident}	[kWh/m ² /day]	incident daily solar energy
G_{POA}	[W/m ²]	plane of array global irradiance
I_{arr}	[A]	array current
I_{sc}	[A]	array short circuit current
P_{MPP}	[W]	power at the maximum power point
t_{amb}	[°C]	ambient temperature
t_{mod}	[°C]	module temperature
V_{arr}	[V]	array voltage
V_{oc}	[V]	array open circuit voltage
V_{MPP}	[V]	array voltage at maximum power point
V_{pp}	[V]	peak-to-peak voltage

Converter related symbols

f_{s}	[Hz]	switching frequency of the converter
I_{con}	[A]	converter current
V_{con}	[V]	converter voltage

Inverter related symbols

f_{s}	[Hz]	switching frequency of the inverter
f_{fund}	[Hz]	fundamental frequency of the voltage/current waveform
I_{phase}	[A]	inverter rms phase current
I_{line}	[A]	inverter rms line current
m_{a}		amplitude modulation index
m_{f}		frequency modulation index
pf		power factor
V_{LL}	[V]	inverter rms line-to-line voltage
V_{LN}	[V]	inverter rms line-to-neutral voltage
ϕ	[°]	phase-shift between current and voltage

Motor related symbols

s	[%]	slip in three phase motor
S_{mot}	[rpm]	speed
SR		speed ratio
T_{mot}	[N.m]	torque
ω	[rad/s]	angular velocity

Pump related symbols

g	[m/s ²]	gravitational acceleration
H_s	[m]	static head
H_{Pr}	[m]	pressure head post discharge head
Pr	[kg/m ²]	pressure
Q	[l/h or m ³ /s]	flowrate
Q_{vol}	[m ³]	volume flow
Re		reynolds number
S_{pump}	[rpm]	pump speed
T_{pump}	[N.m]	pump torque
ρ	[kg/m ³]	density of water (ρ_{oh})

Power, efficiency and uncertainty related symbols

$P_{incident}$	[W]	power from the sun
P_{arr}	[W]	array output power
P_{con}	[W]	converter output power
$P_{inv/act}$	[W]	inverter output power
P_{mot}	[W]	motor output power
P_{pump}	[W]	pump output power
η_{arr}	[%]	array efficiency
η_{con}	[%]	converter efficiency
η_{inv}	[%]	inverter efficiency
η_{mot}	[%]	motor efficiency
η_{pump}	[%]	pump efficiency
η_{subset}	[%]	inverter and motor efficiency
η_{subsys}	[%]	subsystem efficiency
η_{sys}	[%]	system efficiency
U_{abs}	[%]	absolute uncertainty
U_{rel}	[%]	relative uncertainty

Costing related symbols

C	[R]	capital cost: initial or installation
dr	[%]	discount rate
i	[%]	interest rate
LCC	[R]	life cycle cost
M	[R/(n × year)]	maintenance cost
P	[R/year]	amortised annual amount
$PVal$	[R]	present value
R	[R/(n × year)]	replacement cost
SL	[years]	project lifetime
UWC	[cents/m ³]	unit water cost

Chapter One

INTRODUCTION

To date, three phase photovoltaic water pumping systems are not very common. Major obstacles in the development of these systems were the high technological requirements and their associated costs, as well as the comparatively poor efficiency of the inverter and the motor, all of which made these systems an infeasible commercial product with the result that few three phase systems were manufactured. Nowadays the cost of microcontrollers and other digital components has decreased significantly and the performance, reliability and cost factors of analog and power electronic components used in inverters have greatly improved.

Two prototype variable frequency inverters were acquired by Solar Age Namibia (Pty) Ltd. One inverter (referred to as the Solvo inverter) was designed in Germany by Günther Hirschmann at his company Solvo (GmbH). The other inverter (referred to as the MLT inverter) is a South African product designed and built by John Davies at the University of Cape Town.

Both inverters were built in response to the demand for a controller that could drive a locally manufactured motor and pump suitable for deep well applications. One such pump is the progressive cavity pump, an efficient, locally made and widely disseminated product which can be used in conjunction with a three phase motor, also manufactured in South Africa. The demand arose from the need to provide an alternative to diesel, wind and photovoltaic DC pumps which were, up till now, the only technologies available to drive progressive cavity pumps in remote areas.

1.1 Conventions for this dissertation

A photovoltaic pumping (PVP) system in this dissertation consisted of a PV array, a controller, a motor and a borehole pump.

The controller in a PVP system is considered to be the central component since it is responsible for loading the array at or near its maximum power point over the complete operating range and for driving the motor appropriately. The controller is either a DC to DC controller referred to as a converter or a DC to three phase controller referred to as an inverter. Apart from other factors, the efficiency of the array and the motor are also a function of the controller when operating as a system. A PVP system where only the controller is exchanged is therefore regarded as a different system. All tested systems used the same array and pump, but a different controller. Each system is therefore referred to as PVP systems in its own right (usually by the name of the controller).

The system refers to the combination of all four components, the subsystem refers to the controller, motor and pump and the subset refers to the controller and motor combination. A set of components can be any grouping of components but this is specified where necessary.

The array and pump are always discussed first where applicable (since they are the same in all systems).

1.2 Objectives

The purpose of this study was to assess the performance of each system and its components under various operating conditions, to observe the system response when the controller is confronted with difficult and possibly unusual circumstances (start-up, cloudy weather, blocked motor, overload etc), to evaluate conditions of breakdown and to make recommendations towards the further development of the Solvo inverter in particular, and so facilitate the progress to a marketable product.

For comparative purposes an additional, well established photovoltaic pump system (referred to as the Miltek system) was also tested under the same conditions as the prototype systems. This system uses a DC to DC controller which is manufactured in South Africa and a permanent magnet motor which is imported.

A discussion of technical aspects (such as maintenance, protection etc) and cost of the systems completes the objectives of this study and provides an overall assessment of the PVP systems.

1.3 Scope

All discussions and comparisons are limited to PVP's in the subkW power input range and to delivery heads of 60m to 150m.

The systems under test used an array size of 636W_{peak}. The pump delivery head was fixed at 75m. This level remained constant during the test period. The three phase systems both used the same motor.

The dissertation aims to present all the information and specifications of each system in a fairly detailed manner. This is particularly true for the prototype inverters. Attempts are made to explain the results and particular phenomena while clearly pointing out the calculated and occasionally estimated uncertainty in the data. The improvements that are suggested for the Solvo inverter are specified in detail in an appendix but have not been tested for correct operation. This will only be attempted after completion of the dissertation but will be based on the suggestions made in the main text and the appendix.

The comparisons among PVP systems are limited to the three systems under test and a Grundfos system. All three systems are compared to the Grundfos system in terms of performance (by means of a simulation package) and in terms of cost.

1.4 Structure

The dissertation consists of three main areas. Informative (chapter one and chapter two), descriptive (chapter three to chapter five) and evaluative (chapter six to chapter ten).

Information on PVP's in general is provided in chapter two with specific emphasis on three phase systems.

Chapter three contains the complete system description of the three systems and their components. The research questions and the test methodology are discussed in chapter four while the data acquisition system is described in chapter five. All three chapters have their respective appendices.

The results of the component tests for the array and the pump as well as the system performance results of the DC Miltek system are discussed in chapter six. This is followed by the results of the Solvo and MLT three phase systems in chapter seven and eight respectively. Calculation methods are detailed in appendices four, five and six.

Chapter nine suggests improvements for the inverters, with detailed program codes for the Solvo inverter in appendix seven. The comparison between the systems, the performance simulation with the Grundfos system and the cost analysis are contained in chapter ten with back-up information in appendix eight and nine.

1.5 The evaluation criteria

The criteria for PVP evaluation in this study comprised performance evaluation, technical aspects and cost assessment.

Performance evaluation

The performance evaluation of a system is mainly concerned with the efficiency of the components, sets of components or the complete system over a range of input powers under steady array W_{peak} and constant static head. The evaluation of mismatch losses between components is also considered important.

The daily energy efficiency of the components (or set thereof) entails an observation of performance over a typical solar day. It is very useful for comparison to other PVP systems.

A further aspect (not directly linked to the efficiency) is the control algorithm ability to cope with various situations including system start-up and dynamic conditions as well as unforeseen system disturbances.

Other technical aspects

Further to system performance, there are technical aspects of a system which have an effect on the cost of a system and its suitability to a particular site and which may partially guide the choice of a system. These can be divided into system requirements and attributes.

System requirements are taken to include the availability of system components, local or overseas production of components, maintenance and installation requirements.

The system attributes are considerations of the system modularity (separate or joined components), its flexibility, its protection capabilities within the controller, its monitoring features and its user interface (if any).

Cost assessment

The assessment of cost, in particular the life cycle cost and the unit water cost, is a very important criterion since that relates the performance of a system to the user's financial resources. The *price to performance* relation must be optimised unless the technical aspects outweigh the cost aspect due to specific system requirements.

Chapter Two

PHOTOVOLTAIC WATER PUMPING

This chapter deals with photovoltaic pumping in general. Photovoltaic pumps are compared to diesel and wind pumping options. The different photovoltaic pump configurations presently available in southern Africa are reviewed and the prototype systems classified according to the mentioned photovoltaic pump categories. AC and DC photovoltaic pumps are briefly compared to each other on the basis of their main characteristics.

The main section of this chapter is the introduction to three phase photovoltaic pump systems which includes an overview of terminology and explains the most fundamental aspects of three phase inverters. The last section contains a brief discussion on component efficiencies within photovoltaic pump systems and provides some information on how these can be improved.

2.1 Advantages and disadvantages of PV pumping

Photovoltaic water pumps (PVP) offer particular advantages (as well as some disadvantages) over diesel and wind pumping applications in areas where no utility grid is available. These advantages are listed below and are based on the assumption that the delivery head is less than 150m and that the water demand can be realistically met by a PVP system. A photovoltaic pump:

- requires no fuel - operating costs are therefore zero; a diesel generator uses fossil fuels (non-zero operating costs) and, during operation, pollutes the environment with fumes and noise
- allows for relatively modular expansion (minimum expansion is usually equivalent to the number of modules in a series string)
- delivers daily water volume over the whole day and not in a matter of one or two hours like the diesel option (PVP's are a good application for small capacity boreholes)
- requires less maintenance than wind and diesel options; in addition, maintenance is more easily carried out in a PV system
- is an excellent option for remote areas when compared to diesel (especially in Namibia which is a large country with little infrastructure)

Other advantages are:

- autonomous operation (a diesel generator usually needs to be started)
- the utilisation of the solar resource which is more reliable and predictable than the wind resource
- the water demand often correlates well with the amount of solar irradiation received
- the array and the motor are reliable components; if the controller is also reliable then the PVP system becomes more reliable than a windpump

The disadvantages of a PVP system are the skill requirements in the event of controller breakdown and high initial cost. It does however have very low running costs. Cost comparisons depend on factors like maintenance costs, running costs (includes the cost of fuel transportation) and replacement costs for PV, wind and diesel systems. This comparison however is beyond the scope of this dissertation. It has been discussed in detail by Gosnell (1991) and Borchers (1992).

2.2 PV pumping configurations

There are presently three basic photovoltaic pump configurations available in southern Africa that are suitable for static heads in the range of 60m to 150m (a basic configuration in this case is determined by the type of controller, not by the pump). These are the DC system, the AC three phase system and the AC single phase system with battery storage. The block-diagram in Figure 2.1 shows the basic layout.

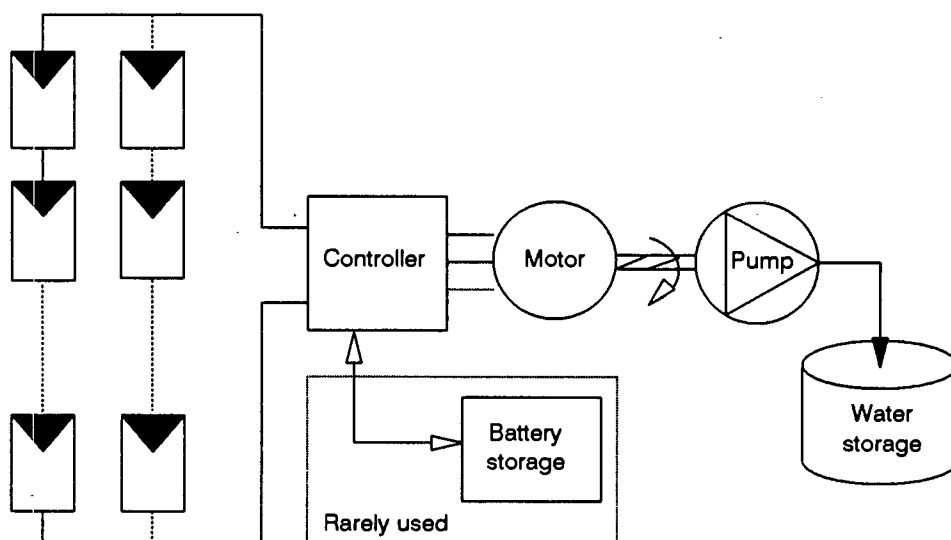


FIGURE 2.1 Possible components in a PVP system

The photovoltaic array consists of mono- or polycrystalline solar cells. The array can be configured in series, parallel or both. It is common to have a fixed array with possibly two or three settings for seasonal changes. Alternatively a tracking array can be used, capable of tracking on a single or dual axis. Iliceto et al. (1987) found that the energy gain over a half year period for a single-axis tracking system was 23.2% and for a dual-axis system 39.7% (at the Adrano PV plant near Milan in Italy). Schmalschläger et al. (1993) concluded that a single-axis tracking system would have cost benefits over a fixed array system. This is true for the particular case but factors like tracking array cost, maintenance requirements, available solar irradiance and type of controller will usually determine which type of array is most suitable.

The controller is the matching device between the array and the motor. Its principle function is to convert a variable current (function of irradiance) to a variable voltage (to control the speed of the motor) while operating at or near the maximum power point of the array. The controller is either a DC to DC converter or a DC to AC single or three phase inverter (the option of direct connection between the array and the motor is not considered for this range of static heads). The common modes of operation of the controllers on the array are at fixed voltage point (fixed voltage operation: FVO) or at maximum power point (maximum power point tracking: MPPT). There are also controllers which make use of optimum voltage point tracking (OVPT). These operate at a fixed percentage (about 75%) of the open circuit voltage which is tested at regular intervals to take account of variations in V_{MPP} due to cell temperature variations.

The DC motors which are commercially available in southern Africa are the brushed and the brushless motor. Both have permanent magnets. The brushed motor requires periodic brush changes which can be problematic in terms of brush wear if the incorrect brushes are used (Burton 1992). Brushless DC motors require additional electronics for the commutation circuit and the shaft position sensor.

The only AC motor used is the squirrel cage induction motor. It is manufactured locally (in South Africa) and costs about a third to a fourth of a DC motor. It is less efficient than a DC motor but virtually maintenance-free.

The pumps used for static heads of 60m to 150m are all borehole pumps. They are either centrifugal, progressive cavity or diaphragm type pumps. Recently piston pumps have also come into use for PV pumping applications in Namibia. A progressive cavity pump has the following characteristics:

- efficiency is maintained well over a wide operating range
- very reliable and may be less prone to corrosion difficulties than a centrifugal pump
- high starting torque

The characteristics of a centrifugal pump are:

- water delivery at a specific head commences when the pump reaches a certain threshold speed (Davis 1993a)
- efficiency decreases when the pump operates at speeds and delivery heads other than the design speed and head (Davis 1993a)
- low starting torque

Diaphragm pumps are mostly limited in their input power to a few hundred Watt. In addition, the membranes used in these pumps have a relatively short lifespan (Whitfield & Bentley 1989) and are very sensitive to water quality. This can be confirmed from experiences at Solar Age Namibia where it was found that diaphragm pumps with an anticipated maintenance interval of two years (for the replacement of brushes and membranes) would usually require a service before the two year period was over. The result is a less reliable pump requiring maintenance at more frequent intervals.

The combination of PVP components into one unit is common. This is mainly the case for centrifugal pumps that are combined with either a DC or an induction motor. These units are submersible. Progressive cavity pumps are also available as submersible units but usually have a higher operating voltage (for example 220V and 380V) which is not always feasible for PV pumping.¹

Two forms of storage can be used in a PVP system, namely battery or water storage. The type of storage chosen depends on site conditions. Batteries are an additional cost and maintenance factor apart from the risk of battery failure. They also introduce losses into the system. Generally it is advised not to use batteries (Schaefer 1985; Burton 1992). However in the case of a small capacity borehole it may be advisable to use batteries to run the PVP in an on/off mode. This gives the borehole time to recover, keeps the drawdown to a minimum, stores the energy from the array in the batteries during off-mode and can operate efficiently when in on-mode due to operation at optimum speed (Baltas & Russell 1987).

Table 2.1 provides a breakdown of the PVP components (excluding the array) and lists some of the available products in southern Africa (systems suitable for 60m to 150m head). All pumps are borehole pumps as opposed to surface mounted pumps. There are certainly further combinations but these are presently not available in southern Africa to my knowledge.

¹ There is a PVP system which uses a submersible 220V pump. It is a Tescon system which until now has not proved reliable due to problems with the batteries and start-up difficulties with the mono-element version at high head (Experiences from Solar Age Namibia).

TABLE 2.1 Available PV pump configurations in southern Africa (60m to 150m)

<i>Configuration</i>	<i>Controller</i>	<i>Motor</i>	<i>Pump</i>	<i>Features</i>	<i>Product(s)</i> ¹⁾
DC	DC to DC (MPPT)	brushless permanent magnet	multi-stage centrifugal	submersible motor & pump (& controller)	• A Y McDonald Solar Sub (Model 21000)
	DC to DC (FVO)	brushed permanent magnet	progressive cavity	surface mounted motor	• Mono Solarlift • Orbit
			piston	surface mounted motor	• Terra Sol ²⁾
			diaphragm	submersible motor & pump	• M&B Sunpump • Waterhog
AC three phase	AC 3 ϕ (MPPT)	induction	multi-stage centrifugal	submersible motor & pump	• Grundfos
AC single phase	AC 1 ϕ (FVO)	induction	progressive cavity	submersible motor & pump; battery storage	• Sunwater by Tescon

¹⁾ Information from the 'Directory of PV pumping equipment' (Davis 1993b)

²⁾ Recent development, manufactured in Namibia by Terra Sol

2.3 Classifying the systems under test

The DC system which is referred to as the Miltek system is essentially a Mono Solarlift PVP system (Table 2.1). The modules and the motor may have different manufacturers but the basic operation is the same. The prototype systems, namely the Solvo and the MLT systems, have the same configuration as the Grundfos system (Table 2.1) but are in a different subcategory since the pump used is a progressive cavity pump and the motor is surface mounted. In addition, the Solvo inverter employs fixed voltage point operation while the MLT inverter uses an indirect form of MPPT by attempting to maximise the speed of the motor. Both prototype systems therefore fall into the same category as the Grundfos system but fill a subcategory that has so far remained empty.

Table 2.2 provides some characteristics of the prototype three phase systems and a three phase submersible centrifugal pump system like the Grundfos system.

TABLE 2.2 Characteristics of the prototype PVP systems and the Grundfos system under deep well conditions

<p>Progressive cavity borehole pump system (for example: the Solvo & MLT systems)</p>	<p>Submersible centrifugal pump system (for example: a Grundfos system)</p>
<ul style="list-style-type: none"> ● potentially higher average daily efficiency ● can be very reliable if the inverter is protected and able to monitor its operating conditions ● can be virtually maintenance-free if the water is of acceptable quality ● high starting torque requirements ● adaption to site possible through change in speed ratio (pulley) ● the pump can be driven with a mechanical back-up power source (wind or diesel) ● labour intensive installation ● motor and pump are locally manufactured; both inverters can be locally produced¹⁾ ● the pump is widely used with diesel and wind energy ● standard components and good service infrastructure 	<ul style="list-style-type: none"> ○ higher peak efficiency at design speed ○ the system is very reliable ○ can be virtually maintenance-free if the water is of acceptable quality ○ starting torque is lower or similar to running torque ○ motor is close-coupled to the pump therefore no speed ratio adjustment ○ no option for a back-up drive ○ simple installation making this system transferable to other sites of similar water-level conditions ○ inverter, motor and pump are imported from Denmark ○ the pump is usually only used with the Grundfos inverter ○ specialised components requiring trained personnel

¹⁾ Solar Age Namibia intends manufacturing the Solvo inverter in Namibia

2.4 Three phase PVP's versus DC PVP's

It is not attempted here to argue for the three phase or the DC PVP case. This section merely offers a listing of the advantages and disadvantages of each configuration. The circumstances, the system quality and the cost will usually determine whether a DC or a three phase system is more appropriate. The details are supplied in Table 2.3.

TABLE 2.3 Comparison of three phase and DC subset characteristics

<i>Three phase PVP option</i>	<i>DC PVP option</i>
<ul style="list-style-type: none"> • lower efficiency for inverter / motor subset over operating range • complex microprocessor and driver circuitry • more components • possibly less reliable and therefore shorter MTBF ¹⁾ • microprocessor controlled (improves reliability) ²⁾ • potential fault monitoring and diagnostic capabilities due to microprocessor • potential user interface • inverter / motor subset potentially cheaper • the PVP <u>subsystem</u> can be locally produced • maintenance-free ³⁾ 	<ul style="list-style-type: none"> ○ higher efficiency for converter / motor subset over operating range ○ relatively simple control and driver circuitry ○ less components ○ possibly more reliable ²⁾ ○ usually analog controlled ○ analog monitoring (less versatile) but there is no reason why a microprocessor cannot be used ○ only with microprocessor ○ inverter / motor subset more expensive ○ the motor has to be imported ○ maintenance-free³⁾ brushless motor (comes at a cost) or minimal maintenance with a brushed motor

¹⁾ MTBF - mean time between failure

²⁾ reliability of a unit is dependent on the design and the time-span that it has been in operation (successful operation confirms reliability)

³⁾ maintenance-free implies a five year period without any attention

2.5 Analog versus digital controller implementation

Both converters and inverters can be implemented in analog or digital control circuitry. However, not all PWM switching schemes can be generated with analog circuitry. There are some trade-offs between analog and digitally based control circuitry (Bose 1986: 315-7):

Digital implementation

- costs, compared to analog hardware, can be significantly reduced
- increased reliability due to reduced parts which will improve mean time between failures (MTBF) as opposed to a high number of electronic components connected together in an analog based three phase inverter
- no problems with time and temperature dependent variations as is the case in analog circuitry (for example drift and offsets)
- software offers flexibility to adapt the inverter to different operating conditions (for example adaption to different motors or change of motor frequency operating range etc). The program can be updated and stored in ROM
- controller output is easily implemented controlled by monitoring control variables such as DC voltage, DC current and / or motor speed
- sophisticated control functions can be implemented to improve efficiency (for example, harmonic elimination PWM (discussed in subsection 2.5.2))
- the microcontroller can be used to protect the power electronics hardware (against overvoltage, overheating, burn-out due to blocked motor etc), to protect the pump against dry-running and to perform diagnostic functions
- microcontrollers can go through a process of 'learning' to optimise performance

Analog implementation

- the response time of the system is faster with negligible delays; delays in digital processing can cause stability problems in feedback control
- a digital control implementation can be costly due to the time requirements for software development
- variables and different processing stages are easily accessed with a multimeter whereas the digital implementation removes the real world dimension

For the above mentioned reasons and the continuing development in digital technology, it is advisable to base at least inverters on digital control circuitry. PVP's are ideal for remote areas but that usually means a lack of skilled personnel in case of breakdowns. The potential of microcontroller based converters to offer diagnostic functions could help unskilled people at the site to get a feeling for what is going on in case of in-operation. Instead of assuming that the converter has broken-down LED's or an LCD display could assist the operator in determining the state of the system.

2.6 Introduction to three phase PV pumps

This section reviews the technicalities of three phase PVP inverters. The basic switch-mode inverter and its different switching schemes are explained. This is followed by a comparison of digital versus analog inverter implementation. Additional aspects of three phase drives are addressed and discussed since these will crop up frequently during the course of this dissertation. The aspects concerned are the voltage to hertz relation, torque pulsations and the function of the DC input capacitors.

The main references for this section are Mohan et al. (1989), Bose (1986) and Murphy and Turnbull (1988). Direct sources are indicated.

2.6.1 AC technical developments

In the course of the last ten years microcontrollers have become more sophisticated and the prices have dropped considerably. It is quite common nowadays that a particular application finds a more effective implementation if it is digitally rather than analog based. This is also the case for the control part of an inverter. Inverter control circuitry could certainly have been digitally based ten years ago (and was too - for example the Grundfos inverter) but it is only today that these inverters are cost effective and offer similar reliability compared to their analog counterparts. A comparison between analog and digital implementation follows in section 2.5.3.

The drawback of three phase inverters are the high number of electronic components compared to a conventional analog based DC to DC converter. Three phase inverters after all have to make use of six switches with six individual drivers to generate a three phase output. This results in higher power consumption (which translates into less efficiency) and a shorter mean time between failures. However recent developments in power electronic components have resulted in improved performance, lower power consumption and greater reliability making them more suitable for a competitive three phase inverter.

2.6.2 Switch-mode inverters

Switch-mode inverters invert the DC voltage at their input to a three phase AC voltage at their output. A diagram of the power module that is used to perform this inversion is shown in Figure 2.2. In most cases the magnitude and the frequency of the output to the motor can be controlled. The switch-mode switching schemes are attractive as the control signals driving the switching devices either turn them on or off. There is no need for control signals to turn the switching device on by degree. That would require complex control circuitry. The main requirement for the generation of a PWM signal is the control of the switching instance.

The most common types of inverters are the pulse-width modulated (PWM) inverters and the square-wave (SQW) inverters. PWM and SQW inverters are also referred to as voltage-source inverters (VSI) as opposed to current-source inverters which are presently only used in high-power AC-motor drives. A PWM inverter can control both

the amplitude and frequency of its output whereas a SQW inverter can only control the frequency of its output. In other words, the DC input voltage has to be varied to achieve variable voltage and frequency operation (this is assuming that each switch of the SQW inverter is on for half a cycle). In PVP applications it is essential to operate at a relatively constant array voltage for maximum power extraction. For this and other reasons, SQW inverters are not suitable for PVP applications and only PWM inverters are considered.

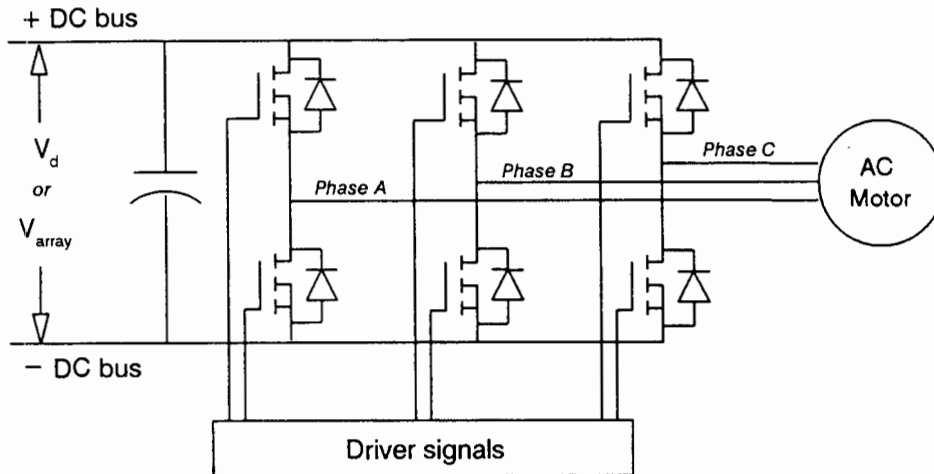


FIGURE 2.2 Basic circuit diagram of a three phase inverter power module
 Source: Adapted from Mohan et al. (1989: Figure 6.21)

There are many PWM switching schemes including sinusoidal PWM, harmonic elimination PWM (also termed optimum PWM), square-wave PWM (also termed multiple-pulse modulation or square-wave pulse switching; not to be confused with the SQW switching scheme mentioned earlier) and current-controlled PWM (also referred to as current-regulated modulation). Only the first three schemes will be discussed as current-controlled PWM inverters are not used in PVP systems.

Definition of terminology

A PWM waveform consists of a number of pulses per cycle (period) which all have the same amplitude. Figure 2.3 shows the pole voltage (phase to negative DC bus voltage) for half a cycle. The pulses differ in width during a cycle (sinusoidal and harmonic elimination) or remain constant in width (square-wave PWM), the latter of which is not shown in the figure. The amplitude of the output signal is varied by increasing or decreasing the pulse-width of each pulse in accordance with the desired output voltage amplitude.

The fundamental frequency of the output signal ($1/T$) is varied by either changing the number of pulses per cycle (while the switching frequency remains constant) or by changing the switching frequency (while the number of pulses per cycle remains constant). Changing the switching frequency ($1/T_s$) alters the signal time base.

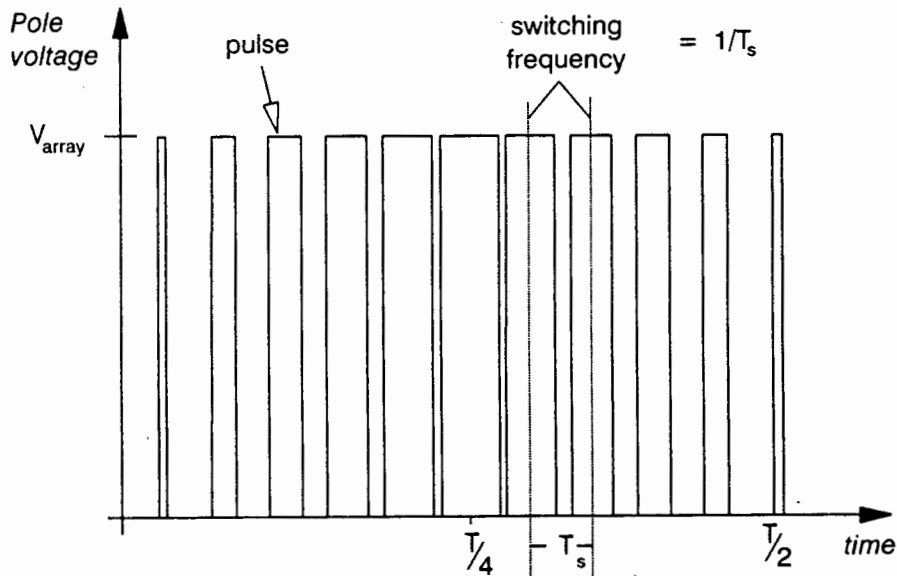


FIGURE 2.3 A PWM signal - half a cycle

Amplitude modulation index m_a

The value of the amplitude modulation index (m_a) is an indication of the peak amplitude of the fundamental frequency component contained in the PWM signal. It can be expressed as:

$$m_a = k \times (V_{\text{peak-sine}} + \tau_{90^\circ})$$

where $V_{\text{peak-sine}}$ is the peak amplitude of the resulting sine-wave and τ_{90° is the time of the widest pulse. k is a constant. This equation has been manipulated since the original equation relates the peak amplitude of a sine-wave to the peak amplitude of a triangular waveform. The latter is used to determine the switching instances when a PWM signal is generated with analog circuitry.

The modulation index can be divided into three regions: a linear region, an overmodulation region and a square-wave region.

In the linear region ($0 \leq m_a \leq 1$) the amplitude of the fundamental component in the output varies linearly with the amplitude modulation index. At $m_a = 0$ the output amplitude is zero.

In the overmodulation region ($1 < m_a < 3.24$) the relation between the amplitude of the fundamental component in the output and m_a is non-linear. The relation becomes proportional to the square-root of m_a (that is for equal increases in m_a the amplitude of the fundamental component rises as the square-root of m_a). In this region the widest pulses at and near 90° start to merge into one another (also referred to as pulse dropping). This changes the harmonic spectrum of the waveform considerably as this introduces low-order harmonics in the current waveform.

In the square-wave region ($m_a \geq 3.24$) the waveform has degenerated into a square-wave (as mentioned earlier, each switch being on for half a cycle). The amplitude of the fundamental component stays constant which demonstrates that a square-wave is a special case of a PWM signal.

Frequency modulation index m_f

The frequency modulation index is the ratio of the switching frequency to the fundamental frequency in the PWM output signal. It is written as follows:

$$m_f = f_s \div f_{fund}$$

Sinusoidal PWM

In sinusoidal PWM the pulse-width of each pulse is sine-weighted. The switching frequency is fixed during a cycle to generate pulses of different width at regular intervals. The switching frequency does not need to stay constant throughout the variable frequency range but can vary from one period to another. It does not, however, change during a cycle. An example of a sinusoidal PWM waveform and the resulting sine-wave is shown in Figure 2.4. The graph displays the line-to-line voltage of the inverter output versus time. The switching frequency (SF or f_s) indicated by the dashed lines running through two adjacent pulses, is the inverse of the time interval (T_s).

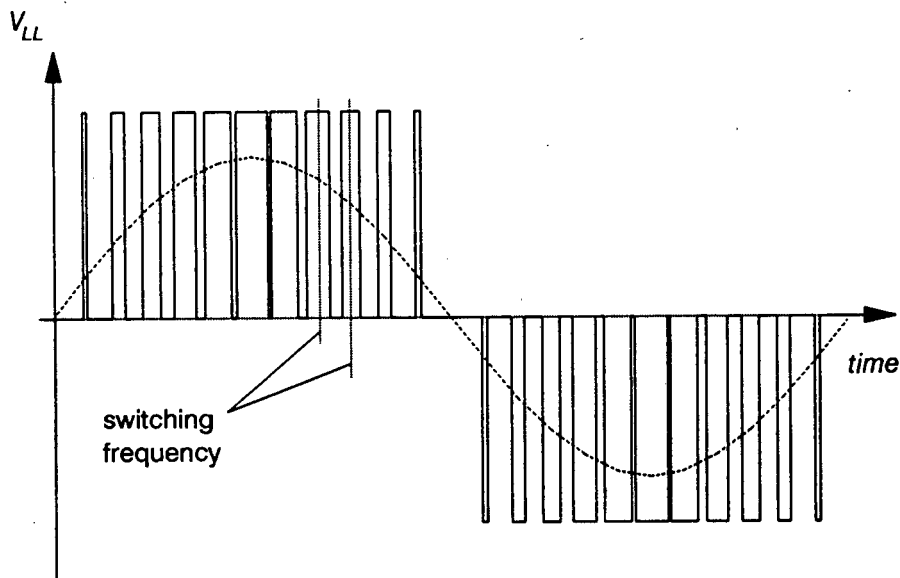


FIGURE 2.4 Sinusoidal PWM waveform
 Source: Mohan et al. (1989: Figure 6-22-b)

The rms line-to-line voltage V_{LL} can be related to the array voltage through the amplitude modulation ratio as follows (Mohan et al. 1989: 132):

$$V_{LL} = 0.612 \times m_a \times V_{arr} \text{ (for } m_a \geq 0 \text{ and } \leq 1)$$

The harmonic frequency spectrum of the PWM signal depends on m_r and m_a where m_r determines where the harmonics will occur and m_a determines the amplitude of the harmonics. When m_r is an integer and $m_a \leq 1$, harmonics appear as sidebands centred around the switching frequency and its multiples (that is at f_s , $f_s \pm 2f_{fund}$, $f_s \pm 4f_{fund}$, $2f_s \pm 1f_{fund}$, $2f_s \pm 3f_{fund}$, $2f_s \pm 5f_{fund}$, $3f_s$, $3f_s \pm 2f_{fund}$ etc). The harmonic spectrum can be improved by adhering to the following:

- choosing m_r to be an integer (referred to as synchronous PWM). If m_r is not an integer (asynchronous PWM) then subharmonics of the fundamental frequency will occur, which will negatively affect the efficiency of a load such as a motor.
- choosing m_r to be an odd integer. This eliminates the even harmonics (that is $2f_s$, $4f_s$ etc but not the sidebands).
- choosing m_r to be a multiple of three. This will cancel out the most dominant harmonics (triplen harmonics) in the line-to-line voltage (that is f_s , $3f_s$, $5f_s$ etc) but not their sidebands.

Under the above conditions the harmonics will occur as sidebands of the SF multiples as can be seen in Figure 2.5. The graph is for one particular amplitude modulation index. The magnitude of the harmonics changes as m_a changes. (The frequency at which some of the harmonics occur is indicated).

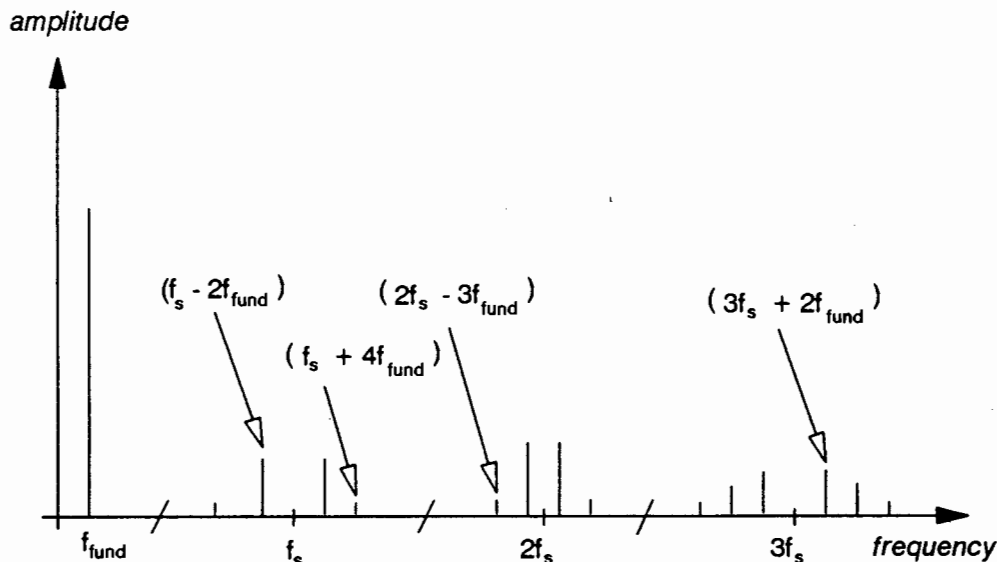


FIGURE 2.5 Frequency spectrum of a sinusoidal PWM signal
 Source: Adapted from Mohan et al. (1989: Figure 6-22-c)

It is possible to increase the rms line-to-line voltage above $0.612 \times m_a \times V_{arr}$ by overmodulating the PWM signal. The maximum attainable rms line-to-line voltage is then $0.78 \times V_{arr}$ (Mohan et al. 1989: 132). Overmodulation causes the odd harmonics of the fundamental frequency to appear (except for the third harmonic and its multiples) which results in torque pulsations and higher motor losses.

At high frequency modulation index ($f_s \gg f_{fund}$), the ripple on the induced current in the motor becomes smaller so that smooth motor rotation is obtained at very low speeds.

Harmonic elimination PWM

This method is a fusion of square-wave switching and pulse-width modulation. It introduces notches in a square-wave at pre-calculated instances with the aim of controlling the fundamental frequency component and eliminating low-order harmonics.

A square-wave consists of odd harmonics and in a three phase inverter the third harmonic and its multiples are cancelled out (triplen harmonics). The remaining harmonics are the fifth, seventh, eleventh, thirteenth and so on. The lowest four harmonics are also the ones that cause torque pulsations and during low speed operation, speed fluctuations. The number of notches per half-cycle determine how many harmonics can be eliminated. Introducing three notches per half-cycle eliminates the fifth and the seventh harmonic. Five notches eliminate the lowest four harmonics. An example is shown in Figure 2.6. The pole voltage is the phase to negative DC bus voltage and a_x are the switching angles.

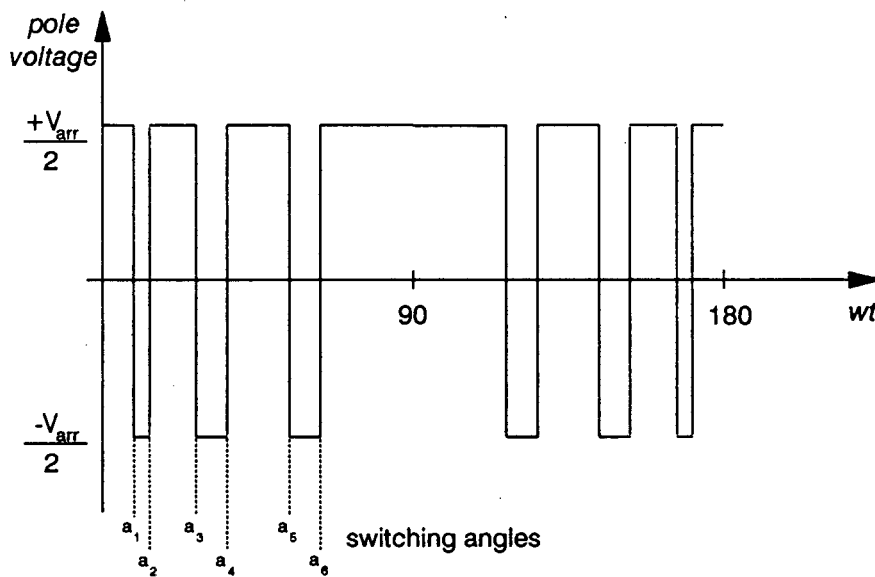


FIGURE 2.6 Harmonic elimination PWM waveform
Source: Murphy and Turnbull (1988: Figure 4.29)

The amplitude of the fundamental voltage is controlled through different values of switching angles while still eliminating the unwanted harmonics. The differences in the switching angle value when changing from one amplitude to another are very small (in the order of 0.1°). The tables for eliminating a specific number of harmonics can be obtained from literature. They are calculated by means of Fourier analysis and have to be solved numerically.

Some additional characteristics:

- as a result of low-order harmonic elimination the next in-line harmonics are boosted
- at low frequency operation the number of notches should be increased to eliminate a higher number of harmonics. Look-up tables then tend to become quite large
- the switching frequency of this harmonic elimination technique is not as such constant during a cycle

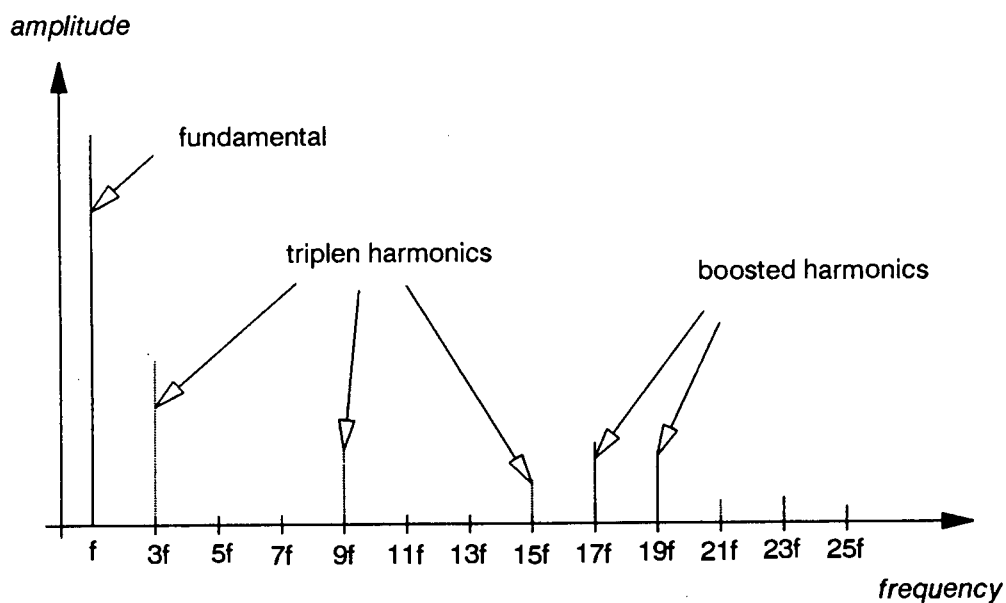


FIGURE 2.7 Frequency spectrum of a harmonic elimination PWM signal
 Source: Adapted from Murphy & Turnbull (1988), Bose (1986) and Mohan et al. (1989)

The elimination of the fifth, seventh, eleventh and thirteenth harmonic is shown in Figure 2.7 which displays the harmonic spectrum as a function of frequency. The triplen harmonics will be cancelled in the line-to-line voltage. The seventeenth and the nineteenth harmonics are boosted. The amplitude of the harmonics will change with changes in the fundamental amplitude of the output signal.

Square-wave PWM

This scheme essentially uses a square-wave where notches are introduced at regular intervals to control the fundamental output voltage. The pulses all have the same width during a cycle. The width is varied to allow for voltage control. The output voltage changes in direct proportion with the amplitude modulation index if $m_a < 1$. At $m_a \geq 1$, the square-wave PWM turns into a plain square-wave.

The harmonics occur as odd multiples of the fundamental frequency and as sidebands of the even multiples of the switching frequency ($2f_s \pm f_{fund}$, $2f_s \pm 5f_{fund}$, $4f_s$ etc). Their magnitude is substantial.

Due to this harmonic spectrum, square-wave PWM inverters give rise to torque pulsations and speed fluctuations at low motor speeds and are rarely used nowadays in AC motor drives.

Sinusoidal modulation versus harmonic elimination switching schemes

Sinusoidal and harmonic elimination PWM are both highly favoured switching schemes. The criteria for evaluating a switching scheme are switching losses and the size of the rms ripple current (harmonics) in the motor:

- Harmonic elimination:
- can reduce the number of switches per cycle and therefore lower the switching losses while eliminating the most the undesired harmonics
 - harmonic losses increase at small m_a and are therefore not well-suited for operation at low voltage and frequency unless more notches are introduced which can result in more switching losses. In addition, the tables containing the switching instances become very large
- Sinusoidal:
- good low speed performance making it a preferred switching scheme for slow processes

2.6.3 The induction motor

The induction motor as used in this application is a three phase, squirrel-cage motor. The stator consists of three sets of windings which are physically displaced by 120° with respect to each other. The rotor consists of electrically conducting bars whose orientations are parallel to the rotor axis. The bars are short-circuited at each end with a ring. This gives it the cage-like appearance and this also highlights the simple and rugged construction of a squirrel-cage induction motor.

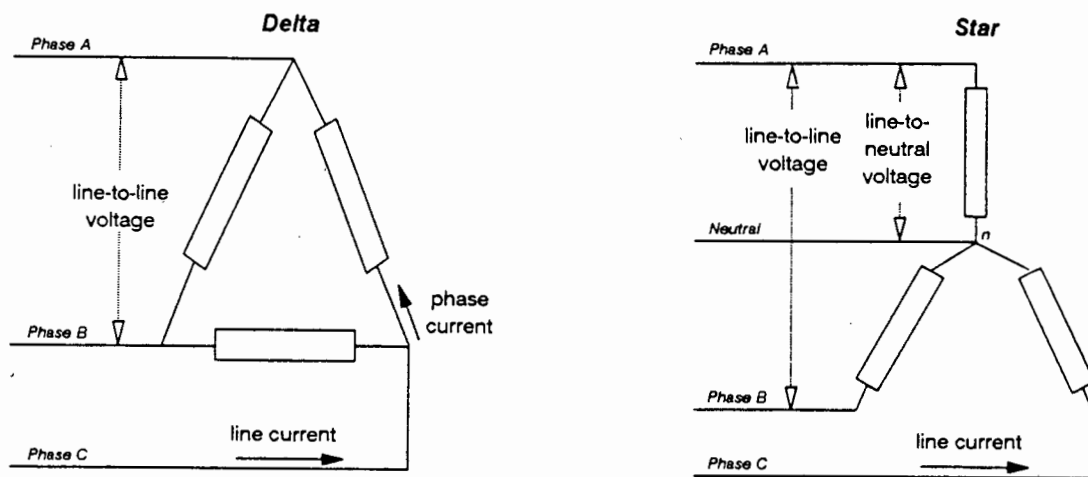


FIGURE 2.8 Delta and star induction motor configurations

The three sets of windings, which are essentially inductors, can be connected in two configurations namely delta and star configuration. This is shown in Figure 2.8. The delta connection is a three lead connection without a neutral. Only the line-to-line voltage can be applied. The specified voltage for an induction motor is always the line-to-line voltage unless otherwise specified. The line current is different from the phase current in terms of amplitude and phase angle. The amplitude of the line current is a factor of root three larger than the phase current.

The star connection is a four lead configuration where the one end of each inductor is connected to become the neutral. The line-to-line voltage is a factor of root three larger than the line-to-neutral voltage. In a delta connected motor the line and phase current are the same.

Motor current

When the motor is excited with a three phase voltage a current is generated in the inductors which is drawn out of the capacitors at the input of the inverter (see Figure 2.2). The harmonic spectrum of the current waveform is completely dependent on the characteristics of the voltage signal applied (amplitude, switching frequency and switching scheme). All voltage signals, except a sinusoidal signal, will result in a ripple superimposed on the fundamental sinusoidal current waveform. The size of the ripple depends on the harmonic frequency spectrum of the applied voltage signal. A

sinusoidal PWM signal results in a smaller ripple amplitude on the current waveform than the ripple caused by a square-wave signal. This can be observed in Figure 2.9 which shows the ripple current as a result of a square-wave (a) and a PWM signal (b). The fundamental current component has been subtracted.

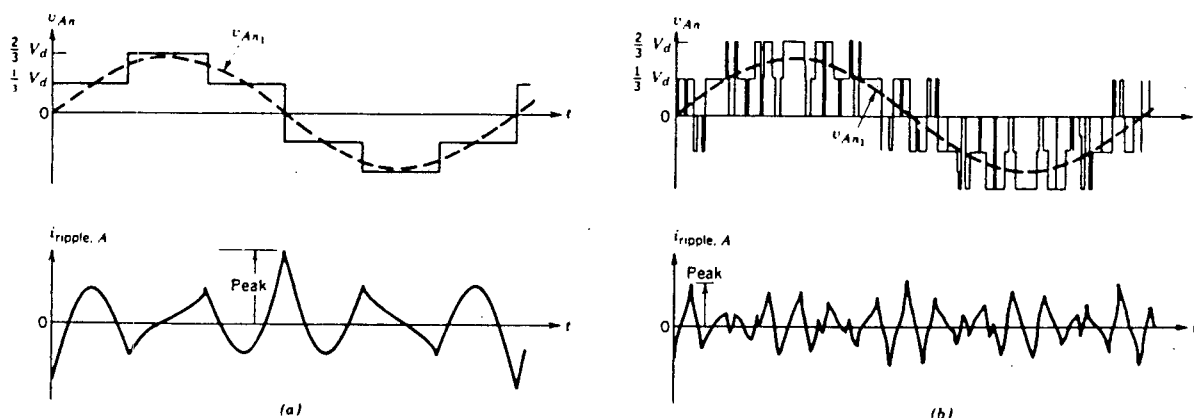


FIGURE 2.9 The ripple on the line current: (a) square-wave and (b) PWM
Source: Mohan et al. (1989: Figure 6-26)

The real or active power transferred to the motor is carried by the fundamental frequency component in the voltage and the current waveform. The power contained in the ripple is lost since the motor does not transfer this energy to its output shaft. Motor performance is therefore improved by minimising the current ripple. This is accomplished by increasing the switching frequency in the case of sinusoidal PWM or by introducing more notches in the case of harmonic elimination PWM. However, this will result in an increase of switching losses in the inverter. Therefore, from the point of view of the inverter and the motor, a suitable switching frequency has to be selected to take account of the switching losses in the inverter and to take account of the reduction in motor efficiency due to the ripple on the current waveform.

Characteristic motor curve at rated voltage and frequency

The characteristic motor torque-speed curve for rated voltage and rated frequency is shown in Figure 2.10. T_{em} is the electromagnetic torque, ω_r is the rotor speed in radians and ω_s is the stator 'electrical speed' in radians. ω_s is directly proportional to the stator frequency and ω_r is directly proportional to the rotor frequency. ϕ_{ag} is the flux of the magnetic field. However, flux is not taken into further consideration here.

The motor, if not overloaded, operates along the solid region of the top graph which is also quite a linear region. The operating point on this curve is determined by the intersection with the load curve. As an example, a hypothetical torque-speed curve of a positive displacement pump has been added (lower curve). The curve has a reasonably low gradient as is characteristic for these type of pumps. It can be seen that the motor is capable of generating a range of torques (between zero to rated torque) without substantial speed changes.

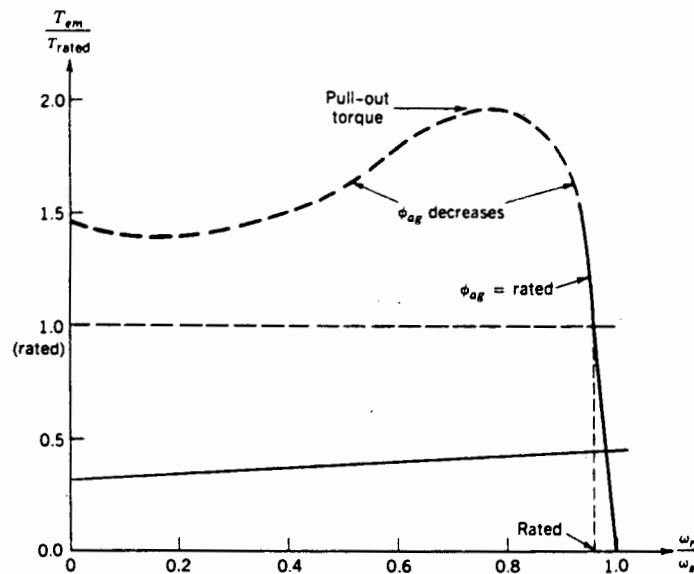


FIGURE 2.10 Induction motor torque versus speed characteristics for fixed voltage and fixed frequency operation

Source: Mohan et al. (1989: Figure 12-3)

The motor traces the dashed section of the curve during start-up (assuming start-up under rated voltage and frequency conditions; for example, 220V and 50Hz). It can be seen that the motor generates a torque well above the rated torque. However, the drawback is that the motor draws a current of six to eight times its rated current during its speed-up period. The maximum torque which the motor can produce is referred to as the pull-out torque.

Characteristic motor curves at variable voltage and frequency

Figure 2.11a shows a family of torque-speed curves at variable voltage and frequency and Figure 2.11b shows the stator voltage (V_s), the magnetising current (I_m) and the rotor current (I_r) which is referred to the stator. The magnetising current and the rotor current combine to give the stator current.

The family of curves in the constant torque region (graph a) are the linear sections of the torque-speed curve shown in Figure 2.10. In the constant power and the high speed region the peak amplitude of the torque curve (the pull-out torque) reduces exponentially. The maximum operating torque (T_{em}) reduces along the constant power hyperbola ($T_{em} \times \omega_r = \text{constant value}$) in the constant power region. During the high speed region the maximum permissible torque reduces exponentially, just like the pull-out torque.

Generating higher than rated torques beyond the rated frequency (f_3) would require a higher voltage than rated voltage or allowing the motor to draw current in excess of its rated current. None of these conditions are desirable and would ultimately lead to break-down. Motor ratings are usually exceeded by overloading the motor. It is less likely that the applied voltage will be in excess of the rated voltage.

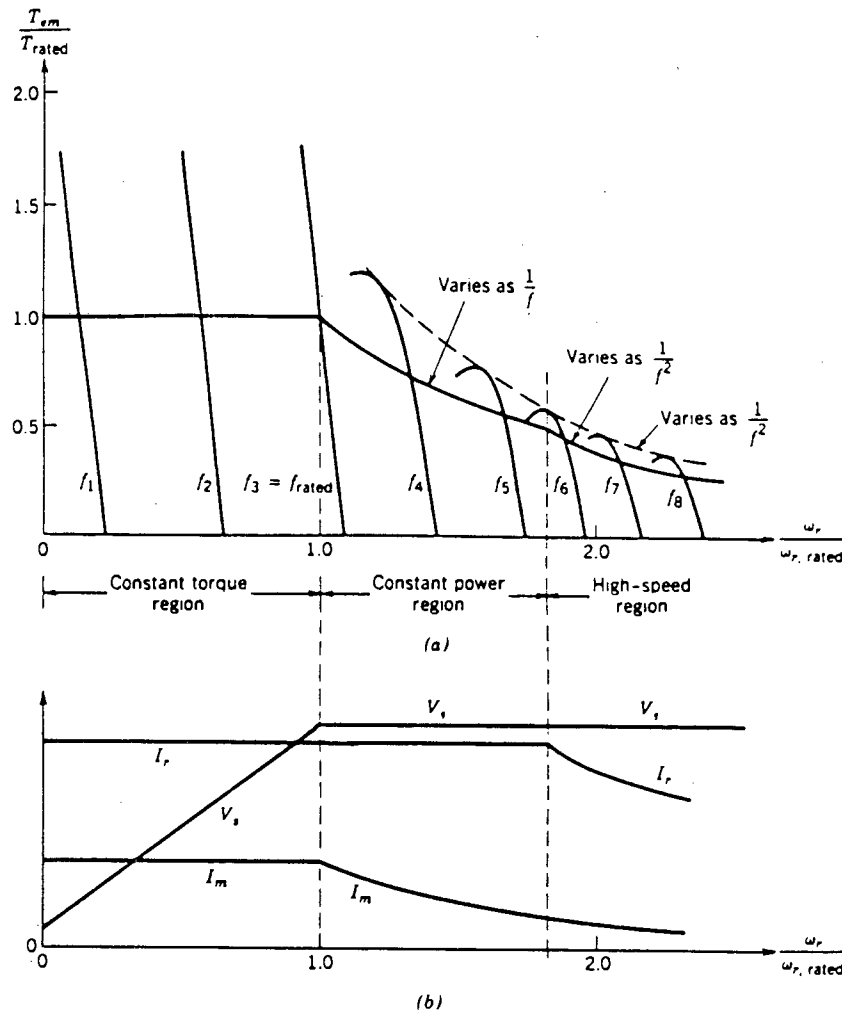


FIGURE 2.11 Induction motor variable voltage and frequency operation: (a) torque versus speed characteristics; (b) stator voltage and current during maximum permissible torque output

Source: Mohan et al. (1989: Figure 12-12)

The stator voltage is non-zero at zero rotor speed (graph b), and in general the voltage drop across the resistance in the stator windings becomes larger relative to the applied voltage as the voltage across the motor terminal is reduced. The boost voltage therefore compensates for this voltage drop.

Figure 2.11 shows that in principle any motor speed can be generated at a particular torque (determined by the load) provided that the motor drive is able to apply the exact voltage and frequency. This is mainly a question of resolution. Should the required resolution be supported by the hardware then there are still the memory requirements which will be high due to many voltage look-up tables.

If the load on the motor output is such that the motor is operating near or at the rated torque over a frequency range which is in excess of the rated frequency then care has to be taken not to overload the motor. This could occur in the region beyond the rated

frequency (that is, $\omega_r \div \omega_{r, \text{rated}} \geq 1$). In PV water pumping applications the motors are usually oversized to allow for efficiency improvements by the motor designer. Therefore, there is no danger in overloading the motor since the motor is consistently operated in the partial load region (about 60% of the rated torque or less).

Voltage to hertz relation

The voltage to hertz (V/Hz) relation is an important aspect of a variable voltage, variable frequency drive. The normal approach is to keep the relation constant (see Figure 2.11). In this case the voltage is linearly related to the frequency. The torque remains constant under these conditions which is broadly suitable for a progressive cavity pump.

Two types of V/Hz relations are prevalent in industry. The synchronous V/Hz range follows a linear V/Hz relation to 50Hz (usually the rated frequency) and then keeps the output voltage constant while the frequency is increased to above the rated frequency (as shown in Figure 2.11b). The sub-synchronous V/Hz range follows a linear relation from 0Hz to 87Hz and therefore maintains a constant torque over the whole range.

In order to match the output of the MLT inverter to a particular motor, Davies (1992) derived a V/Hz relation that is based on maximising the efficiency of the motor over the complete frequency operating range. The resulting equation requires the values for the equivalent circuit parameters of the motor. These have to be found using appropriate tests. The voltage in this V/Hz relation is proportional to the square-root of the frequency. However, some components in the relation are frequency dependent.

2.6.4 Torque pulsations

Torque pulsations can arise from harmonic frequencies in the stator current. The lowest harmonic frequency at which this phenomenon occurs is at the 5th and the 7th harmonic. The fifth harmonic rotates in the opposite direction to that of the rotor and the seventh harmonic rotates in the same direction as the rotor. These two harmonics combine to produce a resulting torque that pulsates at the sixth harmonic frequency. Similarly, the eleventh and the thirteenth harmonic frequencies can produce a pulsating torque at the twelfth harmonic frequency and so on.

Torque pulsations at low frequency (for example the sixth harmonic) can affect the mechanical performance of the motor. They can cause the frame and the rotor to vibrate, resulting in eccentricity which could lead to shaft fatigue. The lifespan of the ball bearings will be reduced and the pulsations may also be harmful to the load. In addition, torque pulsations can amount to speed fluctuations.

Torque pulsations may be significant in square-wave and six-step inverters. Sine-wave and PWM inverters do not have these low order harmonics in their spectra unless the frequency modulation index for PWM inverters is extremely small or the amplitude modulation index is larger than one. However, torque pulsations may occur for other reasons, such as array voltage oscillations (see section 7.3 and 8.3).

2.6.5 The function of DC input capacitance

The DC input capacitance has three principal functions:

- to act as a buffer between the array and the load, in other words, to stabilise the array operating point. The array voltage is switched completely on the load. Without a buffer the operating point would shoot up and down the IV curve of the array, resulting in extremely poor power extraction.
- to store the back-flow of current (reactive power) from an inductive load
- to provide the extra energy to generate the starting torque for a positive displacement pump which can be in the order of 1.5 to 3.8 times higher than the running torque (Vetter & Wirth 1993)

The input ripple on the array voltage (and current) due to the switching of the inverter (or converter) is reduced if the capacitance is increased.

*2.7 Efficiency considerations in PV pump systems

It was stated previously that one of the main disadvantages of photovoltaic water pumping was its high cost. Efficiency considerations therefore gain importance as they may result in some cost savings.

The efficiency of the components and their interaction is discussed in this section. The emphasis is on the aspects which affect the efficiency of a component or the match between two components.

2.7.1 PV pump component efficiencies

Photovoltaic array

Assuming a given type of module with the present commercially available photovoltaic cells, then the main aspects which affect the efficiency of a PV array are its internal mismatch losses and cell temperature variations. Both aspects are discussed below. The information is drawn from Lasnier and Gan Ang (1990).

PV array mismatch

The efficiency of a network of photovoltaic cells (PVC) or modules can be affected by the occurrence of different IV characteristics within that network. The effect is best demonstrated by means of a graph with the IV characteristics of two different PV cells, one low efficiency cell (PVC1) and one high efficiency cell (PVC2). The IV curves in Figure 2.12 are slightly exaggerated (relative to each other) but show the result of mismatching well. These particular PV cells are connected in series. The resulting IV curve is shown by PVC3.

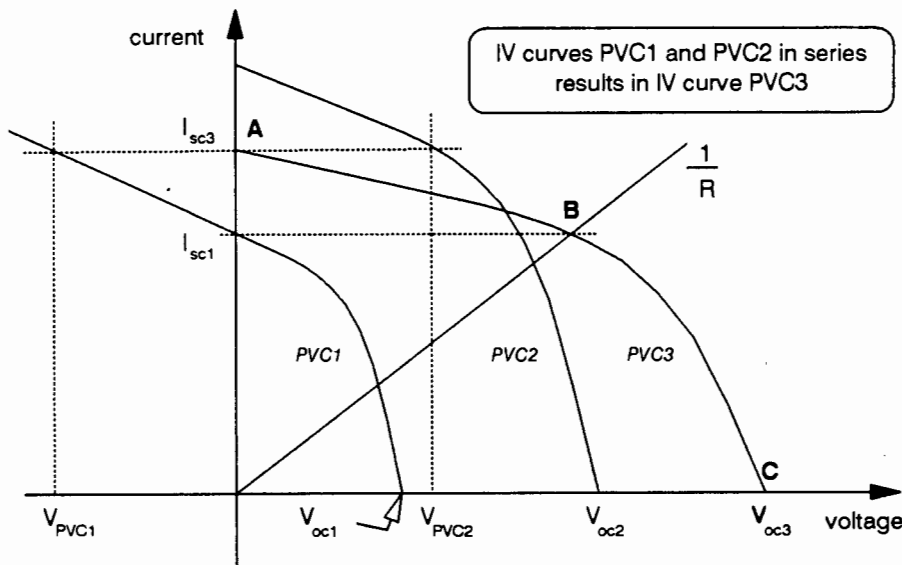


FIGURE 2.12 Matching of two non-identical PV cells in series
 Source: Adapted from Lasnier and Gan Ang (1990: Figure 3.4)

Both PV cells will operate as generators along the B to C region of PVC3. At point B PVC1 generates no power (it has reached its short-circuit current). If PVC3 is loaded such that the operating point is just to the left of point B, then PVC1 will act as a receptor. The current is still flowing through PVC1 but the voltage across it is negative. At point A on PVC3 the short-circuit current has been reached with the effect that the voltage across PVC2 (V_{PVC2}) is equal to the negative voltage across PVC1 (V_{PVC1}). Therefore $V_{PVC2} = -V_{PVC1}$. Under these conditions PVC1 is dissipating power equal to $V_{PVC1} \times I_{PVC3}$. This results in heating and leads to hot spots within a PV module. Besides the likely deterioration the efficiency of such a network is reduced.

The same holds true for a larger network of PV cells or modules. In a long string of series cells/modules a substantial reverse voltage can be applied across a less efficient cell only with a much bigger heating effect.

Mismatched IV characteristics within a parallel network can result in similar effects. In this case the less efficient cell sinks a negative current near the open circuit voltage of the resulting IV curve.

By-pass diodes are used to avoid the above phenomena. These diodes also protect strings of PV cells which may be partially shaded.

In an array where few strings of series modules are connected in parallel, the weakest modules can be separated into one series string and then connected in parallel to the other strings. This ensures that only one string of modules will generate a lower current. If the weak modules were distributed amongst the different series strings of modules then the overall array performance will be poorer. The rule is that the performance of each string will be governed by the performance of its weakest module.

PV cell temperature variations

An increase in the cell temperature results in a marginal increase in the operating current which is due to a decrease in the band-gap energy. However, the operating voltage decreases by a larger percentage than the percentage increase experienced by the operating current. The voltage decrease is due to an increase in the saturation current which is inversely proportional to the open-circuit voltage.

The overall effect of cell temperature on the maximum available array power is that the power decreases by approximately 0.35%/°C (Lasnier & Gan Ang 1990) as the temperature increases (this figure will vary for different types of modules). Consequently the array efficiency is reduced by an increase in cell temperature.

Switch-mode controller

The efficiency of a controller is determined by three quantities namely the power requirements of the control electronics (analog or digitally based) and the drive circuit, by the switching losses and by the conduction losses.

Controller power requirements

The power requirements of the control electronics and the drive circuit are usually constant and include the efficiency of the power supply itself. The efficiency of a switch-mode power supply is higher than the efficiency of a linear regulator-type power supply. The reduction in power requirements of the control and drive circuit electronics is a question of design and choice of components. The use of components that have a low power consumption (for example, CMOS IC's) and an overall reduction in the number of components (for example, single chip computers with on-board ADC and phase comparator) will reduce the power requirements and can hence improve the efficiency. The improvements will be marginal as this area of control electronics and power electronics has been optimised to a large extent.

Conduction losses

The conduction loss refers to the voltage drop which occurs across the switching transistor during periods of conduction (transistor on-state). A small, additional loss is incurred by the power dissipated in the diode across the other transistor (of one particular phase; refer to Figure 2.2).

The magnitude of the voltage drop is dependent on the on-state resistance of the transistor, on the peak line current (squared) which passes through it and on the power factor.

Conduction losses are reduced in power modules which have lower on-state resistance values. This is mainly a question of the available selection of power modules and their cost. It is also common to find converters (and possibly inverters) which use a number of transistors in parallel to reduce the on-state resistance.

Switching losses

The switching losses which occur in the power module (MOSFET or IGBT) during the switching instances are directly proportional to the switching frequency of the controller. The major losses occur during the switch turn-on period whereas the turn-off losses are small in comparison. Turn-off losses are therefore regarded as negligible. The energy lost during turn-on depends on the shape of the line current waveform. The essential parameters are the peak current amplitude (the current overshoots on turn-on), the time base of the signal (from which the charge can be calculated: current \times time) and the array voltage. The per phase dissipated switching power is therefore:

$$P_{\text{switching}} = f_s \times V_{\text{arr}} \times i_{\text{line}} (f^n (\text{time})) \text{ [W/phase]}$$

The term $i_{\text{line}} (f^n (\text{time}))$ represents the charge which is dissipated during turn-on. It is equivalent to the area under the switching current waveform during the switching instance. The total dissipated losses are equal to three times $P_{\text{switching}}$ in the above equation.

The switching losses are constant if the torque requirements and the switching frequency are constant. A progressive cavity pump requires a reasonably constant torque and the variations in the line current are hence small. It is generally assumed that the switching losses are constant under these conditions. They can however be treated as variable losses for a more accurate evaluation by taking account of the variations in the line current.

The switching losses can be reduced by using transistors that have superior switching characteristics (shorter switch-on time) or by decreasing the switching frequency. However, a decrease in the switching frequency affects motor performance negatively.

Induction motor

The efficiency of an induction motor is affected by its design, by the harmonics in its current waveform and by the voltage to hertz relation applied to the motor. Considerations in terms of optimal motor design are not discussed as this goes beyond the scope of the dissertation.

Losses in the presence of harmonics

The harmonics in the voltage and current waveform do not contribute towards the real power transfer to the rotor shaft. This is done solely by the fundamental frequency components. The amplitudes of the harmonic currents generated in the motor inductance are independent of the load. They will be just as large at no-load as at full load (Scholey 1982).

The harmonics in the current waveform result in losses which are primarily due to I^2R (copper) losses. Additional losses are due to core and stray losses as well as harmonic frequency eddy currents and hysteresis. These depend on the design and the material used in the motor. The latter losses are estimated to be in the range of 10% to 20% of the total power losses at rated load (Mohan 1989: 328).

Motor efficiency is improved when the harmonics in the motor current are shifted to high frequencies. This is accomplished by increasing the switching frequency.

Voltage to hertz relation

According to Davies (1992) the voltage applied to the motor has to be proportional to the square-root of the frequency to obtain an optimum efficiency over the whole variable frequency range. Davies also performed a sensitivity analysis which evaluated the reduction in efficiency due to variations in the required torque and the applied voltage. Both analyses showed that the reduction in efficiency is most marked at lower operating frequency. At 20Hz, torque variations of 20% result in a relative motor efficiency reduction of 2.3% (Davies 1992: Figure 31) and voltage variations of 20% result in a relative efficiency reduction of 5.6% (Davies 1992: Figure 32). At 70Hz, similar torque variations result in a relative efficiency reduction of 1.2% (Davies 1992: Figure 31) and similar voltage variations result in a relative efficiency reduction of 3.7% (Davies 1992: Figure 32).

The use of a progressive cavity pump will certainly result in some torque variations and depending on the magnitude of these variations, motor efficiency reductions as discussed above can be expected. If the load characteristics of a pump are very well known and are found to vary by relatively small percentages, then it would be possible to adapt the voltage to hertz relation such that it would meet the torque requirements with minimal losses. The drawback is that the pump speed and inverter frequency have to be correlated to each other - pulley changes would therefore not be desirable once the voltage to hertz relation had been optimised for a particular pump using a pre-determined speed ratio.

Realistically this degree of voltage to hertz adaption is not possible as the required data would not be readily available. Furthermore, it is unlikely that the load characteristics of a pump (especially a progressive cavity pump) would retain its magnitude and shape over a longer period of time making a highly adapted V/Hz relation unwarranted.

Progressive cavity pump

The efficiency of the pump cannot be affected by changes in the installation but only through appropriate changes during its design stage. If a selection of pumps were available, then the most suitable pump for a particular site could be selected. This information is based on a paper by Vetter and Wirth (1992).

The losses which occur in a progressive cavity pump are mainly due to two factors:

- (a) Losses due to slip - not all the water in the cavities is effectively lifted to the top, and a small amount of water slips back to the suction side of the pump;
- (b) Losses due to friction between the stator and the rotor.

A typical efficiency curve is shown in Figure 6.19. The main variables are the pump speed, the pressure head and the interference fit between the stator and the rotor.

Losses as a function of pump speed

The friction losses tend to increase slightly as the speed of the pump increases (Vetter & Wirth 1992: Figure 6). The slip losses are usually close to 100% near zero speed and then decrease rapidly. For the particular type of pump mentioned in the paper (NE 20 Mono pump) the overall efficiency increases from about zero percent at zero speed to reach a peak at a third of its nominal speed and then decreases slightly for the remaining operating range.

Losses as a function of pressure head

The friction losses decrease substantially as the pressure head increases (Vetter & Wirth 1992: Figure 7) especially at low pressure head. Slip losses show a marginal increase as the pressure head increases. The overall efficiency of the pump increases from zero percent at zero head to its optimum efficiency at maximum and rated pressure head.

Losses as a function of the interference fit

The friction losses are virtually proportional to the interference fit. As the interference fit is narrowed (the stator is squeezed more tightly around the rotor) the friction losses increase (Vetter & Wirth 1992: Figure 8). The slip losses decrease rapidly as the interference fit is narrowed. The losses reach a shallow minimum from which they only increase slightly as the stator is fitted tighter to the rotor.

2.7.2 The impact of component interaction on the overall efficiency

The interaction of components can be divided into two categories namely, the mismatch losses and the transfer losses between the components. The losses are listed in Table 2.4. The minimisation of some of these losses can improve the overall performance of a PVP system.

TABLE 2.4 Areas of optimisation in a photovoltaic pump

<i>Inter-component</i>	<i>Mismatch losses</i>	<i>Transfer losses</i>
<i>Sun → array</i>	<ul style="list-style-type: none"> • spectral response • angle of array surface to sun¹⁾ 	<ul style="list-style-type: none"> • particulates and haze in the atmosphere
<i>Array → controller</i>	<ul style="list-style-type: none"> • tuning²⁾ • array operating point³⁾ • size of input capacitor(s)⁴⁾ 	<ul style="list-style-type: none"> • cable copper losses⁷⁾
<i>Controller → motor</i>	<ul style="list-style-type: none"> • none other than the V/Hz relation and current harmonics as discussed in subsection 2.7.1 	<ul style="list-style-type: none"> • cable copper losses⁷⁾
<i>Motor → pump</i>	<ul style="list-style-type: none"> • unreasonable speed ratio⁵⁾ • pulley misalignment⁶⁾ 	<ul style="list-style-type: none"> • friction in belt transmission
<i>Pump → reservoir</i>	<ul style="list-style-type: none"> • too small pipe diameter • sudden pipe expansion • sudden pipe contraction 	<ul style="list-style-type: none"> • discharge head gland packaging⁸⁾ • friction in discharge head bearings⁹⁾ • friction and velocity head losses in pipe network - roughness

¹⁾ If the angle (α) between the direct component of the global irradiance and the normal to the array surface is larger than zero degrees the amount of direct irradiance received is reduced by $(1 - \cos \alpha) \times 100$ [%] percent. The amount of incident irradiation during the course of a day/year can be maximised by the use of different array structures. The options are a fixed array with no seasonal adjustment (worst case), a fixed array with seasonal adjustment, a single axis tracking array and a dual axis tracking array (best case).

²⁾ The most common operating modes implemented by PVP controllers are: fixed voltage operation (FVO), optimum voltage point tracking (OVPT) or maximum power point tracking (MPPT). FVO and OVPT require tuning. The specifications for the modules are required for that. In case of FVO the array voltage should be chosen closest to optimum array operating point by taking account of the most probable average cell temperature for the particular site.

³⁾ Steady state and instantaneous array operating point should be stable, that is no oscillations about an average point as this can diminish the array output power.

- 4) The size of the input capacitor has an effect on the magnitude of the ripple current at the controller input and it affects the capacity to provide the required starting torque. Over-sizing the capacitors is mainly prohibited by cost. An increase in capacitance requires a reassessment of the start-up amplitude programmed into look-up tables since the higher current generation capabilities of the increased capacitance can damage the power module on start-up should it exceed the controller power module ratings.
- 5) The two extremes are: a) a too large speed ratio (small motor pulley) where the motor will reach maximum speed at low input powers and b) a too small speed ratio (large pulley ratio) resulting in torque requirements that cannot be met by the motor (in conjunction with the array current and the DC capacitors).
- 6) Pulley misalignment will result in unnecessary friction in the transmission. The motor pulley can be adjusted until the V-belt plane is at right angle to the motor and discharge head plane where latter planes face each other.
- 7) The voltage-drops over long cables can be reduced by using larger diameter cable; the trade-off is higher cost - an assessment has to be made from case to case.
- 8) Gland packaging material which has less friction than graphite asbestos but also acts as a good seal will reduce losses; Payne (1986) suggests replacing graphite asbestos with P.T.F.E. (a form of teflon).
- 9) These bearings could be replaced with non-contact type sealed bearings (Payne 1986).

3.2 The array

The PV array consisted of twelve monocrystalline modules manufactured by Siemens. However these modules were not all from the same production generation. The breakdown was as follows:

- 3 × M55 ARCO Solar modules (black aluminium frame)
- 4 × M55S Siemens Solar modules (silver aluminium frame, with M6 nuts pressed into the frame to simplify installation)
- 5 × M55 Siemens Solar modules (silver frame, youngest generation)

The specifications and the physical dimensions remained the same for all three types of modules except for a small increase in the short circuit current in the most recent generation of modules. Temperature coefficients were only supplied for the M55S while the specifications of the other two module types included graphs showing the effect of temperature on the array voltage.

3.2.1 Specifications

The data sheet for the Siemens module is attached in appendix A1.1. The Table below lists the specifications of the M55S module. Each module was fitted with two by-pass diodes.

TABLE 3.2 Specifications of a Siemens M55S module

Output ¹⁾	Value	Units
<i>MPP voltage</i>	17.4	V_{MPP}
<i>MPP current</i>	3.05	A_{MPP}
<i>Open circuit voltage</i>	21.7	V_{oc}
<i>Short circuit current</i>	3.35	A_{sc}
<i>Maximum power</i>	53.0	W_p
<i>Efficiency</i>	13.9	%
Temperature performance		
<i>NOCT ²⁾</i>	47	°C
<i>Temperature coefficient of V_{oc}: t_v</i>	- 0.34	%/°C
<i>Temperature coefficient of I_{sc}: t_i</i>	+ 0.04	%/°C
Module Area		
<i>Number of cells per module</i>	36	
<i>Cell area</i>	0.0106	m ²
<i>Module area</i>	0.3812	m ²

¹⁾ These electrical characteristics can vary by $\pm 10\%$ due to manufacturing variations. Standard Test Conditions (STC) are: irradiance of 1000W/m², cell temperature of 25°C and air mass of 1.5.

²⁾ NOCT: Normal operating cell temperature: Irradiance = 800W/m², ambient temperature = 20°C and wind speed 1m/s.

3.2.2 Configurations used

The three electronic controllers under test had different voltage limits on their input. The array therefore had two configurations: one series configuration where all the modules were in series, and one parallel configuration where two strings of six series modules were connected in parallel. The expected output values of the array for both configurations are listed in Table 3.3.

TABLE 3.3 Possible array output values for series and parallel configuration

Output: Series configuration ¹⁾	STC	NOCT²⁾	Units
<i>MPP voltage</i>	208.8	193.2 ³⁾	V_{MPP}
<i>MPP current</i>	3.05	3.08 ³⁾	A_{MPP}
<i>Open circuit voltage</i>	260.4	240.9	V_{oc}
<i>Short circuit current</i>	3.35	3.38	A_{sc}
<i>Maximum power</i>	636	595	W_p
Output: Parallel configuration ¹⁾			
<i>MPP voltage</i>	104.4	96.6 ³⁾	V_{MPP}
<i>MPP current</i>	6.10	6.16 ³⁾	A_{MPP}
<i>Open circuit voltage</i>	130.2	120.5	V_{oc}
<i>Short circuit current</i>	6.70	6.76	A_{sc}
<i>Maximum power</i>	636	595	W_p
Array area			
<i>Total array cell area</i>		4.5742	m ²

- ¹⁾ These values are given as an indication only. Inter-module mismatch and transfer losses have not been taken into account.
- ²⁾ NOCT = 47°C and $G = 800W/m^2$ but here it is calculated for $1000W/m^2$ as this is more representative of Namibian solar irradiance conditions.
- ³⁾ These values assume that the open-circuit voltage and the short-circuit current temperature coefficients are the same for the MPP voltage and current.

3.2.3 Tracking array mechanism

The array was a single-axis, passive tracker with two tilt angles to accommodate seasonal changes. It was manufactured by Zomeworks in the USA. The data sheet is in appendix A1.2. The tracking principle is as follows: The array has a black metal tube on the east and the west side that contains a gas (CFC). Both tubes are connected with a compensating pipe. Both are partly shaded with U-shaped aluminium wings (see appendix A1.2) that partially cover the top surface and the bottom surface of the tube, leaving a section exposed to the sun for heating. These sections are heated in equal amounts when the sun shines perpendicularly on the array. Tracking is accomplished when the sun is not shining perpendicularly onto the array since, under these circumstances, one tube is heated more than the other and the gas then expands and forces most of its weight into the less heated tube. The imbalance in weight causes the array to turn while shock-absorbers prevent fast movement.

3.3 The pump

3.3.1 Specifications

The pump that was used was a S2M Mono borehole pump. This is a positive displacement, progressive cavity, self-compensating stator type pump. It operates up to a head of 150m. The maximum recommended speed is 1200 rpm. The specified minimum starting torque is 3N.m.

The pump data sheet is in appendix A1.3. Figure 3.1a shows the pump characteristics at 75m in a slightly reprocessed form.

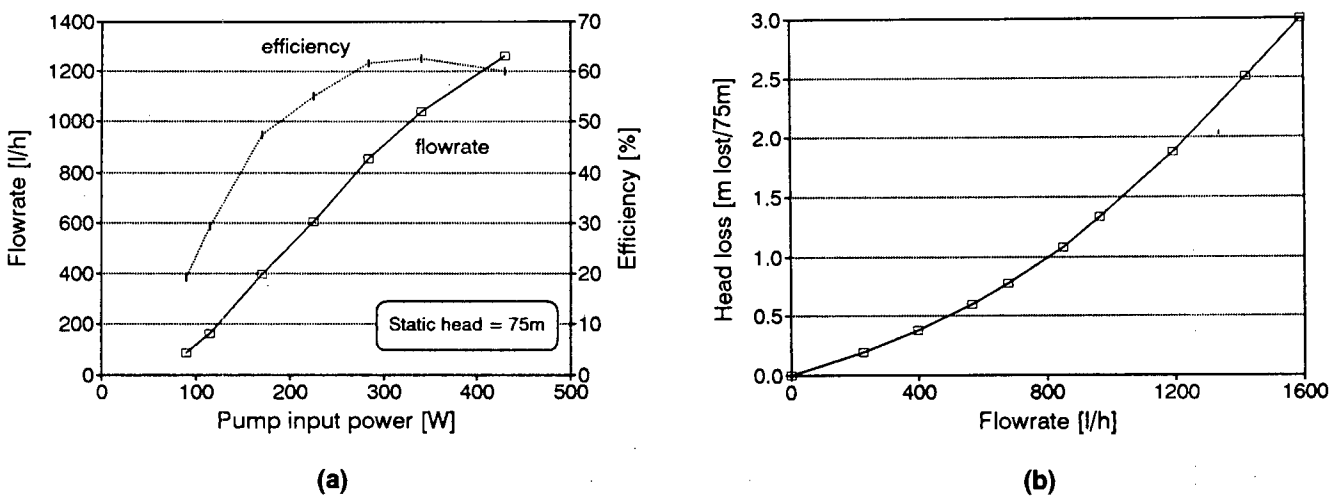


FIGURE 3.1 Supplied data for S2M pump: (a) Flowrate and efficiency of the pump at 75m; (b) Rising main head losses

3.3.2 Installation

The pump was installed at a depth of 90m. The pipe had a diameter of 40mm. The shaft had a diameter of 13mm and was supported by bobbin bearings (one per 1.5m). A graph that shows the head losses as a function of the flowrate in the rising main pipe was supplied by Mono Pumps. The relevant section of the graph (in terms of flowrate) is shown in Figure 3.1b.

3.3.3 Transmission

The power of the motor was transferred to the pump by means of a single V-belt (Super-HC; 10×8mm). The section type was 10N (SPZ) which was the narrowest section available. The pulley on the discharge head assembly had an outer diameter of 250mm. The pitch-centre diameter (PCD) was measured to be 247mm. The motor pulleys that were available for the tests were: 85, 97, 112, 118, 125 and 140 PCD.

3.4 The Miltek DC to DC converter

3.4.1 Specifications

The Miltek converter as used in the tests was a DC to DC converter, model number MEI 400. It was manufactured by Miltek Electrical Industries which has become a subsidiary of United Power Corporation. In the text the converter is referred to as Miltek converter.

TABLE 3.4 Specifications of the Miltek converter

<i>Input</i>	<i>Value</i>	<i>Units</i>
<i>Operating range for fixed voltage¹⁾</i>	45 → 120	V _{arr}
<i>Maximum open-circuit voltage²⁾</i>	200	V _{arr}
<i>Maximum short-circuit current</i>	15	A _{arr}
Output		
<i>Voltage range³⁾</i>	$(0.06 \rightarrow 1) \times (V_{arr} - 1.4)$	V
<i>Maximum pulsed current</i>	25	A
<i>Maximum power</i>	1.8	kW
<i>Switching frequency</i>	2.5	kHz
<i>Efficiency (direct mode)</i>	98	%
Other		
<i>DC Capacitance (200V)</i>	2200	μF
<i>External fuse</i>	10	A
<i>Mode of operation</i>	Fixed Voltage Operation (with direct mode)	

- ¹⁾ This voltage is fixed during converter operation (except in direct mode). For operation near the maximum power point, this voltage can be fixed to roughly $n \times V_{MPP}$ where n is the number of modules in series. Usually $n \geq 3$ and ≤ 8 .
During direct mode the voltage can exceed 120V as the operating point could move down the IV curve.
- ²⁾ This limit is set by the maximum voltage across the capacitors and possibly by the power supply. In terms of modules this means eight ($\times 25V_{\infty}$) for 200V maximum.
- ³⁾ The minimum output voltage is a function of the array operating voltage and the duty ratio of the narrowest pulse that the PWM unit can generate.
The maximum output voltage is a function of the input voltage, the converter current, R_{on} and the load. If the load is well matched then the converter will go into direct mode at full irradiance. At that point the output voltage is close to the input voltage minus the voltage drop across the MOSFET's. At $R_{on} = 0.1\Omega$ and drain current of 14A the voltage drop is 1.4V. This is very small but can be higher if R_{on} increases with temperature.

3.4.2 Configuration of the converter in the PVP test system

The PV array was connected in parallel configuration. Therefore the input voltage was fixed to approximately 92V.

3.4.3 Control algorithm

The converter electronics is implemented purely with analog circuitry. For this reason there is no software. The control algorithm is part of the hardware.

The array voltage is the control variable. If the array voltage is less than the reference voltage then the voltage applied to the motor (converter voltage) is decreased. This results in a decrease in motor speed (motor voltage \propto motor speed). If the array voltage is larger than the reference voltage then the motor voltage is increased. The aim is to have a fixed array voltage and the motor is driven in such a way that this can be implemented.

The converter operation at start-up is linear which means that it does not employ any special routines to overcome the break-away torque of a positive displacement pump (the energy could be generated out of the DC capacitors). The converter is however capable to connect the array directly to the motor (MOSFET in a continuous on-state) once the converter receives sufficient current from the array to supply the pump torque requirements. When the converter enters the direct mode it leaves its fixed voltage operating point and moves towards a higher voltage operating point. This takes place whenever the irradiance increases beyond the threshold value (where the array current meets the required motor current).

3.4.4 Hardware

Figure 3.2 shows a basic block-diagram of the Miltek converter (linear current booster) in the PVP system. Some more detail is given below.

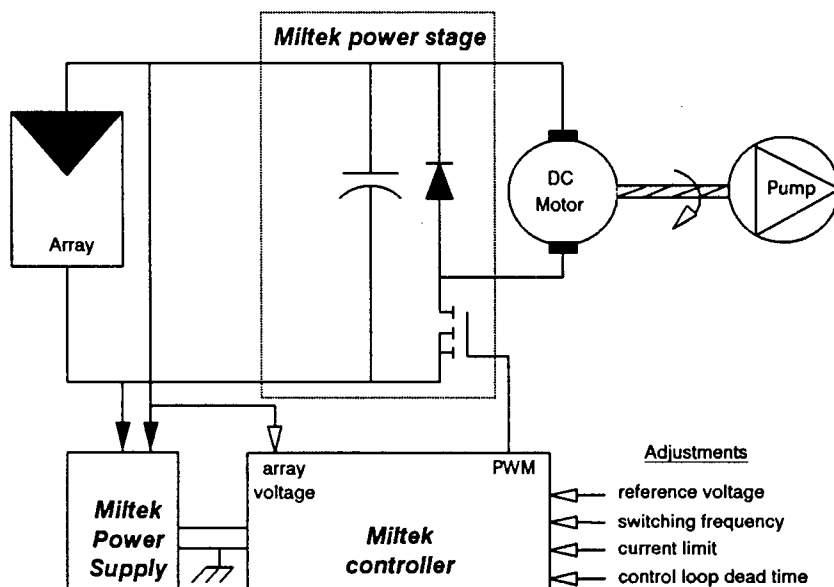


FIGURE 3.2 Basic block-diagram of the Miltek converter

Control and drive circuitry

The converter voltage is varied by pulsing the array voltage. This is achieved with the MOSFET's at a switching frequency of 2.5kHz (factory set). By changing the pulse-width the converter voltage can be increased or decreased. The duty ratio is directly proportional to the output voltage. The PWM signal is provided by the control circuit (implemented with PWM IC SG3524) to drive the MOSFET gates.

Due to superior performance of N-channel over P-channel MOSFET's, N-channel MOSFET's are used to switch the negative DC bus (see Figure 3.2). Therefore the positive array voltage terminal and the positive motor terminal are permanently connected.

Power device

The converter uses three IRF350 MOSFET's in parallel. The ratings of a single MOSFET are as follows:

- maximum drain-source voltage is 400V
- continuous drain current is 14A
- pulsed drain current is 25A
- on-state resistance is approximately 0.3Ω
- maximum power dissipation is 150W

As the three MOSFET's are connected in parallel the on-state resistance (0.3Ω) is reduced to 0.1Ω . This results in lower losses.

A free-wheeling, fast-recovery diode facilitates smooth operation by providing a path for the motor current when the MOSFET's are switched off.

Power supply

This would appear to be a linear voltage regulator. A 25W, $1.5k\Omega$ resistor reduces the array voltage which is fed into a transistor with a Zener clamp at its base. The output is then regulated to the required voltage.

Adjustments

Four potentiometers are provided for adjustments. Only P1 would ideally require tuning. The other three potentiometers are factory-set.

P1: A multi-turn pot to adjust the array reference voltage (FVO). It is usually set to $0.76 \times V_{oc}$ but might require adjustment at the installation site. For various array configurations the fixed voltage can be adjusted over a range of 45 to 150V.

P2: A single-turn pot to adjust the switching frequency. It is set to 2.5kHz.

P3: A single-turn pot to adjust the current limit which is factory-set to 15A.

P4: A single-turn pot to adjust the control loop dead time

3.4.5 Signal profile

The graph below shows the characteristic curves of a DC to DC converter. The converter current ramps up during the on-cycle of the converter voltage and down during the off-cycle. The converter output voltage (pulse height = array operating voltage) is controlled by controlling the width of the pulses (PWM). The fact that the current can flow during the voltage off-cycle is due to the free-wheeling diode.

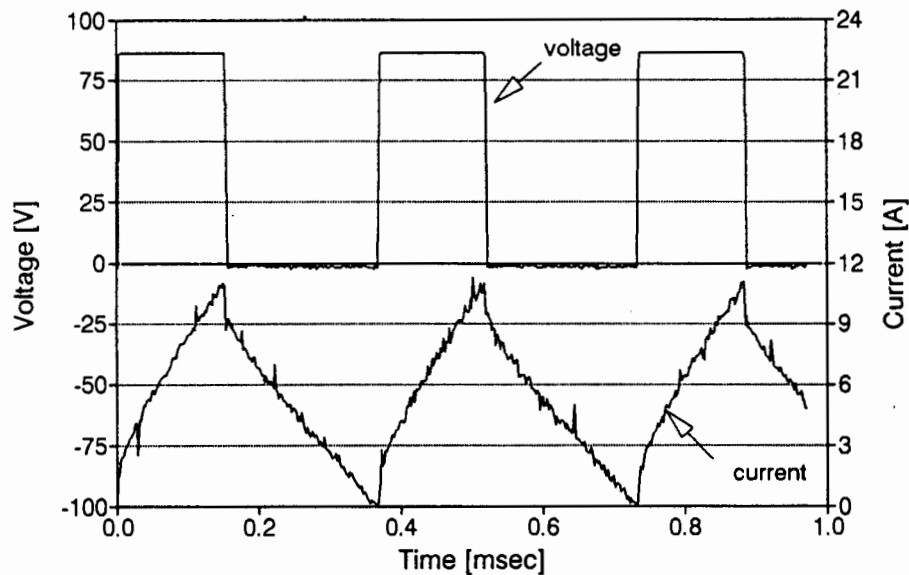


FIGURE 3.3 Characteristic converter output signals

The magnitude of the current is dependent on the load. If the load increases then the current will ramp up to a higher peak value during the on-cycle. There is no phase angle between these two signals which is to be expected from a DC system.

3.5 The Solvo three phase inverter

This three phase inverter was designed and developed by Günther Hirschmann in Germany. The inverter, being still in the prototype phase, does not have a model name/number. Solvo refers to the name of Mr Hirschmann's company and the inverter is referred to as the Solvo inverter.

3.5.1 Specifications

TABLE 3.5 Solvo inverter specifications

<i>Input</i>	<i>Value</i>	<i>Units</i>
<i>Voltage operating range</i>	120 → 190	V_{arr}
<i>Maximum open-circuit voltage¹⁾</i>	270	V_{arr}
<i>Maximum short-circuit current (80°C)</i>	IGBT: 15, FET: 13	A_{arr}
Output	MOSFET BSM 652 F -or- IGBT BSM 15 GD 100D	
<i>Line to line voltage (as programmed)</i>	$(0.184 \rightarrow 0.612) \times V_{arr}$	V_{rms}
<i>Maximum pulsed current at 80 °C</i>	IGBT: 30, FET: 52	A
<i>Maximum power</i>	1.8	kVA
<i>Frequency range (as programmed)</i>	7.6 → 84.7	Hz
<i>Switching frequency (as programmed)</i>	10.3 → 17.5	kHz
<i>Efficiency (estimated)</i>	~ 90	%
Other		
<i>DC input capacitance (350V)</i>	1100	μF
<i>DC side fuse</i>	4	A
<i>Array voltage readings in intervals of:</i>	10	ms
<i>Max. temperature of power module</i>	80	°C
<i>Mode of operation</i>	Fixed Voltage Operation	

¹⁾ This limit is set by the power supply maximum input voltage

3.5.2 Configuration of the inverter in the PVP test system

The PV array is connected in series configuration for this inverter. The input voltage is fixed approximately to 185V. The maximum line-to-line rms voltage is therefore 113V.

3.5.3 Hardware

The inverter consists of two printed circuit boards (PCB). The large PCB holds the DC capacitors, the gate drive circuitry and the power supply. The smaller PCB holds the microcomputer which consists of a microcontroller with its peripheral components. The power module is mounted on the inverter cast-aluminium casing for heat transfer. Both PCB's are fully visible from the top. A single-turn potentiometer for tuning the set-point of the array voltage is mounted on the microcomputer board and can be adjusted from the top (it has been moved to the drive circuit PCB in the more recent prototypes).

Figure 3.4 shows a basic block-diagram of the Solvo inverter. A detailed description follows below.

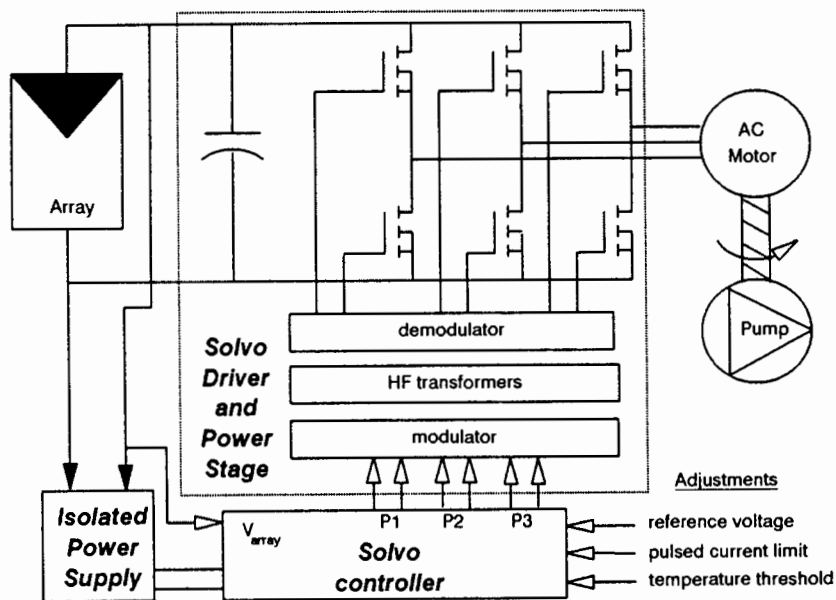


FIGURE 3.4 Basic block-diagram of the Solvo inverter

Microcomputer

The microcomputer consists of the SAB 8031 microcontroller, a dedicated PWM generation IC (SLE 4520), an 8-channel analog-to-digital converter (ADC 0808) that digitises the reference array voltage and a 4kbyte EPROM (2732A) containing the program code. In addition, there is a frequency divider (74LS161), a bus-driver (74HC673) and an IC with six open collector transistors (7406).

The salient features of the SAB 8031 are volatile 128×8 bit RAM, four programmable 8-bit I/O ports, two 16-bit programmable timer/counters, two external and three internal interrupt lines (2 timer and one serial interrupts) with two priority levels, a serial I/O line, an on-chip oscillator and clock circuits. The timers are essential as they can be used (and are) to process the PWM pulses at regular intervals. The controller runs at a clock frequency of 12MHz. This is the recommended clock speed for the 8031 processor and the SLE 4520 PWM IC combination.

The main features of the SLE 4520 are its capability to generate motor frequencies from zero to 3 kHz at switching frequencies of up to 23.4 kHz, to generate an almost unlimited range of waveforms with any phase relationship (smallest increment of 7.5°) and to adapt to different power stages due to a programmable dead time (dead time is essential to avoid bus shoot-through in case the upper and lower device have unintentional switch-on overlap periods). Changing the switching frequency in steps of one microsecond results in a virtually continuous transition from one motor frequency to another.

The SLE 4520 consists of the following functional blocks:

- A crystal oscillator input (a 12MHz crystal is used). The oscillator provides a buffered clock output that is used by the microcontroller.
- Two 4-bit registers for dead time and a divider ratio. The latter sets the clock frequency at which the SLE operates (2MHz). These registers only need to be written once, usually in the initialisation phase of the microcontroller.
- Three 8-bit phase registers which are continuously being written. The values that are received are latched into down-counters on reception of the transfer pulse (SYNC) from the 8031. The zero detector will be low (as the content of the down-counter is still non-zero) which will enable the counters. Therefore the pulse starts and ends when the zero detector goes high. The next pulse is sent when receiving the next transfer pulse.
- An output block, which receives the signals from the phase registers and generates their inverse (to drive six switching devices) and adds the programmed dead time to the pulses. The unit also blocks the output (all signals go high, that is the active switching state is Low) when receiving a High on the Inhibit or the Status line.
- An address decoder that decodes a three bit address from the 8031 to enable one of the five registers to receive data.

The 7406 IC with the open collector transistors has the following functions: Raising the PWM signal voltage to 12V, inverting the PWM signal (the SLE switches active low) and buffering the output of the SLE.

Protection from overheating is provided through a heat sensitive resistor which is mounted on the power module. At a tunable threshold level, a comparator switches to a low logic state activating an interrupt. This results in a state of in-operation until the power module has cooled down sufficiently.

Short circuit protection on the AC side is sensed on the DC side with a torroid-type transformer by measuring the current surge that occurs during a short-circuit. If the current exceeds a particular, adjustable threshold then a flip flop at the SLE 4520 is pulled high which will inhibit any further output. This circuit has a very fast response since it disables the SLE directly.

The inverter is overload protected by a three phase thermal switch. The data sheet for the AEG Mbs 25 protective motor switch is in appendix A1.4.1.

Drive circuit

The most central aspect of the drive circuitry is the provision of an isolated signal to the gates of the power switching devices (Hirschmann 1989a). This gate drive circuitry structure is based on high frequency (HF) transformers rather than opto-couplers. The reason for this choice is that at the time the inverter was developed the available range of opto-couplers did not fulfil the requirements (to be fast and to have a small coupling capacitance).

Besides the advantage of complete isolation between the driver stage and the power module, the gate voltage for the three upper FET's is derived via the HF transformers (see Figure 3.4).

HF transformers are usually sized for a particular frequency. Their design becomes non-trivial if the transformer has to transfer pulses of variable duty cycle (like a PWM signal). The PWM signal is therefore modulated with a frequency higher than the frequency of its narrowest pulse. The narrowest pulse here is $1\mu\text{s}$ (1MHz) and the carrier frequency is 3MHz.

The PWM signal and its inverse is modulated with the 3MHz carrier signal (obtained from the 12MHz clock frequency divided by four) by means of an AND and a NAND gate. The resulting signal is amplified with two push-pull stages and then coupled across the HF transformer. On the secondary side, the PWM signal is restored through the removal of the carrier signal by means of fast rectifier diodes leaving the envelope curve with a superimposed ripple. The 3MHz ripple on the PWM signal is smoothed by the high watt resistor in conjunction with the Gate-Source or Gate-Collector input capacitance of the MOSFET or the IGBT power module. Some additional capacitance (2.2nF or 4.7nF respectively) has been added to further reduce the magnitude of this ripple. The ripple has to be kept below a certain level to avoid ringing after switch-off. A 16V Zener diode limits the voltage spikes that occur when the MOSFET's or the IGBT's are switched on. A PNP transistor decreases the switch-off transition time.

MOSFET power module BSM 652 F

The three phase full-bridge SIMOPAC power module from Siemens consists of six MOSFET's in a single package. Each MOSFET is equipped with a Fast Recovery Epitaxial Diode which make these FET's particularly well suited to switch inductive loads. The MOSFET's are of the N-channel type. Some characteristics of the module are: drain-source voltage of 500V, continuous drain current of 13A (at 80°C), pulsed drain current of 52A (at 80°C), $R_{DS(on)}$ of 0.28 to 0.32 Ω (for $V_{GS} = 10V$), a turn-on time of 150ns and a turn-off time of 420ns.

IGBT power module BSM 15 GD 100D

The IGBT (Insulated Gate Bipolar Transistors) power module has become the replacement for the MOSFET module. It also contains six transistors and has the same physical dimensions as the MOSFET power module. The advantage is that the IGBT is more robust. It has a maximum collector-emitter voltage of 1000V, a continuous collector current of 15A (at 80°C) and a pulsed collector current of 30A (at 80°C). The on-resistance, R_{CE} , is typically 0.15 Ω , compared to 0.30 Ω for the MOSFET. One disadvantage is the switching characteristics which are slightly slower than those of the MOSFET's (turn-on time = 250 ns and turn-off time = 450ns). A data sheet is attached in appendix A1.4.2.

Power supply

A switched-mode power supply has been implemented in this inverter. The input voltage can have any value between 60 to 270V_{DC}. It basically consists of a control IC, a MOSFET and a transformer which consists of two sets of primary and secondary coils. The main primary coil couples the demanded power across and the other primary coil works as a feedback of the power demand on the secondary side. The secondary side coils provide two different voltages (5 and 15V). The control IC used is the TDA 4605. It 'observes' whether the voltage is constant, dropping or increasing and responds by switching the MOSFET accordingly. As a result the secondary side voltages remain almost constant. Rectification takes place on the secondary side of the transformer

3.5.4 Software

Program features

The inverter drives the motor through a maximum of 16 major gears if enough power is available (Gear 0 to Gear 15). Each major gear has 16 minor gears resulting in a maximum of 256 gears for the full frequency range. The present programs only utilise 11 major gears (Gear 5 to Gear 15) resulting in a resolution of 176 gears for the 85Hz frequency range. The inverter starts a run-up through Gear 0 to Gear 4 with an amplitude modulation index of zero. Therefore the resulting line-to-line voltage is zero. The inverter then starts the motor in Gear 5 with a frequency of 7.6Hz. The change in frequency within one major gear is not constant however (for example, if we say

that the full frequency range is equal to 80Hz and the number of major gears is equal to 10; then 80/10 gears is equal to 8Hz frequency-change per major gear which is not true). Typically the change in frequency in the lowest major gear is about 2Hz (Gear 5) and in the highest major gear about 13Hz (Gear 15). Therefore the frequency-changes within a minor gear at low major gears are about 0.12Hz (2/16) and increase to about 0.8Hz (13/16) at high major gears.

The Volts to Hertz relation can only be adapted to the frequency of the major gears and not the minor gears. Therefore the voltage increases are comparatively large (from about 30V to 110V in 11 steps). The shape of the V to Hz curve is stored as sine-weighted PWM values in look-up tables.

PWM generation

When switching at frequencies of up to 15kHz the number of different width pulses that would be required to generate a low frequency fundamental waveform is enormous (a 20 Hz signal would require 375 different width pulses). Such a signal cannot be generated with an 8-bit (= 128) word. Therefore pulses of equal width have to be repeated a fixed amount of times (anything between 1 to 255 times is possible). This repetition value is changed between major gears but remains the same within a major gear. The repetition rate for equal pulses is greater at lower fundamental frequency than at higher fundamental frequency, assuming that the switching frequency stays more or less constant throughout the range of major gears.

The above-mentioned point explains more clearly how the inverter manages to change its fundamental frequency between major gears. A decrease in fundamental frequency is achieved through increasing the number of times that each different pulse is repeated (the effect is almost as if the waveform is being stretched). The opposite is true for an increase in fundamental frequency. The 'jump' in frequency from one gear to another can be minimised by slightly adjusting the switching frequency.

Frequency changes within a minor gear are effected by changing the time-base for the timer interrupt. This is done in steps of 1 μ s. To clarify matters further, the Timer 0 of the 8031 is responsible for sending the three PWM values from the look-up table to the SLE 4520 phase registers. It is also responsible for sending the SYNC (transfer) pulse at regular intervals. These intervals are changed in steps of 1 μ s for a small frequency change in minor gears. Therefore the switching frequency changes by 16 μ s within each major gear. For example, if the switching frequency is equal to 12.5kHz (80 μ s) in the first minor gear then it will be 15.6kHz (64 μ s) in the sixteenth gear. It is up to the programmer and hardware limitations whether or not the next major gear has the same switching frequency spectrum.

The 8031 and the SLE 4520 combination is not able to operate at modulation indexes which are larger than one. Therefore over-modulation is not possible and the voltage of the array at the maximum power point should be high enough to achieve the rated voltage of the motor (at a modulation index of one, the rms voltage is equal to $0.612 \times$ array voltage (Mohan et al. 1989: 132)).

Algorithm

The array voltage (from the ADC at intervals of 10ms) is the only variable used by the control algorithm to determine whether or not the motor frequency should be increased or decreased. As this inverter runs in FVO mode, the software reference value is fixed. The algorithm attempts to remain as close as possible to this value and will increase the motor frequency (ie, increase the load) when the array voltage is larger than the reference value, and decrease the motor frequency when the array voltage is lower.

The algorithm continuously tests the state of the phase reversal switch which can be activated during inverter operation. Should the switch be activated, the algorithm will stop the motor by running down through all the gears. The inverter will start up again after about 5 seconds the motor turning in the opposite direction.

Over-heating is constantly monitored. When it occurs, the motor is switched off and the microcontroller waits until the temperature has decreased to below a particular threshold.

3.5.5 Signal profile

Figure 3.5 shows some of the characteristics previously mentioned. Graph (a) displays the line-to-line PWM pulses. The vertical lines divide the pulses into groups of four which have the same width. This is not easily visible on the graphs but the data values show this clearly. From the number of repeated pulses and the switching frequency (if there were enough resolution) one could calculate exactly in what major and minor gear the inverter is.

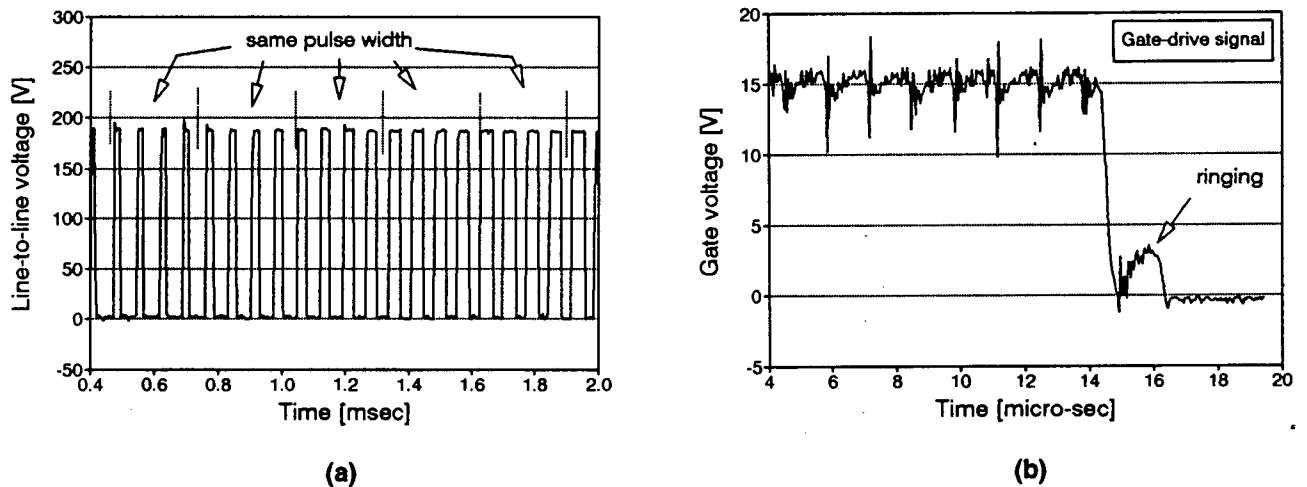


FIGURE 3.5 Some Solvo inverter characteristics

Graph (b) shows the ripple on the gate-drive signal which is the remains of the carrier frequency. A suitable gate-source capacitance has to be selected to reduce the ringing effect without increasing the switch-off time too much.

Figure 3.6 shows a typical current and voltage signal sent out by the inverter in conjunction with a three phase motor.

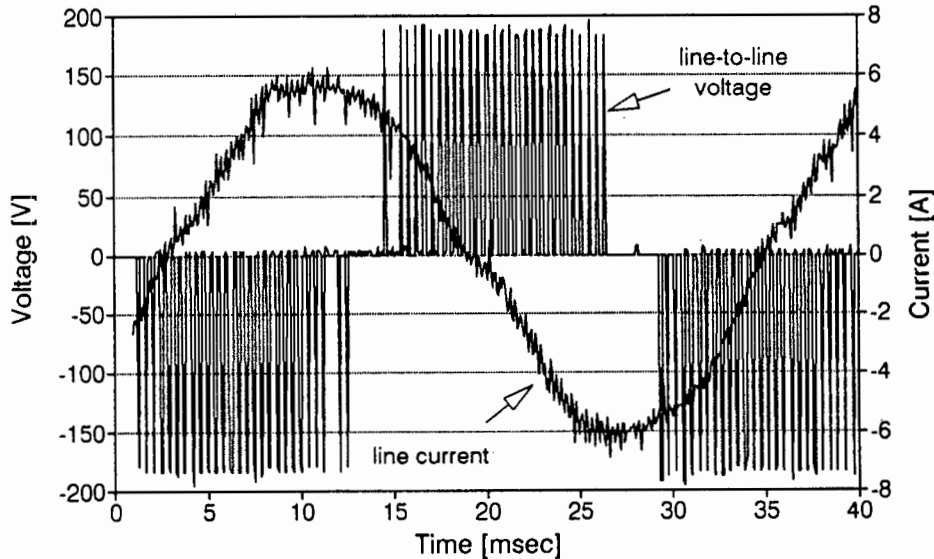


FIGURE 3.6 Current and voltage of the Solvo inverter

3.5.6 Future developments

The new opto-couplers from Toshiba, the TLP 251's, are fast enough to process the PWM signals at this high switching frequency range. They could therefore replace the AND and NAND gates, one of the amplifier stages and the HF transformers, thereby rendering the modulation of the PWM signal unnecessary. This would result in fewer parts, reduced costs and higher efficiency, the latter due to reduced switching losses resulting from shorter rise and fall times (rise time = 200ns and fall time = 100ns). Improved reliability is debatable.

The microcontroller will be replaced with the SAB 80517 which is an 8-bit single-chip microcontroller. It has an on-board phase comparator which would simplify PWM generation when compared to generating the PWM from the 8031 directly. This implementation would result in reduction of parts on the microcomputer board and should increase the mean time between failures.

3.6 The MLT three phase inverter

3.6.1 Specifications

This three phase inverter was designed by John Davies in partial fulfilment of an MSc degree in Engineering at the University of Cape Town. It was developed to the prototype stage at MLT Power Electronics in Cape Town. It is referred to as an MLT inverter in this dissertation.

TABLE 3.6 Specifications of the MLT inverter

<i>Input</i>	<i>Value</i>	<i>Units</i>
<i>Voltage operating range</i>	80 → 120	V_{arr}
<i>Maximum open-circuit voltage</i>	200	V_{arr}
<i>Maximum short-circuit current</i>	8	A_{arr}
<i>Output</i>	MOSFET IRFP 250	
<i>Line to line voltage (as programmed)</i>	$(0.184 \rightarrow 0.73) \times V_{arr}$	V_{rms}
<i>Maximum continuous current at 60 °C</i>	33	A_{rms}
<i>Maximum power</i>	0.5	kVA
<i>Frequency range</i>	3 → 65	Hz
<i>Switching frequency range</i>	0.8 → 6	kHz
<i>Efficiency over main operating range</i>	~ 85	%
<i>Other</i>		
<i>DC Capacitance (200V)</i>	2040	μF
<i>Array voltage readings in intervals ¹⁾</i>	80	ms
<i>Speed reading intervals ¹⁾</i>	2000	ms
<i>Max. temperature of power MOSFET's</i>	150	°C
<i>Modes of operation</i>	Fixed voltage operation Maximum speed tracking	

¹⁾ There is some uncertainty about these values. It is certain however that for every speed reading there were 25 array voltage readings

3.6.2 Configuration of the inverter in the PVP test system

The PV array was connected in parallel configuration for this inverter. The input voltage was adjusted to approximately 95V. The maximum line-to-line rms voltage was therefore 69.3 V at an array voltage of 95V.

3.6.3 Hardware

The inverter consists of two PCB's. One PCB holds the microcomputer which consists of a microcontroller with its peripheral components. The other PCB holds the gate drive circuitry. The power switching devices are soldered onto the gate drive PCB with

their backs mounted to a heat-sink which is attached to the inside of the inverter cast-aluminium casing. The power supply is also mounted on the heat sink. The DC capacitors are attached to the bottom of the drive circuit PCB by means of plastic straps. The microcomputer PCB is mounted above the gate drive circuit PCB. Two multi-turn potentiometers, of the front adjustment type, are mounted on the microcomputer PCB for tuning the array voltage and the motor speed reference voltages. A basic block-diagram is displayed in Figure 3.7 showing the functional blocks of the MLT inverter.

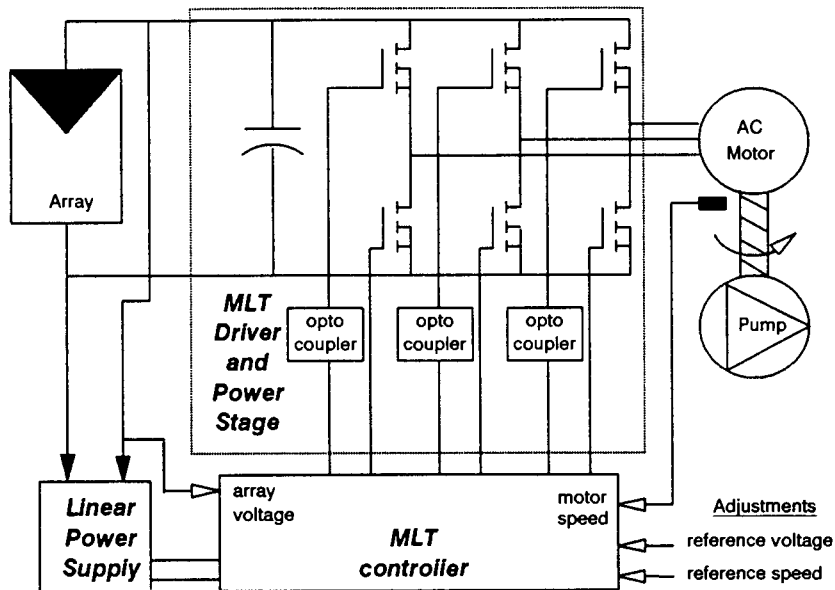


FIGURE 3.7 MLT inverter block-diagram

Microcomputer

The main components on the microcomputer board are the Intel 8031 microcontroller, one 8-channel ADC (ADC 0809) that converts the voltage references for the array and the motor speed, one 8kbyte EPROM (27C64) containing the program code and one 2k RAM chip (6116). A frequency divider in the form of four D-type flip-flops divides the clock frequency by 16 for the ADC. A few NAND gates are used for chip enabling, read, write and status signals etc. A frequency-to-voltage converter (LM331N) and an active LPF (CA7140) make up the speed reference circuit and an oscillator IC (LM555) forms part of the watchdog circuit.

The main features of the 8031 microcontroller were described earlier (subsection 3.5.3). The clock frequency provided to the 8031 is 10MHz. The controller is interfaced to ROM, RAM and the ADC. The PWM signals are latched from the 8031 through Port1 (P1.0 to P1.5) driving the opto-coupler LED's directly.

Speed monitoring is facilitated by means of a magnetic speed sensor. The LM331 is configured as a frequency-to-voltage converter. The signal is converted in the ADC and is read into the 8031 to act as a second level control variable.

The speed sensor signal is also fed to the watchdog circuitry (implemented with the LM555). The circuit provides the logic to the 8031 indicating whether or not the motor is running. If the motor is at standstill, the 8031 is reset with a high on its RST pin of longer than two machine cycles and performs a restart. If the speed sensing option is not used then the watchdog circuit can be supplied with one of the PWM output signals from the microcomputer board.

Drive circuit

This circuit structure is based on opto-couplers. All six PWM signals from the 8031 are coupled via 4N32 opto-couplers. This protects the microcontroller from possible voltage surges due to power device switching. The coupled signals are fed into DS0026 totem-pole drivers which are capable of supplying high current pulses and have, in addition, fast turn-on and turn-off times.

The circuit has a switching aid network to reduce turn-off time. It consists of an RCD snubber circuit made up of a resistor, a capacitor and a diode.

Power device

The power stage consists of six separate IRFP250 MOSFET's. These FET's are based on HEXFET technology which achieves very low on-state resistance (0.085Ω at a drain current of 33A and a temperature of probably 25°C ; the on-state resistance increases to 0.106Ω at a temperature of 60°C). It has superior diode recovery dv/dt capabilities. The internal diode also acts as a Zener diode. Further characteristics include an N-channel type FET and a maximum drain-source voltage of 200V which are suitable for fast switching and are easily paralleled.

Power Supply

The power supply for the microcomputer board uses a linear type voltage regulator. The array voltage is reduced via a 100Ω resistor (50W) and is clamped with a 24V Zener diode at the base of a BUX 84 transistor. The voltage is then sufficiently reduced so that it can be fed into a LM 7815 voltage regulator.

Power to opto-couplers and totem-pole drivers is provided without any isolation. To drive the positive DC bus FET's, the charge from a capacitor (charged in turn from the grounded FET's) is used to produce the power for the gate drive signal.

3.6.4 Software

Program features

There are 103 different fundamental frequencies with a range of 0Hz to 65Hz. The increase in frequency takes place in fixed increments of approximately 0.6Hz.

There are 19 different amplitudes which can be assigned to these frequencies to produce a sensible voltage to hertz (V/Hz) relation. The V/Hz relation was programmed as explained and deduced in the dissertation of Davies (1992), namely that the voltage is proportional to the square root of the frequency.

PWM generation

The PWM generation is based on sinusoidal modulation and harmonic elimination PWM (both discussed in subsection 2.5.2). Sinusoidal modulation is used from 3Hz to 50Hz and harmonic elimination from 50Hz to 65Hz. The harmonic elimination was programmed for eliminating the 5th, 7th, 11th and 13th harmonics.

The core of the program, which is implemented through Timer 1 of the 8031, has the task of:

- deciding whether the inverter is in start-up-mode or already operational;
- executing the control algorithm (that is deciding from the array voltage and motor speed whether to decrease, leave or increase the frequency to the motor);
- generating the PWM table (from ROM) for all six drive signals in external RAM;
- creating a new time-base for PWM signals by changing the values for Timer 0 which is equivalent to increasing or decreasing the fundamental frequency.

The retrieval of the PWM values from external RAM and the actual sequence for latching the PWM signals (through Port 1) for the six MOSFET's are the responsibilities of Timer 0.

The PWM ratios for a quarter cycle and the linearised frequency table are stored in ROM. An additional table serves as an address reference table. It has the same number of elements in it as the linearised frequency table but instead of values it contains addresses. The control algorithm decides on the next output frequency, generates the correct offset in register R7 and loads the start address of the table into the data-pointer (DPTR). Together they point to the memory location of the next frequency (which is a new value for Timer 0). The same offset can now be used to point to the location in the address reference table which contains the actual address of the PWM waveform. This makes assigning amplitudes to particular frequencies easy.

Algorithm

The inverter offers two modes of operation: Fixed Voltage Operation (FVO) and Maximum Speed Tracking (MST).

FVO: The implementation of this algorithm is explained earlier (subsection 3.5.4).

MST: This algorithm requires the array voltage to be tuned to within about $\pm 5V$ of the V_{MPP} . It uses the array voltage for coarse adjustments of the output frequency. Once 25 samples have been taken (every 80msec), the average speed of the last two readings is calculated. If that value is less than the previous average reading then the controller will decrease the array reference voltage if the latter had previously been increased and increase the array reference voltage if it had previously been decreased. If the average speed is higher than the previous average speed then the opposite will take place.

3.6.5 Signal profile

The graphs in Figure 3.8 show the two PWM methods employed by this inverter. The harmonic elimination PWM method looks very similar to overmodulated sinusoidal PWM but, in this case, the switching frequency is not constant.

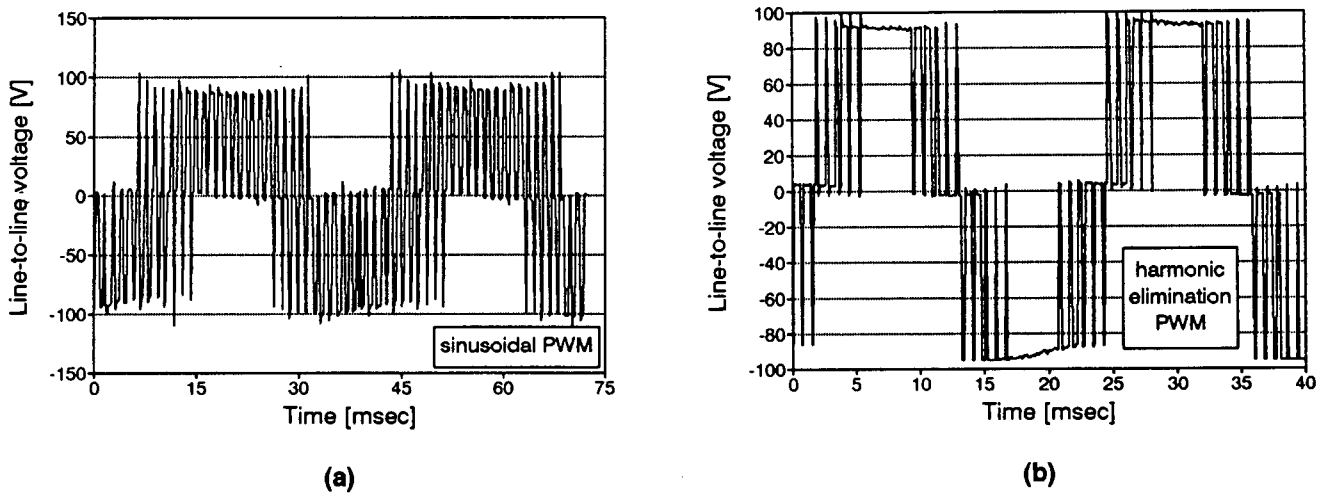


FIGURE 3.8 Sinusoidal and harmonic elimination PWM techniques used in the MLT inverter

Figure 3.6 shows the current and voltage (harmonic elimination PWM) waveform of the inverter when it drives a motor.

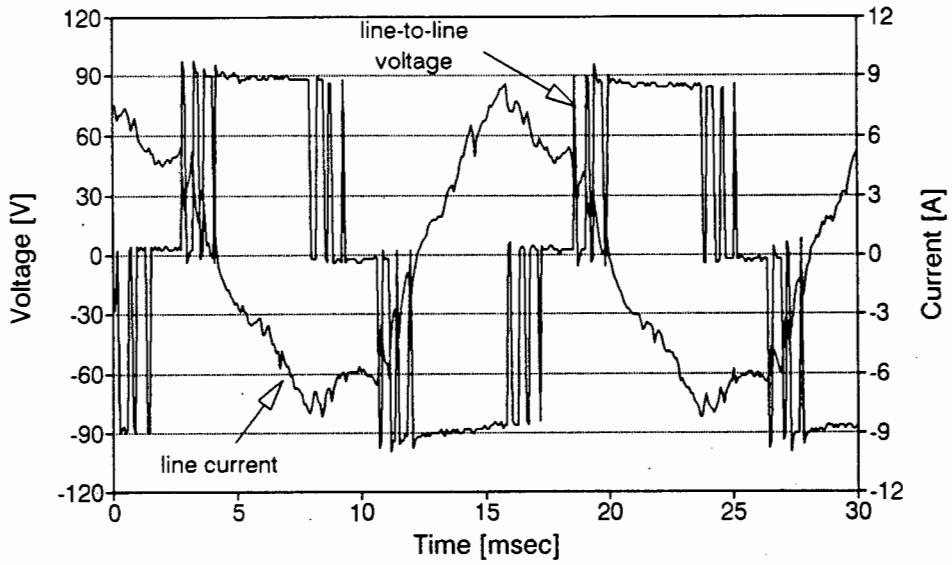


FIGURE 3.9 MLT inverter current and voltage

3.7 The motors

3.7.1 Specifications of the Baldor DC motor

The motor was a permanent magnet motor which was imported from the USA. The maintenance requirements (estimates) are a brush replacement every two years and a bearing replacement every ten tears. The motor frame size was 56C.

TABLE 3.7 Specifications for Baldor DC motor

<i>Input</i>	<i>Value</i>	<i>Units</i>
<i>Armature Voltage</i>	90	V
<i>Amps</i>	10	A
<i>Output</i>		
<i>Power</i>	750	W
<i>Speed</i>	1750	rpm
<i>Efficiency</i>	80	%

3.7.2 Specifications of the GEC induction motor

This motor has been designed by GEC (South Africa) with the specific aim of improving its efficiency to make it more competitive with motors in the PVP market. Its data sheet is attached in appendix A1.5.

TABLE 3.8 Specifications of GEC three phase induction motor

<i>Input</i>	<i>Value</i>	<i>Units</i>
<i>Voltage</i>	110	V_{rms}
<i>Amps (full load, 50Hz)</i>	6.4	A_{rms}
<i>Output</i>		
<i>Power</i>	750	W
<i>Speed</i>	1435	rpm
<i>Efficiency (full load)</i>	78	%

Unfortunately, GEC was unable to provide specifications for variable voltage and frequency due to lack of test facilities.

The material used in the motor was extruded aluminium and the motor frame was a DZ90L frame. The bearings have an estimated lifespan of ten years.

Chapter Four

RESEARCH QUESTIONS AND TEST METHODOLOGY

The first section in this chapter provides a set of research questions regarding the system components and the systems as a whole.

The second section lists the formulae that are used to calculate the power through the components and the complete system. From the equations it can be determined which variables have to be monitored by the data acquisition system to arrive at the answers to the research questions.

The third section gives a brief outline of the test procedures which were adopted to obtain the required data. The test details are all provided in appendix two.

The research questions and the test methodology were to some extent guided by Lasnier's et al. (1988) publication on testing PV pumping systems. The particular emphases, the range of information, and the methods of obtaining this information changed considerably during the preparation and course of the testing phase, to suit the systems under test. However this publication contributed substantially towards the basic approach to the testing phase.

4.1 Research questions

The research questions can be divided into four categories (similar to the PVP evaluation criteria in section 1.5). These are performance, technical and cost related questions as well as those regarding the improvements required to complete the final developmental stage of the prototype inverters.

Performance questions

- What are the component and system steady state performance characteristics over a range of input powers?
- How well do the components compare to their specifications (if these are available)?
- How well are components matched to each other?
- Do the PVP systems cope well with dynamic conditions?
- Does the electronic controller have a capable control algorithm? For example:
 - Can system failure be avoided under most conditions (excluding fatigue)?

- Does the controller employ a special start-up routine?
- Does the algorithm ever get 'lost'?
- Can the controller respond 'intelligently' if motor or pump failure occurs?

Other technical questions

- What are the system requirements (for example, maintenance, installation, spare parts and so on)?
- What are the system attributes (for example, modularity, protection, monitoring and so on)?

Cost inquiry

- What are the life cycle costs of the PVP systems over a twenty year project life?
- What are the unit water costs for each PVP system?

Assessment of required improvements

- What improvements have to be incorporated into the prototype inverters (in particular the Solvo inverter) which are absolutely essential for reliable operation?
- How can the prototype inverters be further optimised from an efficiency point of view?
- What features can be added to the inverter to make it more 'user-friendly'?

It is the performance evaluation in particular that required detailed testing. However this data could also be used for simulation purposes. The technical and costing aspects are evaluated in parts from literature and in parts from the collected data. The assessment of the type of improvements is based primarily on the result of the performance and technical evaluation.

The characterisation of the PVP components (or set thereof) over a range of operating conditions constitutes the monitoring of relevant signals which would yield the efficiency as a function of the input power. Both the efficiency and some signals are important for the evaluation of the performance. This requires answering questions about which parameters have to be monitored to enable a performance evaluation. This is done in the following section.

4.2 Choice of parameters

The equations by which the power out of each PVP component and the efficiency of each PVP component are calculated are listed in this section. The parameters which required monitoring were subsequently selected.

4.2.1 Equations

All equations represent steady state operating conditions and the measured parameters were DC quantities. Therefore all AC signals have been processed to relative DC quantities.

Array input

$$\begin{aligned} P_{\text{incident}} &= \text{plane of array irradiance} \times \text{array area} \\ &= G_{\text{POA}} \times A \quad \quad \quad [\text{W}] \end{aligned}$$

Array output

$$\begin{aligned} P_{\text{arr}} &= \text{array current} \times \text{array voltage} \\ &= I_{\text{arr}} \times V_{\text{arr}} \quad \quad \quad [\text{W}] \end{aligned}$$

Converter output

$$\begin{aligned} P_{\text{con}} &= \text{converter current} \times \text{converter voltage} \\ &= I_{\text{con}} \times V_{\text{con}} \quad \quad \quad [\text{W}] \end{aligned}$$

Inverter output

The power into a delta connected motor is:

$$\begin{aligned} P_{\text{inv}} &= 3 \times \text{phase current} \times \text{line-to-line voltage (instantaneous)} \\ &= 3 \times i_{\text{phase}} \times V_{\text{LL}} \quad \quad \quad [\text{W}] \end{aligned}$$

Since there is no easy access to the phase current (which is the current through one of the motor coils) the line current I_{line} was measured. The three phases were terminated with three resistors in a star formation. The line-to-neutral voltage was measured across one of the resistors. This measurement set-up is equivalent to measurements on a star connected motor.

$$P_{inv} = 3 \times \text{power factor} \times \text{rms line current} \times \text{line-to-neutral voltage}$$

$$= 3 \times \text{pf} \times I_{\text{line rms}} \times V_{\text{LN rms}} \quad [\text{W}]$$

Motor output

$$P_{mot} = \text{angular velocity} \times \text{torque}$$

$$= ((2 \times \pi) \div 60) \times S_{mot} \times T_{mot} \quad [\text{W}]$$

Pump output

$$P_{pump} = \text{water density} \times \text{gravitational acceleration} \times \text{flowrate} \times \text{static head}^1$$

$$= \rho \times g \times Q \times (H_s + H_{Pr}) \quad [\text{W}]$$

System efficiency

$$\eta_{sys} = 100 \times P_{pump} \div P_{incident} \quad [\%]$$

Subsystem efficiency

$$\eta_{subsys} = 100 \times P_{pump} \div P_{arr} \quad [\%]$$

Subset efficiency

$$\eta_{subset} = 100 \times P_{mot} \div P_{arr} \quad [\%]$$

Component efficiency

$$\eta_{comp} = 100 \times P_{out} \div P_{in} \quad [\%]$$

¹ The dynamic head losses are considered to be part of the pumping set. It is therefore included in the efficiency evaluation of the pumping set, the system and the subsystem efficiency.

4.2.2 Parameters

The parameters which were measured are listed in Table 4.1. These were used to conduct a complete steady state analysis of the PVP system.

The array voltage, the line-to-neutral voltage and the torque were also measured instantaneously to provide a more detailed analysis of the signal shape and consequently the controller performance.

TABLE 4.1 The parameters of the PVP system which were measured

PVP system parameters		
G_{POA}	-	plane of array irradiance
t_{mod}	-	module temperature
t_{amb}	-	ambient temperature
I_{arr}	-	array current
V_{arr}	-	array voltage
I_{con}	-	converter current
V_{con}	-	converter voltage
$I_{\text{line rms}}$	-	rms line current
$V_{\text{LN rms}}$	-	rms line-to-neutral voltage
P_{inv}	-	active inverter power
f_{fund}	-	fundamental frequency
T_{mot}	-	motor torque
S_{mot}	-	motor speed
Q	-	flowrate
H_s	-	static head
Pr	-	pressure

The array area (A), the water density (ρ) and the gravitational acceleration (g) as they are used in the equations in subsection 4.2.1 are constants.

4.3 Test methodology

This section contains a brief description of the preparations that took place before the testing commenced and gives a short summary of the tests that were conducted. Test details such as the purpose of the test, the procedure, the logger configuration etc are in appendix two.

Preparations prior to testing

The following is a list of tasks that were generally completed prior to a series of tests. Depending on the circumstances some of the tasks were omitted since they were performed for a previous test. The sequence in which these points are listed was also the sequence in which these tasks were completed.

- Signal calibration: The parameters which required calibration prior to each new test were recalibrated.
- Signal quality: The signal quality of all the signals was established by running the PVP system and the data acquisition as if a test series was in progress. This was most useful when logging in the presence of noise.
- Tuning: This was important since the tests were meant to evaluate the system when it was tuned to optimum performance. This consisted mainly of the array voltage set-point, the optimum pulley ratio between motor and discharge head and an optimum voltage to hertz relation (if applicable).
- Selection of best program: This was only applicable for the Solvo inverter where the necessary equipment was available for one week to generate a number of voltage to hertz relations.
- Estimation of the settling time for the system and the signals: Depending on the type of test a particular settling time was required to ensure that the system and the signal conditioning had settled.
- Commencement of testing

This method could have ensured that most tests were successful. However this was not always the case since there was a good part of learning on the author's side. For example, pre-test results were sometimes incorrectly interpreted or it was found at a later stage that the PVP system had not been optimally tuned at the time of testing.

Situations also arose where the acquired data for a component did not agree with the theoretical expectations. In such cases, the tests were usually repeated a few times to verify in particular the observed phenomena. Ultimately, sound explanations were found (this was the case for the array and the pump).

Outline of tests and methodology

The main test areas were the array, pump, controller and motor performance characteristics of all three systems, the system and subsystem performance, a component-matching evaluation, an algorithm survival test and the system response to dynamic conditions.

The acquisition of component performance data (or set thereof) was greatly simplified by the use of the tracking array. Through manipulating the orientation of the array, conditions could be changed according to the requirements, rather than waiting for suitable conditions to arise. This guaranteed less change in spectral conditions, less change in ambient and cell temperatures, shorter testing periods and less data to process (less data to be discarded).

The main test procedure consisted in moving the array from one setting to another. The data acquisition system was synchronised with a stopwatch so that the input changes to the system would occur at the correct time. Then a particular amount of time was allowed to pass to enable the system to settle.

Chapter Five

DATA ACQUISITION SYSTEM

The data acquisition systems that were used to collect data from the photovoltaic pumping systems are described here. The main data acquisition system consisted of transducers, signal conditioning, a data logger and a computer. These devices are discussed in the first section. This is followed by the method and means of calibration of the data acquisition system and the uncertainty evaluation for the acquired data. The chapter ends in a brief description of a secondary data acquisition system.

The primary data acquisition system was used for the main test period (over five month) and was capable of logging a number of steady state parameters simultaneously. The secondary data acquisition unit was available for one week. It was capable of sampling two signals at a time and had a very large bandwidth.

5.1 Description of the primary data acquisition system

The transducers and the data logger specifications are presented first. Then the signal conditioning circuitry requirements are discussed in view of the signal characteristics that had to be processed by the signal conditioning unit to meet the input requirements of the data logger.

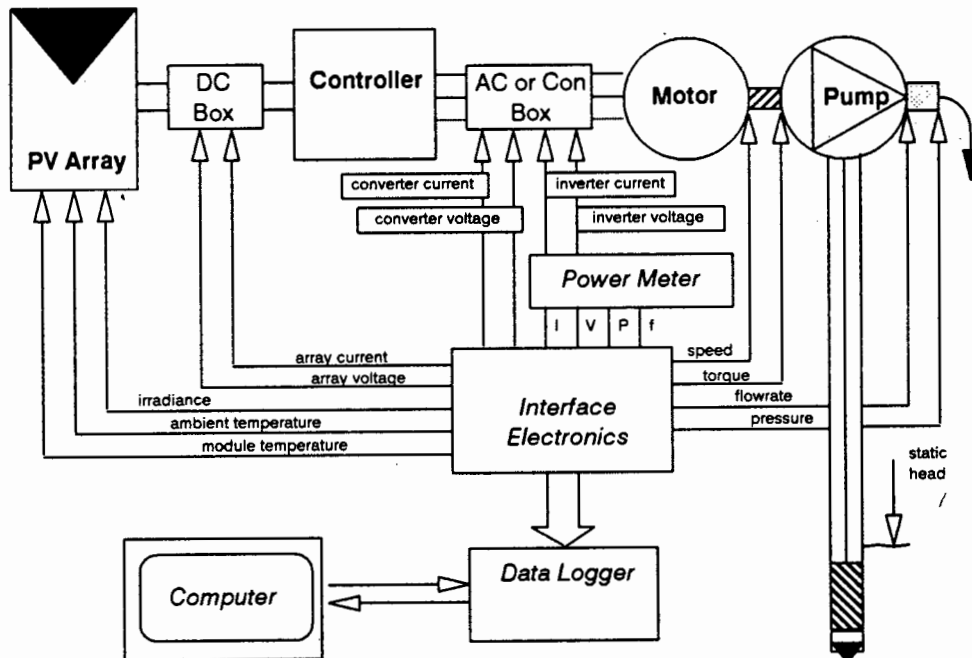


FIGURE 5.1 Block-diagram of the PVP and the primary data acquisition system

The layout of the ground and screen network with respect to the data acquisition system (DAS) and the photovoltaic pumping (PVP) system are also discussed. The section concludes with the limitations and the problems experienced with the primary data acquisition system.

A block-diagram in Figure 5.1 gives an overview of the PVP system. It shows the points at which measurements were taken.

The PVP system consisted of the photovoltaic array, the controller, the motor and the pump. The array output was measured in a box referred to as the DC Box. The controller output was measured in a box referred to as the Con Box (for the Miltek converter) or in a box referred to as the AC Box (for the Solvo and the MLT inverter). All the parameters are listed in Table 5.1 with their designated symbols.

The signal conditioning was implemented in two separate units, namely the interface and the power meter as can be seen in Figure 5.1. As the power meter was meant to be a stand-alone unit it was built in a separate housing with its own power supply. Its output signals are routed through the general interface to the data logger. The power meter converts the instantaneous inverter current and voltage to rms DC reference quantities. Through appropriate processing it generates a reference signal for the inverter frequency and the active power.

TABLE 5.1 Parameters logged by the primary data acquisition system

<i>Component</i>	<i>Parameter</i>	<i>Processed parameters</i>	<i>Symbol and type of signal ¹⁾</i>
<i>Array input</i>	solar irradiance ambient temperature module temperature		G_{POA} A t_{amb} A t_{mod} A
<i>Array output</i>	voltage current		V_{arr} A I_{arr} A
<i>Converter</i>	voltage current		V_{con} A I_{con} A
<i>Inverter</i>	line current line-to-neutral voltage	active power frequency	I_{line} A V_{LN} A $P_{invfact}$ A f_{fund} D
<i>Motor</i>	torque speed		T_{mot} A S_{mot} D
<i>Pump</i>	flowrate static head pressure head		Q A H_s n/a P_r A

¹⁾ 'A' stands for analog parameter and 'D' stands for a digital parameter.

5.1.1 Transducers

Most of the information on the transducers presented here is backed up with specification sheets in Appendix 3.1. The specification sheets for shunts and voltage dividers are not attached.

Irradiance

The solar irradiance was measured with a LI-COR pyranometer (LI-200SZ). It measures the global irradiance which is the combination of direct and diffuse irradiance. The pyranometer is a silicon photodiode sensor which generates a current proportional to the incident solar irradiance. The specification sheet is attached in appendix A3.1.1.

The LI-COR pyranometer was mounted in the plane of the array since a tracking array was used.

Temperature

The cell temperature and the ambient temperature were measured with precision centigrade temperature sensors, type LM35D. This is an integrated-circuit sensor which varies its output voltage linearly with the temperature (The data sheet is in appendix A3.1.2).

The sensor which measured the cell temperature was mounted on the back of a module and insulated with silicone sealant. This gave confidence that the measured temperature was a good estimate of the cell temperature. The ambient temperature was measured in the shade of the modules.

Array voltage and current

The array voltage was measured using a differential operational amplifier with a gain of less than unity.

The array current was measured with a non-inductive shunt (Dale, 0.1 Ω , 1%) in the positive lead (Miltek DC system) or the negative lead of the array in the case of the three phase system.

Converter voltage and current

The converter voltage and current were measured in the same way as the array voltage and current. The current shunt was in the positive lead of the converter output since the converter switches the negative lead to the motor while the positive lead remains physically connected.

Inverter current and voltage

The current was measured with a LEM probe (LA 50-P) which works on the principle of magnetic field compensation. The device is completely isolated and generates a current in the secondary winding which is a thousandth of the current on the primary side. The nominal current rating of this probe is 50A. Accuracy can be improved by having several primary turns if the magnitude of the actual current is considerably less than the nominal value. The power supply requirements are $\pm 15V$ (the data sheet is in appendix A3.1.3).

The inverter voltage was measured by terminating the three phases in a resistor star network. All three resistors had a value of 100k Ω . The line-to-neutral voltage was measured across one of the resistors.

The active (or average) power and the inverter frequency were determined as a result of current and voltage signal processing.

Motor torque and speed

The motor torque was measured using a loadcell (UBG 10kg) which contains a resistor bridge. It requires a 10V excitation voltage and the output is a differential voltage which rides on 5V_{DC} (the data sheet is in appendix A3.1.4).

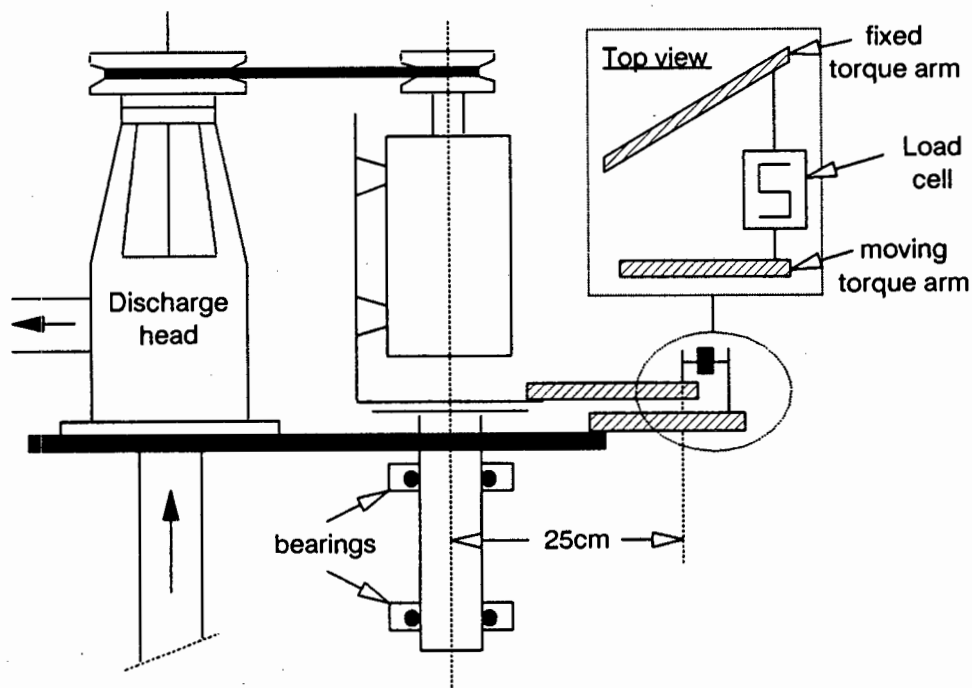


FIGURE 5.2 Torque measurement arrangement

The motor was installed in a vertical position adjacent to the pump discharge head assembly. It was fixed to the L-shaped metal structure as shown in Figure 5.2. The metal structure was fixed on top of a vertical shaft that was supported by two ball bearings. The vertical axis of the motor and the vertical axis of the shaft were made to coincide by moving the L-shaped structure in relation to the vertical shaft. If the two axes do not coincide then the measured torque will not be linear. In addition, the DC and the three phase motor did not have the same diameter which necessitated adjusting the L-shaped structure whenever systems (AC or DC) were changed.

The torque arm extended from the bottom of the L-shaped structure. Its length measured exactly 25cm from the dashed line to the loadcell connection point. It is essential that the torque arm is at 90° to the loadcell otherwise it introduces a cosine factor.

The motor speed was measured by means of an optical switch (Telefunken, TCST 2000) and flags that rotated through the light barrier. The accuracy can be improved by increasing the number of flags that rotate through the aperture (the data sheet is in appendix A3.1.5).

Pump flowrate and head

The flowrate was measured with a flow-meter (Weber flow-captor, Type 4113.30) or with a semi-positive rotary volume-flow meter (Kent, PSM, Size 3).

The flow-captor is non-intrusive and generates a current which is proportional to the speed of the water at the point measurement in the pipe. Through calibration or calculation the water speed can be related to the flowrate. The power supply requirements are 24V (the data sheet is in appendix A3.1.7).

The PSM volume-flow meter had to be read manually (the data sheet is in appendix A3.1.6).

The static head was measured with a probe that was lowered down the borehole. It sounded a beep if it touched the surface. The depth of the water level could be read from markings on the cable.

The pressure head beyond the discharge head assembly was measured using a Wika pressure transmitter (Model 891.14.525). The transducer generates a current proportional to the pressure and can be supplied with 10 to 30V_{DC} (the data sheet is in appendix A3.1.8).

5.1.2 Data logger

The data logger (MS-256) that was used is microprocessor controlled and has provision for eight digital and eight analog channels. Data is transferred to a computer via a serial cable compatible with RS 232 standards.

All eight analog channels and two of the digital channels were used. Since a maximum of eleven analog parameters could be logged per PVP system (see Table 5.1) a choice had to be made to log eight of the most relevant parameters for each particular test.

The data logger specifications are as follow (the data sheet is in appendix A3.1.9):

The shortest log-interval is one second which can be increased in one second steps to a maximum log-interval of twenty four hours.

An analog channel can either be configured as a voltage or as a current input. The voltage input ranges from 0V to 10V and the current input ranges from 0mA to 20mA. The analog to digital converter (ADC) converts data at a rate of 700 measurements/sec/channel. However, this data is only accessible over a minimum average period of one second. Each analog channel can be individually configured to store its values as follows:

Average value	(2 byte)
Average and minimum value	(4 byte)
Average and maximum value	(4 byte)
Average, minimum and maximum value	(6 byte)
Instantaneous value	(2 byte)

The average value gives the average of the signal during the log-interval while the minimum and maximum value that occurs in that interval can also be recorded. The instantaneous value is the value that the ADC converts at the end of the log-interval. The value in brackets shows the required memory-space per log-interval per channel.

The digital channels are transistor-transistor logic (TTL) compatible (pull-up resistor to 5V) and can be configured in gate or event mode where both require two bytes per channel per log-interval. The maximum counting frequency is 175Hz.

The DL can be supplied with either 12 V_{DC}, 30V_{AC} or 220 V_{AC}. This makes it suitable for laboratory conditions (220 V_{AC}) as well as field conditions (12 V_{DC} from a battery).

The DL communicates with a computer in a terminal mode which is very user-friendly and allows direct access to the data by offering a viewing function of either all the analog or all the digital channels or both. The data that is being down-loaded through the serial port to the computer can be converted with a data conversion program (DACO) to a Comma and delimited file format. That file format can be imported into a Quattro Pro spreadsheet for processing.

5.1.3 Signal interface

The signal interface was required to match the signals from the transducers to the signal input requirements of the data logger. This meant that the signal interface had to be able to handle the amplitude and bandwidth of the signal from the transducer and convert it to a DC reference signal with an amplitude between 0V and 10V. Those transducers that generate a DC current output could usually be directly connected to the data logger (except in the case of the line current measurement as the LEM probe output was not a DC signal).

The signals to be processed consisted of DC quantities with a small amplitude (G_{POA} & $t_{mod \& \text{amb}}$), a DC quantity with a large amplitude (V_{arr}), an AC quantity with large amplitude (V_{con}), AC quantities with a small amplitude (I_{arr} & I_{con}) and a low frequency AC quantity with a very small differential amplitude signal (T_{mot}). The flowrate and the pressure could be directly connected.

The bandwidth requirements would seem to be met by 100kHz since the highest switching frequency was 17.5kHz. It was not possible to measure whether any higher frequency harmonic components were part of the array current spectrum during Solvo system operation as no oscilloscope was available at the site and at that time. The power meter BW requirements were evaluated to 5MHz (see subsection 5.1.4). It was decided to rather use wide-band op-amps in case the array current had higher harmonics than the switching frequency.

In the case of small amplitude signals, op-amps with a small input offset voltage were chosen. This also minimised trimming requirements.

The motor torque parameter was the only one that required a differential op-amp with a high common-mode rejection ratio. The resistors and the op-amp were chosen accordingly.

All interface circuit diagrams and their descriptions are in appendix A3.2.

5.1.4 Power meter

The initial information that was available when the power meter was designed was that the inverter to be tested (the Solvo inverter) had a switching frequency of maximum 28kHz. The narrowest pulse was 1µsec. This is the worst case and it was decided to work from the basis of what BW would be required if one wanted to pass 99% of the energy in the pulse.

The calculations were performed on MathCAD using the discrete Fourier transform of a pulse. It was calculated that a BW of $72 \times 28\text{kHz} = 2\text{MHz}$ was required to pass 95% of that pulse. To pass 98% of the energy content required a BW of $180 \times 28\text{kHz} = 5\text{MHz}$. It was decided that a 5MHz BW was acceptable since this scenario is the worst case. Over one cycle the pulses change width since it is a PWM inverter. For instance, a pulse of 2µsec would already pass 99% of its energy content

through 5MHz and a pulse of 4 μ sec would pass 99.5% of its energy content through a 5MHz BW. Calculations showed that a PWM signal switching at 28kHz and with the narrowest pulse being 1 μ sec would pass 99.55% of its total energy content during a cycle (the energy content of each pulse was sine-weighted for this calculation).

The inverter output had to be isolated from the remaining signal conditioning unit since the output did not have a fixed ground reference. This is usually accomplished with isolators. It was decided to use a LEM current probe for the line current measurement. These devices are isolated from the primary current and are therefore referenced to the signal ground from which they receive their operating power. The inverter voltage could have been coupled across an isolator but the BW for the available isolators was 2kHz (AD202). Even the Burr-Brown (ISO122P) does not have a BW close to 5MHz. It was therefore decided to perform the RMS to DC conversion and the instantaneous multiplication on the floating side. The DC quantities of the rms voltage and the active power references were then coupled across with the AD202 isolators. This is shown in Figure 5.3.

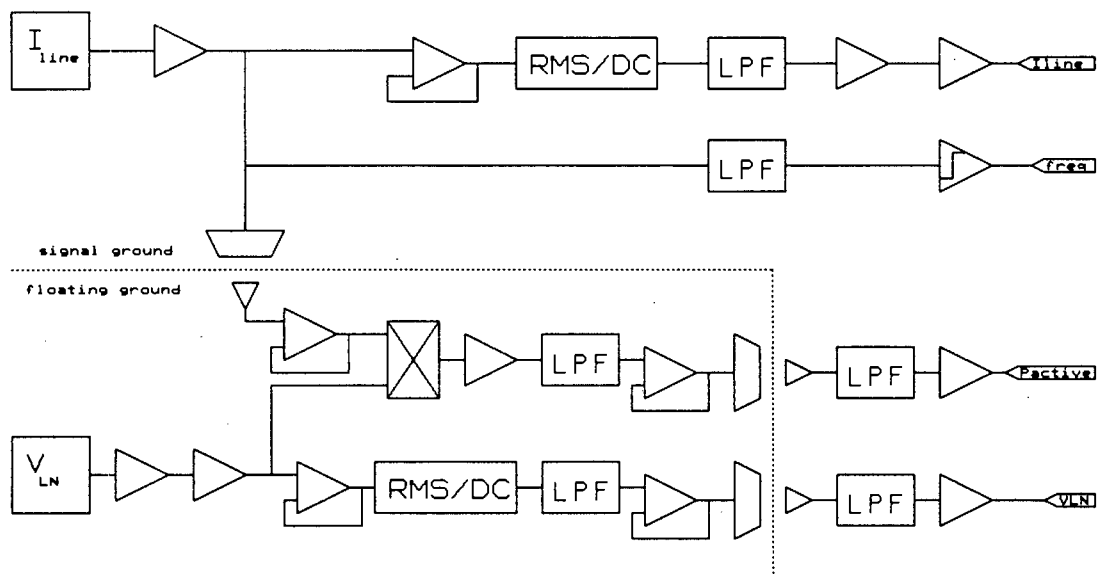


FIGURE 5.3 Block-diagram of the power meter circuitry

This method however required an additional isolator which was powered from the floating side and transfers the current reference signal across to the floating side to be used in the multiplication process.

The criteria for the component choice were therefore sufficient bandwidth, low offset op-amp's for small scale signals, high common-mode rejection ratio for the inverter voltage measurement and a high power supply rejection ratio to reject the ripple on the power supply voltage that was generated with DC to DC converters.

The full circuit diagrams and description of the power meter is in appendix A3.3.

5.1.5 Design procedure for signal processing units

The interface circuitry was not tested on the breadboard but was basically designed on paper and implemented on a 'solder breadboard'. This was then tested to establish proper operation.

The circuitry of the power meter was tested on the breadboard. Unfortunately some of the main components had not arrived and different components with the same function had to be used instead. The circuits were tested for basic performance requirements. Printed-circuit boards were designed on TangoPCB.

Both the interface circuit boards and the power meter circuit board were housed in a metal casing to offer some protection from noise that is usually present near switch-mode inverters and converters.

5.1.6 Layout of the primary data acquisition system

The layout of the data acquisition system with respect to the pumping system and ground becomes important when a noise source like a switch-mode inverter or converter is present.

Refer to Figure 5.1: All cables were screened to minimise interference and the interface-side of the screen was connected to the interface casing. The screen of all the cables on the transducer side was not connected to the PVP system except at one point which was in the AC/Con Box (depending on which system was tested). This was done to avoid earth-loops. The DC box casing, the controller casing, the AC/Con box casing and the motor casing were all connected to each other through using screened cable. The motor casing was at the same potential as the pump due to being installed on the same metal structure. The pump was earthed in the water of the borehole. This was used as the system earth.

The computer and the data logger were connected to the interface with screened cables. In this way, the interface casing which is central to the screen network is connected to the earth through the AC Box (via the power meter or straight in case of DC system) to the pump.

It was found that the signals were more stable when the system ground (the negative array lead in the three phase system or the positive lead in the DC system) was connected to the earth. This was done in the DC Box.

5.1.7 Limitations of the signal processing units

Interface circuitry

The interface circuitry may be limited in terms of range and bandwidth. The range can be altered through changing the magnitudes of the resistors. BW limitations could occur in array current and the converter current and voltage. BW requirements for these circuits are related to the switching frequency of the controller. The BW in the array current and converter current measurement is limited to 1MHz (LM627) at a gain of 15dB (the highest gain in the LM627 circuits) and in the converter voltage measurement to 2MHz at a gain of 6dB. I doubt that any harmonics in that frequency range will still carry any significant amount of energy even when the controller switches at 50kHz.

Power meter circuitry

The inverter current is limited to 50A and a BW of 100kHz. This will be sufficient for most applications. The circuitry is limited to a BW of 700kHz at unity gain. This can easily be upgraded but is not necessary if the transducer is limited to 100kHz. The RMS to DC converter is optimised for a particular bottom threshold frequency, here 50Hz. If signals of lower frequency are of importance then the RMS to DC converter should be reconfigured with larger capacitors to extend the measuring range to a lower fundamental frequency.

The inverter voltage has to be scaled down to $\pm 1V_{pp}$ which is achieved with the differential input resistors to the circuit. The BW is limited to 8MHz which is adequate for all applications. The RMS to DC converters may have to be reconfigured to less than 50Hz if lower frequencies are of more interest.

The active power is limited in terms of bandwidth on the current input side. The reference current is coupled across the isolator (AD202) which has a BW of 2kHz. This is acceptable for an inverter switching at high frequencies (more than 10kHz) but is unacceptable for inverters that switch at low frequencies (less than 5kHz). The reason for this are the low frequency harmonics (larger than 2kHz) that occur in the current spectrum of a low switching-frequency inverter. These still carry a substantial amount of energy and will be attenuated more and more as the frequency of the harmonics exceed 2kHz. The multiplication circuit itself has a BW limitation of 14MHz (LM627) at unity gain.

The frequency measurement will most probably only work for PWM inverters. A variable frequency square-wave inverter has low frequency harmonics that will result in multiple triggering of the Schmitt trigger. If the LPF is set for $f_{-3dB} = 80\text{Hz}$ and the fundamental frequency is tested at 25Hz then the third harmonic at 75Hz is passed through the filter without any attenuation. The hysteresis of the Schmitt trigger could be widened to not respond to the third harmonic but that requires testing.

As the circuit is designed now, the following has to hold true under PWM conditions for the frequency circuit to work correctly:

$$m_f > f_{\max} \div f_{\min}$$

where:

f_{\min} is the minimum fundamental frequency

f_{\max} is the maximum fundamental frequency

m_f is the switching frequency divided by the fundamental frequency

5.1.8 Problems encountered

Inverter voltage

The inverter voltage circuitry was tested in the laboratory and was found to work well. During the field tests however many problems were experienced with this voltage measurement. The interference of the inverter made the measurement of the rms voltage very uncertain. A change in layout of the ground and screen network would have a large impact on the signal. Consequently one did not know which signal level was correct.

The main observation was that the signal did not follow a voltage to hertz relation as it was programmed. The impression was that the signal would rise to a particular level, considerably exceeding the expected value and would remain there with slight variations as the inverter frequency increased. Many alterations to the power meter circuitry and the layout of the data acquisition system were implemented at the site. Some alterations improved the signal stability but the voltage measurement still seemed unreliable with a poor repeatability.

What was interesting was that the power measurement gave very reliable results that followed a more or less linear response with respect to frequency. Both signals had low frequency fluctuations which were due to the array voltage oscillations as will be discussed in section 7.3 and 8.3. However the data logger took the average of this signal which was acceptable for the power measurement but did not improve the voltage measurement reliability. Further investigation with an oscilloscope showed that the multiplier performed its function. The multiplication of the PWM signal and the current waveform could be observed at the output of the multiplier. This also showed the phase angle between the waveforms clearly. However, it was difficult to investigate the rms voltage processing since this all takes place within one IC. Tests were indicating that the measurement problems must have occurred into or after the rms-to-DC converter.

Possible reasons for the uncertain performance of the rms voltage measurement:

- array voltage oscillations

- interference and poor measurement system layout
- transferring floating signal from one PCB to another

The consequence of this is that the inverter voltage measurement is not relied on. It is therefore hardly discussed in the dissertation nor is the power factor evaluated (by $pf = P_{act} \div (I_{rms} \times V_{rms})$) due to the large uncertainty in the voltage measurement.

Flowrate measurement with the flow-captor

During the five months of field testing, a period of four weeks was unwillingly dedicated to the flow measurement with the flow-captor. The results were not satisfactory after that time and the use of the flow-captor as a measurement device was aborted.

The status of the measurement at the end of this time was that the signal was quite unstable and occasionally did not bear any proper resemblance to the motor speed. In addition it was found that an earlier calculation of the Reynolds number was wrong and that a flowrate range from 200l/h to 1000l/h with the pipe diameter used would actually go through a flow profile change. Since the flow-captor measures the speed of the water at a particular point in the pipe a change from laminar to turbulent flow results in a discontinuity of the flowrate versus motor speed relation (it is usually a linear relation). A change in pipe diameter was not feasible since it would have to be decreased to a very small diameter (17mm) making the installation of the flow-captor very difficult. Increasing the diameter was not considered since laminar flow is quite difficult to maintain.

The following was done to stabilise the flow-captor signal:

- removed all air from the flow-captor attachment fitting
- removed non-return valves from the system - unstable elements
- varied intrusion depth of flow-sensing unit
- put unit into top, middle and bottom position of the pipe
- stabilised flow with internal fins
- added silicon around the flow-sensing surface to smooth the flow
- built a lowpass filter to stabilise the signal

Some of these points helped to reduce the signal variations but in my opinion it was not sufficient. In addition the flowrate versus pump speed relation did not maintain a good level of repeatability. As a result of this performance measurements with this device were abandoned before any PV pump testing had commenced.

5.2 Calibration

Table 5.2 below lists the parameters and the devices with which they have been calibrated. The calibration was mostly performed with a Fluke 83 multimeter (data sheet is in appendix A3.5.2) which displayed the actual input to the signal conditioning and the computer terminal program showing the instantaneous input to the data logger. The two displays (Fluke and computer) could then be related to one another with the transfer functions (listed in appendix A3.2 and A3.3).

TABLE 5.2 Calibration of parameters

Parameter	Calibration device & process
<i>Irradiance (G_{POA})</i>	Fluke [μ A] in series with LI-COR output and calibration certificate (in appendix A3.5.1), namely (94μ A/1000W/m ²)
<i>Temperature ($t_{mod/amb}$)</i>	Fluke [mV] and LM35D specification sheet namely 10mV/°C
<i>Array voltage (V_{arr})</i>	Fluke [V_{DC}] and array operation
<i>Array current (I_{arr})</i>	Fluke [A_{DC}] and array operation
<i>Converter voltage (V_{con})</i>	Fluke [V_{DC}] and actual converter operation
<i>Converter current (I_{con})</i>	Fluke [A_{DC}] and actual converter operation
<i>Inverter voltage (V_{LL})</i>	Soar [V_{rms}] (in appendix A3.5.3) and a square-wave signal input to the circuit from a signal generator and a sine-wave input from the electricity grid
<i>Inverter current (I_{line})</i>	Fluke [A_{AC}] and a sine-wave input to the LEM probe from the electricity grid
<i>Inverter power (P_{inv})</i>	Fluke [A_{AC}] and Soar [V_{rms}] with a 220V sine-wave (grid electricity) applied to a resistor
<i>Inverter frequency (f_{fund})</i>	Fluke [Hz] and a sine-wave signal input to the current circuit
<i>Motor torque (T_{mot})</i>	Precision spring and Fluke [V: Min / Max / Mean mode]. Spring calibration with known weights.
<i>Motor speed (S_{mot})</i>	Either correct or wrong. The speed was calculated from recorded data. The measurement was however confirmed with a hand-held tachometer.
<i>Flowrate (Q)</i>	Bucket and S_{mot}

Notes on the calibration of specific parameters:

V_{LL} : There was no way in which the Soar true RMS meter could be used to calibrate the line-to-line PWM voltage out of one of the inverters due to low frequency oscillations on V_{LL} as explained in section 7.3 and 8.3. In addition, the Soar multimeter does not have the bandwidth. For that reason a square-wave (20Hz to 2kHz) and a sine-wave were used for this calibration.

I_{line} : An ordinary sine-wave is acceptable here since that resembles the real conditions well enough. The inverter current will have higher harmonics which would all be converted by the RMS to DC converter.

P_{act} : Due to lack of equipment (only one signal generator and no commercial multiplier) this parameter had to be calibrated with an in phase sine-wave current and sine-wave voltage signal. By varying the load (the number of bulbs) P_{active} could be calibrated over a range of operating signals. In fact the voltage did not receive either a square-wave or a PWM signal for the power calibration.

T_{mot} : The loadcell was calibrated while being installed in the system. Initially three known weights were used which were tied to the torque arm exactly opposite the loadcell (same horizontal and vertical plane) and suspended over a 'frictionless' wheel to meet gravity. The main problem was the frictionless wheel. Calibrations were not repeatable. This led to calibration of the loadcell with a spring which was first calibrated on the three weights. It maintained its calibration well through out the tests. The loadcell however had to be recalibrated every time there was a change in the system. What could be observed was that the gradient of a few sets of samples (one set usually consisted of six samples: 0.25, 0.5, 0.75, 1.0, 1.25 and 1.5kg) was very constant but that variations took place in the offset if the calibration is thought of as being: $T = a \times \text{mass} + C$. The regression fit for a set of samples always had a very good R^2 .

Q: A calibrated one litre container was used to calibrate a bucket at 5litres, 10litres and 15litres. The bucket was used to calibrate the Kent volume-flow meter. The flowrate was related to the motor speed by recording S_{mot} and the difference volume-flow through the Kent meter in a particular time-interval. This was repeated for a range of motor speeds and under steady state conditions.

All calibrations took place under steady state conditions. It was usually attempted to take calibration samples at a few operating points. This gave a better average coefficient for the transfer function or the degree of output adjustment required at the potentiometer but would also reveal non-linearities in the data acquisition system.

5.3 Uncertainty in the measured data

The uncertainty analysis of the acquired data for each parameter is performed in appendix A3.6. The result of the analysis is listed in Table 5.3 below. The uncertainty is stated in absolute and in relative terms. The absolute uncertainty is equivalent to the overall uncertainty and the relative uncertainty is a subset of the absolute uncertainty and excludes errors that have not changed during the test period. The relative uncertainty of a parameter for example, if only calibrated once during the tests, will not include the calibration uncertainty.

The relative uncertainty is significant when comparing any of the three systems to one another. When the systems under test are being compared to different PVP systems other than the ones tested then the absolute uncertainty must be used.

The uncertainty in the efficiency of the components (or a set thereof) has been calculated and is frequently quoted in chapters six, seven, eight and nine. A calculation example is given in appendix A3.7 showing how the uncertainties are derived.

TABLE 5.3 The absolute and relative uncertainties in the logged parameters

Parameter	Absolute uncertainty [%]	Relative uncertainty [%]	of full-scale reading
G_{POA}	8.7	5.5	1250 W/m ²
t_{amb}	5.5	2.3	40°C
t_{mod}	7.6	1.5	60°C
V_{arr}	1.1	0.3	180V
I_{arr}	1.2	1.1	3A
V_{con}	1.1	0.3	90V
I_{con}	1.3	1.0	6A
I_{line}	3.3	3.0	5A _{line}
f_{fund}	0.4	0.4	50Hz
V_{LL}	5.8	2.8	110V _{LL}
P_{act}	6.9	4.4	500W
T_{mot}	3.6	3.4	2N.m
S_{mot}	< 0.8	< 0.8	worst case
Q	6.1	2.2	0.2 → 1m ³ /h
H_s	0.2	0.2	75m

The largest uncertainty was experienced at the array input and at the inverter output, the latter in terms of the line-to-line voltage and the active power measurement. The high uncertainty in the line-to-line voltage measurement was mainly due to the lack of a calibration device. This of course will also affect the power measurement.

5.4 The secondary data acquisition unit

The primary data acquisition system was able to log only steady state signals and so little was known about the AC signal characteristics of some of the parameters. Through courtesy of Solar Age Namibia a newly acquired, hand-held, battery-operated digital storage scope (Phillips PM97) was made available for a one week period at the end of the five months test period.

The PM97 storage scope has a 3dB BW of 50MHz and can sample two signal simultaneously with 512 samples each. The most useful feature of this device is the capability to transmit its data through an optical link to the RS 232 port of the computer. Sampled data could therefore be down-loaded immediately.

This device made it possible to take the evaluation of the prototype inverters to another level of detail since this unit captured data which revealed undesired characteristics of the inverter operation that could not have been observed with the primary data acquisition system. The test methodology in chapter four outlines for which tests the scope was used.

The specifications of the PM97 can be found in appendix A3.8.

Chapter Six

ARRAY, PUMP AND MILTEK SYSTEM PERFORMANCE

This chapter deals with the performance of the array, the pump and the Miltek subset, system and subsystem performance. The Miltek system (or set thereof) serves as a basis of comparison for the prototype three phase inverter systems.

The Miltek system used the same array and pump that were used by the prototype inverters. Therefore only the subset components (electronic controller and motor) were exchanged between systems.

The derivation of the absolute and relative uncertainty in the acquired data is presented in appendix A3.6. The derivation of the stated uncertainty in the efficiency data is given by an example in appendix A3.7. The uncertainty is stated as a plus-minus percentage of a full-scale reading.

6.1 Array performance evaluation

The main evaluation criteria are the array characteristics (are the characteristics similar to the theoretical characteristics and are they reasonably close to the specifications) and the variations in maximum power due to variations in module cell temperature. The latter aspect is analysed in terms of fixed voltage operation (FVO) compared to maximum power point tracking (MPPT).

6.1.1 Array characteristics

The array was tested under various conditions. The input variables were the solar irradiance and the module temperature (measured on the back-surface of the module, covered in non-heat-conductive insulation). The module temperature was used as a reference for the module cell temperature. Array tests were conducted at solar irradiance levels of 200, 400, 600, 800, 1000 and 1100W/m² and module temperatures of 25, 35, 47 and 55°C. Unfortunately, a shade fell on the array at irradiance levels of 200 and 400W/m² due to the aluminium wings that form part of the array tracking mechanism. This was realised too late. The data at these irradiance levels are therefore omitted as the power output is reduced due to the shading. The effect that the shading had on the current-voltage (IV) curve of the array will be shown later.

The larger part of the tests were conducted with the array in series configuration. The reason for this was the strain on the loads due to twice the current being produced in the parallel configuration and due to the method of testing which used AC switches to switch the loads. The sparking was obviously more severe in parallel configuration.

Figure 6.1 shows the IV output characteristics (Graph a) and the deduced power curve

(Graph b) at a module temperature of 47°C. The array is in the series configuration.

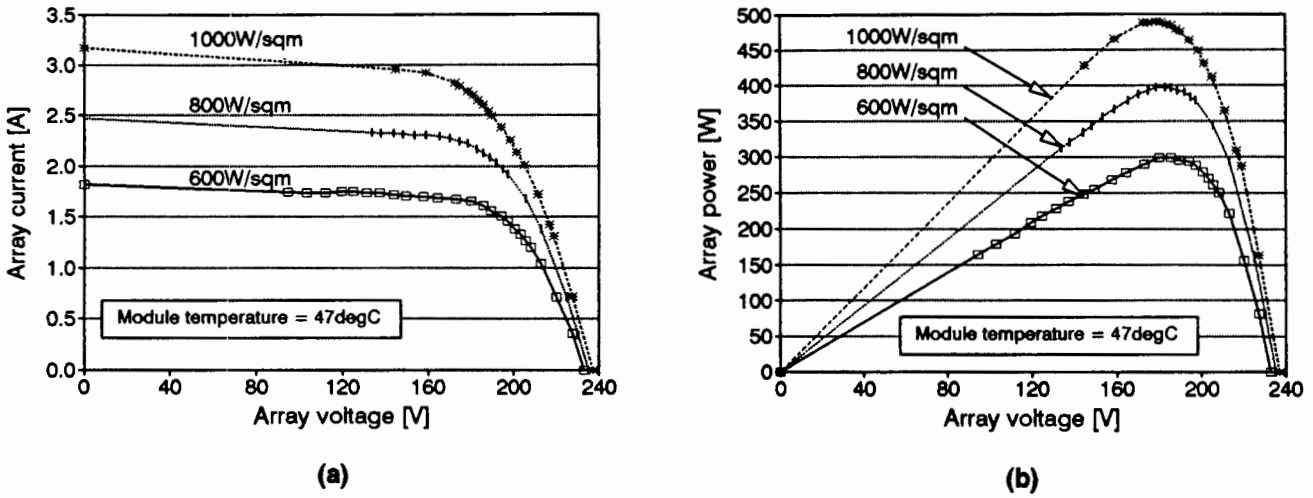


FIGURE 6.1 Array characteristics as a function of irradiance: (a) IV curves; (b) power curves

The shape of the IV curves is as expected. The short circuit current and the power out of the array increase proportionally in the region from 600W/m² to 1000W/m².

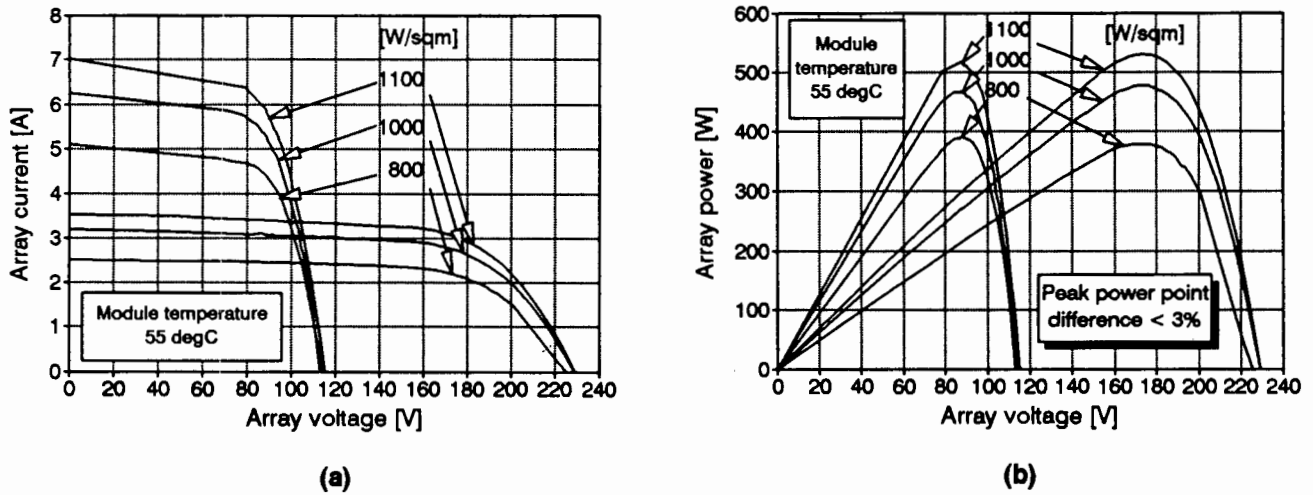


FIGURE 6.2 IV and power curves for the series and parallel configured array

Figure 6.2 shows the IV (Graph a) and power curves (Graph b) for the parallel and the series array configurations. The difference in peak power of the series and parallel array configuration is less than 3%. That is acceptable, since the relative uncertainty of the solar irradiance data is $\pm 5\%$. If the IV curves are superimposed on each other (through appropriate scaling, for instance converting parallel to series: $I_{\text{parallel}} = 2 \times I_{\text{series}}$ and $V_{\text{parallel}} = \frac{1}{2} \times V_{\text{series}}$) the shapes coincide well with the largest deviation being 3.1%.

The behaviour of the array characteristics under constant solar irradiance but with

variable module temperature is displayed in Figure 6.3.

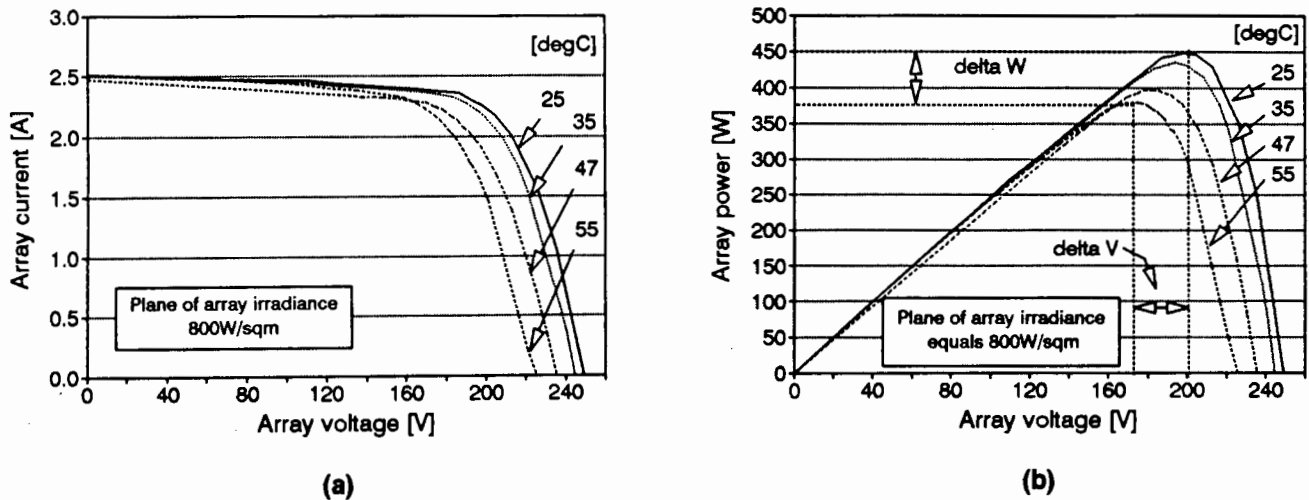


FIGURE 6.3 Array temperature characteristics: (a) IV curves; (b) power curves

The increase in module temperature results in a decrease of open circuit voltage and hence a decrease in the maximum power point (MPP) voltage. The drop in open circuit voltage is generally slightly larger than the drop in MPP voltage. This is not visible in the graph and the data also does not indicate this relationship. The test conditions may have changed during the test. The decrease in MPP voltage can be seen in the adjacent graph where delta V represents the range in which the MPP voltage drops due to the temperature increase. Delta W represents the consequent drop in MP. Subsection 6.1.3 discusses this in detail.

I conclude that the array behaves as expected. Now it remains to be seen how closely the key characteristics of the array agree with the specifications in order to meet the first criterion specified at the beginning of this section.

6.1.2 Array efficiency compared to the specifications

The comparison between the acquired data and the specifications is based on the efficiency at MPP. The data from the specifications are processed to the level of the acquired data by a method described in appendix A4.

The graphs in Figure 6.4 show the measured and the specified efficiency at maximum power as a function of the solar irradiance. The measured efficiencies maintain a relatively flat relation to the irradiance over half the operating conditions (600W/m² to 1000/1100W/m²). The efficiency graphs at 25, 35, 47 and 55°C are relatively flat. The specified efficiency on the other hand has a logarithmic relation to irradiance. Over the range of 200W/m² to 1100W/m² the efficiency is reduced by about one percent at constant cell temperature. As low irradiance levels are generally received by the array at an angle and not due to obstructions like clouds or dust in the air, I would expect the efficiency to decrease more rapidly due to reflections on the glass covering the PV

cells. Nevertheless, the specifications as they are represented in Figure 6.4 will do, since the comparison only takes place for irradiance levels of 600W/m² and higher.

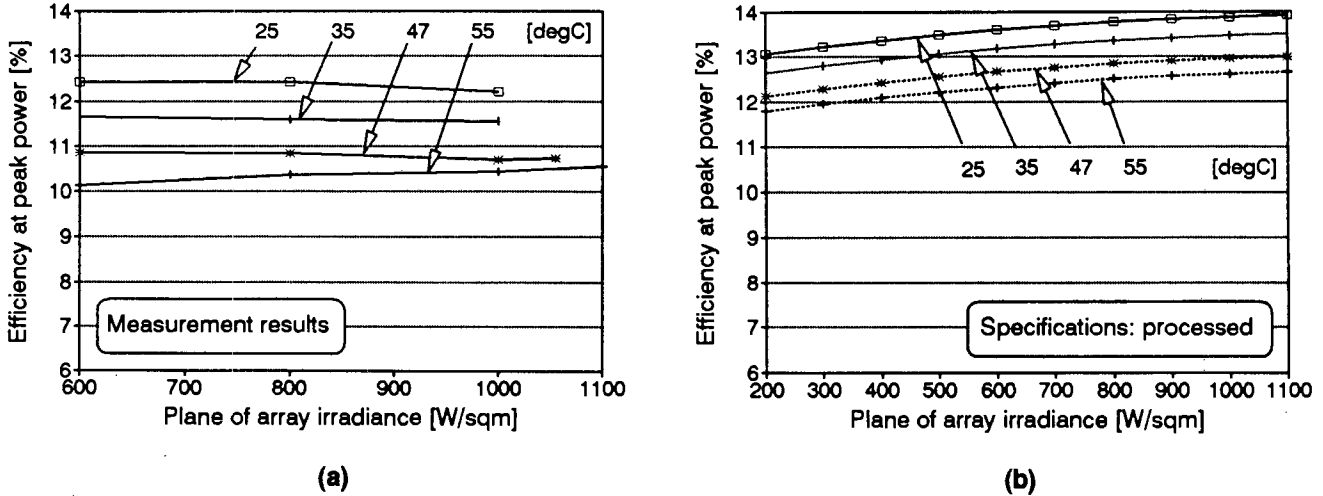


FIGURE 6.4 (a) Measured array characteristics; (b) Specifications

The comparison between the specifications and the measured results is shown in Figure 6.5. The graph shows the percentage difference in efficiency between the specifications and the measurements at 600, 800 and 1000W/m² for module temperatures of 25, 35, 47 and 55°C. The difference at 1000W/m², 25°C is 12%.

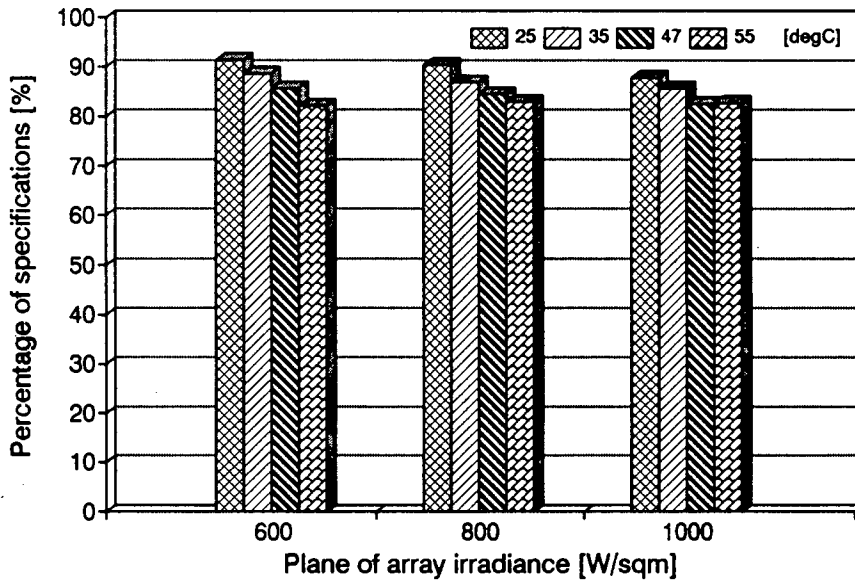


FIGURE 6.5 The measured results as a percentage of the specifications

Two trends can be observed. The differences between the specifications and the measurements increase with:

- a) increasing module/cell temperature and

b) increasing solar irradiance

where the effect of a) is larger than the effect b).

Possible reasons for these differences: There will certainly be some mismatch losses between the individual modules as a result of differently shaped IV curves and differing values of open-circuit voltage and short-circuit current. As specified in chapter three (System description) the array contains modules from three different production generations. If these mismatch losses are as high as 5% then the array performance would already be within the $\pm 10\%$ of the specifications for lower cell temperatures. Another reason could be the uncertainty in the array efficiency data which is:

$$\begin{aligned} U_{\text{abs}} (\eta_{\text{arr}})_{1000\text{W/sqm}} &= 13.4\% \\ U_{\text{abs}} (\eta_{\text{arr}})_{600\text{W/sqm}} &= 19.8\% \end{aligned}$$

The uncertainty is very large due to errors like calibration, drift, spectral variations and uncertainty in the calibration of the module temperature. But since the graph exhibits definite trends, it is more the fixed error that carries weight (the calibration and the long term drift error). Most of the tests were conducted within a few days and it was felt that spectral conditions were stable (that is clear blue Namibian sky, no wind, no dust). The array performance could therefore be well within the specifications considering the uncertainty in the data but it could just as well be way outside the specifications.

Note the increase in percentage compared to the specifications at 1000W/m^2 for 47°C and 55°C . I would consider this to be due to an error or errors in the measurements or even an unnoticed change in conditions.

I conclude that the array may well have performed within the specifications at 25°C cell temperature. The temperature coefficients seem to be higher though than specified, unless the increase in cell temperature results in altered IV shapes causing larger mismatch losses or the temperature sensor might have under-measured.

6.1.3 Fixed voltage operation in relation to the MPP

The PVP systems under test either employ Fixed Voltage Operation (FVO) or Maximum Speed Tracking (MST) as a mode of operation on the array IV curve. MST is ultimately a form of MPPT if correctly implemented. It is of interest to establish the losses in array power for this particular array due to operation at a fixed voltage while the cell temperature and the level of irradiance vary during the course of a day.

Figure 6.6 shows how the MPP decreases due to changes in cell temperature and how the MPP moves with respect to the array voltage as a result of changes in cell temperature and solar irradiance levels.

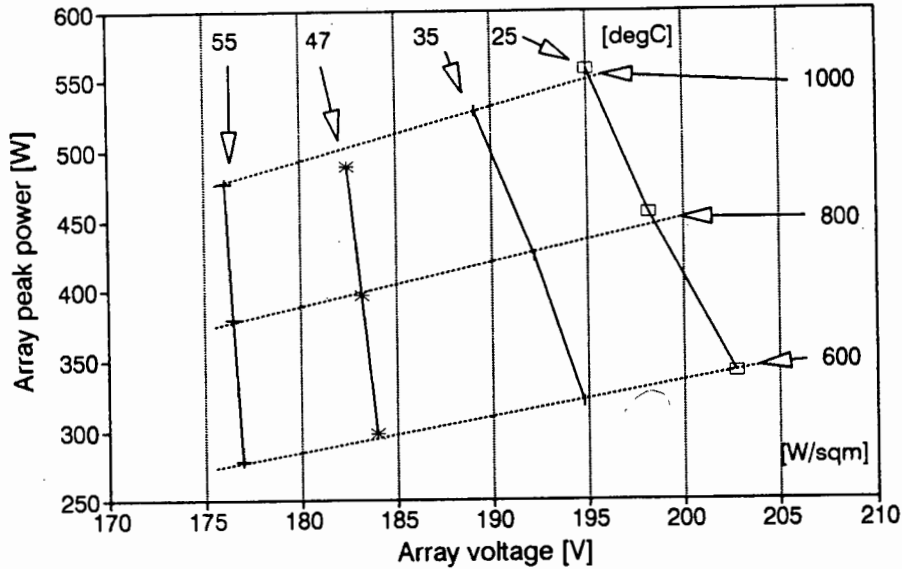


FIGURE 6.6 Array peak power as a function of the array voltage for different irradiance levels and module temperatures

Figure 6.7 and Figure 6.8 show how the power relative to the MPP decreases under certain conditions.

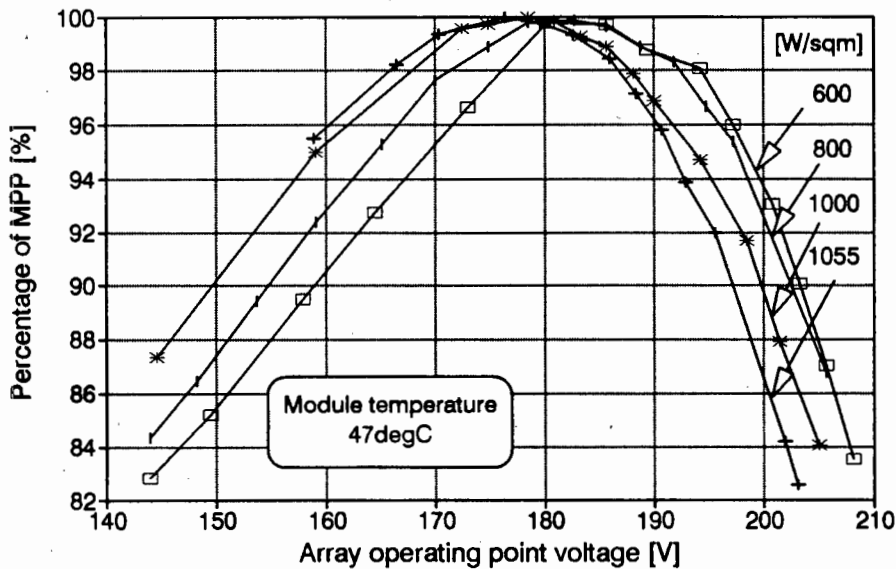


FIGURE 6.7 Percentage decrease in array output power relative to the MPP as a function of irradiance

Figure 6.7 displays the variations as a function of irradiance while the cell temperature is constant at 47°C. The graph shows that the loss in power is relatively small due to variations in solar irradiance if a suitable fixed voltage point is selected. At 180V the losses are less than 0.5% for the shown levels of irradiance. At 170V the losses would vary from 0.5% to 5%. The further the fixed voltage point moves away from 180V, the

larger the losses. The losses also increase more rapidly to the right of 180V than to the left. This is due to the shape of the array power curve as could be seen in Figure 6.1.

The losses as a function of solar irradiance are similar at different, constant cell temperature. The real impact on FVO power loss though, is due to variations in cell temperature, as shown at constant solar irradiance of 800W/m² in Figure 6.8.

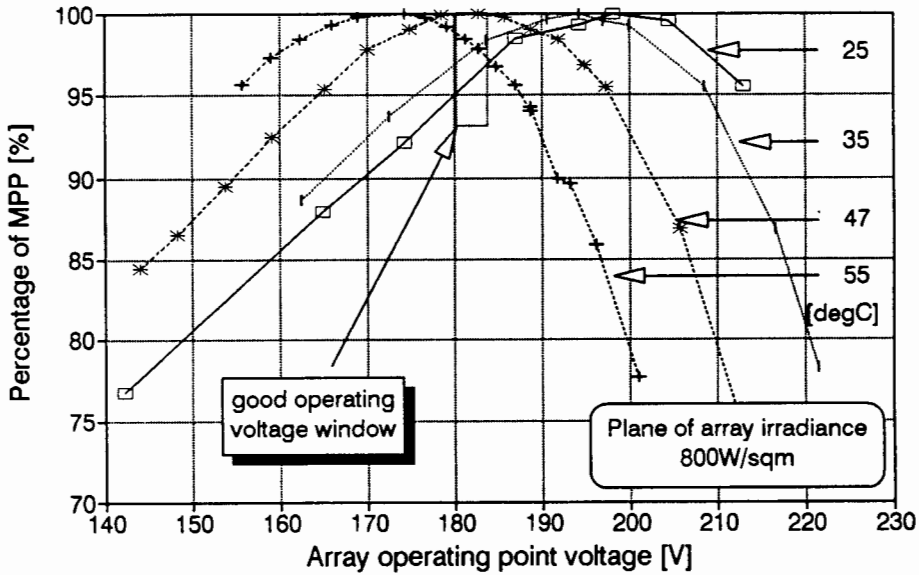


FIGURE 6.8 Percentage decrease in array output power relative to the MPP as a function of module temperature

At this particular irradiance, the average minimum losses (3%) would occur at 185V for all cell temperatures. The graph demonstrates the importance (for a FVO system) of knowledge about the average module temperatures that can be expected at a particular site. At 190V power losses could be as high as 7% at 55°C and at 200V as high as 20% at 55°C or 7% at 47°C. The window that is being indicated in the graph would suggest the optimum fixed voltage point range for a site where the average cell temperature might be 40 to 50°C.

6.1.4 The effect of shading on the IV curve

The Figure 6.9 shows how a hard shade on the array will change the shape of the IV curve. Two IV curves are displayed, one at 200W/m² and one at 400W/m². The power curve at 400W/m² is also displayed. The shade fell over the long side of two modules, shading between none to two columns (of three) of the modules. It can be seen in the graph that the bend in the IV curve at 200W/m² occurs below half the short-circuit current (Line B). The bend in the IV curve at 400W/m² occurs at more than two-thirds of the short-circuit current (Line A). The reason for this behaviour is that the shade is larger at 200W/m² than at 400W/m². As the shade is reduced while the irradiance is being held constant the 'bend' moves up the IV curve until it disappears in the knee of the IV curve resulting in an increase of the short circuit current. The short-circuit

current is about 67% of the estimated short-circuit current at $200\text{W}/\text{m}^2$ and 91% of the estimated short-circuit current at $400\text{W}/\text{m}^2$. This may possibly be an indication of the amount of shading (33% shade at $200\text{W}/\text{m}^2$ and 9% at $400\text{W}/\text{m}^2$).

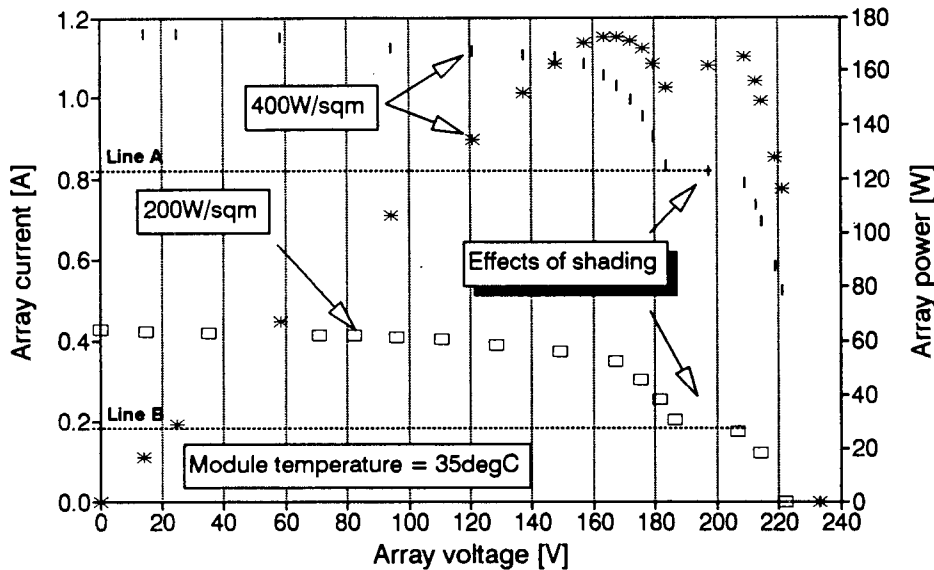


FIGURE 6.9 Effects of shading on the characteristic array curves

6.1.5 Tracking versus fixed array

As a matter of interest it was thought to compare the difference in water delivery of using a passive tracking array (as installed) and a passive tracking array which is facing east in the morning (external intervention, not part of the features of a passive tracking array) and a fixed array. The results of this test cannot be used to make general deductions on the pro's and con's of a tracking array since it would require testing for different day-length and with different solar irradiance profiles.

The test procedure was as follows: The tracking array was fixed for one whole day, left to track for the next day and moved to the east-facing position (the night before) on the third day. All the system data was recorded instantaneously over the whole day in thirty second intervals except for the third day where it was recorded until mid-day. The different shapes of the daily irradiance profiles can be seen in Figure 6.10.

The tests were conducted in mid-April, so day-lengths were approximately average (over a year). The irradiance profile of the fixed array (profile A) is very similar to a sine-wave. The profile of the tracking array (profile C) that has been moved to an east-facing position is a shape between a sine and a square-wave, that is, the area is larger. The irradiance profile of the tracking array (profile B) left to itself is missing the first hour of the day. That is the time it takes for the sun to heat the tube sufficiently for realignment from west to east. Then the plane of array irradiance rises quite sharply, hits a flat peak (which is not very pronounced) at about 11^{00} and then follows the path of the normal passive tracking array (profile B & C, after 12^{00}). The reason for the peak is that at that moment the vertical plane through the sun and the north-

south tilt axis of the array is perpendicular to the surface of the array. As the irradiance comes down from the peak (11⁰⁰ to 12⁰⁰) the sun has 'overtaken' the array and from then onwards the array lags slightly behind the sun. This effect is normal (and actually essential) for these types of tracking devices. The average irradiance of profile B between 10⁰⁰ and 12⁰⁰ is 1.4% higher than for profile C.

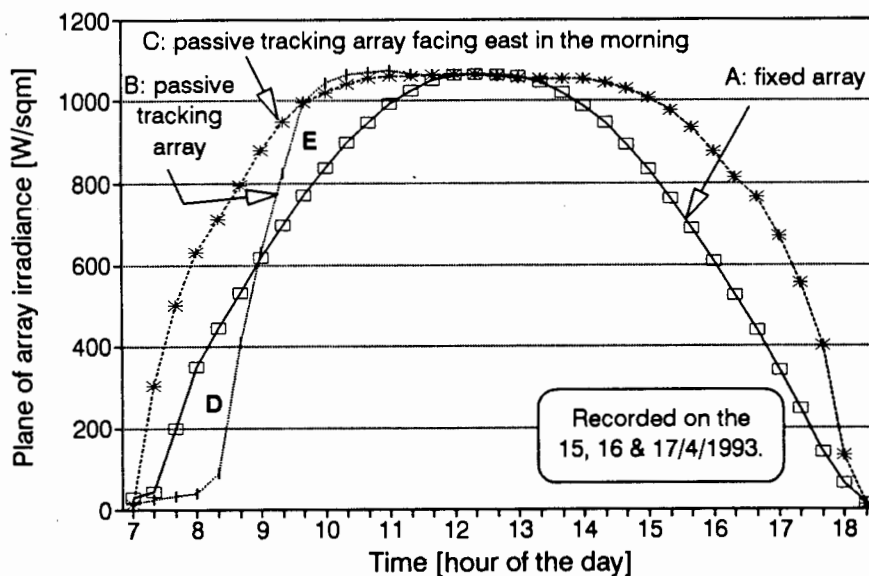
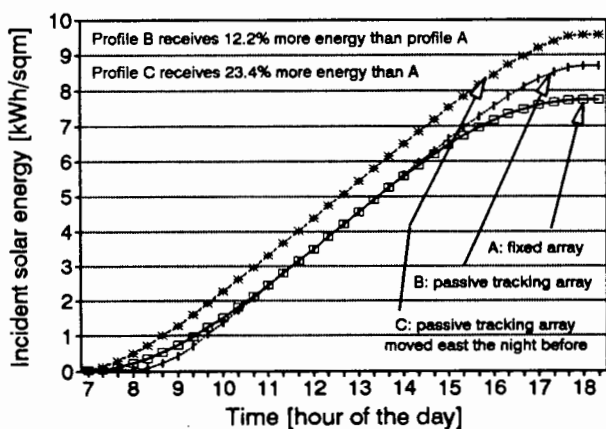
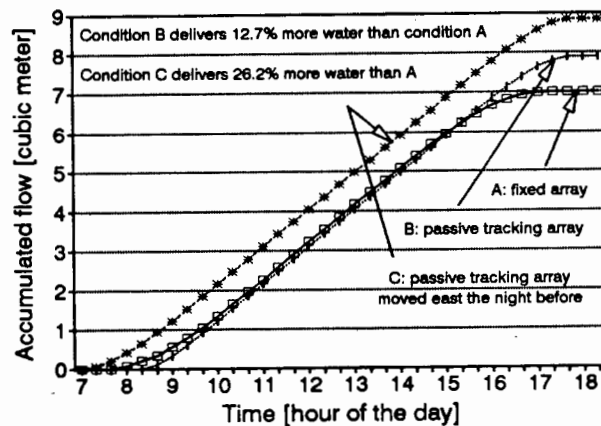


FIGURE 6.10 Fixed versus tracking array for a particular day

Another way of viewing these irradiance profiles is to look at the cumulative irradiation over time. This is shown in Figure 6.11a.



(a)



(b)

FIGURE 6.11 (a) Cumulated solar irradiation and (b) accumulated flow for a fixed and two types of tracking arrays

The vertical axis represents the incident solar irradiation in kWh/m^2 . The profile A exceeds profile B until 11⁰⁰ where they become equal. Therefore area D and E in Figure 6.10 are equal. Then profile A and B have equal values until 14⁰⁰. This means that up until this moment there has been no gain from using a passive tracking array. Only from 14⁰⁰ until sunset does the tracking array perform better than a fixed array. Comparing profiles A and C shows that the gain for the tracking array is made in the morning and in the afternoon. At the end of this particular day the irradiation profile B has received 12.2% more energy than irradiation profile A. Irradiation profile C received 23.4% more energy than profile A.

Figure 6.11b shows the accumulated flow as a function of time. The particular PVP system that was installed while these tests were conducted was the Miltek DC system, operating at a static head of 75m. Therefore this graph incorporates a specific subsystem efficiency (that is, other subsystems will show different magnitudes of accumulated flow). Compared to the fixed array, volume-flow profile B will deliver 12.7% more water and profile C will deliver 26.2% more water on these particular days in the year, under the same solar and spectral conditions and when using this particular Miltek PVP system at a static head of about 75m.

Comparing profiles A and C in graph (a) and (b) (Figure 6.11) the percentage gain in water delivery in is higher (26.2%) than the percentage gain in irradiation (23.4%). This is due to the general trend of PVP systems in that class to operate more efficiently at higher irradiance levels than at lower levels. Since profile C is above an irradiance level of 1000W/m^2 for two hours longer (see Figure 6.10) one can expect the system to be more efficient and deliver more water.

6.2 Pump performance evaluation

This section discusses the performance of the pumping set and the pump itself. The pumping set can be separated into a few functional blocks as shown in Figure 6.12:

- the V-belt transmission from motor pulley to discharge head pulley;
- the discharge head, which transfers the mechanical power from motor to pump;
- the transmission shaft supported by bobbin bearings;
- the borehole pump itself;
- the water pipe which also holds the transmission shaft - together these are referred to as the rising main;
- the discharge head outlet which forms one unit with the discharge head drive, namely the discharge head assembly (the term discharge head always refers to the unit that transfers the power to the pump - not to be confused with the head over which the pump delivers water);
- the post discharge head pipe network which includes all the pipes and bends up to the reservoir.

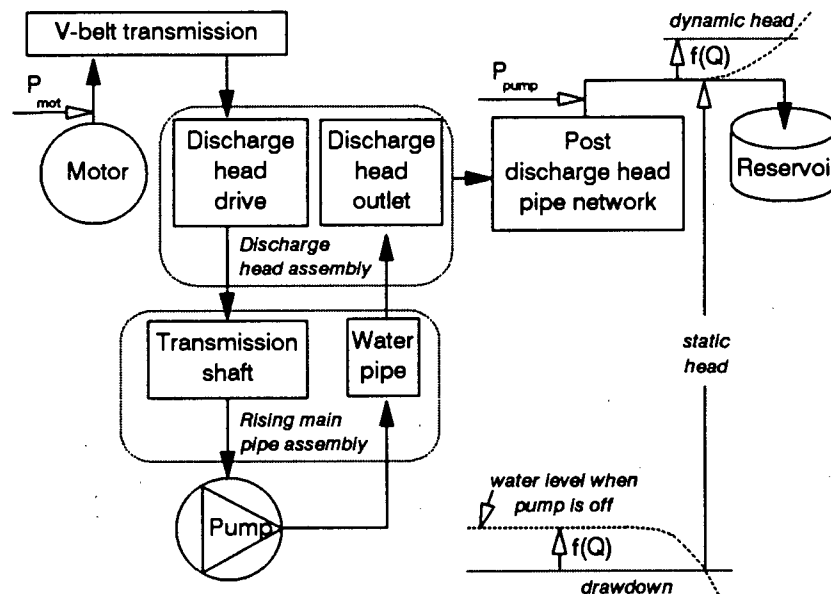


FIGURE 6.12 Block-diagram of the pumping set

The static head (Figure 6.12) is the height difference between the water level in the borehole and the outlet pipe at the reservoir. The water level drawdown in the borehole depends on the flowrate and is included in the static head. The dynamic head includes the friction and the velocity head losses which are found in the rising main water pipe, the discharge head outlet and the post discharge head pipe network.

The pumping set performance is evaluated by relating the motor output power (motor torque \times motor speed = P_{mot} ; see Figure 6.12 for measurement point) to the pump hydraulic output power ($\rho \times g \times Q \times H_s = P_{\text{pump}}$). Therefore, as indicated in the diagram, the pumping set includes the efficiency of the transmission, the discharge head, the transmission shaft, the pump, the water pipe, the discharge head outlet and the post discharge head pipe network. The losses that occur in the water pipe, the discharge head outlet and the post discharge head pipe network are represented by the dynamic head which varies with the flowrate. It should be noted that another convention is frequently used where the dynamic head is added to the static head to give the total head. This is not the case here. The dynamic head is treated as losses. This convention is maintained throughout the dissertation where the pumping set performance is evaluated rather than the pump performance itself.

Figure 6.12 is useful for the evaluation of the pump performance as the different losses that occur in the pumping can be separated from the pump. The evaluation of the losses occurring in the pumping set is in subsection 6.2.4 and the pump efficiency is evaluated in subsection 6.2.5.

The flowrate and the drawdown in the borehole have been correlated to the pump speed. The torque characteristics are discussed with reference to shape and instability. Next the efficiency of the pumping set at different heads is evaluated and then the losses are assessed in order to compare the performance of the pump to the specifications. The section ends with a conclusion on the type of pump used and a comparison to an Orbit pump.

The pumping set performance was measured using the Miltek DC system. The speed ratio for the V-belt transmission was 1.98.

6.2.1 Flowrate and drawdown correlations to pump speed

Due to the tedious nature of reading the volume-flowmeter and measure the drawdown in the borehole it was thought to be simpler to correlate the flowrate and the drawdown to the pump speed.

The flowrate of a positive displacement pump should be linearly related to its speed over the main operating range (here 150 rpm to 1000rpm), as indicated by performance specifications (appendix A1.3), while it may be slightly non-linear near low speed. The latter has not been tested for deliberately. The fact that the static head changes by about 2m due to drawdown carries little weight here as the flowrate has quite an inelastic relation to variations in head.

The borehole water level maintained a very constant head throughout the six months of testing (at non-pumping conditions and after waiting for at least 10min after the pump had stopped; this time value was found through observing the 'charge' curve of the water-level in the borehole after pump standstill). It could also be mentioned here that another two boreholes were situated about 150m from the test site borehole. Each of these boreholes delivered 9m³/h. During one-and-a-half hours of pumping at the

other two boreholes and after another one hour of no pumping no drawdown could be measured at the test site borehole. The assumption that the water level in the borehole would drop repeatedly to the same level at a particular pump speed (after allowing for a 3 min minimum settling time) is therefore justifiable.

Flowrate

The correlations were found to be:

$$Q = 1.05 \times S_{\text{pump}} - 67.5 \text{ [l/h] for } \underline{75\text{m}}$$

$$(R^2 = 0.9994, \text{ Standard error of Y estimate} = 6.67)$$

$$Q = 1.05 \times S_{\text{pump}} - 78.5 \text{ [l/h] for } \underline{82\text{m}}$$

$$(R^2 = 0.9996, \text{ Standard error of Y estimate} = 5.72)$$

These equations were each deduced from two sets of data. At 75m one set contains eleven observations and the other one contains seventeen observations. At 82m the first set contains nine and the second contains twelve observations. The repeatability of the speed coefficient was good. The maximum standard error of the coefficient amongst all four data sets was 0.00657.

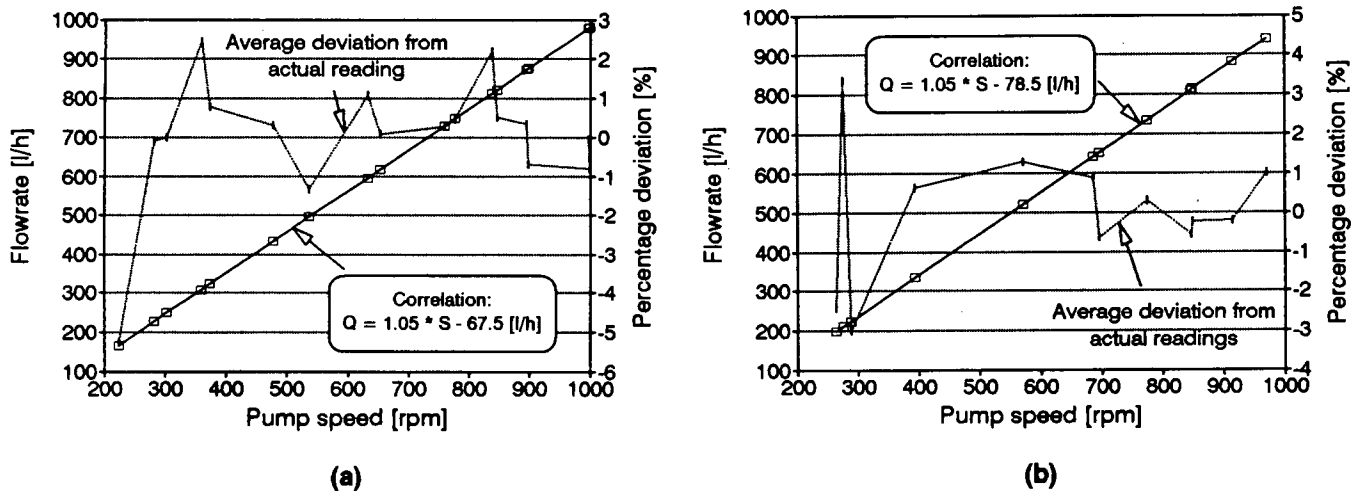


FIGURE 6.13 Flowrate to pump speed correlation: (a) at 75m and (b) at 82m

The largest percentage deviation was found to be -5% and +3.5% for 75m and 82m respectively. Both occurred near low pump speeds. Above 400rpm the deviations were less than 2.2%. This is shown in Figure 6.13 for 75m (Graph a) and 82m (Graph b).

Drawdown

The effects of drawdown were incorporated, through correlation with pump speed, in the following equation:

$$H = 0.9 \times 10^{-3} \times S + 1.6 \times 10^{-6} \times S^2 + C$$

where C is 74.28m (when pumping into pool) and 81.33m (when pumping into the reservoir). H is the sum of the static head measured to the pump discharge head plus the drawdown plus the static head from the pump discharge head to the point of delivery.

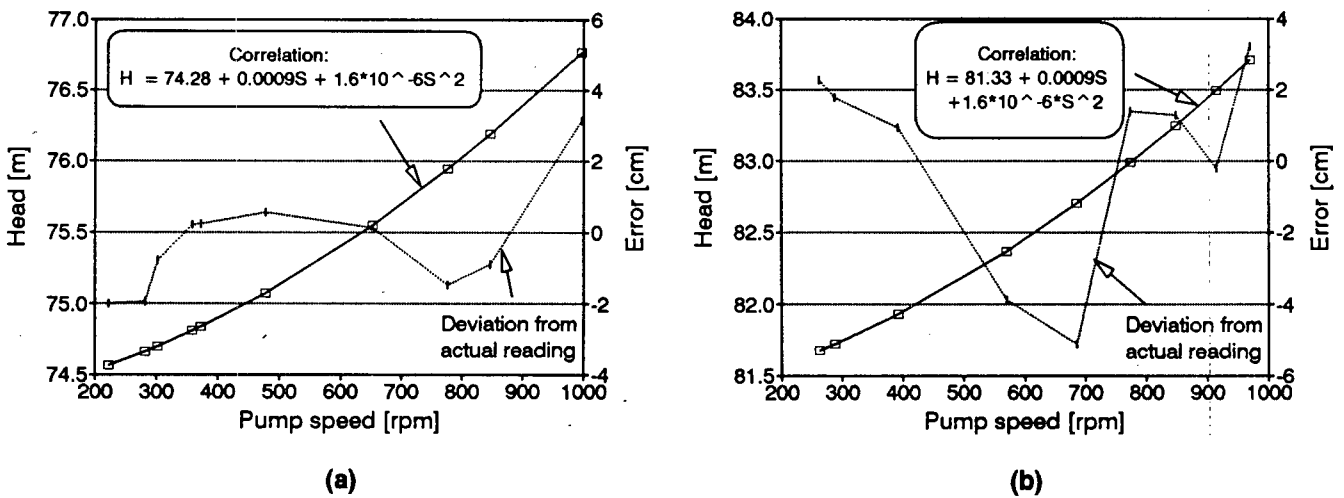


FIGURE 6.14 Drawdown to pump speed correlation: (a) 75m and (b) 82m

The maximum deviation from the manually measured curve is ± 5 cm (less than 0.1%) as can be seen in Figure 6.14.

6.2.2 Torque characteristics of the pump

Once it was realised that the torque speed characteristics were not as expected a lot of tests were conducted that just focused on the shape of the torque curve as a function of speed. The graph shown in Figure 6.15 illustrates a typical steady state torque curve at 75m over the maximum operating range that the DC system can provide. The rising main pipe is filled with water at the start (due to a non-return valve at the bottom of the pump).

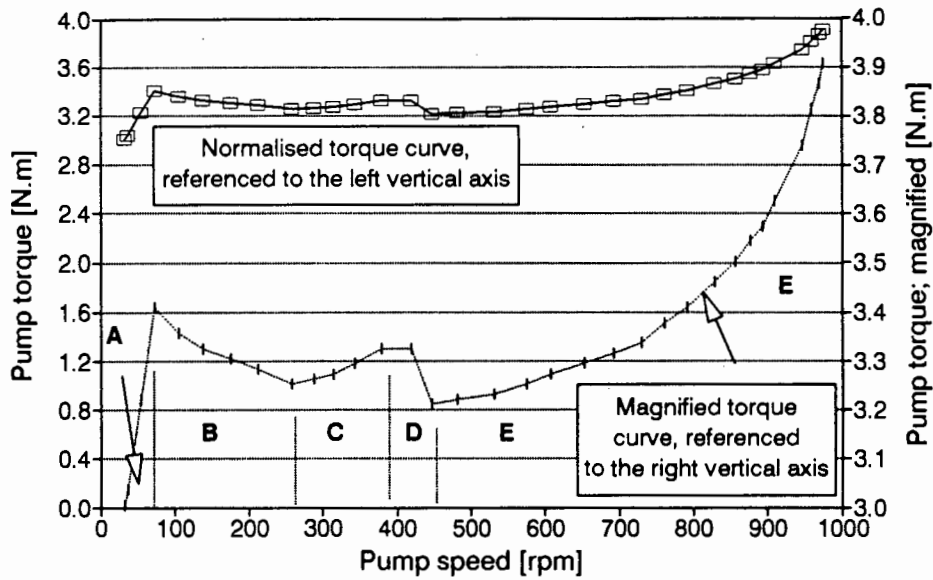


FIGURE 6.15 Typical torque versus speed characteristics of the pump

I discussed this curve with Rob Waites of Orbit Pumps to get some clarification on this unexpected shape. Referring to Figure 6.15 it is attempted to explain the different sections of the graph. Suggestions made by Mr Waites are indicated with his name.

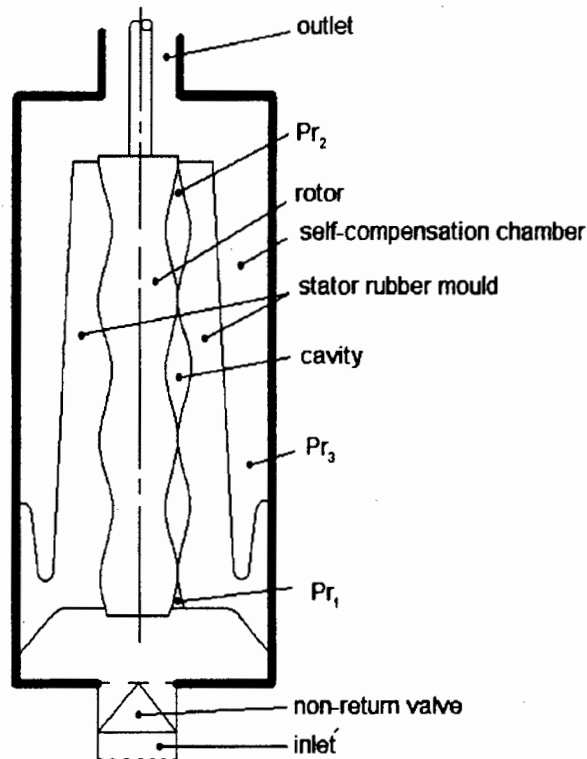


FIGURE 6.16 Diagram of a self-compensating stator, progressive cavity pump
 Source: Adapted from Payne (1986)

Figure 6.16 shows a diagram of a self-compensating rotor/stator set for explanatory purposes. Note that the stator rubber is only attached at the bottom. The self-compensation chamber therefore fills with water and has the pressure from the column of water in the rising main pipe.

- Region A:** The tests have shown that no water is delivered in this region. The slip is therefore one and the pressure is the same across the rotor/stator set ($Pr_1 = Pr_2$). It is also the same on the outside of the stator ($Pr_{1&2} = Pr_3$). The torque increase must therefore be due to friction as the speed increases.
- Region B:** In this region the pump has started to deliver water. The non-return valve is now open and a pressure differential is formed across the stator ($Pr_2 > Pr_1$). It could be that the stator is twisted slightly here resulting in a decrease in torque.
The pressure on both sides of the stator is equal resulting in a decrease in torque [Waites].
- Region C:** Here the pressure on the outside of the stator (Pr_3) is larger than on the inside (gradient of Pr_1 and Pr_2). The stator is 'pressing' on the rotor and the torque increases. Self-compensation is taking place. [Waites]
- Region D:** The stator twists (ie. moves out of its rest position) slightly to try to conform to the shape of the rotor. The slip increases and the torque will consequently decrease. [Waites]
Data shows that this region is completely steady state, that is the pump does not just slip through this region but can settle anywhere on that line. The interpretation of Mr Waites would also suggest that the flowrate in that region cannot be linearly related to the pump speed as was assumed in the flowrate versus pump speed correlation but looking at the available data that was collected for this correlation, I could not find excessively large errors in that speed region at all.
- Region E:** At the transition to region E the stator has moved back to its rest position. Again, the pressure on the outside of the stator is larger than on the inside and the stator will therefore compensate. The torque will carry on increasing exponentially until the pump cannot get any more liquid into the pump as the Net Positive Suction Head (NPSH) is reached (a point where the cavities are being emptied faster than they can be filled up again; the pressure of the liquid is dropped so much that it gets close to the vapour pressure; this though happens around 1400 to 1500rpm). The slip becomes zero when the NPSH is reached. [Waites]

According to Rob Waites the torque requirements in regions A and D are very unpredictable and unrepeatable. This cannot be confirmed for region A. The two data sets obtained (there are only two sets of data logged with the DC system that show

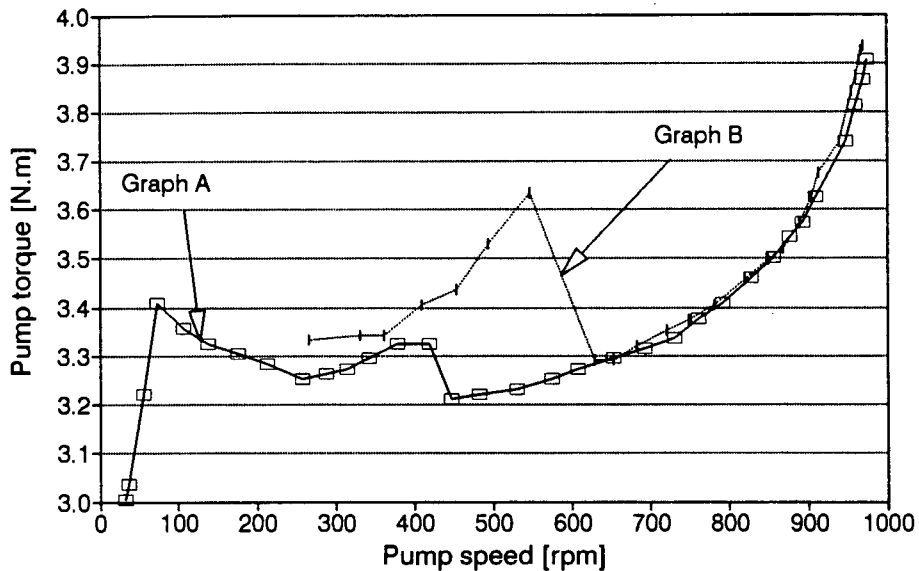


FIGURE 6.17 Two distinct torque versus speed profiles

region A) followed the same straight line. The instability of region D can be confirmed. What is particularly uncertain is at what speed the region D or the transition from region C to D will occur and how 'wide' region D will be. Figure 6.17 shows the previous graph (Graph A) with another graph obtained a month earlier (Graph B). Region C is very wide and the torque rises quite sharply. A possible explanation:

One particular difference between the test methodology for obtaining Graph A and Graph B was the movement of the array. When the data for Graph B was obtained the array was moved very gently which was not the case for Graph A, where the array was moved in more discrete steps (this difference was not really intentional). Another important point is that the shape of Graph B was never obtained with any of the AC systems. The shapes were all rather like Graph A. One characteristic of the AC systems is that they exhibit torque pulsations at a rate of about 1Hz. The point is that the transition from compensating stator (region C) to slightly twisted stator (region D) might occur sooner if the system is disturbed through discrete steps in input power or torque pulsations (AC systems only).

As a possible explanation: Graph A represents the shape of the torque-speed characteristics when the system is slightly disturbed (moving the array in discrete, small steps or torque pulsations) and Graph B represents the undisturbed torque-speed characteristics.

The shape of Graph B has a negative effect on the efficiency of the pump at that speed range (region C to D). Yet this may be the route the DC system might take every day if undisturbed.

The uncertainty in the torque measurement data is:

$$U_{\text{abs}}(T_{\text{pump}})_{4\text{N.m}} = 3.6\%$$

$$U_{\text{abs}}(T_{\text{pump}})_{3\text{N.m}} = 4.7\%$$

This uncertainty is lower than one would expect. The loadcell and the measurement circuit are both of high accuracy. The largest error is introduced from the calibration process. The loadcell signal was calibrated with a precision spring that in turn was calibrated by three known weights.

Hysteresis

The general shape of the curve remains when the speed is decreased, yet it is quite unpredictable at what stage the torque will increase (transition E to D). It could enter region D at a higher speed than on the way up or vice versa. Both cases were observed.

Starting torque requirements

The starting torque is a function of the static head and the rotor/stator interference fit (Vetter & Wirth 1992). The static head remains constant for this pump. The interference fit is likely to vary over a longer period of time due to wear. If the wear is corrosive it might increase the starting torque requirements.

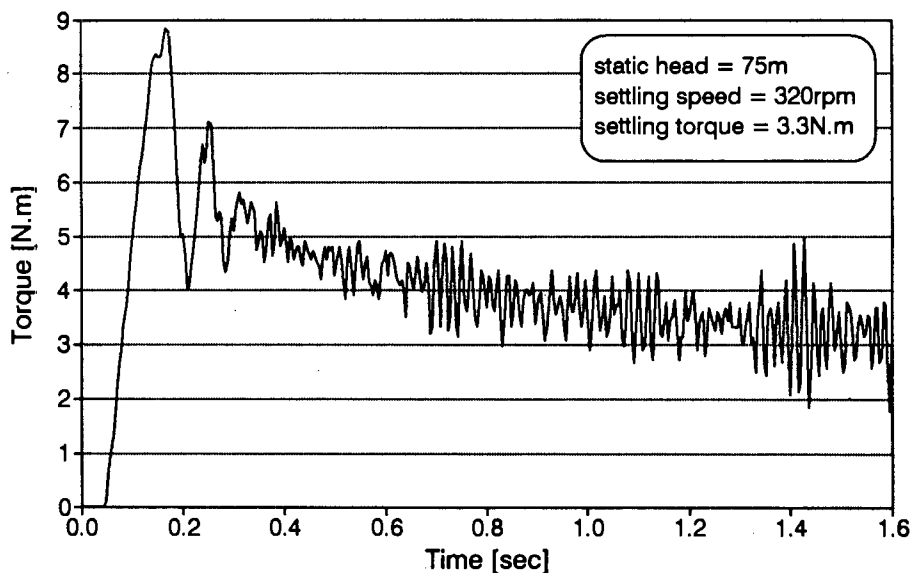


FIGURE 6.18 Torque at the start-up of the pump

The starting torque required for the first start in the morning will be somewhat higher than the requirements for a second start. Figure 6.18 shows the instantaneous torque curve at start-up. The pump had run prior to this start-up. The torque reaches a peak of 9N.m which is in the order of 2.2 to 2.8 times the running torque.

6.2.3 Characteristics of the pumping set at different heads

The pump performance will first be evaluated for the standard operating head as it was used during the test period (around 75m). As a few torque-speed curves were encountered the effect on the pump efficiency due to these variations in torque will be analysed. Then the pump will be evaluated at larger heads. Simulation of smaller heads was impossible. The larger heads could be simulated with a constant pressure valve but these cannot keep the pressure constant for different flowrates unless a non-trivial control loop is constructed. Herrmann et al. (1987) provides a detailed description of an indoor test-loop that is based on such a control loop.

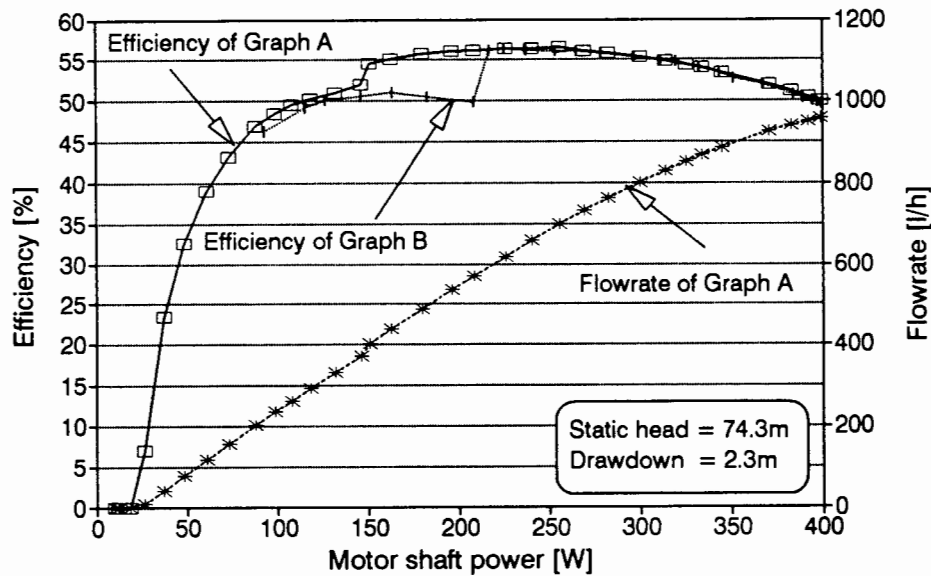


FIGURE 6.19 Pumping set efficiency and flowrate characteristics versus motor shaft power

As it is not really the aim to evaluate the pump performance in detail, the 'constant' pressure valve option was used for approximate observation of how the pump efficiency is affected by higher heads.

Evaluation of the pumping set performance at standard head (75m)

The graphs in Figure 6.19 show the typical efficiency curves (for Graph A and B of Figure 6.17) and the flowrate. The peak efficiency of the pumping set is 56% and it stays above 50% for input power range of 120 to 400W. At input powers of 150W to 220W the efficiency of Graph B (high torque peak) is 5 to 7% lower than Graph A.

Evaluation of the pumping set performance at larger heads (82m and higher)

Four sets of data are represented in Figure 6.20. Graph (a) shows the efficiency of the pumping set versus the motor shaft power. Graph (b) shows the variations in head versus motor shaft power for the efficiency data. Two sets are realistic pump conditions (pumping into the pool and the reservoir) with minor head variations due

to drawdown in the borehole. The other two sets are simulated with the pressure valve and have head variations of up to 10m. Nevertheless, the conclusion can be drawn that the pump efficiency increases with increasing head. This is more noticeable at high power input than at lower power. This is to be expected as the pump can be installed up to a depth of 150m.

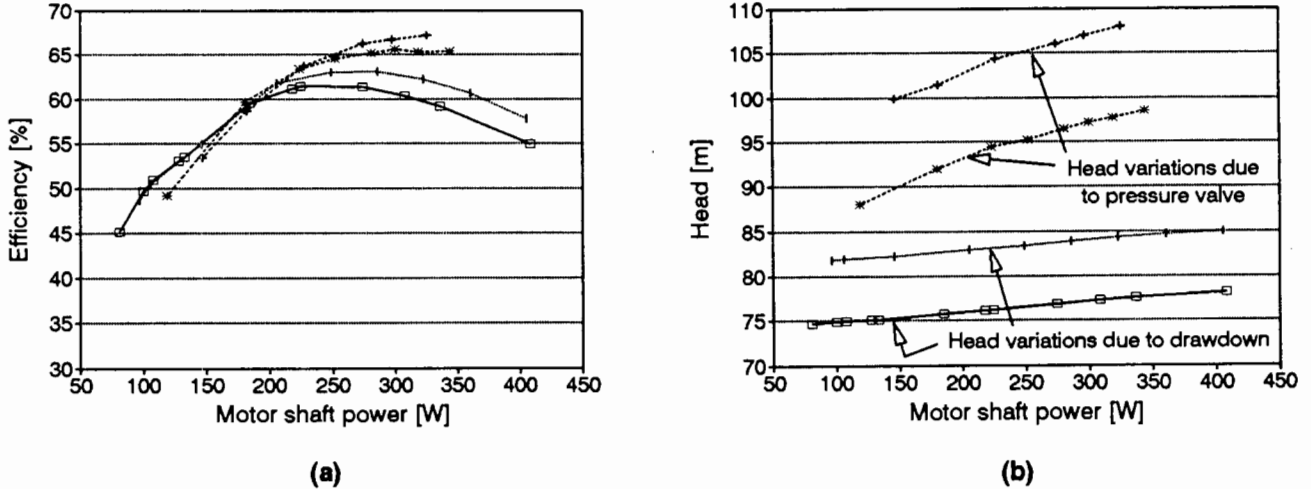


FIGURE 6.20 (a) Pump efficiency over a range of heads; (b) head variations (key to Graph a)

The pumping set reaches an efficiency of 67% at a head of 108m. As the head decreases to 100m the efficiency reduces to 54%. This reduction in efficiency is related to low input power levels rather than a decrease in head.

6.2.4 Pumping set losses

The aim of this section is to evaluate all the losses that occur in the pumping set. These are consequently subtracted from the pumping set performance data to yield the efficiency of the pump itself. The resulting data is used for comparison to the manufacturers specifications. The discussion is based on the diagram of Figure 6.12.

Mechanical losses

These can be divided into V-belt transmission losses, discharge head losses (bearings, anti-reversing mechanism and gland packaging) and transmission shaft friction losses. An attempt was made to measure the V-belt transmission losses with the method proposed in the test methodology. This was unsuccessful. The slip is most probably too small and is flooded by the measurement error. The discharge head losses and the shaft friction losses were not measured.

Gosnell (1991) estimated these latter losses to be 7% and Payne (1986) estimated these losses to be 12%. For this evaluation they will be assumed to be 10%. Since the pump is usually treated as a single unit (motor output to water delivered) an error in this estimation does not effect the evaluation of any of the system components.

Hydraulic losses

These losses are equivalent to the dynamic head which is the sum of the friction head losses (friction of the water on the inside of the pipe wall) and velocity head losses (local velocity losses due to valve, bends, contraction and other general obstructions). The dynamic head losses increase with the square of the flowrate. These losses occur in the rising main water pipe, in the discharge head outlet and in the post discharge head pipe network.

The rising main water-pipe losses were not measured but rather evaluated from a graph supplied by Mono Pumps. It is a graph of the head losses in the rising main pipe as a function of the flowrate. The curve is slightly exponential. Head losses increase from zero meter at zero flow to 1.4m at 1000l/h, for a head of 75m.

The discharge head outlet losses were assumed to be negligible since the installation used 32mm pipe which does not result in significant head losses due to pipe contraction since the flowrate is low.

The post discharge head pipe network losses include velocity head losses due to a number of bends in the network and due to the Kent volume flowmeter and due to the head losses as a result of friction. These losses were measured but no significant pressure increase above the static head could be measured. Hence these were considered to be negligible.

6.2.5 Comparison to pump specifications

The graphs shown here were extracted from the specification sheet of the pump (appendix A1.3). The specifications are presented slightly differently in the sheet. They have therefore been processed.

The performance of the pump has been isolated for this subsection by taking account of the mechanical and hydraulic losses (section 6.2.4) which occur in the pumping set.

Figure 6.21 shows the flowrate and torque at 75m as they were measured and as they are specified. The measured flowrate is slightly lower than the specified flowrate. At 1000rpm this difference evaluates to be 5.8% lower than the specified value. This decreases to zero at 150rpm. I find this difference plausible and acceptable. Besides the uncertainty in the flowrate the assessment of losses may not be accurate enough. If they have been underestimated then the pump performance will evaluate lower.

The absolute uncertainty in the flowrate data is:

$$U_{\text{abs}}(Q)_{200 \rightarrow 1000 \text{ l/h}} = 6.1\%$$

The largest uncertainty is introduced through the calibration of the volume flowmeter. This had to be calibrated by running water into a bucket whose markings had to be aligned with the water-line. The volume flowmeter itself had an accuracy of about 2%.

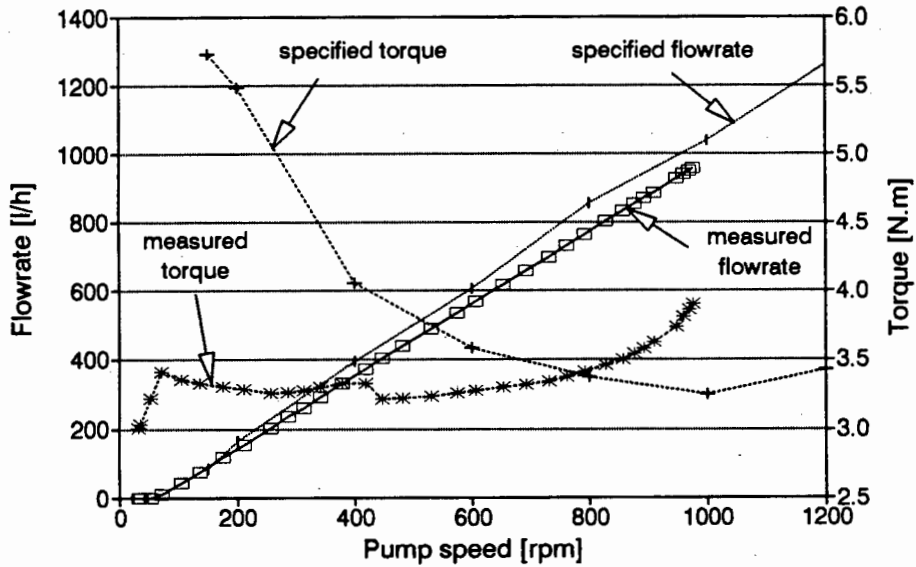


FIGURE 6.21 Measured torque and flowrate compared to specifications

The torque curve deduced from the specifications does not seem to be plausible. It is unrealistic to require such a large torque at 200rpm (nearly double the running torque) and then decrease to a minimum torque at 1000rpm. One would expect the torque to increase steadily from low operating speeds to high operating speeds due to the effect of the self-compensating stator. The principle behind the self-compensating stator is to reduce the torque on start-up. However, the stator does not compensate immediately after start-up but requires a pressure head from the static head and from the flowrate. As compensation takes place, the torque will increase.

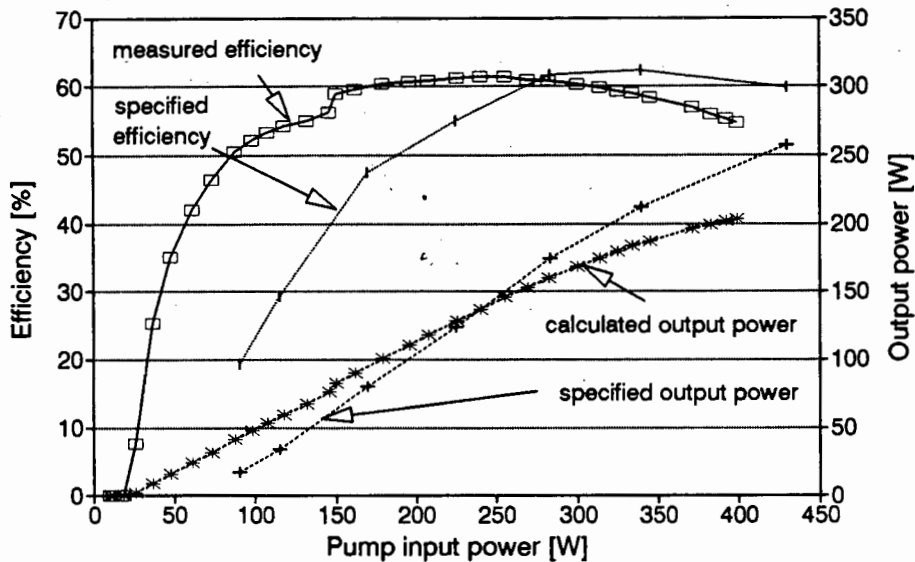


FIGURE 6.22 Measured pump efficiency and out put power characteristics compared to the specifications

The torque was calculated from the input power and the pump speed. The measured and specified torque curve have only an intersection at about 850rpm in common. Unfortunately this undermines the efficiency comparison as the input power is definitely incorrect for pump speeds of less than 800rpm.

Figure 6.22 displays the efficiency and output power of the specified and the measured data. Both output power graphs have their shape in common but have different gradients. That is acceptable. The efficiency curve from the specifications has a predictably lower efficiency near low input power due to an unrealistic torque characteristic. The shapes are similar but peaks are displaced by 100W. The difference in peak efficiency is about 2%. That is good. If the torque curve would be flatter below 800rpm, the specified efficiency curve would move to the left towards the measured efficiency curve.

The uncertainty in the pump efficiency data is:

$$U_{abs}(\eta_{pump})_{400W} = 7.1\%$$

$$U_{abs}(\eta_{pump})_{200W} = 7.8\%$$

Figure 6.23 shows the efficiency of the pump as a function of pump input power. The measured and the specifications data are indicated with the ellipses. The graph indicates that the measured values show a better efficiency near lower input powers (up to 270W). This is due to the unrealistic torque curve.

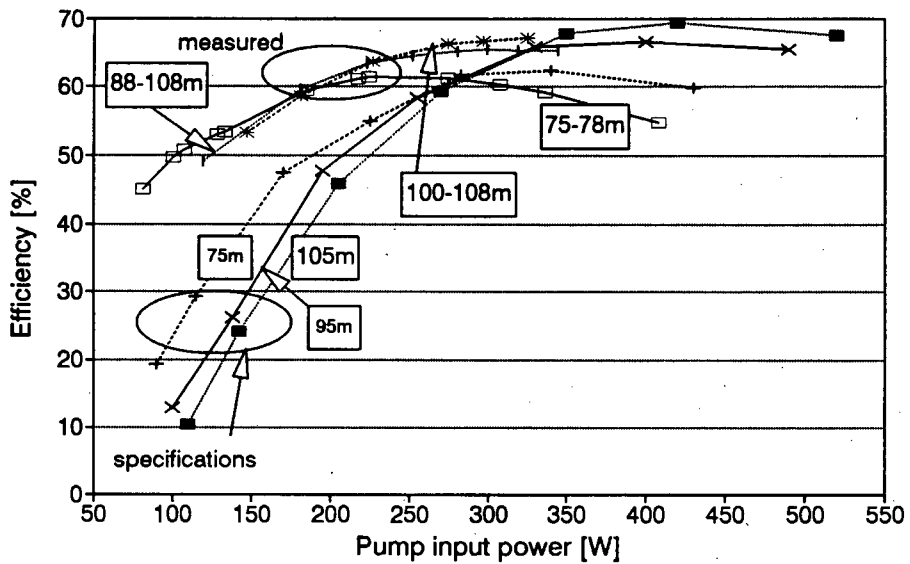


FIGURE 6.23 Measured efficiency compared to specifications over a range of heads

6.2.6 Conclusion on the type of pump used

The self-compensating stator pump was originally designed for hand-pump applications up to a maximum speed of 200rpm (Payne 1986). In the opinion of Rob Waites it is therefore not suitable for PVP applications which usually exceed this speed. Mono Pumps though, sell this type of pump as a solar element for speeds up to 1200rpm.

Mr Waites suggested to rather use a standard moulded element pump like the Orbit 0102. The torque curve is a straight line and has no unstable areas. The starting torque would be higher but that can be overcome with intelligent start-up routines (not for the present Miltek DC converter).

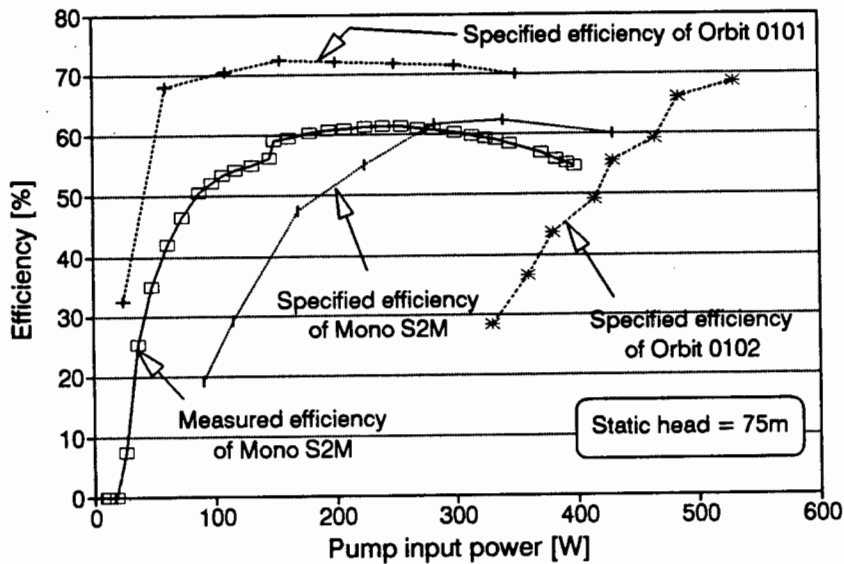


FIGURE 6.24 Efficiency of the Mono S2M and the Orbit 0101 & 0102 pump

Figure 6.24 shows the specified efficiency of the Mono S2M pump, the Orbit 0102 pump, the Orbit 0101 pump and the measured data of the Mono S2M pump. The Orbit 0102 can be installed to a depth of 150m. At 75m the efficiency curve is still rising. It does reach a good efficiency from 450W onwards (that is larger than 60%) but this particular system produces a maximum motor output power of 400W. This pump is therefore not suitable. The Orbit 0101 is designed for static heads up to 75m. It would therefore be operating at its pressure head limit. It shows an excellent efficiency (more than 70%) over most of its input power range (100W to 350W). This element would be an alternative to the present choice. Unfortunately its input power range is too narrow and it is operating at its maximum head. I am not sure what the effect would be if the pump would receive an input power of 400W and operated at heads larger than 80m.

6.3 Miltek system performance analysis

This is the PVP system that the prototype inverter systems will be compared with. It is a well established system which has proved to be reliable under long term running conditions.

The converter and the motor performance are analysed as separate components and as a subset of the complete system. Then the overall performance of the system and the subsystem is evaluated on an instantaneous and a daily energy efficiency basis.

System tuning

The system was tuned with regard to the operating point on the array and the optimum motor pulley size.

The fixed voltage point was set to about 91V. This was found to be close to the MPP at cell temperatures of 47°C (refer to Figure 6.8). Average cell temperatures were in the region of 40°C (windy) to 55°C (no wind) on a sunny day.

The choice of motor pulley was guided by three criteria (discharge head assembly pulley remained constant, being 247 pitch centre diameter):

- the converter should only enter the direct mode (where fixed voltage operation stops, but efficiency across the converter increases) close to the maximum daily irradiance level (estimated to be 1050W/m² over the year)¹
- the pump speed at high irradiance levels should be maximised which in turn maximises the flowrate
- the start-up delay should be minimised

The first criterion will require the pulley diameter to increase (higher torque therefore higher converter current and therefore higher array-current-threshold before entering direct mode), the second criterion depends on the motor efficiency at different torque levels and the third criterion will require the pulley diameter to decrease (less torque, less converter current and therefore earlier start-up). The last criterion should not be over-emphasised as the system uses a tracking array which means that system start-up conditions can be reached earlier in the day (on clear days).

¹ This criterion has been simplified. For true optimisation two effects have to be taken into account. One, the higher efficiency of the converter in direct mode but with reduced array output due to operation away from the MPP (in direct mode). Two, the lower converter efficiency at lower array input powers. The threshold voltage at which the direct mode is to occur is evaluated by finding the point of minimum losses (of effect 1 & 2) over the period of a year for the particular site. This of course is not possible for lack of data prior to installation. In addition, this evaluation would be relatively tedious. It was therefore decided to remain close to the MPP of the array by selecting a pulley for which the direct mode would occur near higher irradiance levels.

Figure 6.25 shows at what irradiance level the converter progresses into direct mode for different size pulleys. The pulley with a pitch centre diameter (PCD) of 112mm enters the direct mode at about 850W/m^2 and the pulley with a PCD of 140mm does not go into direct mode at all. The best choice from this graph would be pulley 125 which just goes into direct mode.

From the point of view of power extraction out of the array, pulley 112 extracts 6.5% less power (at more or less the same irradiance level) than pulley 125 as it operates at an array voltage of 97V. Consequently it does not manage to reach the same speed as pulley 125. Similarly for pulley 118 although here the array power difference is 4.4%.

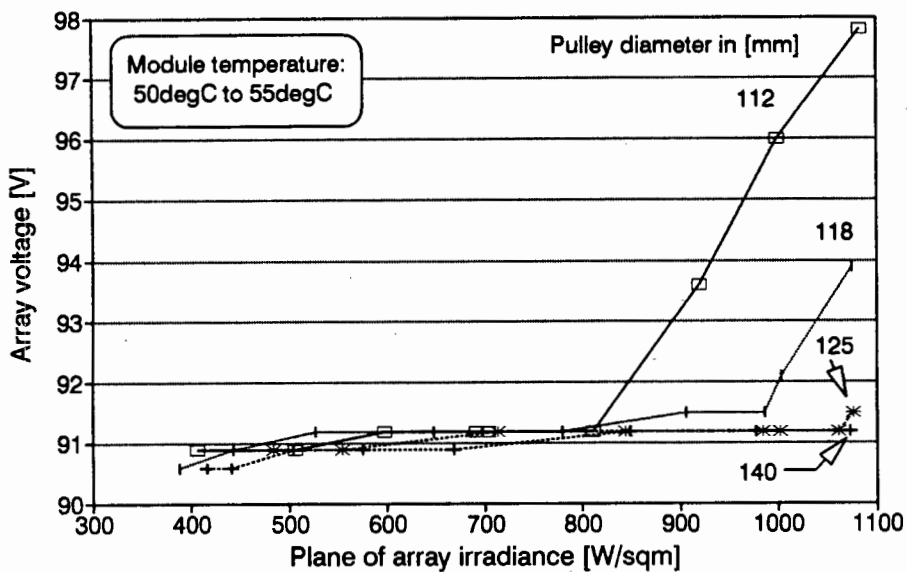


FIGURE 6.25 Array voltage as a function of irradiance for different pulley diameters

Pulley 125 and 140 have similar performance data. Taking the first (just going into direct mode) and the third criterion (early start-up) into account it was decided to choose the 125 pulley.

It was noted later that the transition into direct mode did not always occur at the same irradiance level but could occur 100W/m^2 earlier (temperature and load variations). It also became apparent that start-up time-delay between the 125 and the 140 pulley is not very long, about 15min. Therefore a 140 pulley would also have been acceptable.

6.3.1 Converter and motor performance

Efficiency at standard head (75m)

The converter starts operating at an input power of 50W as shown in Figure 6.26. The efficiency reaches 80% at 100W and then increases linearly to 97% at 520W.

The three percent losses at maximum input power (for this particular configuration) are due to conduction losses in the MOSFET's and due to power consumption in the control electronics. The switching losses are zero as the converter has changed to direct mode (in direct mode the converter ceases to switch such that the array is directly connected to the motor).

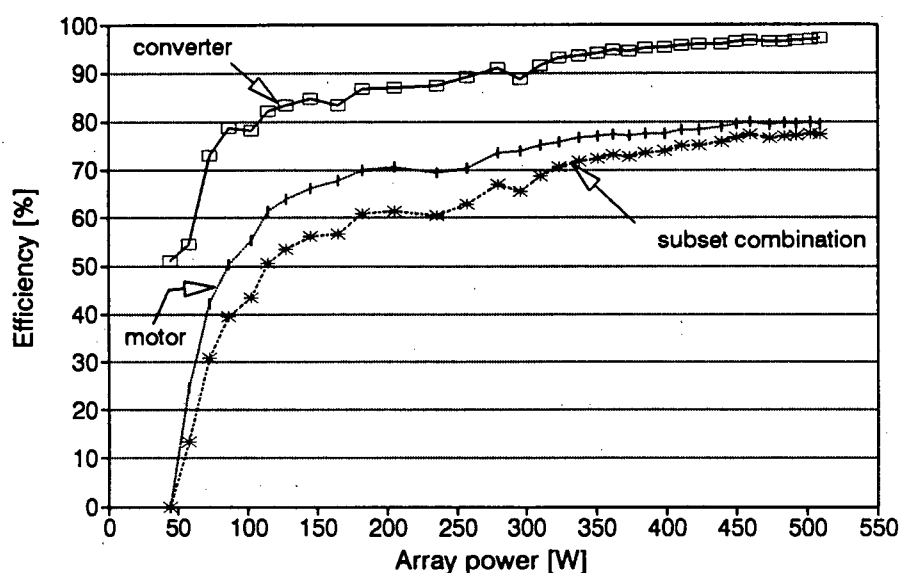


FIGURE 6.26 Miltek converter, motor and subset efficiency versus array power

The uncertainty in the converter efficiency data is:

$$\begin{aligned}
 U_{\text{abs}}(\eta_{\text{con}})_{500\text{W}} &= 3.0\% \\
 U_{\text{rel}}(\eta_{\text{con}})_{500\text{W}} &= 1.7\% \\
 U_{\text{abs}}(\eta_{\text{con}})_{250\text{W}} &= 4.3\% \\
 U_{\text{rel}}(\eta_{\text{con}})_{250\text{W}} &= 3.2\%
 \end{aligned}$$

The motor efficiency rises sharply at 50W array power from zero percent to 60% at 120W and then rises more slowly (with a decreasing gradient) to 80% at 520W. The subset efficiency rises above 60% at an input power of 180W and reaches a maximum at 77.6%.

The uncertainty in the motor efficiency data is:

$$\begin{aligned}
 U_{\text{abs}}(\eta_{\text{mot}})_{480\text{W}} &= 4.1\% \\
 U_{\text{rel}}(\eta_{\text{mot}})_{480\text{W}} &= 3.6\% \\
 U_{\text{abs}}(\eta_{\text{mot}})_{250\text{W}} &= 5.6\% \\
 U_{\text{rel}}(\eta_{\text{mot}})_{250\text{W}} &= 5.0\%
 \end{aligned}$$

The uncertainty in the subset efficiency data is:

$$\begin{aligned}
 U_{abs} (\eta_{subset})_{500W} &= 4.4\% \\
 U_{rel} (\eta_{subset})_{500W} &= 3.6\% \\
 U_{abs} (\eta_{subset})_{250W} &= 5.9\% \\
 U_{rel} (\eta_{subset})_{250W} &= 5.4\%
 \end{aligned}$$

The converter efficiency is quoted at 98%. That will be at full load which is 14A and 120V and most probably in direct mode. Under full load conditions and in direct mode the converter is likely to be more efficient due to the constant losses (for example control electronics) becoming smaller in relation to the total power processed. Therefore the measured maximum efficiency of 97% indicates that the converter lives up to its specifications in direct mode. This specification however is not very informative, since when the controller is performing its fixed voltage operation function, conversion efficiencies are lower than in direct mode, while in direct mode the cessation of voltage tracking can imply reduced array efficiencies through deviation from the MPP voltage.

The motor efficiency reaches a maximum of 80%. Although the specifications did not specify the efficiency literature suggests that DC motors generally have an efficiency of 75 to 85%.

Efficiency at higher heads

The load on the pump was increased from the usual 75m head to 82m (pumping into a different reservoir), to 88 - 87m and to 100 - 107m where the last two were simulated with a pressure valve. The effect on the efficiency for the converter (Graph a) and the motor (Graph b) is shown in Figure 6.27.

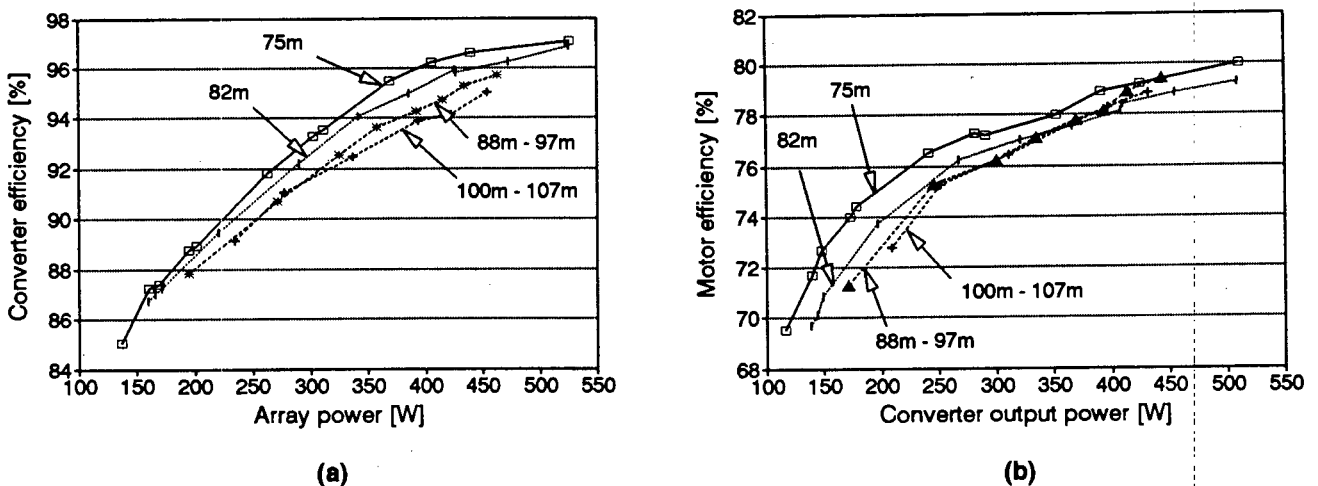


FIGURE 6.27 (a) Converter efficiency and (b) motor efficiency over a range of heads

The converter efficiency tends to decrease with a larger load on the motor. The reason for this is larger conduction losses as more converter current is required to generate a higher torque for the pumping set. The motor efficiency at higher heads is lower at low input power. The graph gives the indication that the efficiency of the motor improves for higher heads as the input power increases in relation to the efficiency at the standard head (75m). That would make sense as the motor is operating under partial load conditions. The output is rated at 750W and the output power here is about half of that. One would therefore expect the efficiency of the motor to increase for larger loads and increased input power.

Characteristic converter and motor curves

These are shown in Figure 6.28 where the converter current and the pump torque are displayed as a function of array power (Graph a). The adjacent graph (b) shows the converter output voltage and the pump speed. The graphs show the proportionality that exists in DC drives between their electrical and their mechanical quantities.

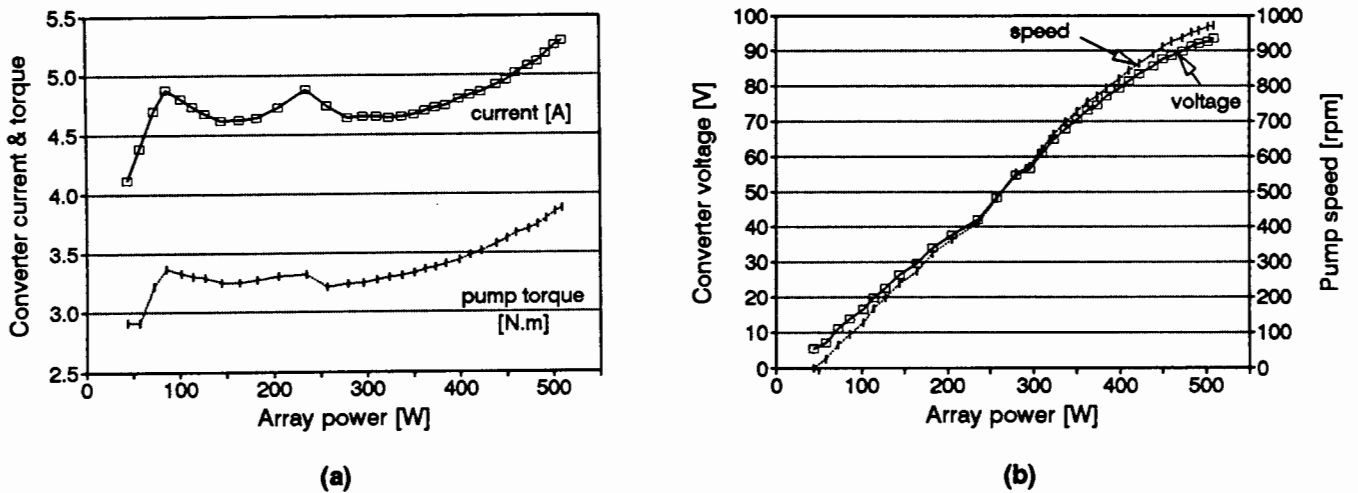


FIGURE 6.28 Characteristic converter and motor (referred to pump) curves

6.3.2 Array operating point characteristics

The control algorithm is implemented in hardware. The algorithm maintains a fixed voltage point by controlling the motor speed which it does by switching the array voltage with a pulse-width modulation scheme.

Figure 6.29 shows the graphs of the array voltage and the array current. The voltage stays within one volt of its fixed voltage point until about 950W/m² (also note the ADC resolution which is amplified times thirty here). The converter progresses to direct mode where the voltage rises sharply (relative to the fixed voltage point) and the gradient of the current decreases slightly. That is due to the IV characteristic of the array. At this point the array current is large enough to supply the motor directly and is therefore able to maintain the torque that the pump requires.

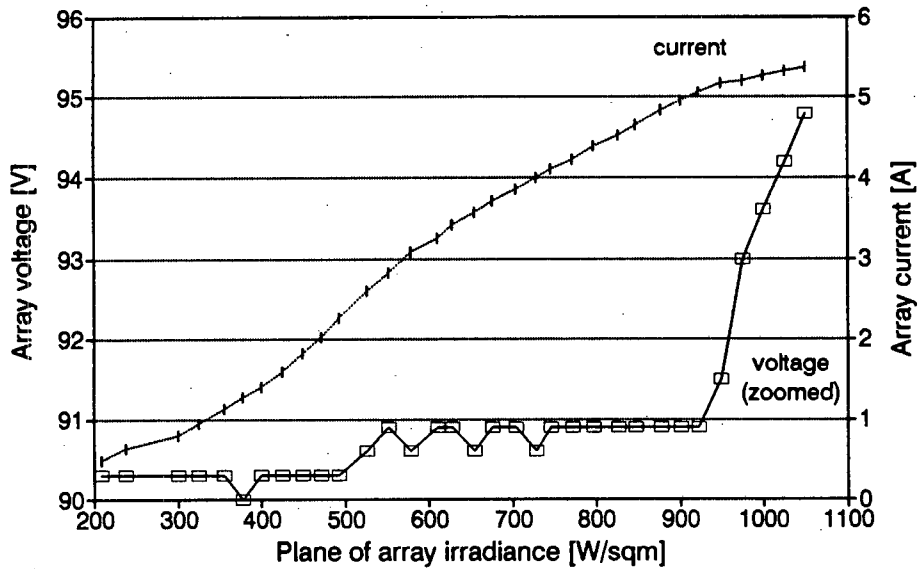


FIGURE 6.29 Miltek converter fixed voltage operation (with direct mode)

During direct mode the converter cannot control the motor speed which is then controlled by the level of irradiance. It can just observe whether the array voltage drops below the fixed voltage point. If this happens the converter starts switching again and thus regains control.

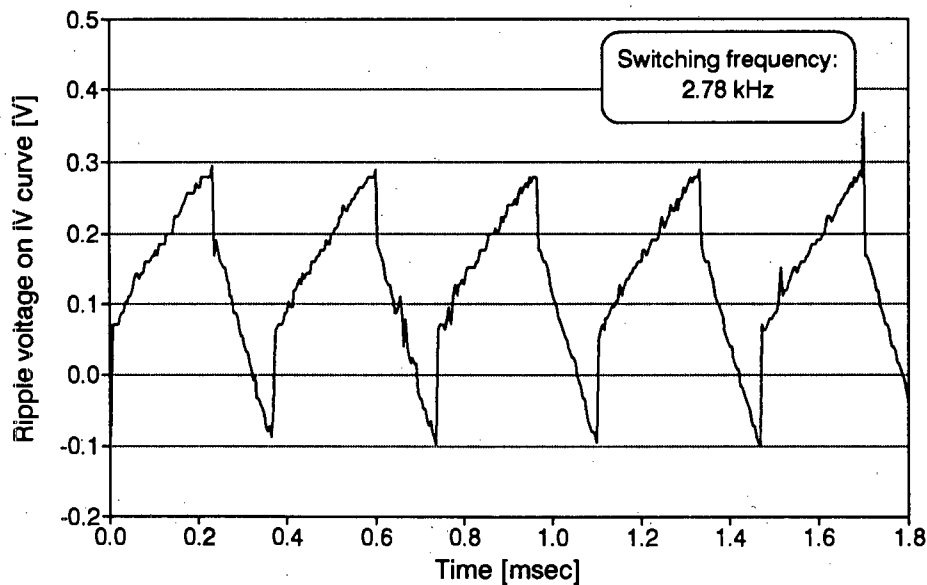


FIGURE 6.30 Ripple on the array voltage due to converter switching scheme

The input ripple due to the switching of the array voltage is shown in Figure 6.30. It has a peak-to-peak voltage of 400mV. The loss that this would cause in array power due to operation away from the MPP is less than 0.02 %. But since the converter operates in fixed voltage mode the losses due to that (discussed in subsection 6.1.3) are far higher than the losses due to the input ripple.

6.3.3 General observations

Two aspects are discussed here, namely how the converter responds to dynamic conditions and the time-delay due to a linear start-up routine in the early morning.

Dynamic conditions

An appropriate test to evaluate the dynamic capabilities of a system is to apply a step-up or a step-down to the input. That was done by disconnecting one of the two strings that were connected in parallel (array configuration: 2×6). The input power to the converter was thus halved (step-down) or doubled (step-up) instantaneously relative to its previous input power. The test result is shown in Figure 6.31.

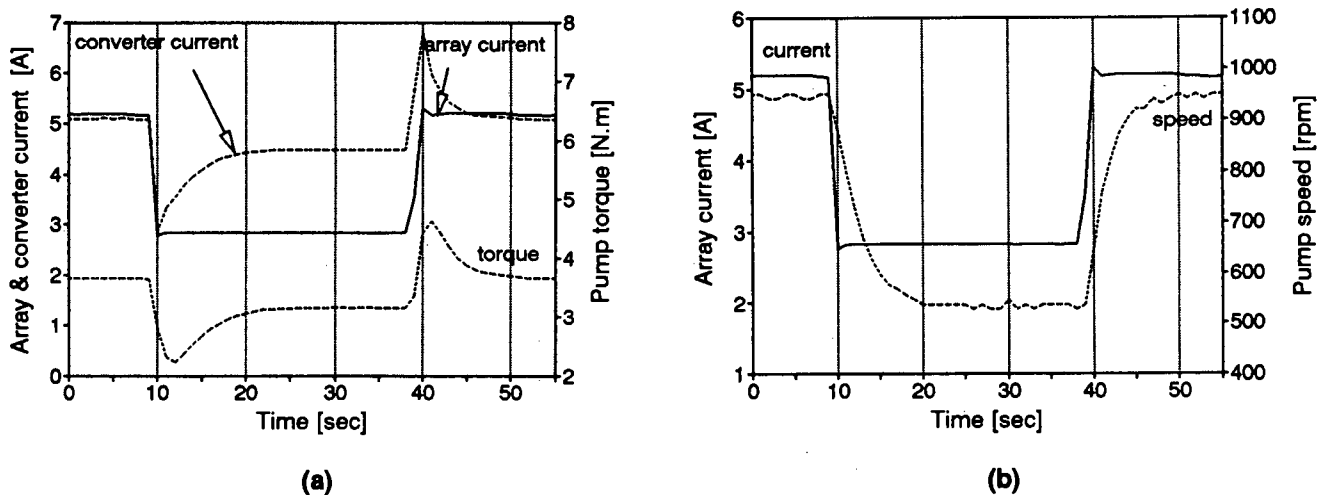


FIGURE 6.31 Response of the subsystem to an array-current step input

Both graphs display the step-down and the step-up of the array current (solid line). Graph (a) also shows the converter current and the pump torque. Both curves drop rapidly but then increase logarithmically to the torque required by the pump and the current required by the motor under the new steady state conditions. The transition of the converter current from the rapid decrease to the logarithmic increase is very sharp which shows how fast the converter responds. The transition for the pump torque is smoother. The same can be observed for the step-up. It takes the system 11sec to settle to a new steady state value. Graph (b) shows the pump speed in addition to the array current.

System start-up

The start-up of the PVP system depends on the ability of the converter to generate a large current at its output while the input current is still very small. Figure 6.32 shows the conditions at start-up as a function of time. This is the first start in the morning.

The non-zero pump speed in Graph (a) indicates when the start-up occurs, here at thirteen and a half minutes on the horizontal axis. The array current has a value of 0.88A and the array power has a value of 80W. The minimum power required from the array to keep the pump turning was measured to be 47W at 0.52A (measured as the array power decreases). From the graph this condition occurs at about 1min. It follows therefore that the system could have operated already 12min earlier if it had employed a non-linear start-up routine where it would use the energy in the input capacitors to overcome the break-away torque of the pump. The gain would be minimal, at the rate of irradiance increase shown in the graph, and in general the proportion of daily irradiation received between 50W/m² and 80W/m² is insignificant.

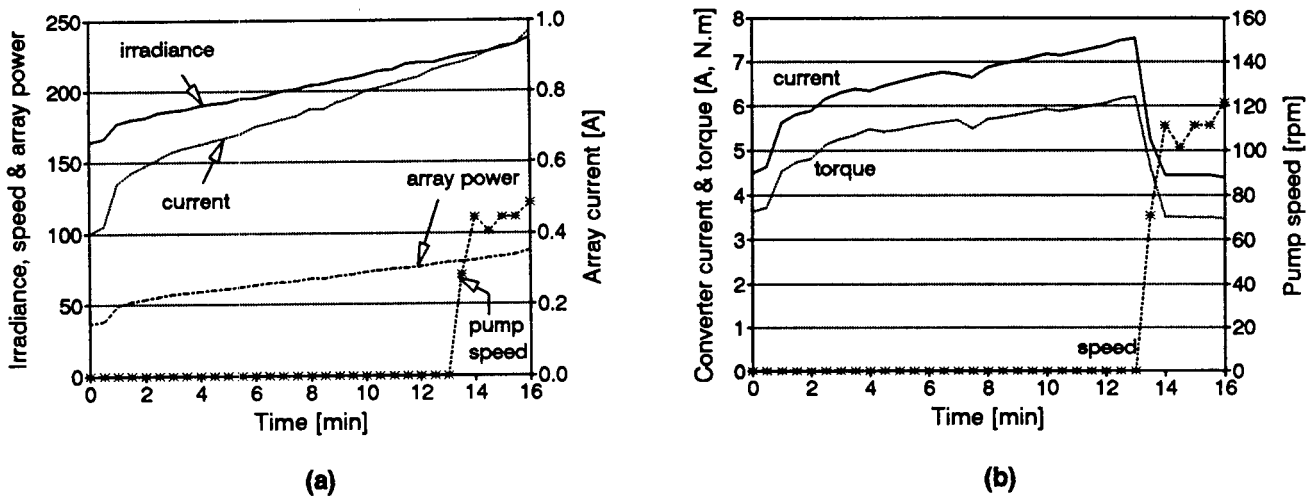


FIGURE 6.32 System status prior to start-up

Graph (b) shows the converter current and the pump torque. They increase more or less linearly after the first minute. The graph shows that the running torque is a lot lower than the start-up torque and the build-up to the start-up torque.

6.3.4 System performance

The aims of this subsection are to present the data of the Miltek PVP system and subsystem instantaneously and to present it on a daily basis for different amounts of daily solar irradiation. The daily energy efficiency of the components, the subset (controller and motor), the subsystem and the system and the volume flow are presented for standard solar days from 2kWh/m²/day to 8kWh/m²/day. The emphasis in this subsection is on the shape of the graphs more than the performance values that the system achieves. The latter will be discussed in more detail in the comparative chapter (chapter ten).

In addition, a solar irradiance profile for a single-axis tracking array has been generated, based on the solar irradiance profile in Figure 6.10. It is referred to as a tracking solar day. The system performance for a standard solar day and a tracking solar day will be compared.

Instantaneous performance

The graphs in Figure 6.33 represent the system and the subsystem performance with corresponding flowrate.

The system efficiency reaches a maximum of 4.5% from 700W/m² to 950W/m² and then decreases to 4.2% at 1060W/m². The flowrate increases in a straight line in the 700W/m² to 950W/m² region. The gradient then reduces (as the efficiency reduces) and it reaches a peak value of 950l/h at an irradiance level of 1060W/m².

The subsystem efficiency reaches a maximum of 42%. It remains above 40% for array powers of 320W to 480W.

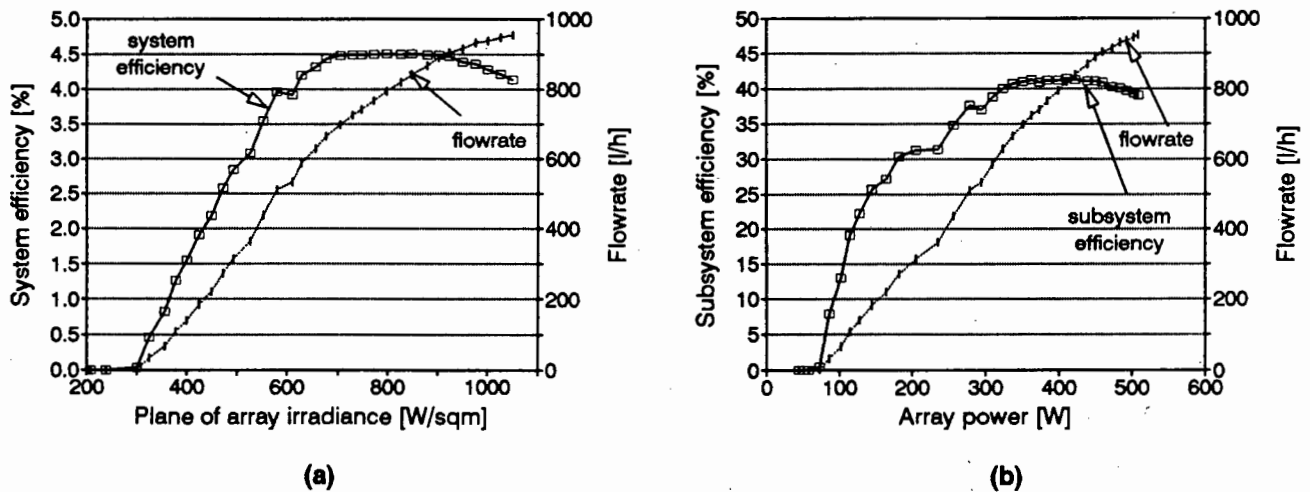


FIGURE 6.33 (a) Miltek system performance and (b) subsystem performance

The shape of the efficiency curves are similar in the upper half of the operating range. They both model the pump efficiency curve quite well in that region (refer to Figure 6.19), including the non-smooth section of the graph at 500W/m² to 650W/m² and 230W to 300W respectively which is due to the torque characteristic of the pump (refer to Figure 6.15). The first half of the system efficiency curve resembles a straight line whereas the subsystem efficiency has a more logarithmic curve (similar to the pump efficiency curve again).

The uncertainty in the system efficiency data is:

$$\begin{aligned}
 U_{abs} (\eta_{sys})_{1050W/sqm} &= 12.0\% \\
 U_{rel} (\eta_{sys})_{1050W/sqm} &= 6.9\% \\
 U_{abs} (\eta_{sys})_{750W/sqm} &= 15.7\% \\
 U_{rel} (\eta_{sys})_{750W/sqm} &= 9.4\%
 \end{aligned}$$

The uncertainty in the subsystem efficiency data is:

$$\begin{aligned}
 U_{\text{abs}} (\eta_{\text{subsys}})_{500\text{W}} &= 6.6\% \\
 U_{\text{rel}} (\eta_{\text{subsys}})_{500\text{W}} &= 2.5\% \\
 U_{\text{abs}} (\eta_{\text{subsys}})_{350\text{W}} &= 6.7\% \\
 U_{\text{rel}} (\eta_{\text{subsys}})_{350\text{W}} &= 2.8\%
 \end{aligned}$$

The uncertainty in the flowrate data is:

$$\begin{aligned}
 U_{\text{abs}} (Q)_{200 \rightarrow 1000\text{lh}} &= 6.1\% \\
 U_{\text{rel}} (Q)_{200 \rightarrow 1000\text{lh}} &= 2.2\%
 \end{aligned}$$

The subsystem efficiency proves to be the most reliable data for comparison since the absolute efficiency only reaches 6.7% at two thirds of the input power. The system efficiency is largely dominated by the errors that can occur in the pyranometer.

Daily energy efficiency performance

The profile of the standard solar day (SSD) and tracking solar day and the method of calculation that was used to derive the data that follows below are presented in appendix A5.

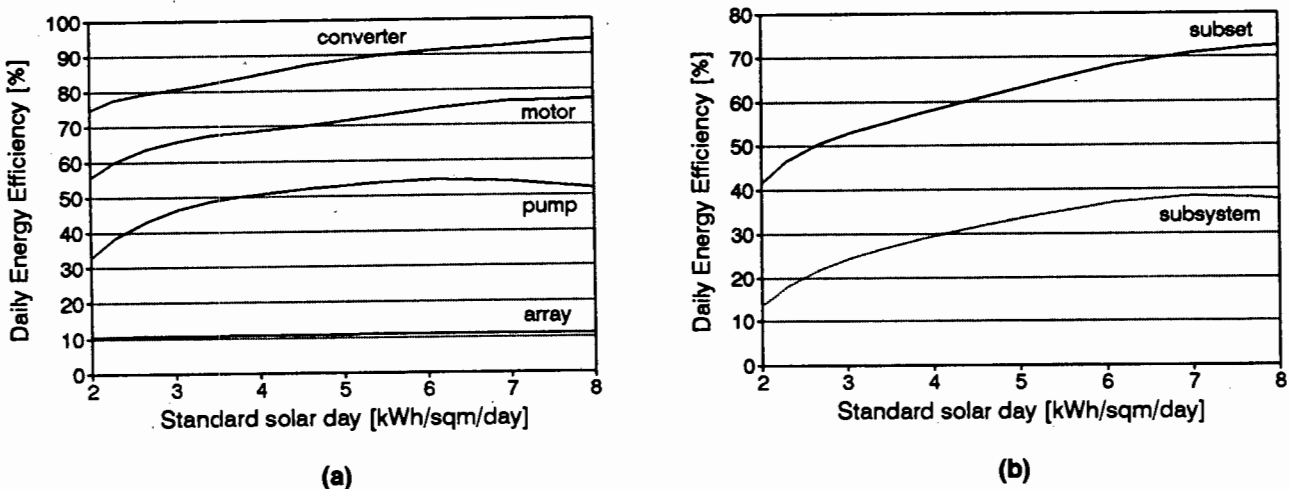


FIGURE 6.34 Miltek system daily energy efficiency (a) system components and (b) subset and subsystem

The daily energy efficiency (DEE) of the components is displayed in Graph (a) of Figure 6.34. The array maintains an efficiency of more than 10% from 2kWh/m²/day to 8kWh/m²/day (the instantaneous array performance data was only used from 600W/m² to maximum irradiance levels, below 600W/m² was assumed to be constant since data in that region was unreliable as discussed in section 6.1). The DEE of the converter progresses from steeper to flatter gradients but is still rising at 8kWh/m²/day having reached a value of 94.3%. The motor reaches a nearly constant value at 77% with little tendency to increase. The DEE of the pumping set reaches a peak of 54.4%

at a SSD of 6.1kWh/m²/day. It then starts decreasing since the instantaneous efficiency curve of the pumping set decreases after reaching a maximum of 56%.

The DEE of the subset (controller and motor combined) and the subsystem are shown in Graph (b) of Figure 6.34. The subset efficiency maintains a positive gradient over the whole simulated daily energy range. It reaches 72.5% at a SSD of 8kWh/m²/day. The DEE of the subsystem reaches a peak of 38.3% at 7kWh/m²/day and then decreases. This is due to the pump performance and occurs at higher SSD values (as opposed to 6.1kWh/m²/day) since the subset efficiency is still increasing.

The DEE of the system reaches a peak of 4.18% at 7kWh/m²/day and consequently decreases for the same reason that the DEE of the subsystem decreases. This is shown in Figure 6.35. The volume-flow is fairly linear and delivers 7.3m³ for a 8kWh/m²/day SSD.

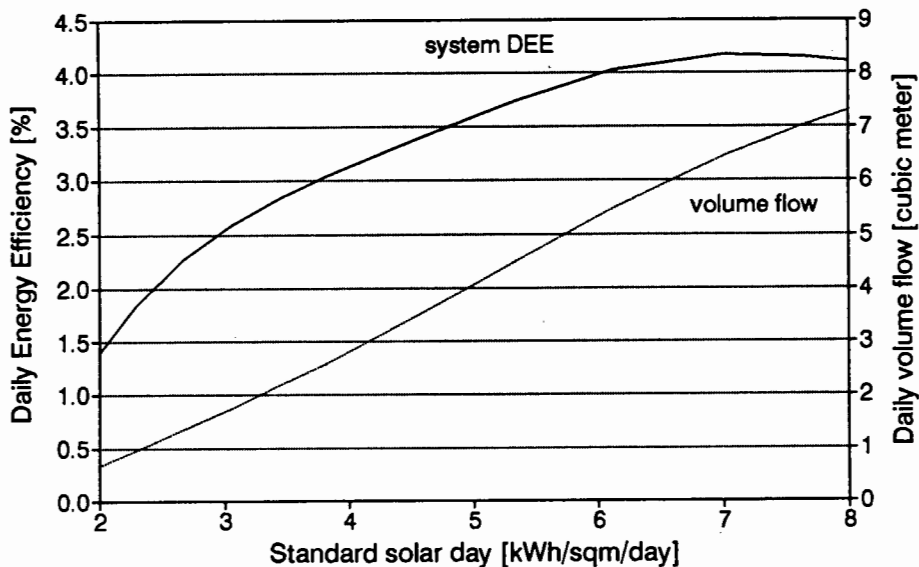


FIGURE 6.35 Miltek system daily energy efficiency and daily volume flow

As explained in appendix A5 the tracking solar day (TSD) is evaluated to observe whether a tracking array will bring the three phase PVP system performance relatively closer to the DC PVP system. It is also evaluated to observe the relative gain between a fixed array and a tracking array for each individual system.

Graph (a) in Figure 6.36 shows the comparison between a TSD and a SSD. It displays the graphs for the DEE of the system and the accumulated flow over the day. The system DEE has a fixed difference of about 0.3 percentage points over most of the different daily operating profiles. The difference reduces to 0.06 percentage points for high noon peak irradiance levels. This is due to the relatively large reduction of the pump efficiency at these high input power levels.

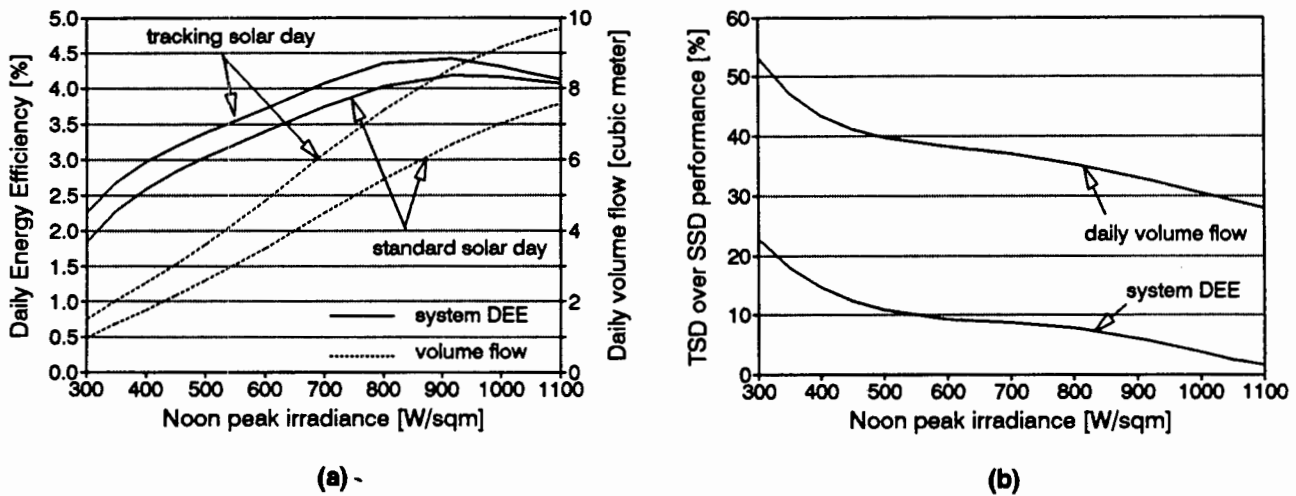


FIGURE 6.36 Tracking solar day and standard solar day for Miltek system DEE and volume flow: (a) performance and (b) percentage of TSD over SSD

Graph (b) shows the percentage difference between the SSD and the TSD by using the SSD as the base value and evaluating the percentage value by which the TSD exceeds the SSD. The difference between the TSD and the SSD becomes larger as the noon peak solar irradiance decreases. At 1100W/m² daily peak irradiance the DEE of the system under TSD conditions exceeds the SSD condition by about 1.5% whereas the volume-flow exceeds it by about 28%. These values increase as the energy content of the different profiles decreases. At 800W/m² daily peak irradiance the TSD DEE of the system exceeds the SSD DEE by 7.5% and the volume flow by 36%. The shape of these two graphs is as expected since the efficiency at lower irradiance levels is poorer and the SSD.

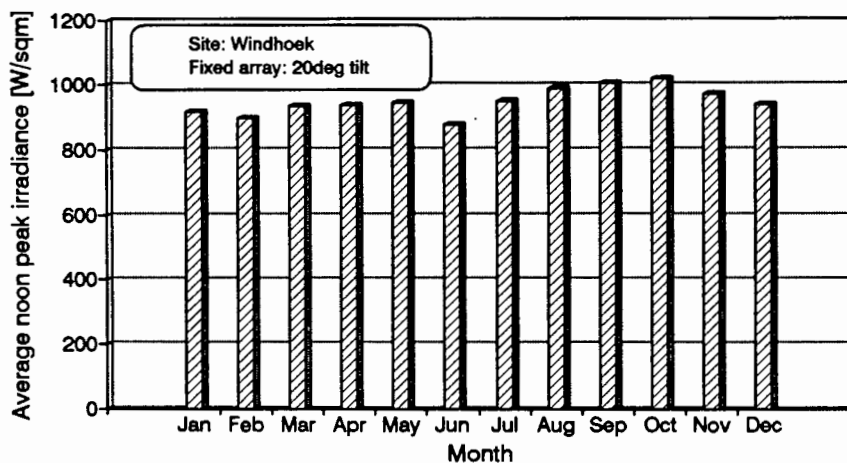


FIGURE 6.37 Average noon peak irradiance on a tilted surface at Windhoek

Figure 6.37 shows the average noon peak irradiance levels received at Windhoek on a 20° tilted surface over a year. The noon peak irradiance was calculated from long term recordings of the global and diffuse irradiance components using the program Solar Tilt (Cowan 1992).

Chapter Seven

SOLVO SYSTEM PERFORMANCE ANALYSIS

The chapters on the prototype inverters (chapters seven and eight) each stand on their own and can be read independently of one another. Because of this there is a small amount of duplication with the result that some introductory paragraphs are the same or similar.

This chapter presents and discusses the Solvo inverter and motor efficiency, the steady state array operating point characteristics, the dynamic array operating point characteristics, the voltage to hertz relation, the control algorithm characteristics and general observations on the system. This is followed by the instantaneous system and subsystem performance evaluation and by the daily energy efficiency evaluation of the components and the system.

The derivation of the absolute and relative uncertainty in the acquired data is presented in appendix A3.6. The derivation of the stated uncertainty in the efficiency data is given by an example in appendix A3.7. All uncertainties are stated as a plus-minus percentage of a full-scale reading.

System tuning

The system was tuned with regards to the array operating voltage (it is a fixed voltage point algorithm) and the pulley size. In addition two programs were available that contained different voltage to hertz relations, therefore had different start-up and different operating characteristics.

The voltage point was fixed to a steady state value of about 182V. This was found to be close to the MPP at cell temperatures of 47°C (refer to Figure 6.8). Average module temperatures were in the region of 40°C (windy conditions) to 55°C (no wind) on a sunny day during March to May.

The choice of motor pulley was guided by two criteria (the pulley of the discharge head assembly remained the same for all tests, being 247PCD):

- the inverter should be able to just reach its programmed maximum output frequency at the maximum irradiance level
- the start-up time delay should be minimised

The choice was between a pulley size of 85PCD (pitch centre diameter), 97PCD and 112PCD. The smallest pulley managed to reach its maximum output frequency (85Hz) before reaching the maximum irradiance level. The 112PCD pulley would delay the start-up due to slightly higher torque requirements from the motor and so it was

decided to choose the 97PCD pulley which nearly managed to reach the full output frequency at full irradiance making it the most suitable pulley.

Two programs with different voltage to hertz relations were generated using a Turbo-Pascal program written by Hirschmann (1989b). The graphs are shown in Figure 7.1. One program had a linear relation between the voltage and the frequency with a voltage boost near zero hertz (referred to as the linear program) and one program had a square-root relation between the voltage and the frequency, also with a voltage boost near small frequencies (referred to as the log program). The square-root relation was adapted from Davies' (1992) dissertation and scaled to the output voltage range and frequency range of the Solvo inverter. This was not necessarily optimal but offered the most practical solution in the circumstances at hand during the field tests (which is where the voltage to hertz relations were programmed into EPROM's).

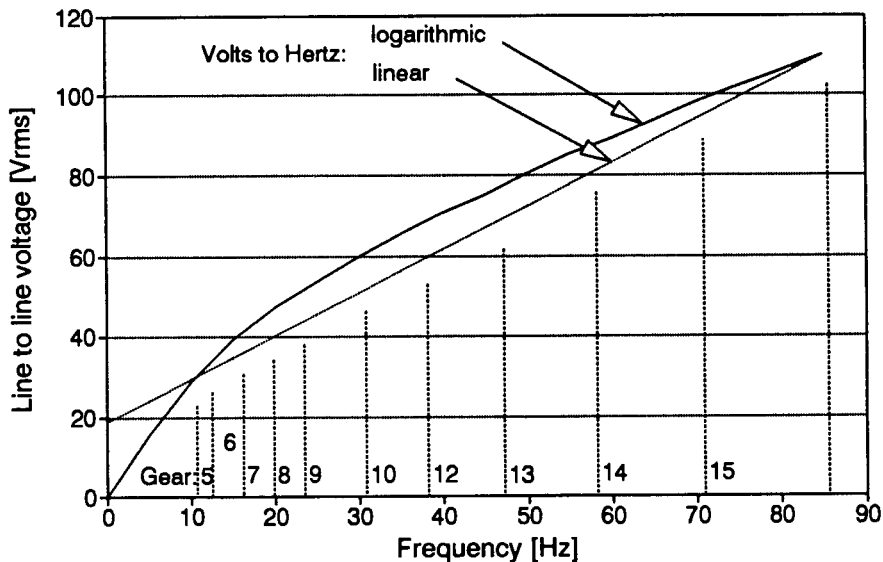


FIGURE 7.1 Linear and logarithmic voltage to hertz relation

The choice of voltage to hertz relation was guided by two criteria:

- the program should drive the inverter-motor subset most efficiently resulting in an optimised pump speed over the full operating range
- the program should result in as early a start-up as possible

It was found that the subset efficiency with the log program at low array power (100W to 200W) was better by an average of 6% than the linear program. In the mid-operating region (250W to 350W) the linear program proved to have a better subset efficiency than the log program, the average difference being 3%. Towards the full operating input power (350W to 550W) the efficiencies were similar. The log program resulted in a slightly higher pump speed (15 rpm on average) than the linear program. It was also found that the log program operated better in the low input power region. It runs more smoothly and has a lower start-up and cut-out threshold. Therefore the choice was for the log program.

7.1 Inverter and motor performance

This section deals with the inverter, the motor and the subset efficiency at standard and simulated higher head as well as with the characteristic inverter and motor curves.

7.1.1 Efficiency at standard head (75m)

The inverter efficiency includes the losses due to the dynamic array operating point characteristics (as will be discussed in section 7.3). It does not include the losses due to steady state operation away from the MPP. It also does not include the mismatch losses between the inverter and the motor which are caused by the harmonics in the current waveform. These losses are included in the motor efficiency.

The uncertainties in the efficiency results are stated at the end of each discussion.

The inverter efficiency is evaluated over an input power range of 150W to 540W. The inverter starts operating at an input power of about 110W. Figure 7.2 shows the first data point at an array power of 150W with an efficiency of 31%. The efficiency rises to 84% over the input power range from 150W to 360W. It then stays constant at 84% up to 540W.

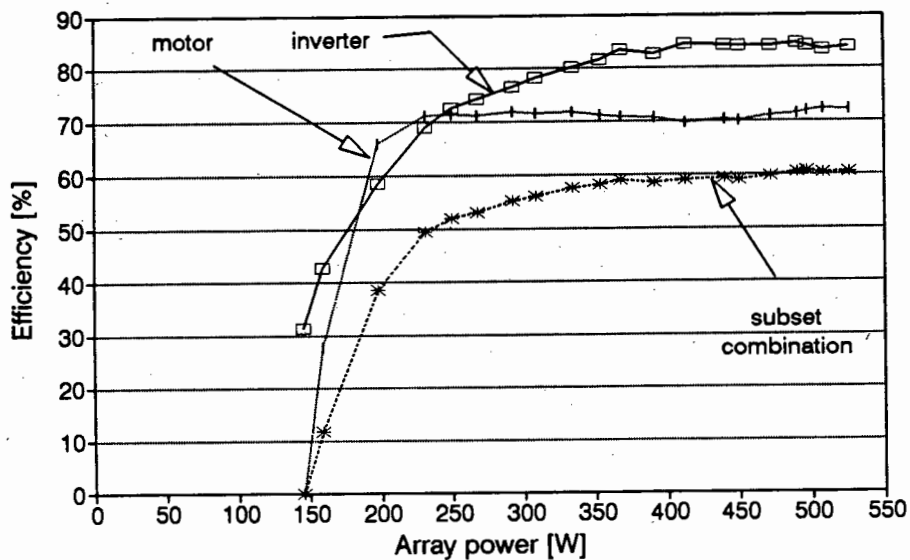


FIGURE 7.2 Solvo inverter, motor and subset efficiency versus input power.

The uncertainty in the inverter efficiency data is:

$$\begin{aligned}
 U_{\text{abs}} (\eta_{\text{inv}})_{500\text{W}} &= 8.4\% \\
 U_{\text{rel}} (\eta_{\text{inv}})_{500\text{W}} &= 5.3\% \\
 U_{\text{abs}} (\eta_{\text{inv}})_{250\text{W}} &= 19.2\% \\
 U_{\text{rel}} (\eta_{\text{inv}})_{250\text{W}} &= 12.3\%
 \end{aligned}$$

The inverter losses decrease from about 100W at 150W input power to about 65W and then increase to 85W at 540W input power as can be seen in Figure 7.3. The losses can be divided into constant and varying losses. The constant losses consist of the power supply losses (comparatively small since the inverter uses a switch-mode power supply), microcomputer power requirements and the drive circuit power requirements. The drive circuit is quite intricate as the PWM signals are modulated with a carrier, then amplified in two stages and coupled across HF transformers. This will require more power than conventional drive circuits. The constant losses have been measured to be about 18.6W ($216V \times 0.086A$) but will be taken as 20W.

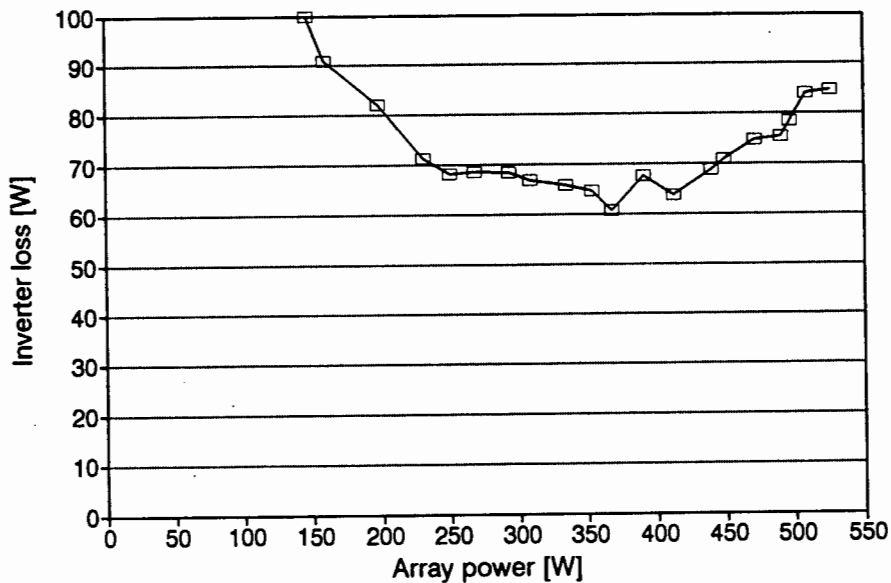


FIGURE 7.3 Solvo inverter losses

The varying losses are the switching losses and the conduction losses. The switching losses can be calculated (Hexfet Power MOSFET Designers Manual 1987: I-141) from the linearised current switching waveform (which has not been sampled on the oscilloscope). The essential parameters are the array voltage (here constant), the line current and the time base. This results in the energy lost during switch-on and switch-off (it is likely to be very small since the current ripple on a high switching-frequency generated current waveform is small). This value is multiplied by the switching frequency to evaluate the losses in one phase. Therefore the switching losses vary linearly with changes in switching frequency. The switching frequency of the inverter changes within a major gear since the inverter changes the output frequency through changing the switching frequency. The average switching frequency within a major gear has been programmed to decrease from about 15.5kHz at low fundamental frequency (10Hz to 30Hz) to 11.2kHz at high fundamental frequency (70Hz to 85Hz). The tendency is therefore for the switching losses to decrease.

The conduction losses in one leg of the three phase bridge are a function of the on-state resistance of one MOSFET and the line current that is passing through it as well as the power dissipated in the source-drain diode of the other MOSFET (which is turned off). These losses can be calculated (Hexfet Power MOSFET Designers Manual

1987: I-145) if the line current, the power factor, the on-state resistance and the diode forward voltage-drop are known. The conduction losses are varying because the torque requirements of the pump are not constant. Therefore the conduction losses will somewhat follow the shape of the line current with a minor peak at 250W input power and another higher peak at the end of the operating range.

None of the varying losses have been measured but the conduction losses can be calculated as mentioned. That will give an idea of the switching losses. The conduction losses are equal to:

$$3 \times [0.462 \times \text{pf} \times I_{\text{peak}}^2 \times R_{\text{DSon}} + \text{LF} \times 0.068 \times I_{\text{peak}} \times V_{\text{SD}}] = 9\text{W to } 14.8\text{W}$$

for $\text{pf} = 0.4$ (estimated), $R_{\text{DSon}} = 0.32\Omega$, $I_{\text{peak}} = 6\text{A to } 8\text{A}$, $\text{LF} = 3$ (load factor, from HEXFET manual) and $V_{\text{SD}} = 0.7\text{V}$). The constant losses were measured to be 20W. Therefore the total losses excluding the switching losses would be 29W (low input power) to 35W (high input power). The switching losses would therefore have a magnitude in the range of 71W (at low fundamental frequency) to 50W (at high fundamental frequency) which is relatively high. The inverter losses have a low between 350W to 450W (that is, they are below 70W) which is where the line current is the lowest.

The occasional bumps in the curve will stem from the relatively large changes in voltage from one major gear to another, from variations in the switching frequency and from the load characteristics of the pump (see Figure 6.15).

The motor efficiency (Figure 7.2) rises sharply to 72% at an array power of 230W and remains there to the end of the operating range with a slight dip to 70%. The specifications for the motor are only available at 50Hz with input powers exceeding the operating range under which the motor was tested. Nevertheless, at 530W input power (50Hz and line voltage = 70V) the specified motor efficiency reaches 75.6% and 73% for 110V line voltage. The motor therefore comes very close to the specifications, reflecting the low harmonic content in the current waveform since the inverter switches at very high frequencies. The motor dissipated very little heat which is an indication that the present harmonic energy was small. It is surprising though that the efficiency curve is so flat. One usually does not expect the motor efficiency to be good at low input powers. The motor was specifically designed for small power applications by GEC. I would not be able to explain why the motor exhibits such a good efficiency at low input power.

The uncertainty in the motor efficiency data is:

$$\begin{aligned} U_{\text{abs}} (\eta_{\text{mot}})_{420\text{W}} &= 9.2\% \\ U_{\text{rel}} (\eta_{\text{mot}})_{420\text{W}} &= 6.6\% \\ U_{\text{abs}} (\eta_{\text{mot}})_{250\text{W}} &= 14.5\% \\ U_{\text{rel}} (\eta_{\text{mot}})_{250\text{W}} &= 9.8\% \end{aligned}$$

The subset efficiency of the inverter and motor combined shown in Figure 7.2 reaches 50% at 230W input power and reaches about 60% at 370W input power where it remains. The subset efficiency is the most important gauge in terms of the efficiency evaluation of inverter and motor for the following reason: Inverter efficiency can be increased by decreasing the switching frequency. This results in a higher current ripple on the line current with effect of increased motor heating and consequently a reduced motor efficiency. The aim is therefore to find the maximum efficiency of the combination as a function of the switching frequency if such a switching frequency exists. From a measurement point of view, the uncertainty in the subset efficiency is lower than the uncertainty of the inverter or motor efficiency.

The uncertainty in the subset efficiency data is:

$$\begin{aligned}
 U_{\text{abs}}(\eta_{\text{subset}})_{500\text{W}} &= 4.5\% \\
 U_{\text{rel}}(\eta_{\text{subset}})_{500\text{W}} &= 4.2\% \\
 U_{\text{abs}}(\eta_{\text{subset}})_{250\text{W}} &= 5.3\% \\
 U_{\text{rel}}(\eta_{\text{subset}})_{250\text{W}} &= 4.9\%
 \end{aligned}$$

7.1.2 Efficiency at higher heads

The result for the subset efficiency at different head is shown in Figure 7.4. Unfortunately only two sets of the acquired data were valid. The one head is at 75m and the simulated head is at 105m (by using a larger pulley).

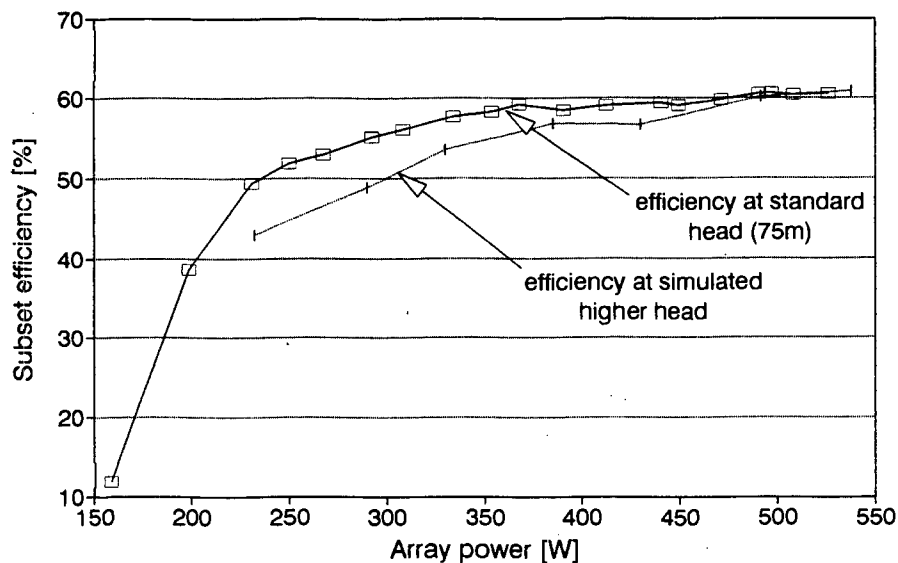


FIGURE 7.4 Solvo subset efficiency at one higher simulated head

The graph shows that the subset efficiency at higher head is lower in the low input power region but reaches the same efficiency towards the end of the operating range. The inverter efficiency decreases due to higher current requirements from the motor. This will result in higher conduction and switching losses which are a function of the current squared and the current magnitude and shape respectively.

An improvement in the motor efficiency while operating along a new load curve (that is higher head, or different pulley size) is mainly dependent on how optimally it is driven by the inverter in terms of its voltage to hertz relation and harmonic content. A number of parameters have to be known to make a comment on this. However these are not available.

The inverter and motor efficiency are likely to improve if, for example, the array was doubled in size to 24 modules (two strings of 12 modules in series) since only the variable losses would increase assuming that a larger motor pulley would be used. The subset efficiency of the simulated higher head shows this trend in that it reaches the same efficiency at high input powers and would probably increase beyond the 75m subset efficiency if more power was available.

7.1.3 Characteristic inverter and motor curves

The characteristic curves of the inverter and the motor under these particular load conditions are shown in Figure 7.5.

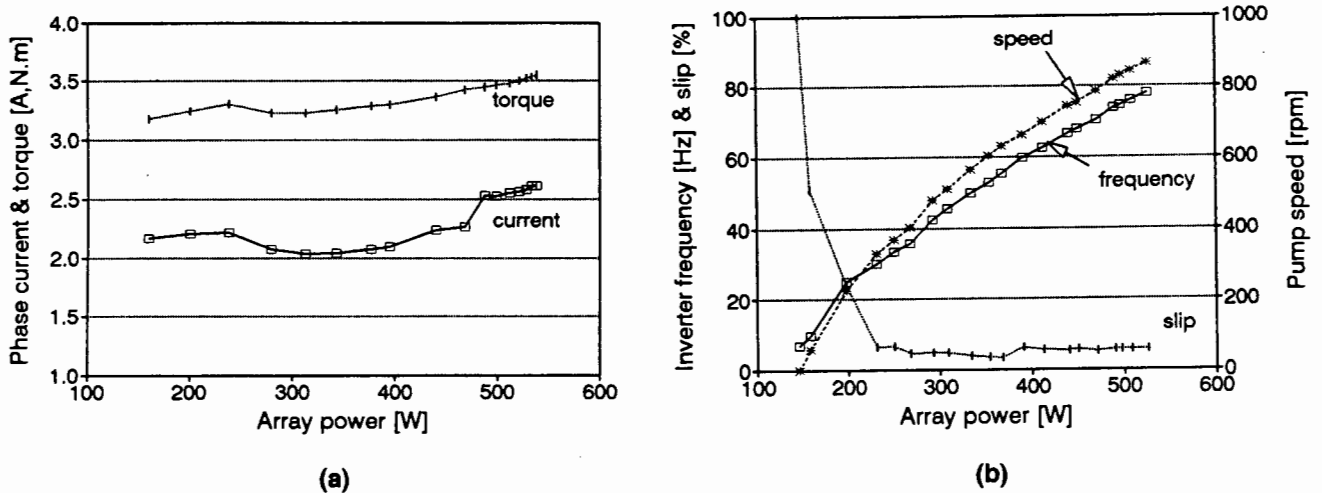


FIGURE 7.5 Characteristic subsystem curves: (a) Phase current and pump torque; (b) frequency, slip and pump speed

The inverter current follows the pump torque curve quite closely (graph a). The discontinuity at about 480W array power is due to a large change in inverter output voltage (from major gear 14 to 15).

The frequency (Figure 7.5b) follows a reasonably straight line (with a tendency towards a logarithmic shape) and the slip between the inverter frequency and the rotor of the motor drops rapidly from 100% to 5%. The slip is 100% at 140W array power since the rotor has not started turning yet. The pump speed curve has a similar shape to the frequency curve which is to be expected.

The inverter voltage has been omitted due to large measurement uncertainties.

7.2 Steady state array operating point characteristics

The Solvo inverter offers one type of control algorithm namely fixed voltage operation (FVO). Under steady state conditions the average array voltage showed that FVO was implemented well as can be seen in Figure 7.6.

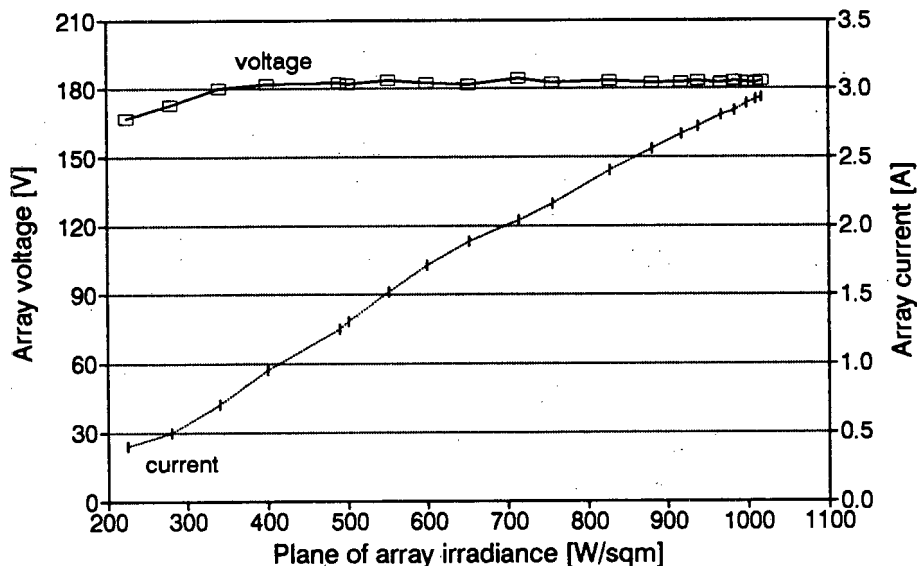


FIGURE 7.6 Fixed voltage operation of Solvo inverter

This shows the average array voltage and the average current as a function of the irradiance. Towards low levels of irradiance the inverter loses its operating point and the array voltage decreases.

7.3 Dynamic array operating point characteristics

The mean array voltage proved to remain close to the set-point to which it was tuned. However the instantaneous voltage had quite a large movement about that mean value. As this could result in a diminished array output and can have a negative impact on the motor performance the effect of this array voltage oscillation is analysed here.

It is common for switch-mode inverters to have a ripple voltage on the DC-side input which is due to the switching scheme employed by the inverter. The magnitude of the ripple is dependent on the switching frequency of the inverter (inversely related). Its frequency is the same as the switching frequency. However, the ripple discussed here (referred to as an oscillation voltage) is the result of the type of control algorithm implemented in the inverter (a detailed analysis of the control algorithm is in section 9.1). This section purely evaluates the impact of the oscillation voltage on the array performance and on the shape of the PWM inverter output signal. The effect of a larger input capacitance on the array voltage oscillation is also evaluated.

7.3.1 Shape of oscillation waveform

The typical oscillation waveform at the input to the Solvo inverter is displayed in Figure 7.7. This waveform is riding on the mean array voltage as shown in Figure 7.6.

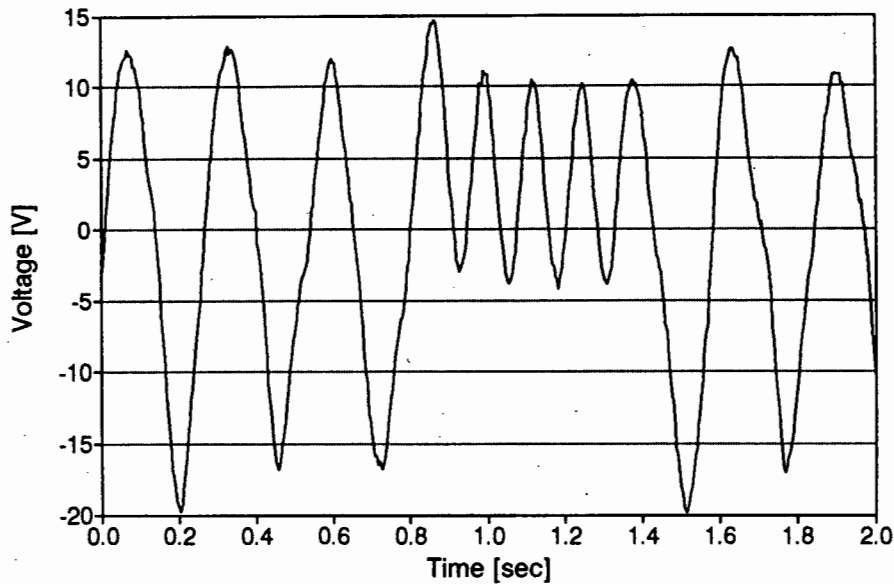


FIGURE 7.7 A typical array voltage oscillation waveform riding on $182V_{arr}$

The oscillation waveform has sine-wave characteristics. It has two distinctive waveforms that differ in amplitude and frequency. One waveform has a peak-to-peak amplitude of about 20V to 30V at a frequency of 3.8Hz and the other waveform has a peak-to-peak amplitude of 10V to 15V at a frequency of 7.6Hz (approximately double the other waveform). No statement can be made whether the one or the other waveform occurs more or less often at particular operating conditions. The waveforms do not change significantly with changes in input power. The waveform can also contain a ripple at the switching frequency of the inverter. This occurs mainly near low input power levels. The amplitude of the waveform increases if the FVP is moved to the left of the MPP and decreases if the FVP is moved to the right of the MPP. The shape of the waveform remains unaltered.

7.3.2 Array power losses

In order to assess the impact of the oscillation on the array output, the waveforms from above were superimposed on the steady state array operating point by using information of a characteristic array power curve. The method of calculation is described in appendix A6.

Figure 7.8 shows the result of this procedure. The two lines represent the two oscillation waveforms displayed in Figure 7.6. The peak-to-peak amplitude is varied by scaling the oscillation voltage amplitude. The operating point on the array is at MPP. Therefore the percentage power loss is zero at oscillation amplitude of zero. The windows display the most commonly found peak-to-peak amplitudes of the oscillation.

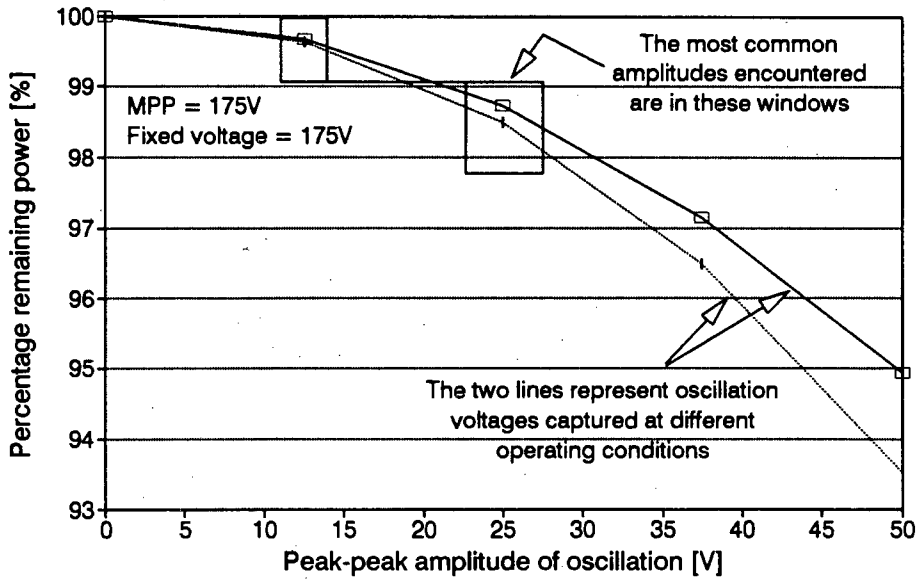


FIGURE 7.8 Percentage of remaining array power versus a range of oscillation waveform amplitudes while operating (on average) at MPP

Power losses of half a percent for the small oscillation waveform and one-and-a-half percent for the large oscillation waveform can be expected.

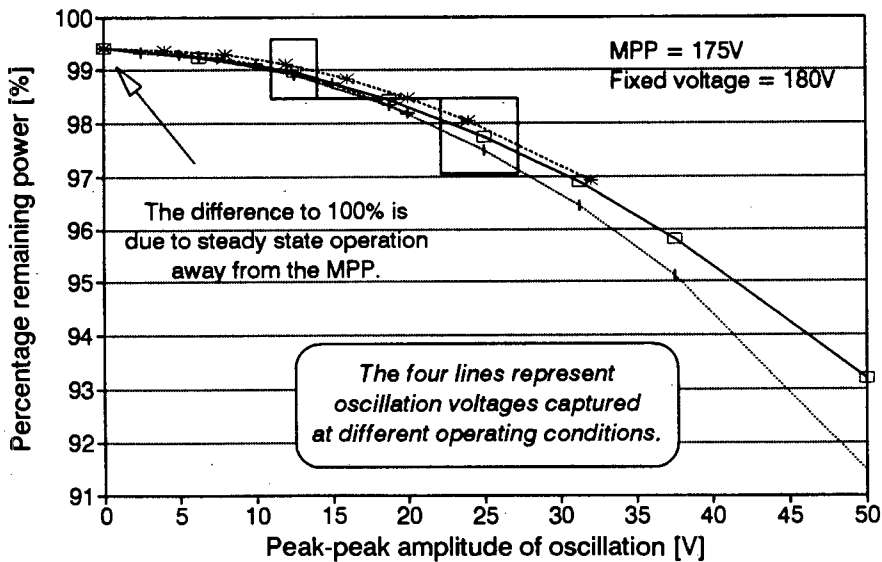


FIGURE 7.9 Percentage of remaining array power versus a range of array voltage oscillation amplitudes while operating (on average) 5V to the right of MPP

Figure 7.9 shows operation away from the MPP by +5V. The power loss for that alone is about 0.6%. The graph displays four different oscillation waveforms that were sampled. The lines diverge only slightly. The windows indicate the most common amplitudes.

It is interesting to observe the effect on the power loss when the operating point on the array is moved to higher and lower voltages with respect to the MPP. This is shown in Figure 7.10. The MPP is at 175V. Two operating points are chosen in symmetrical pairs around the MPP namely 170 & 180V and 165 & 185V. The graph shows that the power loss at higher array operating voltage is larger than at operating points below the MPP voltage. This is to be expected due to the shape of the array power curve. At really large oscillation amplitudes (25V and more) the power loss is less at lower array operating voltages than at the actual MPP voltage (cross-over is indicated by ellipses). This is due to the disproportionately larger power losses on the right-hand side of the power curve. They will therefore exceed the losses incurred by operating to the left of the MPP.

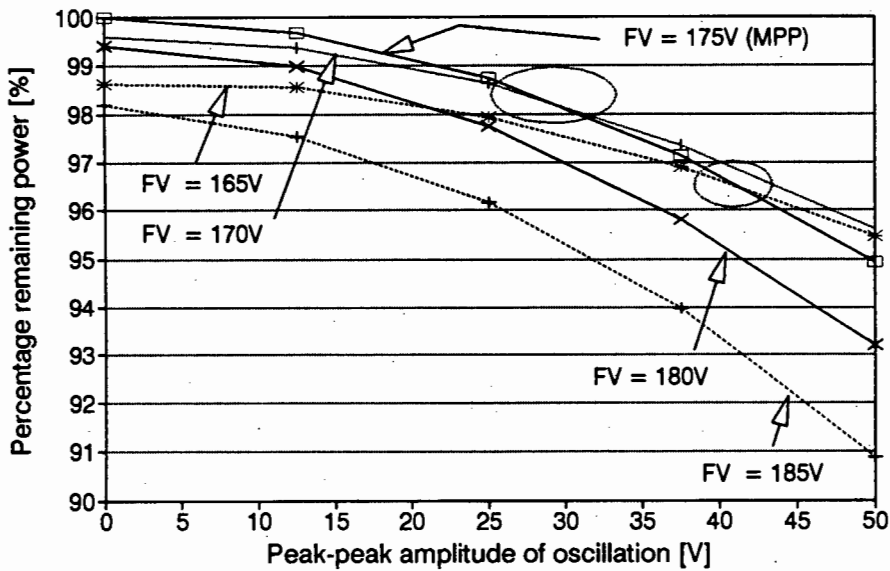


FIGURE 7.10 Percentage remaining array power versus the same array oscillation waveform but oscillating around different operating points

The measurements of the array current and voltage, as they have taken place, are equivalent to the situation of zero amplitude oscillation waveform (refer to Figure 7.8 and 7.9). The array output would have to be derated by the difference in power loss between zero amplitude and actual amplitude. The inverter efficiency would have to be increased by a factor as its input power is actually less than measured. This was not done since the losses incurred are due to the particular operating characteristics of the inverter. The losses are treated like mismatch losses but are evaluated with the inverter rather than the array.

7.3.3 PWM envelope

The PWM output voltage of the inverter will be characterised with the same oscillation voltage as on the array voltage. This means that the pulse height which is equivalent to the magnitude of the array voltage will vary in the same manner as the array voltage. However, the time base of the array oscillation and the inverter switching frequency are very different.

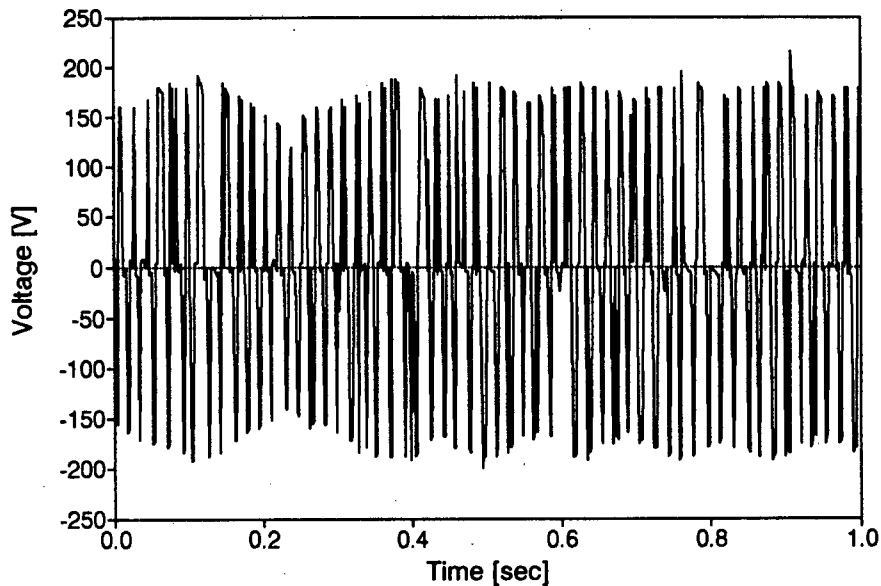


FIGURE 7.11 PWM envelope curve of the Solvo inverter

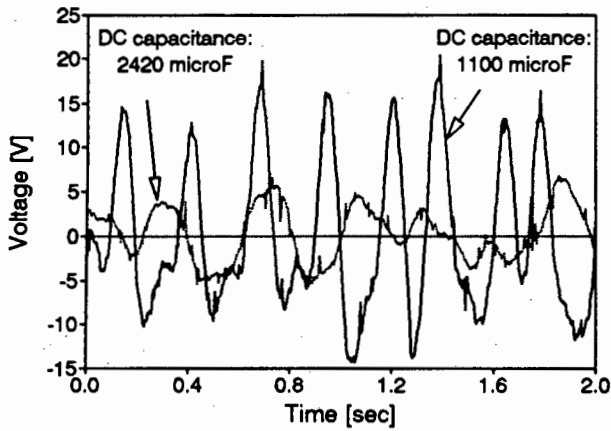
This can be seen in Figure 7.11 where the array voltage oscillation is superimposed on the envelope curve of the PWM voltage (one line in the graph contains the PWM pulses for half a period - they are merged due to lack of resolution for this time-base).

7.3.4 Effects of increased input capacitance

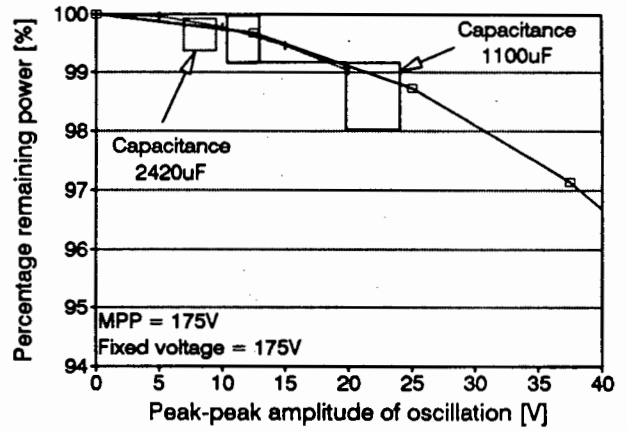
The input capacitance was increased from 1100 to 2420 μF . This has the effect of damping the system by presenting the inverter with a more stable voltage supply. The previous tests were then repeated at the same conditions. Only one shape of oscillation waveform was observed. Graph (a) shows two oscillation waveforms operating across different sized capacitors and graph (b) shows the calculated array losses due to the particular range of amplitudes that each waveform occurs in.

The oscillation peak-to-peak amplitude is reduced from around 25V and 15V to 10V as can be seen in Figure 7.12. The frequency of the oscillation has decreased.

The power extraction from the array improves from $98.7\% \pm 0.3\%$ to $99.6\% \pm 0.2\%$ at MPP as shown in Figure 7.12. This also has the effect of decreasing the envelope voltage on the PWM signal but that data is only available for the MLT system (Figure 8.11 and 8.14).



(a)

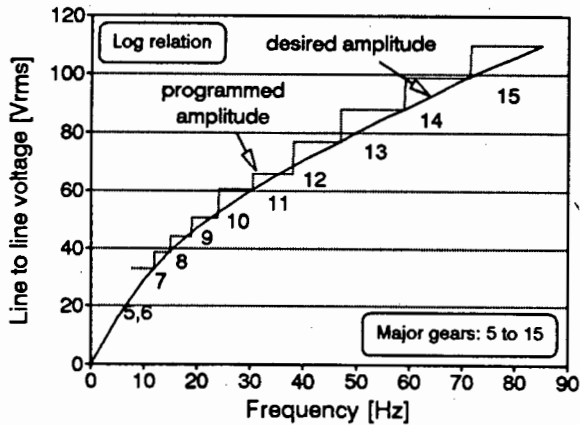


(b)

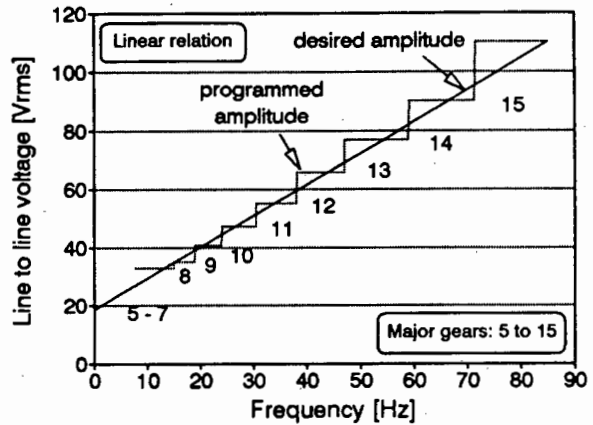
FIGURE 7.12 Effects of larger DC input capacitance: (a) array oscillation waveforms; (b) percentage remaining array power

7.4 Voltage to hertz relation

As pointed out in chapter five a considerable amount of difficulty was experienced with the rms voltage measurement. Nevertheless, a few points can be discussed without proper knowledge of the signal and some points can be discussed in comparison.



(a)



(b)

FIGURE 7.13 Programmed voltage to hertz relation: (a) logarithmic relation; (b) linear relation

A lot of care was taken to find a suitable and well performing Voltage to Hertz (V/Hz) relation. The voltage boost at low frequency was selected by trial and error and the general V/Hz relation was based on two approaches. One approach is the linear relation which was taken from textbooks and is quite a standard approach, referred to as sub-synchronous V/Hz relation, or here as the linear V/Hz relation. The other approach was taken from the dissertation of Davies (1992). Davies found the parameters of the motor under test and derived an equation to approximately minimise the losses of the motor over the complete operating range. The result was a V/Hz relation where the voltage was proportional to the square-root of the frequency. This is referred to as the logarithmic relation. The voltage amplitudes that were programmed are shown in Figure 7.13.

As can be seen from the graphs the program runs through 10 major gears. It receives a new amplitude for each major gear and uses that amplitude for all sixteen frequency steps within each major gear. The resolution in terms of voltage amplitudes is therefore low and consequently undermines the effort of deriving an optimum V/Hz relation.

The frequency range of both programs is 6Hz to 85Hz. The advantage of that is the ability to choose a smaller motor pulley resulting in lower torque requirements from the motor under the same load conditions. In addition the system will be able to run over longer periods of the day. The program cannot overmodulate which is not essential here as sufficient voltage is available from the array.

The array voltage oscillations, as discussed previously, are projected directly on the PWM voltage at the output of the inverter and can be found through the envelope curve of the PWM signal (see Figure 7.11). The PWM voltage will have amplitude variations in the range of 15V to 30V around 180V (see oscillation voltage in Figure 7.7) resulting in rms voltage variations of 4.2% ($7.5V/180V$) to 8.4% ($15V/180V$).

7.5 Observed control algorithm characteristics

A number of observations have been made on the performance of the control algorithm and especially on situations where the algorithm does not perform as expected. The observations will be described here. Proposals towards overcoming some of the control algorithm problems are made in chapter nine.

Basic control algorithm implementation

The array voltage oscillations as were discussed in section 7.3 are the result of a too simplistic control algorithm that does not take account of the settling time of the system. A thorough description and proposed solutions are given in section 9.1 as both inverters have the same problem.

Stuck motor drive

During normal, continuous operation, the system responds to variations in irradiance levels as expected. When the irradiance drops to a particularly low level (due to a thick cloud for example) it causes the motor to stop running which is as expected. The inverter still receives sufficient power to operate its control electronics (that is it has not reset). As the irradiance level increases again the motor fails to start up. Measurements have shown that power is being used and it was very audible that the inverter was attempting to drive the motor. During this process the inverter loses its array operating point and drops from 180V to 80V. As the power from the array increases again the array voltage moves back to 180V and the rms line current is in the region of 7A where usually it is in the region of 3.5A to 4.5A.

A similar phenomenon takes place when the motor is stopped through an external force (for example braking the pulley of the discharge head assembly with a shoe) while about 350W of power is available from the array. The inverter loses its operating point (it has to) and sits at about 80V for 3sec and then goes back to 180V. The motor does not start though. It is as if the inverter is in the wrong gear. Both these phenomena can ultimately lead to the burn-out of the power module.

Tests where the pump was deliberately blocked were conducted. This can ultimately be a realistic situation (pump dry-running can result in break-away torque requirements from the pump which the motor might not be able to generate). It was observed that the array voltage remains at 180V (array current during the test was about 2A), that the line current was about 7A and that the output frequency to the motor was about 9Hz (major gear five). The power module burned-out after 90sec.

Non-essential states of operation

The system goes through a few modes during start-up and stopping procedures. The modes are confined to periods from the time when the inverter starts operation (that is, it receives enough power for the controller to operate) to the time when the system is running smoothly. The modes can be divided into four categories: The first mode

is the heating-mode, the second mode is the jerking-mode, the third mode is the sine-mode and the last mode is the running-mode.

- In the heating-mode the motor is at standstill, the irradiance is below 220W/m^2 , the array operating voltage is between 60V to 100V (as opposed to 180V) and the inverter is delivering current to the motor. It sounds as if the current is pulsed at a rate of 1.5Hz. It can be assumed that the inverter is attempting to drive the motor in its first gear of operation which is major gear number five (in the assembler program).
- In jerking-mode the motor is jerked in regular intervals. The no-operation intervals between the jerks become shorter in time as the input power increases. This mode prevails from irradiance levels of about 220W/m^2 to about 330W/m^2 . The steady state array operating point is maintained reasonably well as can be seen in Figure 7.6. The inverter is still in major gear number five.
- In sine-mode the motor now moves continuously but the speed seems to be varying sinusoidally. This mode occurs at irradiance levels of about 330W/m^2 to 380W/m^2 . The program is either in major gear five or six. The pump does not deliver any water yet.
- In running-mode the motor runs smoothly and delivers water as soon as it enters this mode.

The non-essential modes are therefore the heating and the jerking-mode. They cause unnecessary wear for the motor. The sine-mode can be tolerated but is also not essential since no water is delivered.

Missing phase

It occurred once that one phase had a bad connection. Unfortunately it was the phase where the measurements were taking place. Therefore nothing can be said about the line current. The motor did continue operation but the question is: Will the inverter experience a break-down due to operation on only two phases. It can be assumed that the line current will exceed the normal values and that the inverter will find it difficult to get the motor started meaning it might operate in low major gears for quite a while. For proper precautions this may have to be investigated again. On the other hand people may be of the opinion that a missing phase is an improbable event.

7.6 General observations

Dynamic conditions

An appropriate test to evaluate the dynamic capabilities of a system is to apply a step-up or a step-down to the input. That was achieved by covering two of the 12 modules in series and then uncovering the modules. This simulates a voltage step but due to the IV characteristics this also translates into a current step. This method poses a disturbance to the system (similar to a thick cloud) which the controller has to correct with an adequate response time. The result is shown in Figure 7.14.

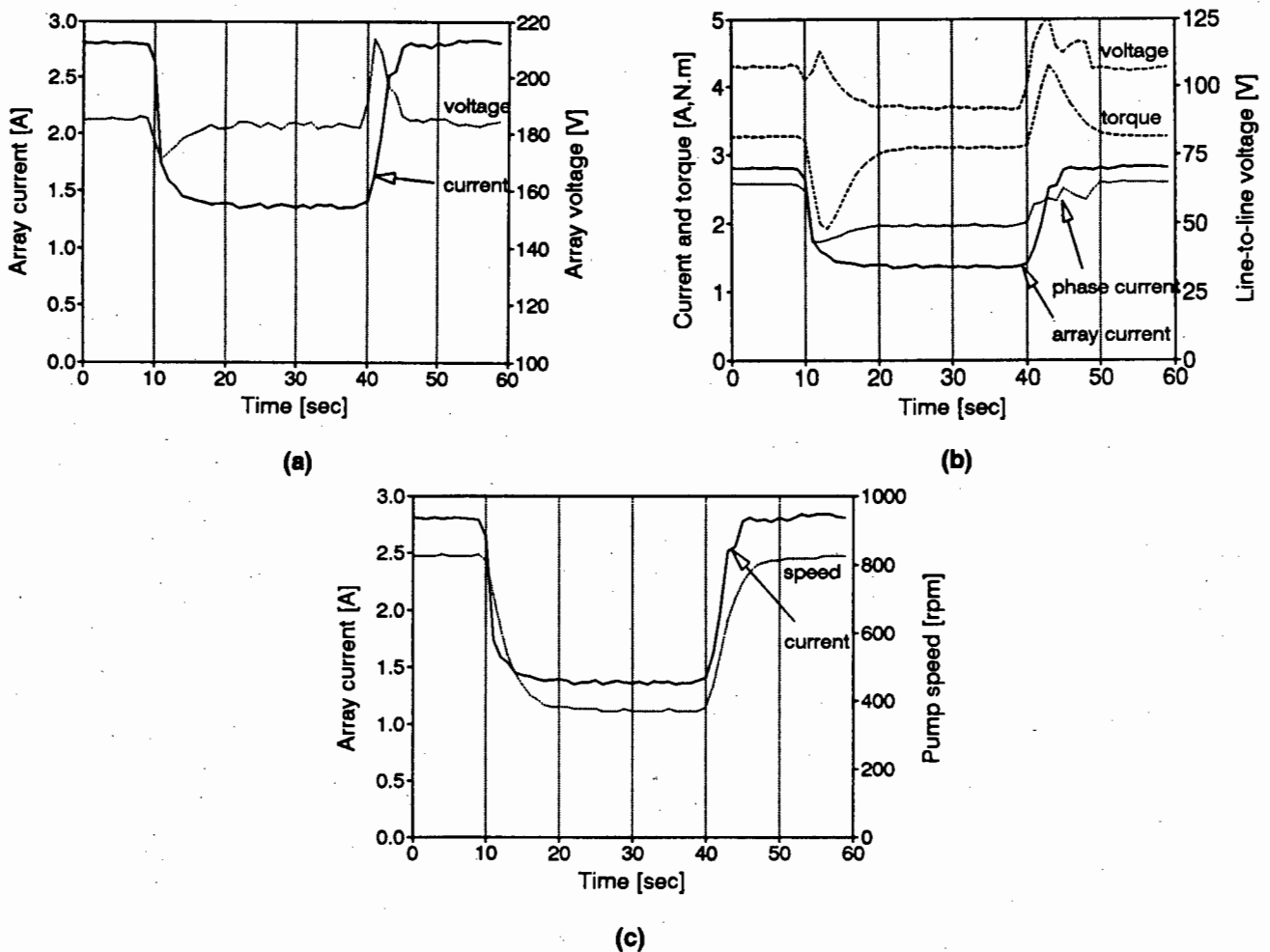


FIGURE 7.14 Solvo system response under dynamic conditions: (a) Array voltage and current; (b) array current, phase current, line voltage and torque; (c) array current and speed

Graph (a) shows the array current and the array voltage versus time. As the modules are covered the array voltage drops by 15V from 185V and after 10 sec settled back to its fixed voltage point. On uncovering the modules the array voltage rises sharply to 210V and drops back to 185V within 5sec. Due to this behaviour the array current does not drop and rise as fast as in the Miltek converter (there is an inherent delay

due to the sampling of the array voltage). This is an advantage rather than a disadvantage since the inverter is protecting itself indirectly.

Graph (b) shows the array current, the line-to-line voltage, the inverter phase current and the torque. Torque drops rapidly during a moment of 'free-wheeling' and then rises to the new torque requirements. So does the inverter current. On step-up the torque overshoots and then settles to its new value. The inverter current does not follow that trend which makes sense since the array voltage in that moment is quite high (210V) resulting in a high line-to-line voltage.

Graph (c) shows the array current with the pump speed. It takes the pump speed about 10 sec to settle to its new value.

System start-up

The system starts smooth operation between irradiance levels of 380W/m² to 400W/m². The power out of the array is 181V×0.85A = 154W. Prior to this, the inverter manages to overcome the starting torque at lower irradiance levels, with the help of its DC capacitors as described in section 7.5, but fails to operate smoothly and simply keeps jerking the motor.

The array voltage was sampled under conditions where the motor does not perform a start-up and under conditions where the motor does perform a start-up (Figure 7.15). Graph (a) shows the array voltage when the motor does not run, where the irradiance level is below 380W/m². Graph (b) shows the condition where the motor operates smoothly, at irradiance levels in excess of 400W/m².

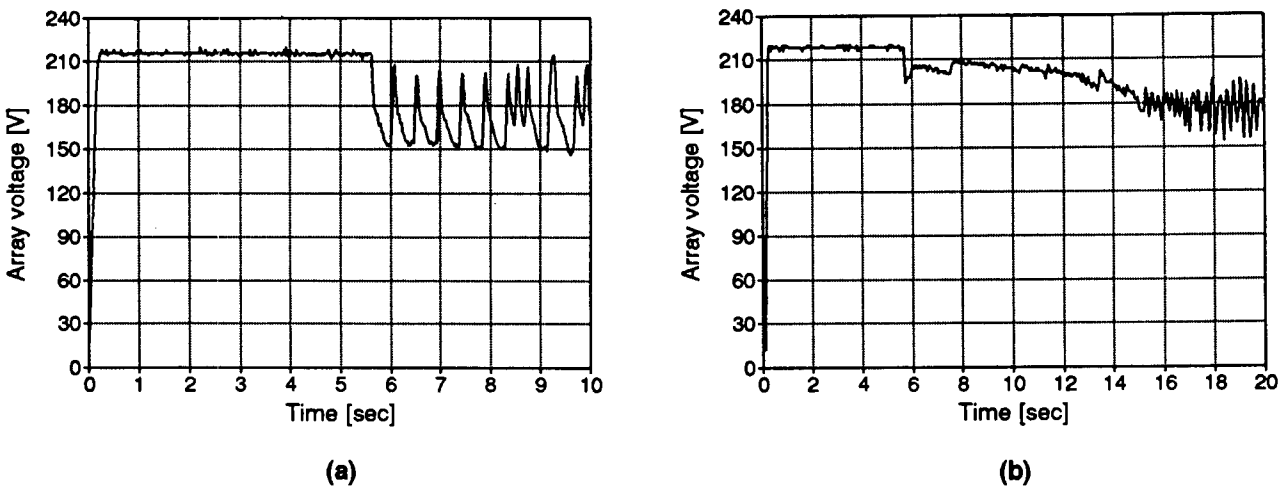


FIGURE 7.15 Array voltage at start-up: (a) Start failure; (b) start success

Graph (a) shows how the array voltage collapses to 150V, meaning the inverter is drawing too much current and therefore slipped over the knee of the IV curve. Since the motor failed to start the array voltage swings back to nearly open circuit voltage and then it seems as if the inverter tries to start the motor during each oscillation.

Graph (b) shows how the array voltage drops to about 195V, then increases a bit and then slowly drops to its set operating point of about 178V (in this case). The normal array voltage oscillations can be observed. The difference between these two graphs is that sufficient current is available from the array at the prevailing conditions during the sampling of graph (b).

Inverter tuning difficulties

Tuning requires a measurement device that takes the average of the array voltage (due to the array voltage oscillation) such that the fixed voltage can be set to the desired value. An ordinary digital multimeter is not sufficient as the average needs to be taken over a period of a few seconds. A multimeter with an averaging feature or a low-pass filter with a long time constant are required to tune the array operating point.

PWM switching scheme

This inverter uses a particular method to generate its PWM voltage at different frequencies. The variables that are changeable are the switching frequency (f_s) and the number of equal-width pulses that can be repeated within one fundamental cycle. What is of interest is how the repetition of equal-width pulses will affect the frequency spectrum of the output voltage. A general PWM scheme (not overmodulated, synchronous, refer to subsection 2.6.2) has in the worst case (m_f is even) its first harmonic at the switching frequency with additional sidebands, its next harmonics only as sidebands of twice the switching frequency, its next harmonics at three times the switching frequency with additional sidebands and so on (use Figure 2.5 as a reference but note that conditions are different). Using repetitive equal-width pulses will introduce harmonics at $3f_s$, $5f_s$, $7f_s$ and so on that are larger in amplitude than the harmonics occurring in a general PWM schemes. This type of harmonic spectrum certainly degrades motor efficiency but the impact cannot be assessed here. Therefore the advantage of a high switching frequency drive are compromised to some degree.

Torque pulsations

Torque pulsations were briefly discussed in chapter two (subsection 2.6.4), in the context of harmonic frequencies occurring in the current waveform. However in the Solvo and MLT systems, lower frequency torque pulsations were physically observed. Measurements conducted to establish the frequency and magnitude of these torque pulsations did not provide data that could be interpreted usefully, so attempts were made to count the pulses manually. Repeated tests led to the conclusion that the pulsations had a frequency of about 4Hz (20 pulses in 5sec). If the pulsations have the frequency of the array voltage oscillations (which could be expected) then this result comes close to the 3.5Hz oscillation. The faster oscillation recorded in array voltages would not be as detectable (higher frequency and smaller amplitude) as the slower oscillation voltage. There is further discussion on torque pulsations in section 9.1.

7.7 System performance

The aim of this section is to present the data of the Solvo PVP system and subsystem instantaneously and on a daily basis for different amounts of daily solar irradiation. The daily energy efficiency of the components, the subset (controller and motor), the subsystem and the system and the volume flow are presented for standard solar days from 2kWh/m²/day to 8kWh/m²/day. The emphasis in this subsection is on the shape and trends of the graphs. The performance values are also briefly discussed but further discussion takes place in the comparative chapter ten.

In addition, a solar irradiance profile for a single-axis tracking array has been generated, based on the solar irradiance profile in Figure 6.10. It is referred to as a tracking solar day. System performance predictions for a standard solar day and a tracking solar day are compared.

7.7.1 Instantaneous performance

The graphs in Figure 7.16 show the system and subsystem efficiencies and the flowrate as a function of irradiance and array power respectively.

The system efficiency reaches a maximum value of 3.9% from 700W/m². Above 700W/m² the flowrate follows a nearly straight line reaching a maximum value of 850l/h just below 1000W/m². The subsystem efficiency reaches a value of 33% from 350W array power onwards. This curve shows to some extent the characteristic unevenness that is transferred from the non-linear pump load curve.

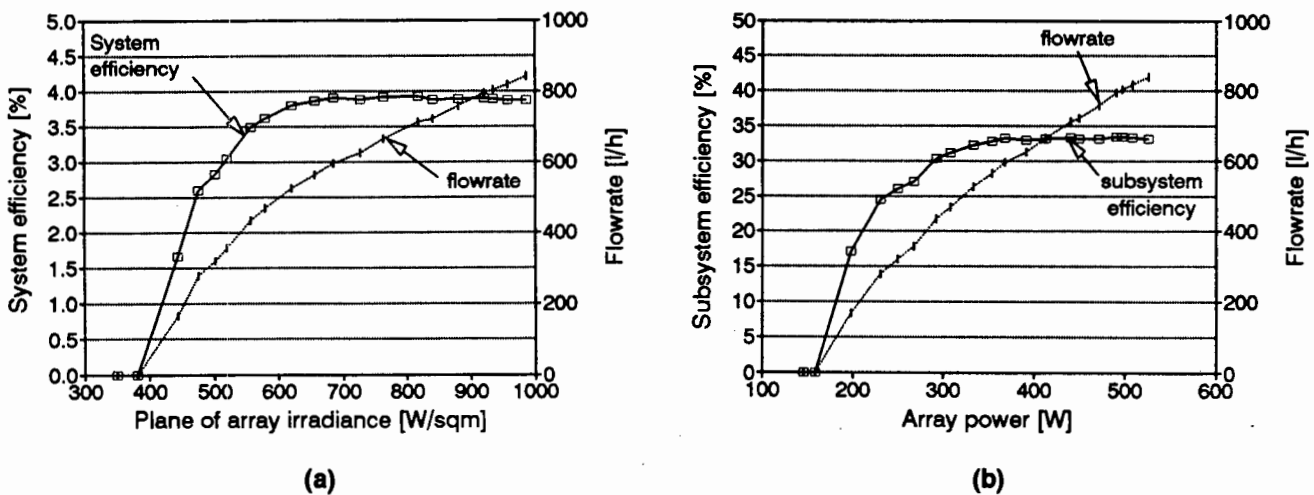


FIGURE 7.16 (a) Solvo system performance and (b) subsystem performance

The uncertainty in the system efficiency data is:

$$\begin{aligned}
 U_{\text{abs}} (\eta_{\text{sys}})_{1050\text{W/sqm}} &= 12.1\% \\
 U_{\text{rel}} (\eta_{\text{sys}})_{1050\text{W/sqm}} &= 6.9\% \\
 U_{\text{abs}} (\eta_{\text{sys}})_{750\text{W/sqm}} &= 15.7\% \\
 U_{\text{rel}} (\eta_{\text{sys}})_{750\text{W/sqm}} &= 9.4\%
 \end{aligned}$$

The uncertainty in the subsystem efficiency data is:

$$\begin{aligned} U_{\text{abs}} (\eta_{\text{subsys}})_{500\text{W}} &= 6.3\% \\ U_{\text{rel}} (\eta_{\text{subsys}})_{500\text{W}} &= 2.5\% \\ U_{\text{abs}} (\eta_{\text{subsys}})_{350\text{W}} &= 6.5\% \\ U_{\text{rel}} (\eta_{\text{subsys}})_{350\text{W}} &= 2.9\% \end{aligned}$$

The uncertainty in the flowrate data is:

$$\begin{aligned} U_{\text{abs}} (Q)_{200 \rightarrow 1000/\text{h}} &= 6.1\% \\ U_{\text{rel}} (Q)_{200 \rightarrow 1000/\text{h}} &= 2.2\% \end{aligned}$$

The subsystem efficiency presents itself as the data with the lowest uncertainty and therefore the most reliable for comparison to other systems (absolute uncertainty in the region of 6.4%). The largest uncertainty is introduced through the flowrate calibration. The relative uncertainty at full input power is 2.5% and increases minimally as the input power decreases. Subsystem efficiency data can therefore be used with good reliability for comparison among the three PVP systems. The absolute uncertainty in the system efficiency is high as a result of the pyranometer errors. The relative uncertainty remains relatively high as the spectral response error in the pyranometer cannot be assessed.

7.7.2 Daily energy efficiency performance

The daily energy efficiency (DEE) is calculated by dividing the total energy out of a component/system by the total energy into a component/system over the course of a standard solar day. Therefore the DEE's of components are partly dependent on surrounding component performances and matching. For example, the inverter DEE depends on the performance of the array: poor array performance will result in a poor DEE of the inverter. The method for daily energy efficiency calculations is presented in appendix A5.

The DEE of the components, subset and subsystem is shown in Figure 7.17. The inverter DEE increases from 15% to 78% ending with a small gradient towards a SSD of 8kWh/m²/day. The motor reaches a nearly constant value at 71%. Its shape follows its instantaneous efficiency curve. The pumping set reaches a peak at 55% and does not increase any further beyond a SSD of 7.3kWh/m²/day.

Both the subset and the subsystem efficiency curves become flatter at higher daily irradiation levels. They reach values of 56% and 31% respectively at 8kWh/m²/day. Subsystem efficiency is zero at 2.3kWh/m²/day. Subset efficiency is zero at 2kWh/m²/day.

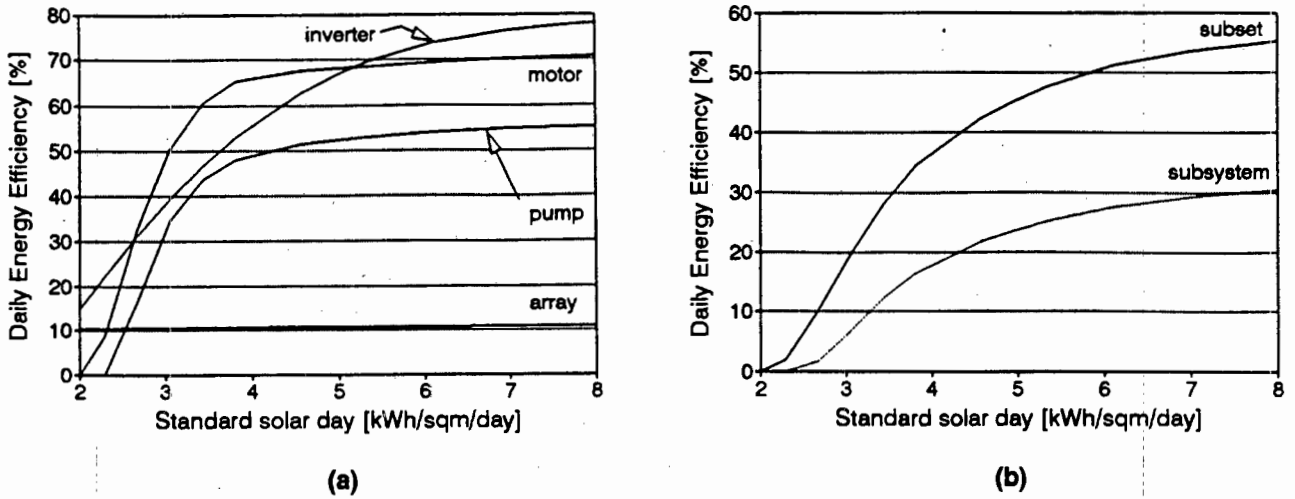


FIGURE 7.17 Solvo system daily energy efficiency: (a) components and (b) subset and subsystem

Figure 7.18 displays the DEE of the system and the daily volume flow as a function of the standard solar day. System operation starts beyond 2.3kWh/m²/day. The system efficiency reaches 3.3% at 8kWh/m²/day and the system delivers 5.85m³ over such a day.

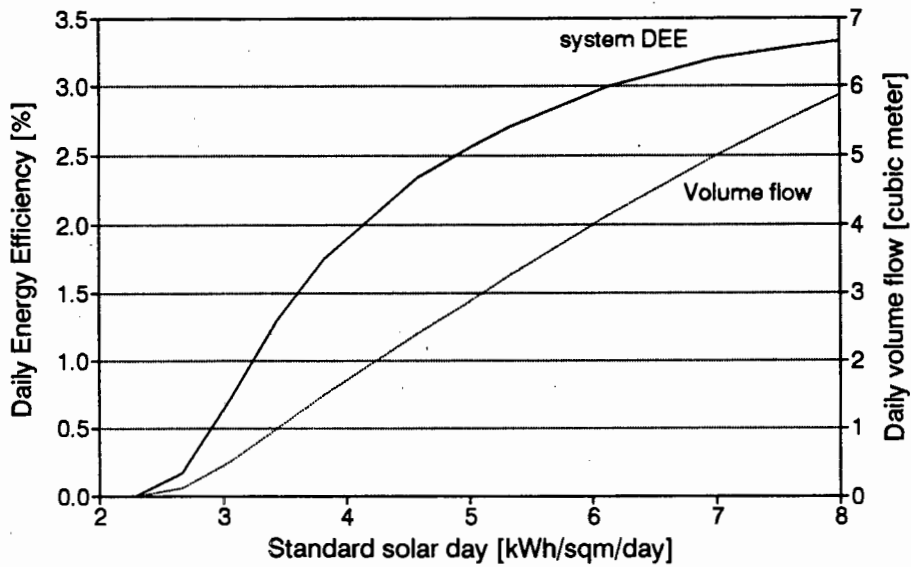


FIGURE 7.18 Solvo system daily energy efficiency and daily volume flow

The comparison between a standard solar day and a tracking solar day (TSD) is shown in Figure 7.19. Displayed are the DEE of the system and the volume flow. The difference between the SSD and the TSD based on the SSD is shown in the adjacent graph.

The difference between the DEE of the system at SSD and TSD is about 7% at 1100W/m² noon peak irradiance. The difference increases as the daily peak irradiance decreases and rises to 20% at 600W/m² and reaches 60% at 350W/m² where the subsystem ceases to operate for SSD conditions. The shape of the volume flow curve is similar but has a higher percentage difference. At 1100W/m² noon peak irradiance the difference is 35% and reaches a value of 53% at 600W/m².

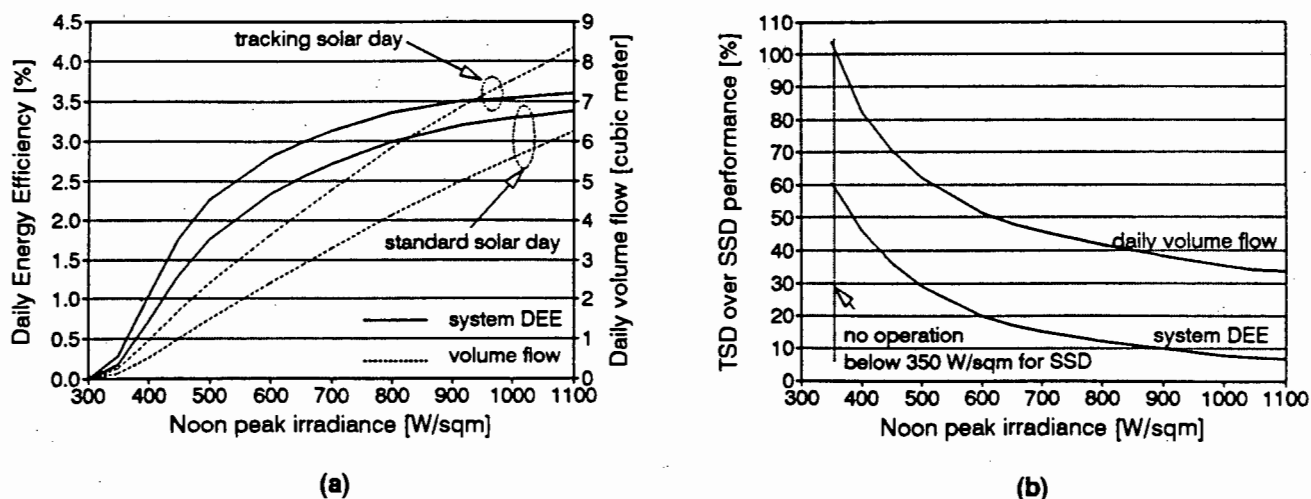


FIGURE 7.19 Tracking solar day and standard solar day for the Solvo system DEE and the volume flow: (a) performance and (b) percentage of TSD over SSD

This graph shows that a tracking array becomes more beneficial in comparison to a fixed array at sites where the solar irradiance levels are generally low, like in the region of 600W/m² to 800W/m² (sites with less than 600W/m² noon peak irradiance should probably not consider PVP's). On the other hand, sites with such low noon peak irradiance levels will have a higher proportion of diffuse irradiation and will therefore not benefit from a tracking array as much as indicated in Figure 7.19 above.

As indicated in chapter six (subsection 6.3.4), the average noon peak irradiance levels for Windhoek never fall below 900W/m² on a tilted surface with an angle of tilt equal to 20°.

Chapter Eight

MLT SYSTEM PERFORMANCE ANALYSIS

The chapters on the prototype inverters (chapters seven and eight) each stand on their own and can be read independently of one another. Because of this there is a small amount of duplication with the result that some introductory paragraphs are the same or similar.

This chapter presents and discusses the inverter and motor efficiency, the steady state array operating point characteristics for fixed voltage operation (speed sensor disconnected) and maximum speed tracking, the dynamic array operating point characteristics, the voltage to hertz relation, the control algorithm characteristics and general observations on the system. This is followed by the instantaneous system and subsystem performance evaluation and by the daily energy efficiency evaluation of the components and the system.

The derivation of the absolute and relative uncertainty in the acquired data is presented in appendix A3.6. The derivation of the stated uncertainty in the efficiency data is given by an example in appendix A3.7. All uncertainties are stated as a plus-minus percentage of a full-scale reading.

System tuning

The system was tuned for two modes of operation, one being fixed voltage operation (FVO) and the other being maximum speed tracking (MST). In both modes of operation the array operating point was adjusted and a suitable pulley size was selected. The MST mode required additional adjustment at the speed potentiometer.

The array voltage was adjusted to a steady state value of about 90V for both operation modes. This was found to be close to the MPP at cell temperatures of 47°C (refer to Figure 6.8).

The choice of motor pulley was guided by two criteria (the pulley of the discharge head assembly remained the same for all tests, being 247PCD):

- the inverter should be able to just reach its maximum programmed output frequency at the maximum irradiance level
- the start-up delay should be minimised

For FVO the pulley choice was between 97PCD (pitch-centre diameter), 112PCD and 118PCD. The 97PCD pulley reached its 65Hz output frequency at 1000W/m² and did not respond to higher irradiance levels. The 118PCD pulley reduced the operating range of the system considerably, that is the system would only start up at high levels

of irradiance (eg. 850W/m^2). The 112PCD pulley permitted start-up to occur at about 750W/m^2 which is still higher than for the 97PCD pulley. But then the 112PCD pulley managed a higher pump speed (about 40rpm higher on average) over the complete operating range. The 112PCD pulley was consequently chosen for FVO.

For MST the pulley choice was between the 118PCD and the 125PCD pulley. It was not very clear from the sampled data which pulley performed better over the whole operating range as both pulleys managed higher pump speeds at particular irradiance levels. The 118PCD pulley reached a higher maximum speed at the same level of irradiance and would also start up earlier. The 118PCD pulley was therefore chosen.

The speed potentiometer had to be adjusted in MST mode. This was not required to maximise speed but rather to enable the motor to start up at the lowest possible input power level (the tuning difficulties are discussed in subsection 8.6). The case occurred where the motor turned at a constant speed of about 170rpm ($S_{\text{pump}} = 90\text{rpm}$, virtually no water is pumped) even though it could potentially turn a lot faster since it was receiving substantially more power than required for start-up.

8.1 Inverter and motor performance

This section deals with the inverter, the motor and the subset efficiency at standard and at higher head as well as the characteristic inverter and motor curves.

8.1.1 Efficiency at standard head (75m)

The efficiencies of the subset components are discussed only briefly for fixed voltage operation but more elaborately for maximum speed tracking.

The inverter efficiency includes the losses due to the dynamic array operating point characteristics (as will be discussed in section 8.3). It does not include the array output losses due to steady state operation away from the MPP. It also does not include the mismatch losses between the inverter and the motor which are caused by the harmonics in the current waveform. These losses are included in the motor efficiency.

The uncertainties in the efficiency results are stated for MST operation but not for FVO. However they are likely to be very similar in magnitude.

Fixed voltage operation

The FVO operating range of the subsystem is quite narrow. Subsystem operation starts at an input power of about 350W. Operation was tested up to 500W. The result is shown in Figure 8.1.

Both components maintain a fairly constant efficiency value. The inverter remains at about 90% and the motor at about 67%. The resulting subset efficiency is 60%.

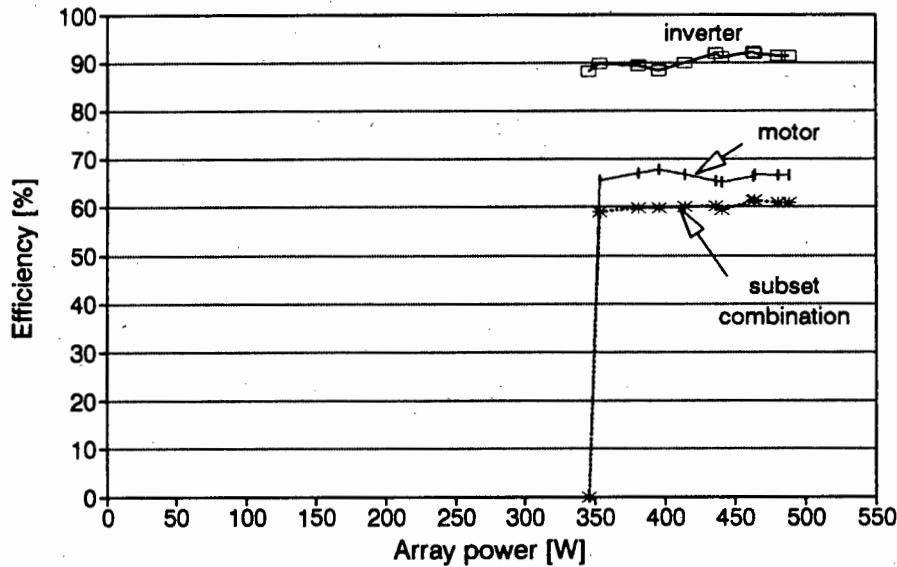


FIGURE 8.1 MLT inverter, GEC motor and subset efficiency versus input power: Fixed voltage operation

Maximum speed tracking

The inverter and the motor efficiency have been recorded from 120W to 510W array power. This is displayed in Figure 8.2. The inverter starts with an efficiency of 70% that rises to over 90% at 300W. It remains at about 92% and rises to 94% on the last data point which is at 510W (confirmation of this data point was found in three separate data sets).

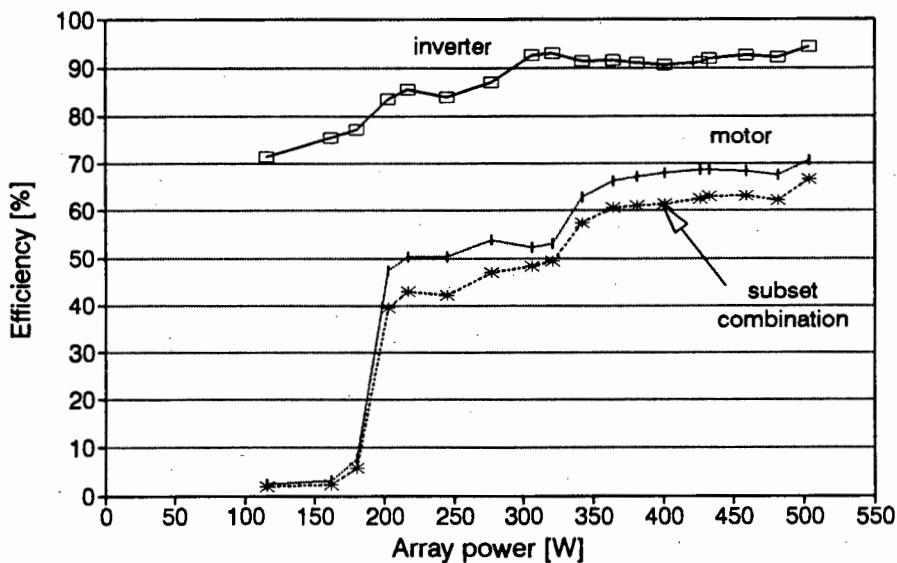


FIGURE 8.2 MLT inverter, GEC motor and subset efficiency versus input power: Maximum speed tracking

The uncertainty in the inverter efficiency data is:

$$\begin{aligned}
 U_{\text{abs}} (\eta_{\text{inv}})_{500\text{W}} &= 7.6\% \\
 U_{\text{rel}} (\eta_{\text{inv}})_{500\text{W}} &= 4.8\% \\
 U_{\text{abs}} (\eta_{\text{inv}})_{250\text{W}} &= 16.7\% \\
 U_{\text{rel}} (\eta_{\text{inv}})_{250\text{W}} &= 10.7\%
 \end{aligned}$$

The inverter losses, Figure 8.3, are on average between 30W and 40W with a low of 23W between 300W and 350W input power. The losses can be divided into constant and varying losses. The constant losses consist of the power supply losses, microcomputer power requirements and the drive circuit requirements. The power supply losses are likely to be relatively high as a voltage regulator circuit is used. The microcomputer and drive circuit power requirements have been approximated by Davies (1992: 71) to be 200mA at 15V which is equivalent to 3W. This power has to be produced from the array operating voltage which is about 90V. The power supply losses are therefore equivalent to $75\text{V} \times 200\text{mA} = 15\text{W}$. The resulting constant losses are consequently 18W but will be taken to be 20W (since the array voltage can also operate at 100V).

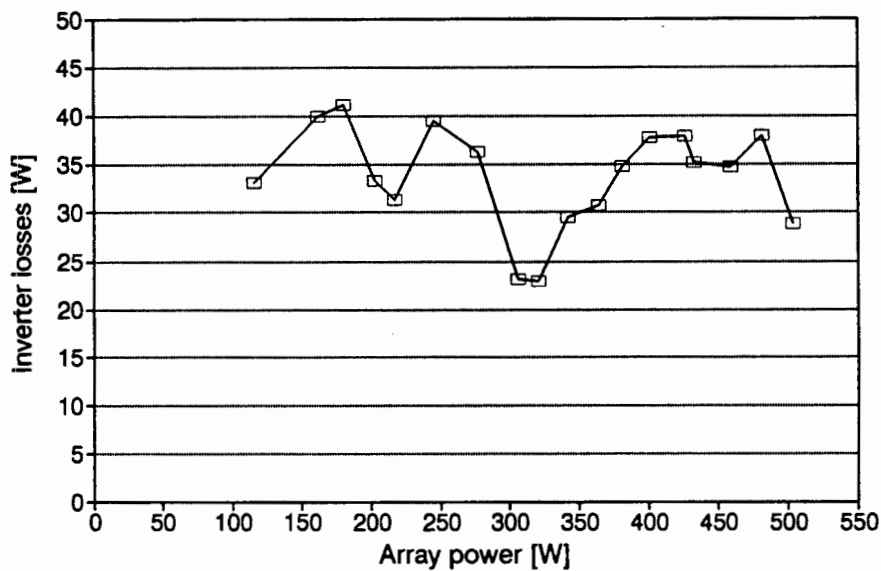


FIGURE 8.3 MLT inverter losses: Maximum speed tracking mode

The varying losses are the switching losses and the conduction losses. These vary because the line current varies to some degree. In addition to this the switching losses also vary due to changes in the switching frequency. Both can be taken from Davies' dissertation (1992) as they are calculated under similar conditions (that is the line current is about 3A and the array voltage is 95V). The switching losses are therefore (Davies 1992: Figure 42) 6.5W at 20Hz, 7.5W at 35Hz and 3.6W at 50Hz. The inverter changes from sinusoidal PWM to harmonic elimination PWM at 50Hz, hence the drop in switching losses. The conduction losses were calculated for a maximum line current but will usually be less than that. Davies (1992: 70) calculated them to be 10W. For a minimum line current of 2.5A (see Figure 8.5 a) this loss evaluates to 2.3W.

Combining all the losses results in 37.5W maximum and 26W minimum. This is in agreement with the inverter losses as they are displayed in Figure 8.3. However, the minimum of the graph, occurring at 310W input power, does not logically correspond to the calculated values since the line current is at its maximum (see Figure 8.5) between 300W to 320W (pump torque peaks slightly and inverter voltage drops). This means that the conduction losses and the switching losses will be high. Consequently the inverter efficiency should be low at this point but actually goes through a peak. I am not able to find an explanation for this behaviour unless the drive parameters programmed into the inverter are unsuitable for the motor in this region or it could be possible that the program changes to harmonic elimination at 40Hz instead of 50Hz (the MLT inverter documentation was not up-to-date). It was also possible that the measurement equipment might have experienced some disturbances due to inverter switching frequencies. However it is certain that this inverter efficiency curve was very repeatable (observed in at least five different data sets) and that it was logged under steady state conditions.

The motor efficiency (Figure 8.2) is about 3% for input powers of 120W to 160W (the motor runs at a base speed of 30rpm) and then rises fairly sharply to about 50% where it more or less remains until 330W input power. It then rises to about 67% / 68% until 510W input power is reached. It then reaches 70% on the last data point which occurs at 510W input power. The motor as tested therefore comes to within 6% of the motor specifications (at 50Hz, 70V_{LL} it is 75.6%). This is acceptable as the motor receives some frequency harmonics as can be seen in the distorted line current waveform in Figure 3.9.

The shape of the motor efficiency curve seems to follow the shape of the pump efficiency curve once more than 200W input power is received. Here therefore it could be that the pump load requirements feed through and determine the shape of the motor efficiency curve. The shape and the magnitude are of course also affected by the harmonic content of the current waveform and the time-base at which the switching frequency is changed. The change in PWM switching scheme was expected at about 400W array power (inverter frequency of 50Hz) but at that point there is no discontinuity. Which of these factors determines the shape would have to be tested with a linear load.

The uncertainty in the motor efficiency data is:

$$\begin{aligned} U_{\text{abs}}(\eta_{\text{mot}})_{475\text{W}} &= 8.3\% \\ U_{\text{rel}}(\eta_{\text{mot}})_{475\text{W}} &= 6.1\% \\ U_{\text{abs}}(\eta_{\text{mot}})_{250\text{W}} &= 14.5\% \\ U_{\text{rel}}(\eta_{\text{mot}})_{250\text{W}} &= 9.8\% \end{aligned}$$

The subset efficiency (Figure 8.2) is 3% at input powers of less than 160W. Between 200W and 330W the efficiency is increasing from 40% to 50% and reaches 60% at an input power of 370W. It reaches 66% on the last data point at 510W input power. The shape of the curve is very similar to the motor efficiency curve since the inverter efficiency curve is reasonably linear.

The uncertainty in the subset efficiency data is:

$$\begin{aligned}
 U_{\text{abs}}(\eta_{\text{subset}})_{500\text{W}} &= 4.9\% \\
 U_{\text{rel}}(\eta_{\text{subset}})_{500\text{W}} &= 4.2\% \\
 U_{\text{abs}}(\eta_{\text{subset}})_{250\text{W}} &= 5.6\% \\
 U_{\text{rel}}(\eta_{\text{subset}})_{250\text{W}} &= 4.9\%
 \end{aligned}$$

The uncertainty in the subset efficiency is lower than the individual inverter or motor efficiency. Due to a partly 'programmable' efficiency of the inverter and therefore indirectly a partly 'programmable' efficiency of the motor it was decided to use the subset performance as the most appropriate gauge for the inverter/motor evaluation (that is the inverter-motor combination has to be optimised not the inverter by itself). From a measurement point of view this is supported due to lower uncertainties in these data sets. The lower uncertainty is mainly due to high-accuracy components of the array current and array voltage data acquisition circuits.

The bumps that generally occur in the graphs of the efficiency curves are due to changes in output voltage and probably due to the unstable torque characteristics of the load.

8.1.2 Efficiency at higher head

The tests that were conducted to evaluate the inverter and the motor performance as the static head increases were only partly successful. Unfortunately the power meter was not correctly connected. Nevertheless, the data for the subset can be evaluated.

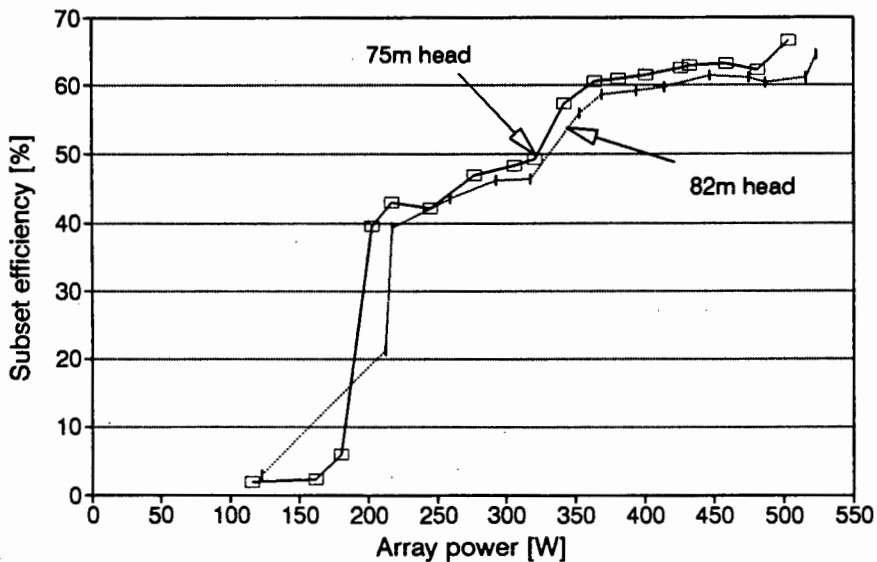


FIGURE 8.4 MLT subset efficiency at two static heads

Figure 8.4 shows the subset efficiency at two heads which are not that far apart. The efficiency at 75m is slightly better than the efficiency at 82m. The average difference is 2%.

Should the available input power be increased than the subset efficiency would increase due to an increase in inverter and motor efficiency (constant losses in the inverter reduce relatively and the motor efficiency increases as it gets closer to its design operating conditions).

8.1.3 Characteristic inverter and motor curves

The characteristic inverter and motor curves under the particular load conditions are shown in Figure 8.5. The inverter line current has similar tendencies to the torque curve of the pump (Graph a). Both reach a peak at 300W array power although the change in current is quite marked. This may well be due to inverter voltage variations due to array voltage variations (compare to array voltage in Figure 8.7).

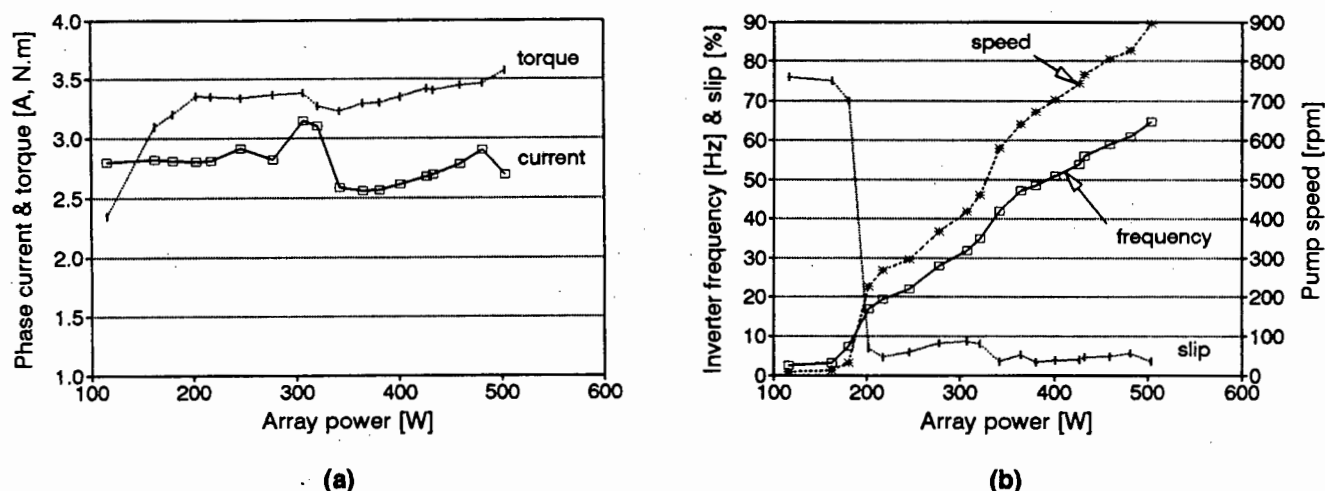


FIGURE 8.5 MLT characteristic subsystem curves: (a) phase current and pump torque; (b) frequency, slip and pump speed

The frequency and the pump speed have the same response curve (graph b). The speed curve exhibits a particular tendency of the MLT system. The motor runs at a base speed of about 30rpm (ie $S_{pump} = 15\text{rpm}$ on the graph; speed ratio is about 2) until it reaches a particular power threshold from where it then speeds up to about 400rpm (ie $S_{pump} = 200\text{rpm}$). The slip decreases rapidly once the motor leaves its base speed. A small peak occurs at 300W array power which corresponds to an increase in the phase current (graph b).

8.2 Steady state array operating point characteristics

The MLT inverter has two principal operating modes which are fixed voltage operation (FVO) and maximum speed tracking (MST). Both were tested extensively. It has to be stated clearly though that in retrospect the MST mode of operation was not tested correctly as it was not given sufficient time to seek its maximum speed at each data acquisition point.

Fixed voltage operation

The mean array voltage (5second average) is displayed in Figure 8.6. The voltage remains at about 93V. The maximum deviation found in a data set was 4.5V. Usually it was about 3V maximum.

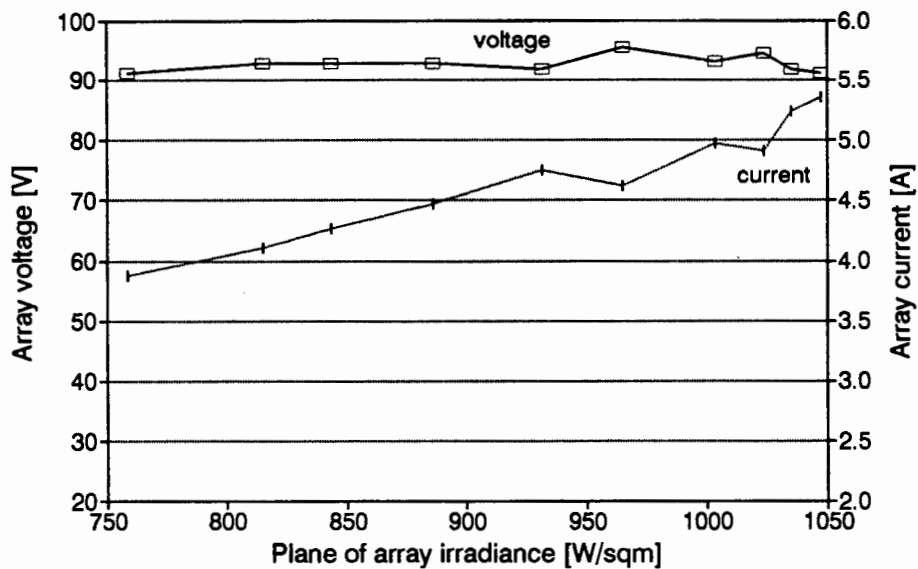


FIGURE 8.6 Fixed voltage operation of the MLT inverter

Below 750W/m² the system failed to reach a steady state operating point. The inverter would 'run up' the IV curve of the array from about 120V but would pass through the array voltage set-point and sit at about 35V. Only when the level of irradiance was in excess of 750W/m² would the system start proper operation.

Maximum speed tracking

I was unable to assess how long it would take the inverter to find its maximum speed operating point and therefore indirectly move towards the MPP. It was thought that the hunting for the maximum speed would be accomplished within a good 30 seconds. It became clear from the data though that this was not the case. The implications are twofold: One, the performance of the MST program cannot be evaluated properly here due to poor test procedure as the system requires a few minutes to track the maximum speed and two, the possibility that MST algorithm cannot be properly implemented under the conditions of array voltage oscillations described in section 8.3.

The latter point will be argued for in subsection 8.5.3. The data is nevertheless shown in Figure 8.7.

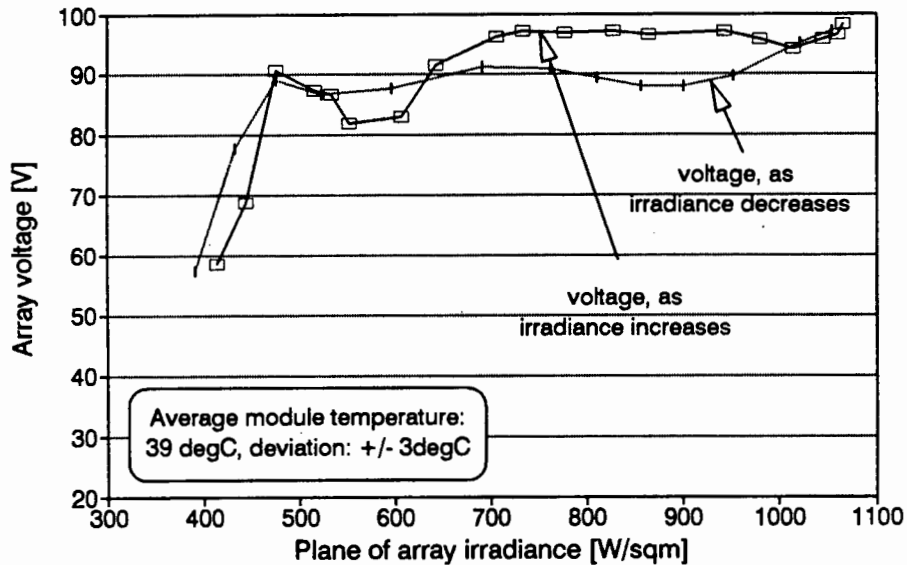


FIGURE 8.7 MLT inverter-control of the array operating point while in maximum speed tracking mode

The array voltage is displayed for increasing and decreasing irradiance (the system received a settling time of 25sec for each data point). It was originally thought that the inverter exhibited hysteresis. That is why the module temperature is specified. The inverter traces out two paths for increasing and decreasing irradiance (consistent for three data sets). While the irradiance level increases the voltage is generally higher as opposed to when the irradiance level decreases. This behaviour gives the impression that the MST program drives its reference voltage window to the top limit as the irradiance increases and to the bottom limit as the irradiance decreases. The impact of the speed tracking algorithm thus has quite a substantial impact on the fixed voltage tracking algorithm. This should not be the case since the program takes one speed sample for every twenty-five voltage samples and therefore indicates that the MST program is not operating as it should or is prevented from doing so (further discussion in subsection 8.5.3).

The MST evaluation would have included calculating the MPP co-ordinates (current and voltage) from the collected array data based on the plane of array irradiance and the module temperature that prevailed when the MLT system was tested. This would have been compared to the operating point co-ordinates that the MLT inverter traced out on the IV curve of the array.

8.3 Dynamic array operating point characteristics

The mean array voltage proved to remain quite close to the set-point to which it was tuned (FVO only). The instantaneous voltage though has quite a large movement about that mean value. As this could result in a diminished array output and can have a negative impact on the motor the effect of this array voltage oscillation is analysed here.

It is common for switch-mode inverters to have a ripple voltage on the DC-side input which is due to the switching scheme employed by the inverter. The magnitude of the ripple is dependent on the switching frequency of the inverter (inversely related). Its frequency is the same as the switching frequency. The ripple discussed here (referred to as an oscillation voltage) is the result of the type of control algorithm implemented in the inverter (a detailed analysis of the control algorithm is in section 9.1). This section purely evaluates the impact of the oscillation voltage on the array performance and on the shape of the PWM inverter output signal. The effect of a larger input capacitance on the array voltage oscillation is also evaluated.

8.3.1 Shapes of oscillation waveforms

The typical shapes of oscillation waveforms that were encountered are displayed in Figure 8.8.

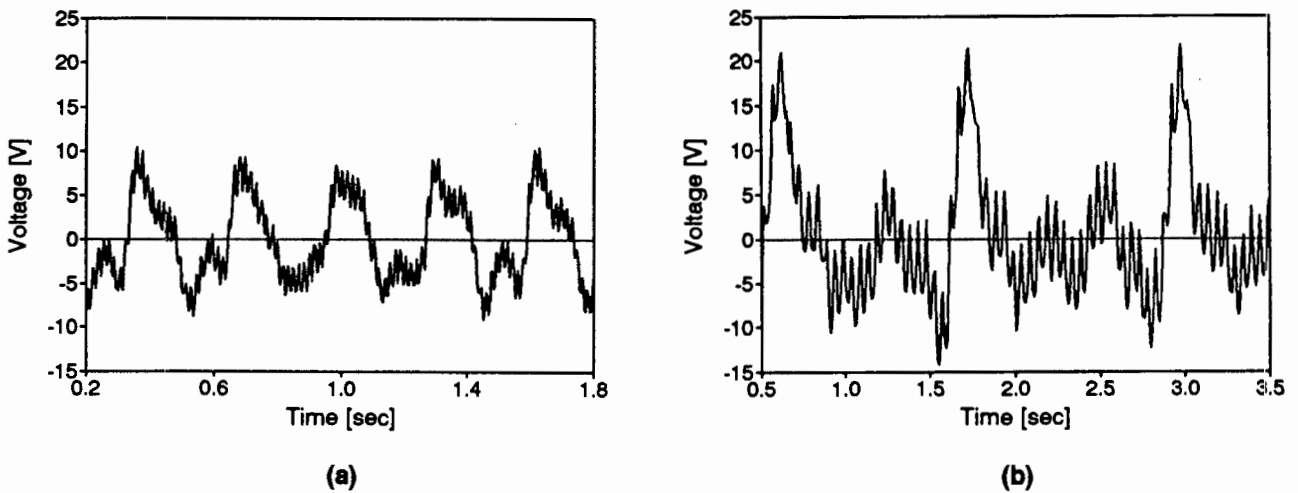


FIGURE 8.8 Typical array voltage oscillation waveforms riding on $90V_{arr}$

They have different amplitude and different shapes. The superimposed ripple is caused by the switching of the inverter. The frequency of the oscillation voltage in graph (a) is 3.4Hz with a peak-to-peak amplitude of about 16V. The oscillation voltage in graph (b) has a frequency of 1.7Hz but that is not really obvious. The peak-to-peak amplitude of the signal is about 30V. The period between the large positive amplitude spikes is in the range of 1.1sec to 1.3sec. Shorter and longer periods have also been observed namely 800msec to 1.7sec.

At what fundamental inverter frequencies both oscillation waveforms occur is not known. However the shape and magnitude do not vary considerably at different levels of input power.

8.3.2 Array power losses

In order to assess the impact of the oscillation waveform on the array output, the two waveforms from above were superimposed on the steady state array operating point by providing information of a characteristic array power curve. The method is described in appendix A6.

The result of this procedure is shown in Figure 8.9. The two lines represent the actual oscillation waveforms. The amplitude of the waveform is scaled to simulate waveforms of smaller and larger amplitude. Waveform 1 represents graph (a) in Figure 8.8 and waveform 2 graph (a). Over the whole peak-to-peak amplitude range waveform 1 has larger array losses than waveform 2. Therefore the integral of oscillation waveform 1 is larger than the integral of waveform 2.

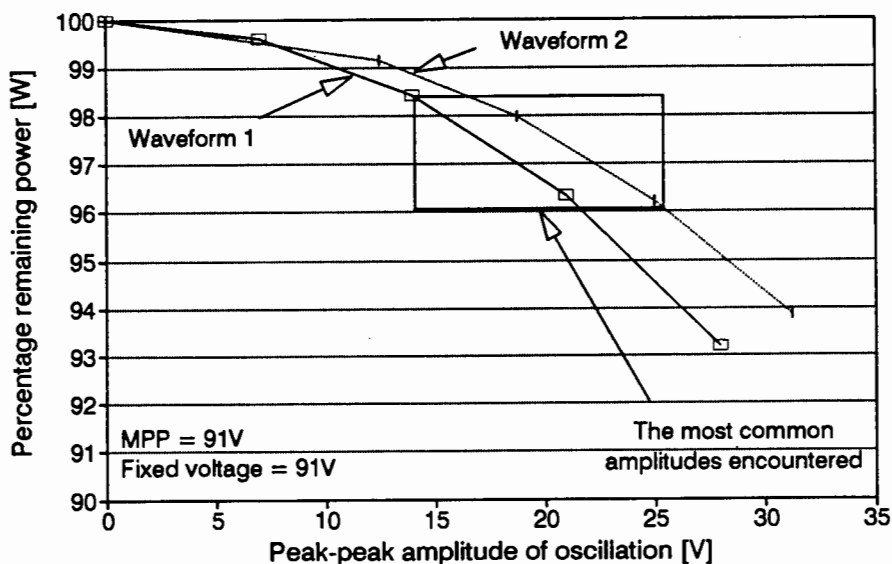


FIGURE 8.9 Percentage of remaining array power versus a range of oscillation waveform amplitudes while operating (on average) at MPP

The oscillation waveform operates around the MPP at 91V. Therefore the array losses are zero at zero peak-to-peak oscillation amplitude. The window indicates the amplitude range that was encountered resulting in array output losses of 1.5% to 4%.

Figure 8.10 shows the effect of operation away from the MPP. The array output losses due to operating 4V above the MPP are shown at zero peak-to-peak amplitude. They are about 1.3%. Due to the shape of the array power curve the losses due to the oscillation waveform are not equivalent to their losses at MPP plus the offset (that is 1.3%). For example, the losses at 25V_{pp} are 6% at an operating voltage of 95V and 3.8% at MPP (3.8% + 1.3% < 6%).

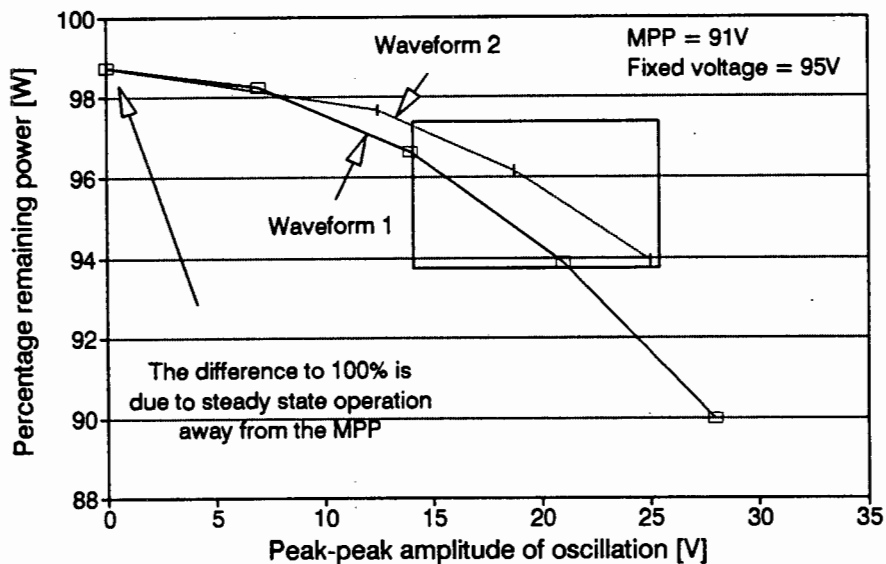


FIGURE 8.10 Percentage of remaining array power versus a range of array voltage oscillation amplitudes while operating (on average) 4V to the right of MPP

The impact of an oscillation waveform increases as the operating voltage increases beyond the MPP voltage and the impact decreases as the array voltage becomes lower than the MPP voltage (see Figure 7.10).

The array current and array voltage measurements, as they have taken place, are equivalent to conditions of zero oscillation amplitude. The array output would have to be derated by the difference in power loss between zero amplitude and actual amplitude. The inverter efficiency would have to be increased by a factor as its input power is actually less than measured. This was not done since the losses are incurred due to the particular operating characteristics of the inverter. These losses are therefore treated as mismatch losses but are put on the inverter's account.

8.3.3 PWM envelope

Since the inverter uses a switch-mode scheme to drive its output the array voltage oscillations will be transferred to its output voltage. This can be seen on the PWM envelope curve shown in Figure 8.11.

The time-base for the oscillation waveform is usually longer (about 3.5Hz) than the fundamental frequency of the output signal (3Hz to 65Hz). For example, at 50Hz fundamental frequency the output voltage will go through 14 cycles as the oscillation waveform goes through one cycle.

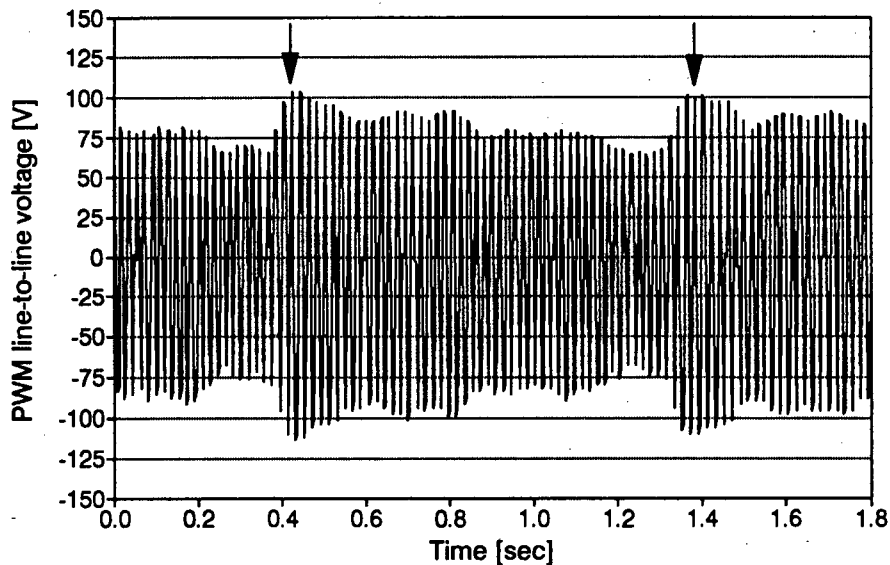


FIGURE 8.11 PWM envelope curve of the MLT inverter

8.3.4 Effects of increased input capacitance

The input capacitance was increased from $2040\mu\text{F}$ to $6740\mu\text{F}$ to observe the impact on the array voltage oscillations. It essentially dampens the system by providing a stiffer voltage supply.

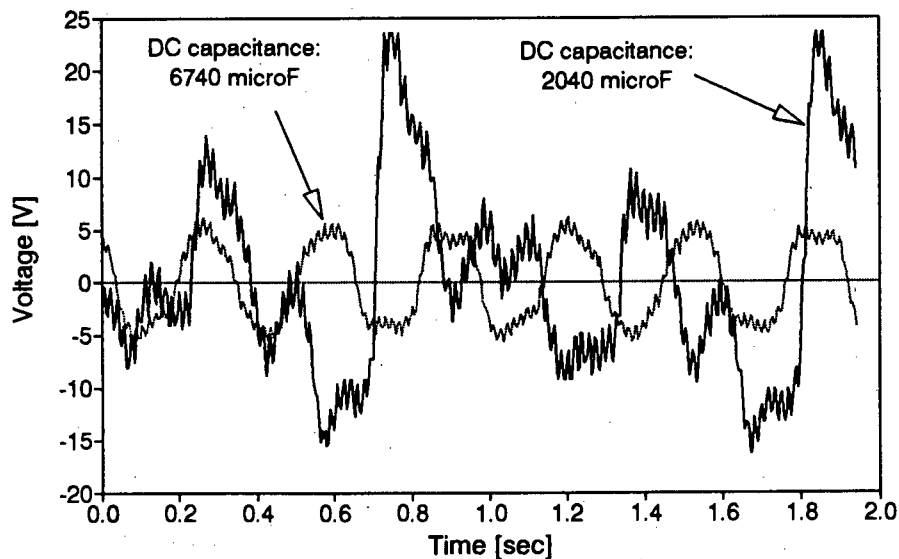


FIGURE 8.12 Effects of a larger DC input capacitance on the oscillation waveform

The oscillation voltage decreased to $10V_{pp}$ in amplitude while the frequency hardly changed (3.2Hz). Figure 8.12 shows the graph.

Array power losses

Figure 8.13 shows that the array output losses have been reduced from the 1.5% to 4% range to the 1% to 3% range. This is not a lot considering that the input capacitance was increased by a factor of 3.3.

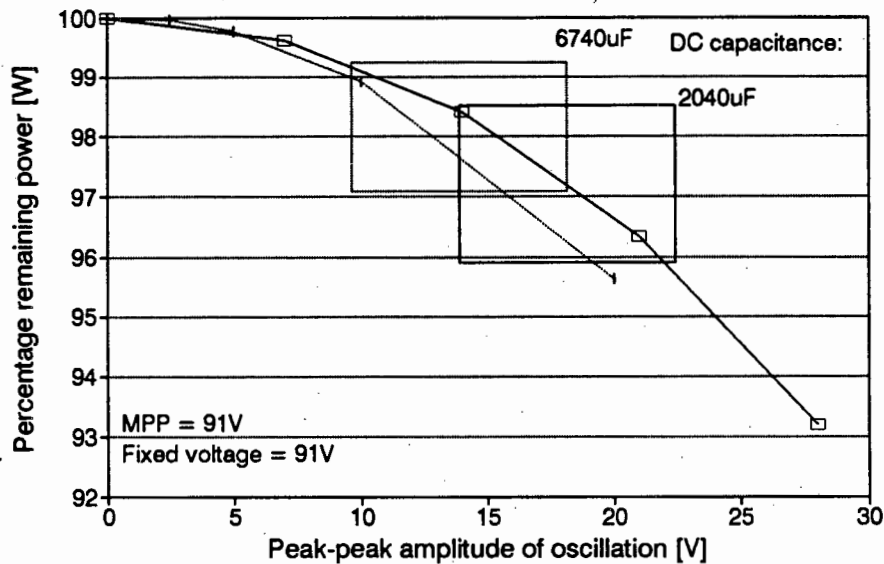


FIGURE 8.13 Percentage remaining array power with larger DC input capacitance

The oscillation waveform shape as in Figure 8.8b was not sampled again for the increased capacitance condition. It does however still occur as will be shown. But this is the reason why the window for the increased capacitance still stretches down to 3%.

PWM envelope

The change in the envelope curve, Figure 8.14, is interesting in that most of the oscillations have been reduced considerably (compare to Figure 8.11) except for an oscillation occurring every 1.2sec (at the arrows). The same oscillation can be observed in Figure 8.11 (arrows) and it probably has the same shape as seen in the graph in Figure 8.8b but with a reduced oscillation voltage between the peaks.

This phenomenon is most likely due to another form of oscillation. I have found no reasonable explanation for its source.

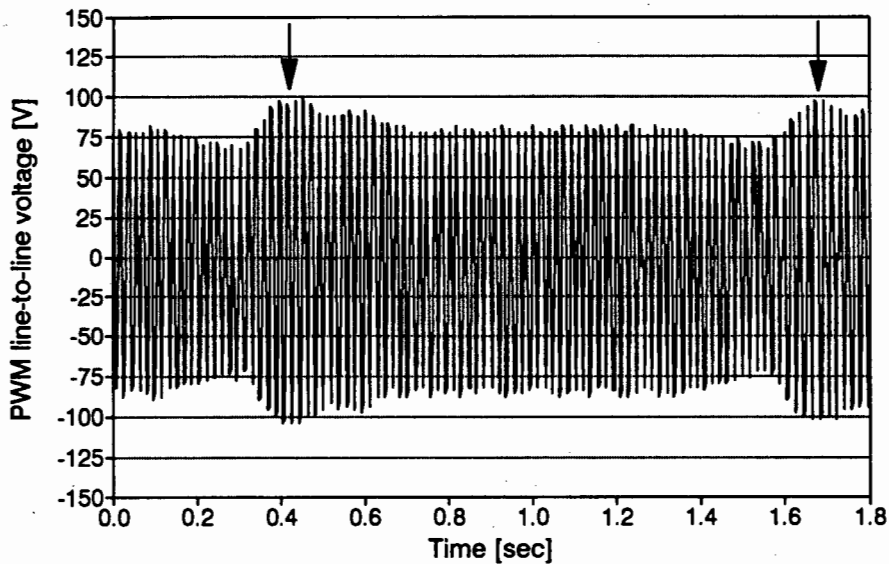


FIGURE 8.14 PWM envelope curve with larger DC input capacitance

8.4 Voltage to hertz relation

This section discusses the voltage to hertz relation of the MLT inverter on a general level and does not rely on the measured line-to-line voltage.

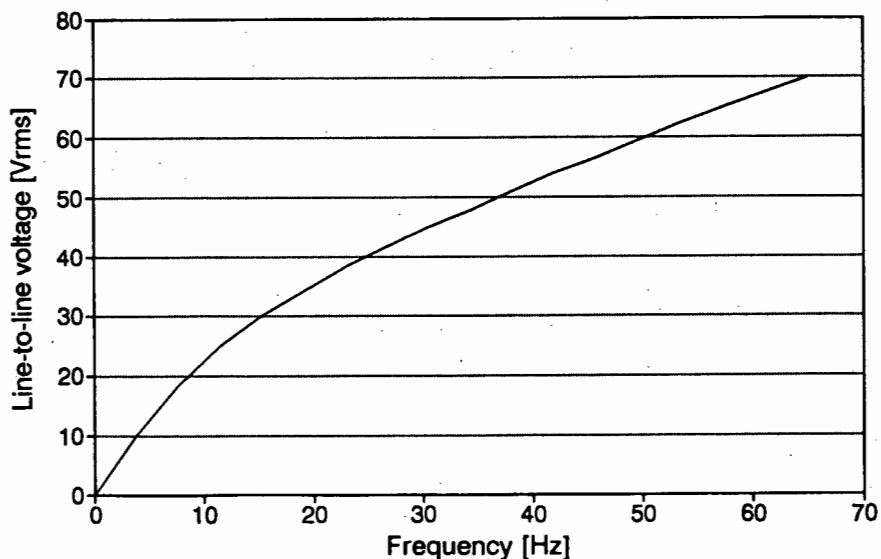


FIGURE 8.15 Programmed voltage to hertz relation of the MLT inverter
Source: Adapted from Davies (1992: Figure 29)

Figure 8.15 shows the programmed voltage to hertz (V/Hz) relation that was derived by Davies (1992) and programmed into the voltage look-up table. The derivation consisted of minimising the losses for the motor over the complete operating range.

The line-to-line voltage in the low frequency range will be boosted and will not run down to zero volts. The V/Hz curve will not be implemented continuously but is approximated by nineteen amplitudes. The best case would be 3.26Hz per amplitude division which would result in 19 amplitude steps spread evenly over 3Hz to 65Hz. I cannot find any reference as to whether this is the case. In my opinion the hardware offers the flexibility to assign amplitudes in these frequency ranges.

The array voltage oscillations, as discussed in the previous section, result in equal variations of the PWM voltage. Consequently, the PWM voltage will vary by 7.9% to 13.2% ($15V_{pp}/2/95V$ and $25V_{pp}/2/95V$ respectively). That is extremely high and undermines the careful derivation for an optimum V/Hz as performed by Davies.

The benefits of generating the PWM signals directly out of the microcontroller are realised in its ability to generate an overmodulated PWM signal. Through these means a larger line-to-line voltage can be generated than in an inverter with a maximum modulation index of one. A modulation index of one would result in a maximum rms voltage of $0.612 \times V_{arr}$ which gives $58V_{rms}$ for 95V array voltage (Mohan et al. 1989:132). With overmodulation a rms voltage of 74.1V can be generated from 95V. However that voltage would have degenerated into a square-wave resulting in undesirable low frequency harmonics. This inverter utilises overmodulation in combination with harmonic elimination and therefore can generate a higher rms voltage while eliminating the 5th, 7th, 11th and 13th harmonics.

8.5 Observed control algorithm characteristics

A number of observations have been made regarding the performance of the control algorithm. Both FVO and MST implementations have some characteristics which may be undesirable or non-essential. These are discussed below.

8.5.1 Basic control algorithm implementation

The array voltage oscillations as discussed in section 8.3 are the result of a too simplistic control algorithm that does not take account of the settling time of the system. A thorough description and suggestions are given in section 9.1 as both inverters have the same problem.

8.5.2 Fixed voltage operation

Narrow operating range

The operating range of the inverter is too narrow with the FVO program installed, as can be seen in Figure 8.17 in section 8.7. At irradiance levels of less than $750W/m^2$ (but larger than $540W/m^2$) the subsystem performs a start-up but passes through its operating point on the array IV curve and settles at an array voltage of 35V. The motor stalls and a restart may take place. In MST operation the subsystem is able to run at much lower input power levels.

FVO but not entirely FVO

It was found that the FVO program does not use the array voltage as its only control variable for its decision making. The microcontroller has a reset circuit that requires a square-wave at its input in order not to reset the microcontroller. This is provided from one of the PWM signals when running in fixed voltage mode (FVO). The inverter responds differently though when the speed sensor is connected to this reset circuit (called the watchdog circuit) which also feeds into the speed-sensing circuit. This is very obvious since the inverter is then able to operate at much lower input powers, very similar to the MST program.

Therefore, firstly, the FVO program uses the speed signal for control purposes (other than reset) but should use the array voltage as its only decision parameter. Secondly, it is possible that the PWM signal at the input to the watchdog and speed sensing circuit may affect the performance of the FVO program negatively (for instance the narrow operating range).

Non-essential states of operation

During FVO operation and feeding a PWM signal to the watchdog circuit the following non-essential states of operation could be observed:

- In the heating-mode the motor was at standstill but was being driven by the inverter. The irradiance was less than 540W/m^2 with the array voltage varying between 25V and 70V. The inverter did not exit this state after five minutes.
- In shaking-mode the motor performed a start-up from 120V but ran past its set-point voltage of about 95V and settled at an average array voltage of 35V where the motor just shakes. It usually restarted after one to five minutes but longer intervals were observed where operation was then terminated through my interference. Only when the irradiance exceeded 750W/m^2 were start-ups successful.

These states of operation should be avoided as they cause unnecessary wear on the subset components and none of these modes can ever deliver water.

8.5.3 Maximum speed tracking

Implementation of MST in the presence of array voltage oscillations

The fact that the steady state PWM voltage has a superimposed oscillation on its rms voltage has several implications as already pointed out. An additional implication is the effective execution of the maximum speed tracking control algorithm.

The MST program samples the array voltage every 80msec and the speed reading every 2sec (25 voltage samples for one speed sample). An average of the previous two speed samples is taken and compared to the current speed sample. The decision

on whether to increase or decrease the reference voltage is based on this process (the reference voltage is the set-point to which the actual array voltage is compared).

Two factors make the successful implementation of the maximum speed tracking program doubtful. One is the long sampling time of the speed signal (compared to the array voltage sampling time) and two are the possible minor speed fluctuations due to the array voltage oscillations. If minor speed fluctuations are present or any other disturbances in the load are present it is questionable if the present sampling time will provide sufficient accuracy for finding the maximum speed point.

Non-essential states of operation

The MST algorithm has similar states of operation to the FVO algorithm. The difference is that the range of irradiance levels at which they occur is narrower.

- In heating-mode the inverter feeds the motor with a current even though the motor does not turn. Maybe consecutive start-up routines are executed but that is neither measurable nor audible. It seems like the inverter attempts to start the motor continuously. The average array voltage is about 55V.
- Shaking-mode occurs at about 400W/m^2 while the inverter frequency is about 4Hz to 5Hz. No water is delivered.

Both these states of operation do not need to occur as the inverter should 'see' from its speed circuit that the motor is not running.

Blocked pump

A blocked pump was simulated by reversing the phases of the motor to reverse its direction of rotation. The pump's reversal pins stop the motor from turning. The motor tries about every 2sec to start the motor. It sounds like a current pump. It maintains a relatively good operating point (between 80V to 95V) and produces an output frequency of about 3.6Hz to 4.1Hz. The inverter was switched off after five minutes without incurring any damage.

8.6 General observations

Dynamic response

An appropriate test to evaluate the dynamic capabilities of a system is to apply a step-up or a step-down to the input. That was achieved by either disconnecting one string of modules (step-down) or by reconnecting one string of modules (step-up). The result for a step-up in MST mode is shown in Figure 8.16.

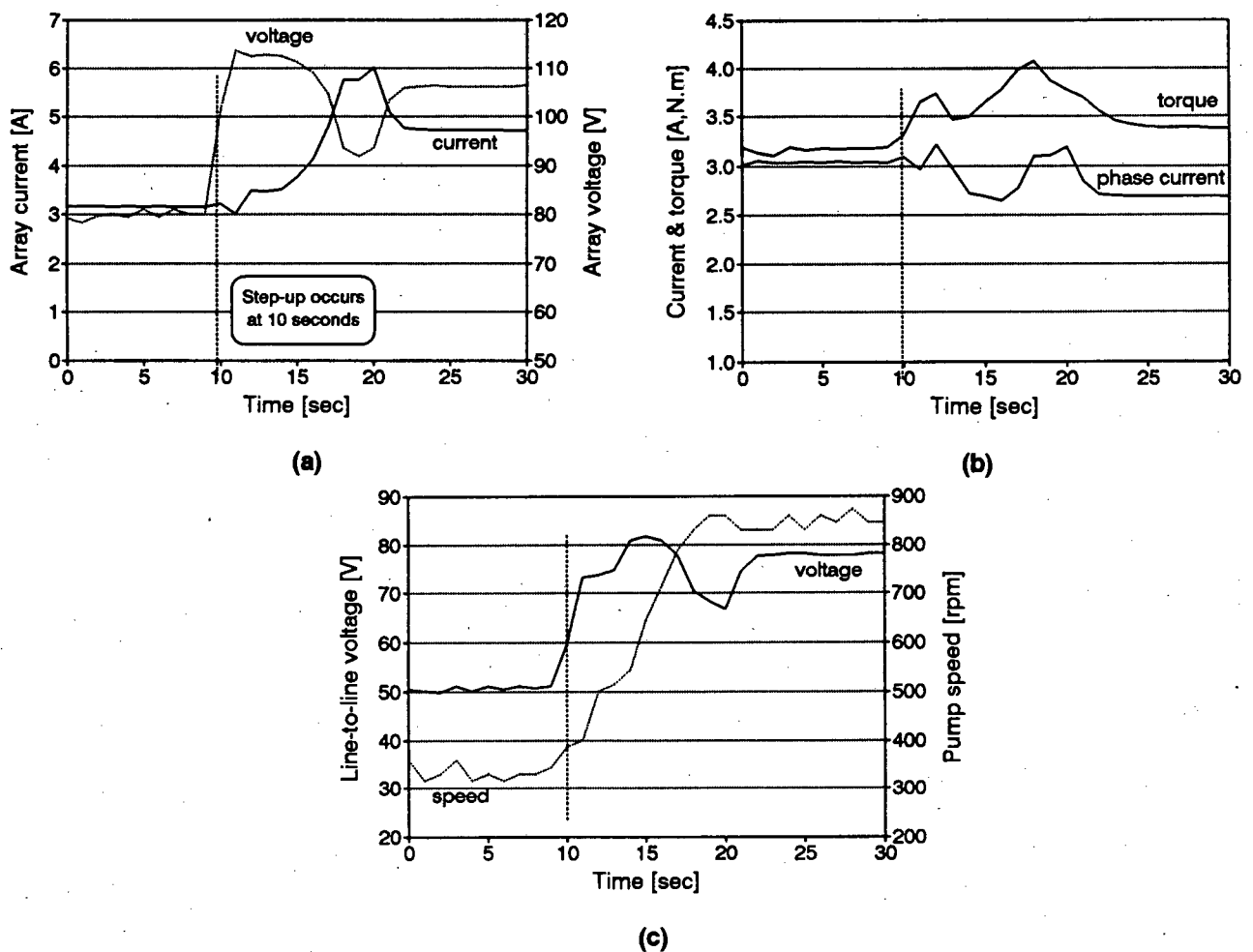


FIGURE 8.16 MLT system response under dynamic conditions: (a) array voltage and current; (b) phase current and pump torque; (c) line-to-line voltage and pump speed

The response is interesting in that it is not the array current that steps-up but the array voltage which steps-up from 80V to 113V, then decreases to 93V while the array current reaches a peak and then rises again to 106V. The response is also slower since its sampling frequency is only 80msec (compare to Solvo response where the voltage is sampled every 10msec). Pre- and post-step array operating points are not good but this may be due to the inability of the MST program to operate properly in the presence of array voltage oscillations.

The inverter line current and the torque both show the same response: a small peak for the array voltage peak and a larger peak for the array current peak.

The inverter line-to-line voltage follows the step-up of the array voltage quite closely. It does not have a choice since it is a PWM signal. It settles at a very high line-to-line voltage ($78V_{\text{rms}}$) since the array voltage has settled at 106V. The pump speed rises to its new value within 10sec.

Tuning problems

Setting the fixed voltage point requires a measurement device capable of displaying the mean voltage measured (due to array voltage oscillations).

Tuning for FVO while the inverter is operating gives the impression that the fixed voltage point is not very adjustable. That is, the multi-turn potentiometer is turned but the array voltage does not respond. However, on the next start-up one may find that the inverter runs past its optimum voltage point and settles at 35V for shaking-mode (which means that the array reference voltage is now set too low). The best way is to turn the potentiometer in small steps and do a restart after each new setting to observe whether the inverter will operate closer to the desired operating point once it has reached steady state conditions.

Tuning for MST involves setting the array voltage potentiometer first with the FVO program and then inserting the MST program. Now the voltage window in which the MST program can hunt for the maximum speed should be tuned correctly (that is the FVP must be tuned to sit in the middle of the desired window in which one would most likely find the MPP). Then the speed potentiometer requires adjustment, not to maximise speed, but to allow the system to start-up at as low a power threshold as possible. In a brief discussion with John Davies we could not find a logical explanation of why a particular range of speed settings on the potentiometer prevents system start-up from base speed at lower irradiance levels (initially the inverter required $900\text{W}/\text{m}^2$ array input power to leave base speed for normal operation).

System start-up

The subsystem starts operation (in MST mode) at an irradiance level of $460\text{W}/\text{m}^2$ which is equivalent to about 200W out of the array. These values can vary widely since they are dependent on cell temperature and array operating point.

The system starts up at lower irradiance levels but does not manage to reach a steady state operating point. This gives the impression that the system could operate with an improved algorithm.

Torque pulsations

Torque pulsations were briefly discussed in chapter two (subsection 2.6.4), in the context of harmonic frequencies occurring in the current waveform. However in the Solvo and MLT systems, lower frequency torque pulsations were physically observed. Measurements conducted to establish the frequency and magnitude of these torque pulsations did not provide data that could be interpreted usefully, so attempts were made to count the pulses manually. Repeated tests led to the conclusion that the pulsations had a frequency of about 1.2Hz (5 pulses in 4sec). This result comes close to the frequency of the large peak oscillation (period of 1sec to 1.5sec) as shown in Figure 8.8b, Figure 8.11 (arrows) and Figure 8.12 (DC capacitance of 2040 μ F) 3.5Hz oscillation. The faster oscillation recorded in array voltages would not be as detectable (higher frequency and smaller amplitude) as the slower oscillation voltage. There is further discussion on torque pulsations in section 9.1.

8.7 System performance

The aim of this section is to present the data of the MLT PVP system and subsystem instantaneously and on a daily basis for different amounts of daily solar irradiation. The daily energy efficiency of the components, the subset (controller and motor), the subsystem and the system and the volume flow are presented for standard solar days from 2kWh/m²/day to 8kWh/m²/day. The emphasis in this section is on the shape and trends of the graphs. The performance values are also briefly discussed but further discussion takes place in the comparative chapter ten.

In addition, a solar irradiance profile for a single-axis tracking array has been generated, based on the solar irradiance profile in Figure 6.10. It is referred to as a tracking solar day. System performance predictions for a standard solar day and a tracking solar day are compared.

8.7.1 Instantaneous performance

The graphs in Figure 8.17 show the instantaneous performance of the MLT system and subsystem in FVO mode (no speed sensor connected).

The narrow operating range becomes very apparent when compared to Figure 8.18 below. Both system and subsystem efficiencies are flat and reach values of 3.4% and 33% respectively which is also lower than those achieved with maximum speed tracking.

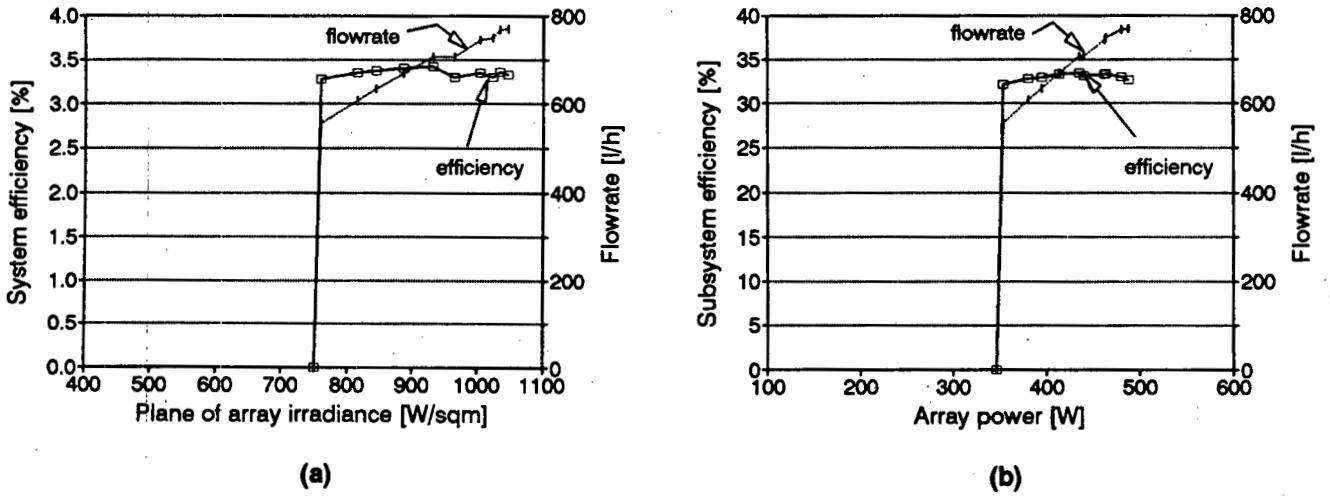


FIGURE 8.17 FVO operating mode: (a) MLT system performance; (b) MLT subsystem performance

The system and subsystem performance graphs, Figure 8.18, for MST mode of operation reach values of 3.7% at 700W/m² and 35% at 360W respectively. Both graphs show that the system first operates at base speed where the flowrate is zero and then jumps to an improved operating point. Both graphs show an unevenness in their efficiency and flowrate curves which is mainly due to the pump characteristics and a non-optimised voltage to hertz relation in that particular region.

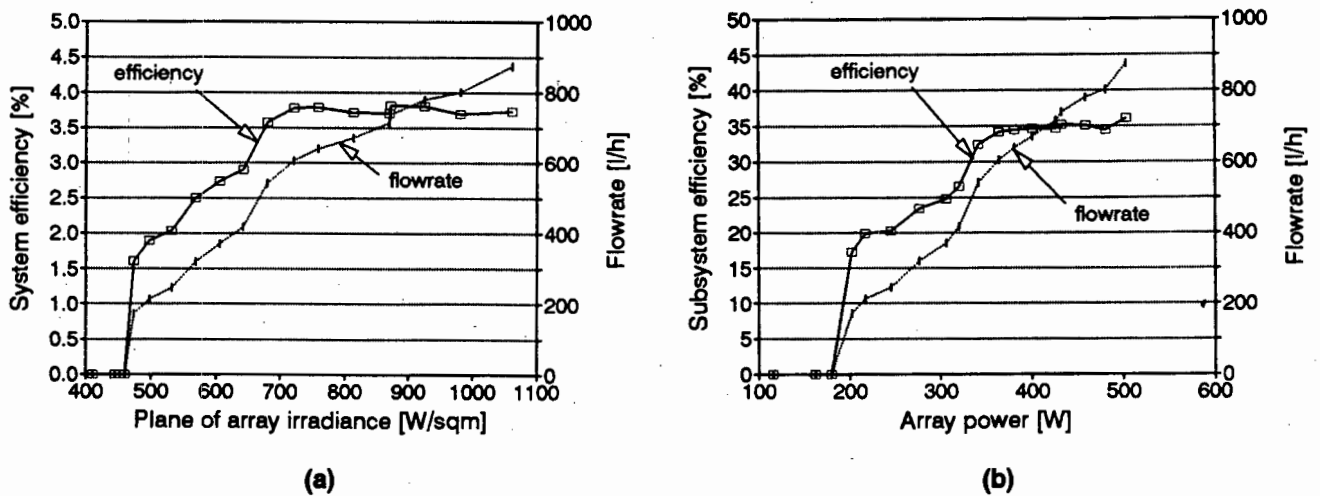


FIGURE 8.18 MST operating mode: (a) MLT system performance; (b) MLT subsystem performance

The uncertainty in the system efficiency data is:

$$\begin{aligned}
 U_{abs} (r_{sys})_{1050W/sqm} &= 12.1\% \\
 U_{rel} (r_{sys})_{1050W/sqm} &= 6.9\% \\
 U_{abs} (r_{sys})_{750W/sqm} &= 15.7\% \\
 U_{rel} (r_{sys})_{750W/sqm} &= 9.4\%
 \end{aligned}$$

The uncertainty in the subsystem efficiency data is:

$$\begin{aligned} U_{\text{abs}} (\eta_{\text{subsys}})_{500\text{W}} &= 6.6\% \\ U_{\text{rel}} (\eta_{\text{subsys}})_{500\text{W}} &= 2.5\% \\ U_{\text{abs}} (\eta_{\text{subsys}})_{350\text{W}} &= 6.8\% \\ U_{\text{rel}} (\eta_{\text{subsys}})_{350\text{W}} &= 2.9\% \end{aligned}$$

The uncertainty in the flowrate data is:

$$\begin{aligned} U_{\text{abs}} (Q)_{200 \rightarrow 1000/\text{h}} &= 6.1\% \\ U_{\text{rel}} (Q)_{200 \rightarrow 1000/\text{h}} &= 2.2\% \end{aligned}$$

The subsystem efficiency provides the data with lowest uncertainty. The uncertainty in the system efficiency stems from the large errors in the irradiance measurement.

8.7.2 Daily energy efficiency performance

The daily energy efficiency (DEE) is calculated by dividing the total energy out of a component/system by the total energy into a component/system over the course of a standard solar day. Therefore the DEE's of the components are partly dependent on surrounding component performances and matching. For example, the motor DEE depends on the performance of the array and the electronic controller. The DEE of the motor may therefore change with a different array and controller. The method for daily energy efficiency calculations is in appendix A5.

Fixed voltage operation

The DEE of the components, the subset and the subsystem are shown in Figure 8.19.

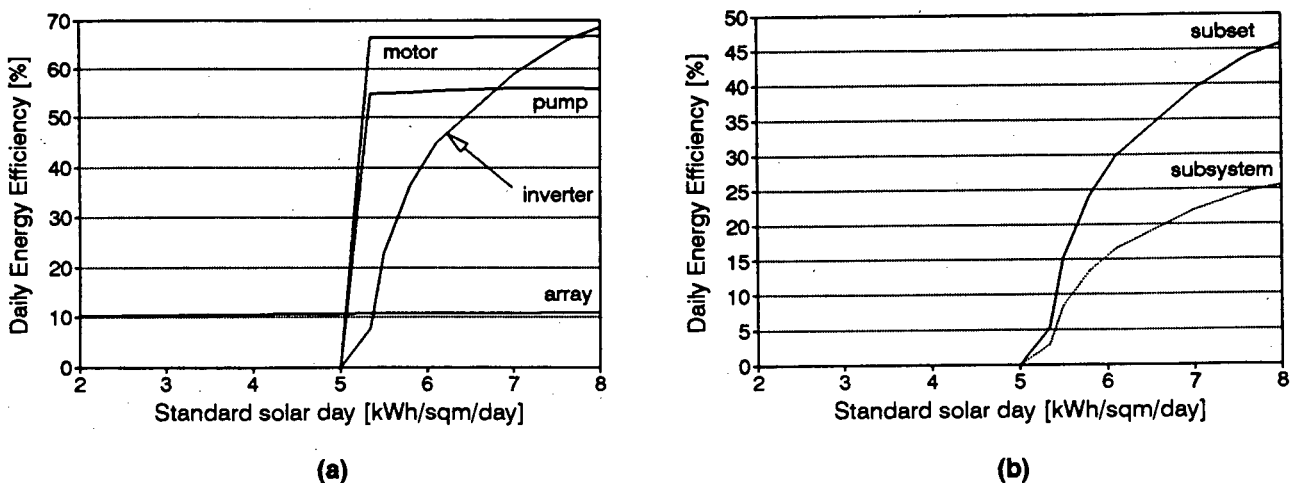


FIGURE 8.19 MLT system in FVO mode: (a) DEE of components and (b) DEE of subset and subsystem components

Subsystem operation starts with standard solar days (SSD) of more than 5kWh/m²/day. The inverter performs poorly because the subsystem starts operation when receiving power in excess of 350W. The inverter probably starts operation at 50W already but since the algorithm is unable to achieve steady state operation at input powers lower than 350W its DEE has to be poor. The DEE curve of the motor is very flat, being 66%, since its instantaneous efficiency curve is also flat.

The DEE of the subset and the subsystem are both increasing with only a slight reduction in gradient. Subset DEE and subsystem DEE reach 46% and 26% at 8kWh/m²/day respectively.

Figure 8.20 shows the DEE of the system and the daily volume flow. Both gradients decrease slightly and system DEE reaches 2.7% and volume flow delivers 4.8m³ for a SSD of 8kWh/m²/day.

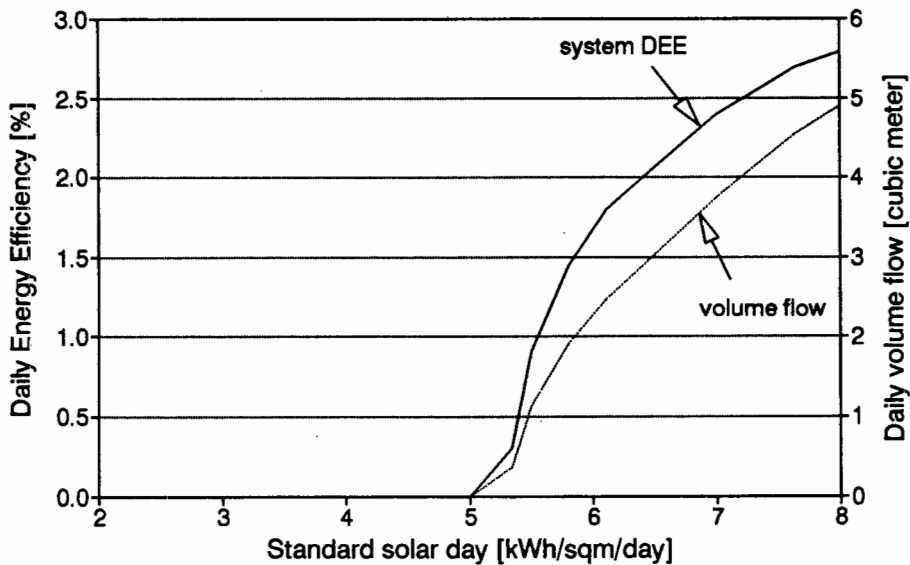


FIGURE 8.20 MLT system in FVO mode: system DEE and daily volume flow

The comparison between a standard solar day and a tracking solar day (TSD) is shown in Figure 8.21. The DEE of the system and the volume flow are chosen as the main base for comparison. Graph (b) shows the difference between the TSD and the SSD basis on the SSD.

The difference between the SSD and the TSD for the DEE of the system is 18% at 1100W/m² noon peak irradiance. As the noon peak irradiance decreases the difference increases. At 800W/m² the difference is 40% and reaches 90% at 700W/m². This is close to where the subsystem ceases to operate under SSD conditions while still operating under TSD conditions. The volume flow follows the same shape but at a much higher differential percentage. At 1100W/m² the percentage difference is 48%, at 800W/m² it is 78% and at 700W/m² it is 138%.

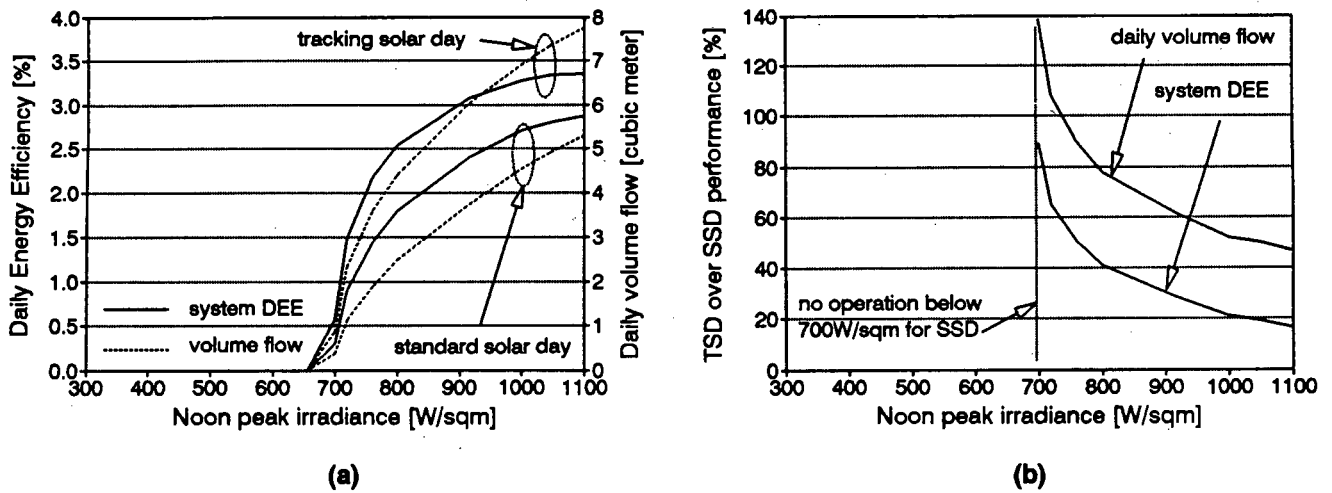


FIGURE 8.21 Tracking solar day and standard solar day for the MLT system DEE and volume flow in FVO mode: (a) performance and (b) percentage of TSD over SSD performance

Maximum speed tracking

The DEE's of the MLT system using the maximum speed tracking algorithm are very different to the fixed voltage operation data. Figure 8.22 shows the DEE of the component, the subset and the subsystem. The inverter now maintains a better DEE over a range of SSD values. The DEE is 55% at 2kWh/m²/day and 90% at 8kWh/m²/day. The gradient becomes flatter towards higher SSD values.

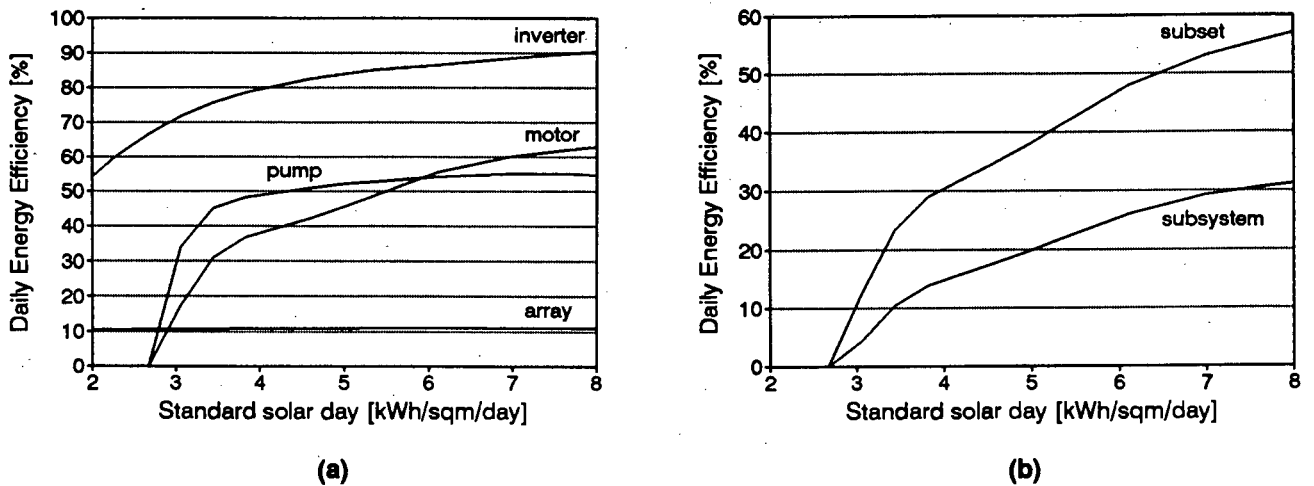


FIGURE 8.22 MLT system in MST mode: (a) DEE of components and (b) DEE of subset and subsystem components

The DEE of the motor seems to go through three discrete gradients, becoming flatter with increasing daily energy. This particular shape will be due to the efficiency curve of the motor (see Figure 8.2). Motor operation starts at a SSD larger than

2.6kWh/m²/day. The motor reaches 30% quickly and then progresses to the next gradient where it reaches 60% at 7kWh/m²/day. The DEE of the pumping set increases very steeply at low daily energy content. It reaches a peak of 55% at 7kWh/m²/day.

The DEE of the subset and the subsystem are both increasing with only a slight reduction in gradient. Subset DEE and subsystem DEE reach 57% and 32% at 8kWh/m²/day respectively.

Figure 8.23 shows the DEE of the system and the daily volume flow. The system efficiency curve passes through three discrete gradients, the middle one being linear over the range of 4kWh/m²/day to 7kWh/m²/day. It reaches 3.4% at 8kWh/m²/day. The volume flow has a smaller gradient from 3kWh/m²/day to 5kWh/m²/day than above 5kWh/m²/day. The load requirements of the pump that shape this curve (see also flowrate in graph (b) of Figure 8.18).

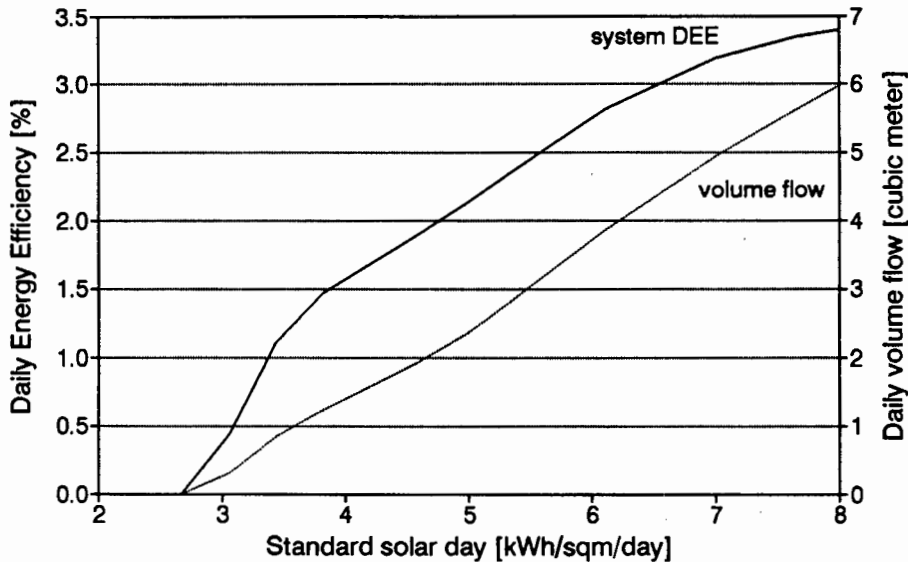


FIGURE 8.23 MLT system in MST mode: system DEE and daily volume flow

The comparison between TSD and SSD is shown in Figure 8.24 with the emphasis on the DEE of the system and the daily volume flow delivered.

The difference between the SSD and the TSD for the DEE of the system is 9% at 1100W/m² noon peak irradiance. As the noon peak irradiance decreases the difference increases. At 600W/m² the difference is 20% and reaches 60% at 400W/m². This is close to where the subsystem ceases to operate under SSD conditions. The volume flow follows the same shape but at much higher differential percentages. At 1100W/m² the difference is 36%, increasing linearly to 52% at 600W/m² noon peak irradiance. The curve then becomes hyperbolic as it increases to 100% at 400W/m² where the subsystem with SSD profile ceases operation.

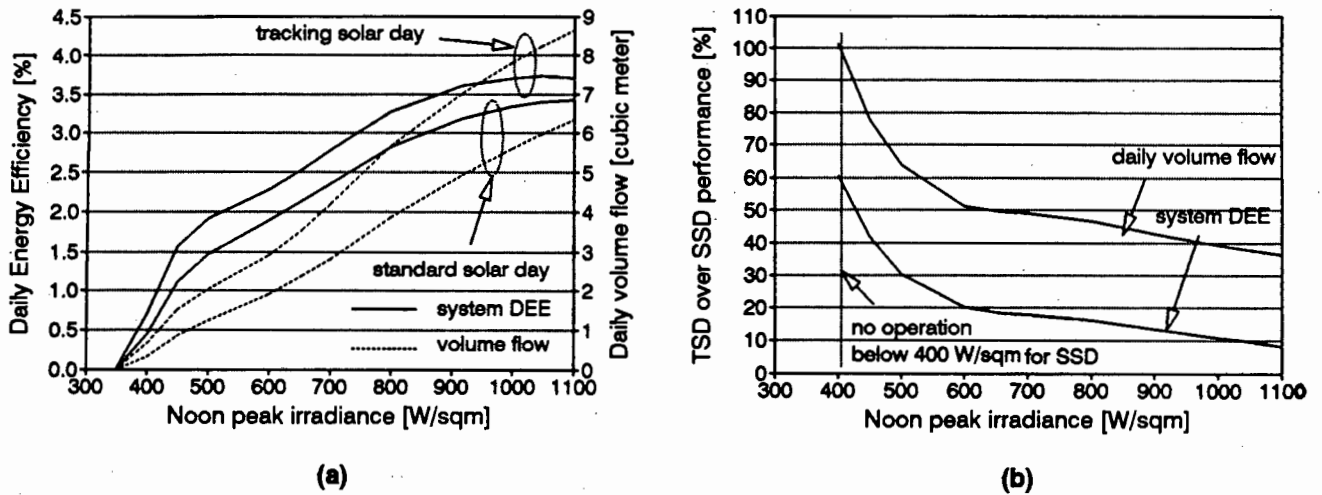
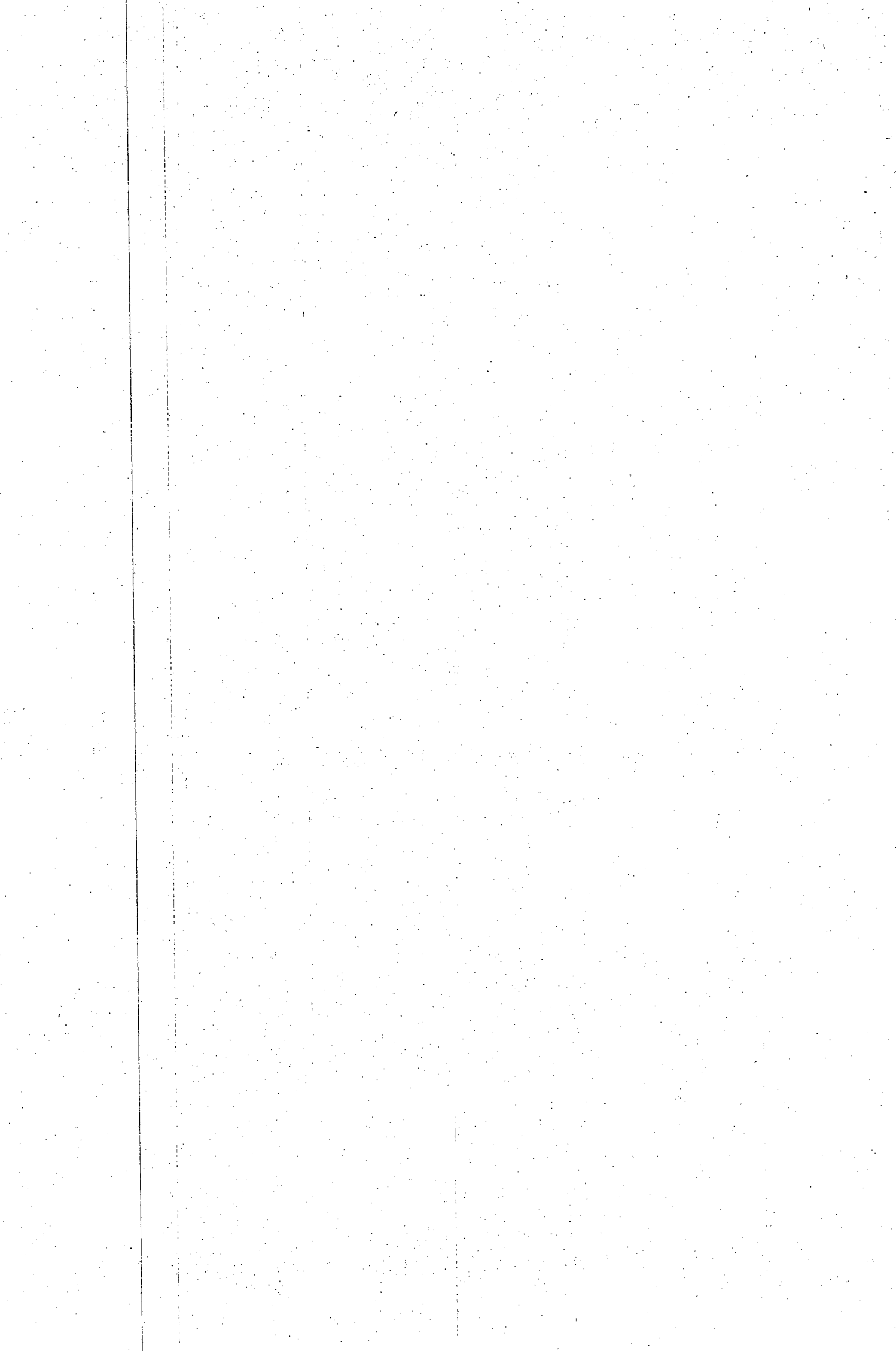


FIGURE 8.24 Tracking solar day and standard solar day for the MLT system DEE and daily volume flow in MST mode: (a) performance and (b) percentage of TSD over SSD performance

This demonstrates the gain of a tracking array particularly for mid-region noon peak irradiance levels ($600\text{W}/\text{m}^2$ to $800\text{W}/\text{m}^2$). However sites with such low irradiance levels usually have a higher component of diffuse irradiation in which case a tracking array does not provide as much performance improvement as demonstrated in Figure 8.24b.



Chapter Nine

PROPOSED IMPROVEMENTS FOR THE PROTOTYPE INVERTERS

This chapter discusses the aspects of the prototype inverters that require improvements. The main emphasis is firstly on avoiding inverter/system break-down and secondly on improving the inverter (and motor) performance.

A serious challenge for all the suggested proposals is to make sure that these will work for all possible installation circumstances like for example different peak Watt array size, different operating voltages, different pulley ratios and for a range of heads. If changes for different circumstances cannot be avoided then these should be implementable with minimum software alterations or hardware settings.

The first section deals with the basic control algorithm as it is implemented in both inverters. The second section proposes ways of avoiding undesired states of operation that occur in the inverters. Section three discusses some realistic aspects of the voltage to hertz relation. Section four proposes a Solvo inverter with a lower switching frequency and section five briefly lists a few of the remaining MLT inverter software problems.

The last two sections discuss hardware additions concerned with protecting the inverter and general design considerations.

Most of the sections deal with the MLT and the Solvo inverter as both exhibit similar problems. Program code details are only supplied for the Solvo inverter (it was the initial aim to evaluate the Solvo inverter and to develop it into a marketable product). However, since both inverters use the same microcontroller it would be possible to use some of the proposed routines with the MLT inverter (a few minor alterations would be necessary). Marc Baret, who is a student at the University of Cape Town, is currently redesigning parts of the MLT inverter. He is likely to implement essential program changes himself.

9.1 Control algorithm evaluation

The array voltage oscillations discussed in section 7.3 and 8.3 are the result of the type of control algorithm that has been implemented in the Solvo and the MLT inverter. This section deals with the reasons for this behaviour and provides some suggestions towards the design of a suitable controller.

As a reminder, the array voltage oscillations result in low frequency oscillations on the average steady state line-to-line voltage which compromises an optimum voltage to hertz relation with the effect of a marginally decreased motor efficiency. The

oscillations also result in low frequency torque pulsations and possibly minor speed fluctuations. It is therefore essential to revise the algorithm to improve overall performance and stability. In addition the monitoring that is being suggested in section 9.2 could be implemented with more certainty.

9.1.1 Problem analysis

The control algorithm which decides whether to increase, decrease or retain the previous output frequency is shown in a flowchart in Figure 9.1. This algorithm has been implemented in both inverters. The MLT inverter evaluates the speed reading in addition to the array voltage when in MST mode and does incremental changes to the reference voltage after every twenty-fifth array voltage reading (Davies 1992: 88-9). Due to the slower sampling rate of the speed signal, it is assumed that the speed algorithm does not interfere with the voltage control algorithm. The Solvo inverter takes a voltage sample every 10msec and the MLT inverter takes a voltage sample every 80msec. Each frequency interval has a PWM voltage amplitude assigned to it by means of a look-up table (see chapter three, subsection 3.5.4 and 3.5.4). The algorithm consequently only needs to change the frequency.

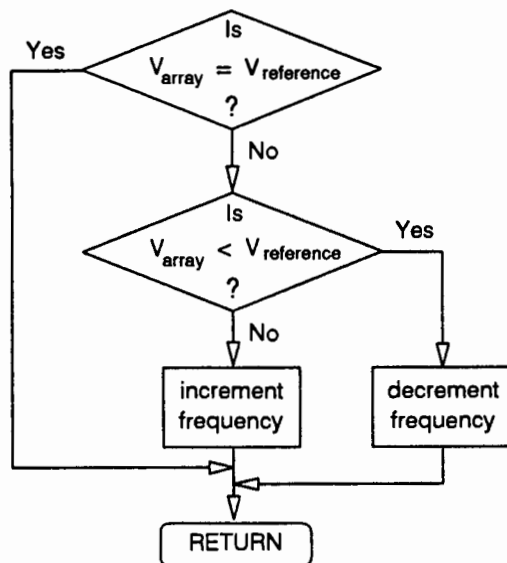


FIGURE 9.1 The basic control algorithm as currently implemented in the prototype inverters

The algorithm compares the actual array voltage to the programmed reference voltage. If they are equal then the inverter will retain its previous frequency and continue operation. This is of course never the case in the tested systems, since the array voltage is oscillating with a frequency of 1.7Hz to 7Hz. Therefore it will continually either increase or decrease the frequency to the motor in a multiple of single steps.

Figure 9.2 shows the array voltage oscillations, the inverter output frequency and the motor acceleration as a function of degrees. All values displayed in the graph are only

reference values. The array voltage has an average of $6V_{ref}$, the frequency has an average of $3Hz_{ref}$ and the motor acceleration has an average of zero $rad.s^{-2}_{ref}$. The x-axis uses degrees to show the phase shifts. One cycle (360°) could be equivalent to anything between 143msec (7Hz) to 590msec (1.7Hz).

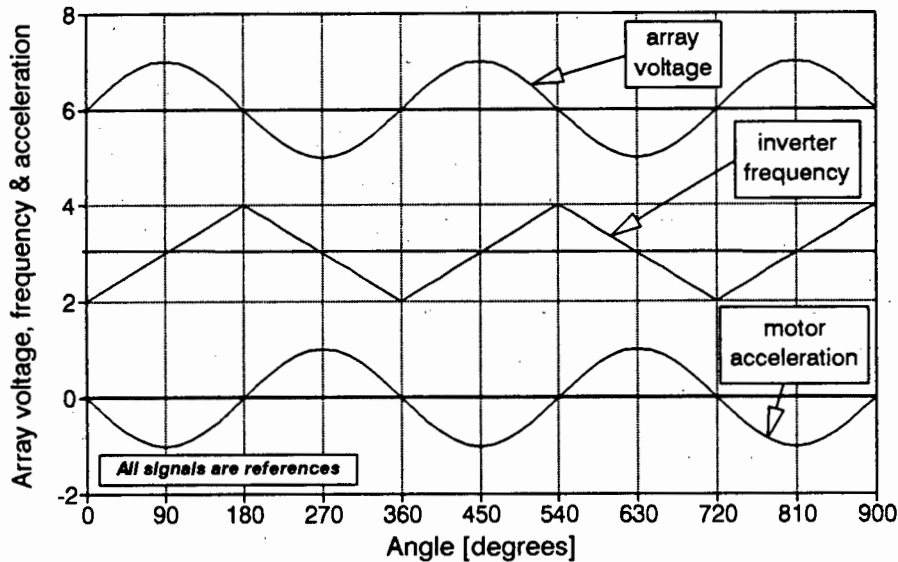


FIGURE 9.2 Signal shape and relation to currently implemented control algorithm

The algorithm, using the above flowchart, will increment the inverter frequency from 0° to 180° as shown and will decrement the frequency when the array voltage is between 180° to 360° . For the Solvo inverter, that means that the algorithm will take between 7 ($140msec/2/10msec$) to 16 ($330msec/2/10msec$) samples per half cycle. Therefore it increments the frequency 7 to 16 times during the first half of the cycle and decrements it the same amount of times during the second cycle. Looking at the graph one can see that the frequency lags 90° behind the array voltage oscillation.

The motor accelerates during periods of array voltage decrease (motor acceleration results in a higher current demand and consequently the array voltage has to decrease) and decelerates during periods of array voltage increase (decrease in current demand). The motor acceleration lags 180° behind the array voltage oscillation.

The rms voltage will take the same shape as the array voltage, ie with an oscillation voltage on the average rms voltage (it may however occur that the inverter frequency change, due to the triangular waveform, results in different voltage amplitudes from the look-up table - then the average rms voltage will vary). Therefore the rms voltage leads the frequency by 90° but is in anti-phase with the motor acceleration. Since both the inverter frequency and the inverter voltage affect the motor torque one can expect quite a complex torque waveform due to the phase-shift between the voltage and the frequency. This point also clarifies why the voltage to hertz relation cannot be maintained.

The torque pulsations are expected to have a frequency similar to the array voltage oscillation frequency or higher. Only the low frequency pulsations could be felt. Since the power ratings of the systems are small (500W maximum motor input power) it is not clear to what degree the pulsations are detrimental to the motor (the pump should be unaffected by torque pulsations as the V-belt and the transmission shaft to the pump will dampen the pulsations). If the torque pulsations could not be avoided through a revision of the control algorithm this would warrant investigation since the system is to be marketed as virtually maintenance-free.

9.1.2 Suggestions towards the design of a suitable controller

Block-diagram of the control system

The block-diagram in Figure 9.3 shows all the relevant components in the control system which consist of the PVP system, a controller being the microcomputer, a data hold circuit and the analog-to-digital converter (ADC). The controller, the data hold circuit and the ADC are physically part of the inverter. The control variable, the array voltage, is compared to the reference voltage. The controller decides how to drive the motor/pump set at the next interval T . T is equivalent to the sample time. The data hold circuit is the dedicated PWM IC in the Solvo inverter and part of the microcontroller in the MLT inverter. The PVP system includes the power module in the inverter which drives the motor/pump set. The power module receives the drive signals from the data hold circuit and its power from the array. The irradiance is treated as a disturbance, having a potentially large random component. It does however control the available amount of power and therefore the rate of output (flowrate).

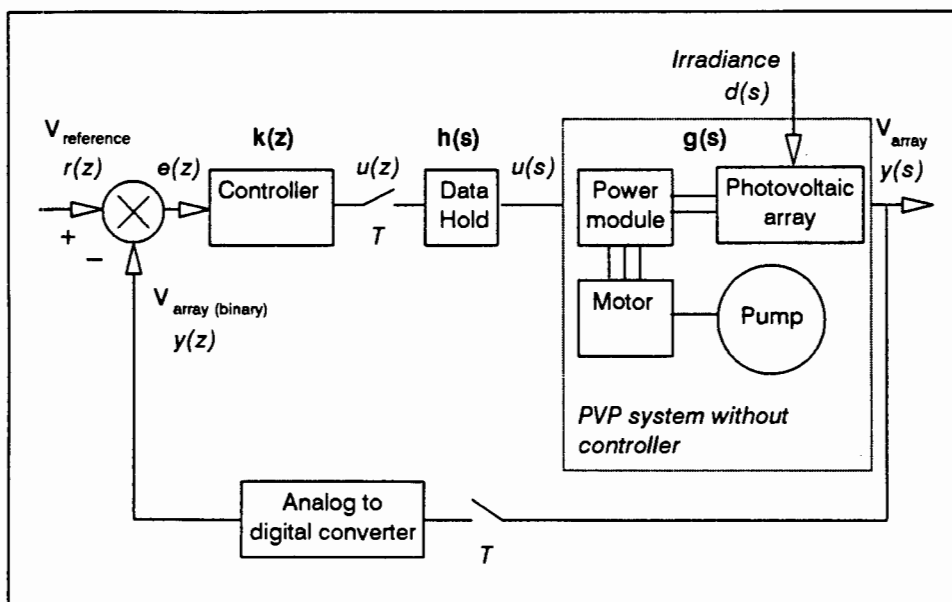


FIGURE 9.3 Control diagram of a PVP system with fixed voltage operation

The bold parameters are the transfer functions of the individual blocks and the italic parameters refer to the input or the output variable of a block. The transfer function of the PVP system is designated by $g(s)$. If the transfer function is known then a suitable controller $k(z)$ can be designed. The block-diagram consists of a continuous (analog) part and a discrete (digital) part. The PVP system without the controller forms the continuous part of the whole system. The variable 's' designates the continuous domain (Laplace transform). The digital part is formed mainly by the controller which takes samples of the control variable at regular intervals T . The variable 'z' designates the discrete domain (z-transform).

The problem of finding a suitable control algorithm is complicated by the following factors:

- The output variable of the PVP system which effects changes in the output frequency (and voltage, via look-up tables) to the power module is the array voltage (flowchart in Figure 9.1). However, the response of the array voltage to changes in output frequency can be non-linear for two reasons. Firstly, because of the non-linear IV characteristics of the array and secondly because of non-linear motor/pump transfer functions at different operating frequencies (for example, the motor/pump set will respond differently to equal changes in the frequency at 20Hz operation and 60Hz operation).
- The controller controls the frequency to the motor in order to control the load (motor/pump set) in order to control the array voltage. This feedback loop is therefore characterised by an inherent lag.
- The transfer functions are likely to change for different installations. For example, changes in the type or size of pump, delivery head, pulley ratio and inverter input capacitance could change the response characteristics. A suitable controller should be able to cope with the possible variations in the transfer functions, or cope with specific installations in which case a range of controllers for a range of installation conditions would be required.
- There are practical difficulties in obtaining the transfer functions of a PVP system since the system requires the controller to reach an acceptable operating point on the array. Further, it is difficult to get inside the system to effect independent step inputs, as discussed further below.

These factors make it non-trivial to find a suitable controller using the conventional approach.

Conventional approach

Although the system has non-linear aspects, there may be a sufficiently linear narrow region around the array voltage operating point to allow for effective linear control.

The conventional procedure for obtaining an appropriate controller is to find the transfer function of the system $g(s)$ (refer to Figure 9.3) by applying a step input to the system at $u(s)$. This means that the power module should receive a frequency step (for example from 40Hz to 50Hz) with a corresponding voltage step due to the programmed voltage to hertz relation. By observing the response of the array voltage $y(s)$ a transfer function can be calculated from the settling time and the gain. The controller $k(z)$ can be evaluated in conjunction with $g(s)$ subject to a few constraints like overshoot, maximum error signal and maximum time allowed to settle to within a certain percentage of the final value.

This approach is clear in theory but could pose difficulties in practice. One possible approach would be to program the controller with a fairly wide deadband in which it does not change the output frequency. Once the controller reaches this deadband it may have reached a temporary steady state without the presence of array voltage oscillations. This state could be detected by the controller (with some intentional delay to allow for steady state settling) and could be used to trigger a discrete pre-programmed frequency step input to the power module. There would be a corresponding change in voltage due to the fixed V/Hz relation.

With no further control, the array voltage should settle at a new array operating point, showing the array voltage response to the step under these conditions. The response could be investigated for a range of conditions. For example:

- a) at different array operating voltages, while the irradiance is constant;
- b) at different inverter operating frequencies, while providing sufficient power at each frequency;
- c) for different frequency step sizes - within limits (as to not settle near short-circuit current);
- d) different pulley sizes;
- e) different delivery heads;

It does not seem practical to combine a single controlled frequency step with a corresponding change in irradiance. This might limit the applicability of the information gained.

Possible options for modification

The scope of the dissertation did not extend to a systematic investigation of improved control algorithms for the prototype inverters. However, this question is of practical importance, and will hopefully be taken further in the future.

It is possible that the present algorithm (or alternatives) could be adapted to resolve the observed problems. Some of the options which could be considered are sketched below. Without establishing the transfer functions however it is not possible to make definite recommendations. The suitability of any of the listed options would need to be investigated in detail.

Deadband controller with saturation

This basic controller would incorporate the present algorithm but with a deadband (Anand 1974). A deadband is a region in which the controller does not change its output (that is the controller maintains its present frequency to the power module). The width of the deadband might be $\pm 2V$ to $\pm 4V$ around the reference array voltage. If the controller manages to remain within the deadband then the array power output losses would be reduced. Once the difference between the reference voltage and the actual array voltage is larger than the deadband the controller drives the power module as usual. This form of algorithm is still very simplistic but might reduce the amplitude of the array voltage oscillations.

Sampled average with deadband

This controller would incorporate a deadband but would also use a linear algorithm to evaluate a number previous error samples in conjunction with the present error sample and then determine by what amount the frequency has to be changed.

Controller with regions and deadband

A discrete state space controller (Anand 1974) could be considered with defined regions around the reference voltage which become narrower closer to the reference voltage. The closer the array voltage is to the reference voltage the longer the time-interval before the output frequency is changed. This is shown graphically in Figure 9.4.

The error signal is equivalent to the reference voltage, $r(z)$, subtracted from the actual array voltage, $y(z)$. The zero line in the graph is therefore the reference voltage. When the error signal is positive the frequency will be increased and when the error signal is negative the frequency will be decreased. All regions have the same sampling time but will only effect a change in the output frequency after a number of samples.

In terms of the Solvo inverter algorithm, region A is the region where control changes would take place at the sampling frequency, every 10msec. The error signal (in this example) has to be larger than $\pm 12V$. Region E is the deadband where no changes

in output frequency will occur. Here the error signal magnitude will be within $\pm 1V$. The intervals in which region B, C and D will effect changes have to be selected by trial and error. The following has to hold true though: Interval D > interval C > interval B > interval A (for example A = 10msec, B = 20msec, C = 40msec and D = 90msec).

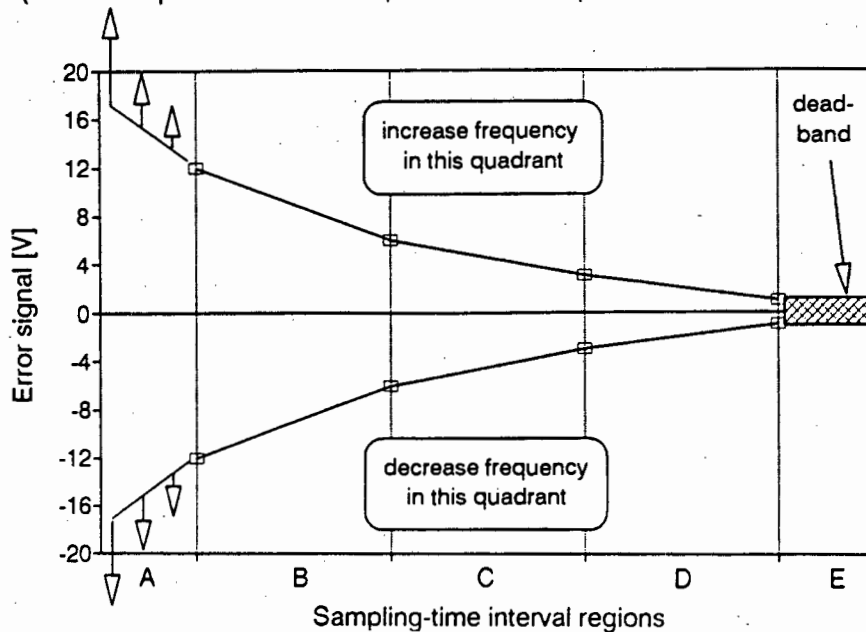


FIGURE 9.4 Graphical representation of a controller with regions and a deadband

This type of controller could allow the motor/pump set to settle close to the reference voltage while still maintaining a fast enough response time when the array voltage moves too far away from the reference voltage.

A flowchart and program code, for this approach were developed for the Solvo inverter (appendix A7.1), but have not been tried out. The program could also be tested for the MLT inverter, with minor adaptations.

Fuzzy logic control

The observed problems in the present algorithm could almost certainly be resolved through fuzzy logic control but it is doubtful whether the degree of complexity and non-linearity would warrant this. If, however, installation-dependent factors lead to a problematic range of transfer functions, requiring excessive customisation for effective conventional algorithms, then a more robust and versatile fuzzy control algorithm could be worthwhile.

9.2 Monitoring of undesired states of operation

9.2.1 Incorrect array operating point

Both inverters can lose their average fixed voltage point on the array and operate at a very low array voltage. Under these conditions the inverter usually still operates but the motor will have stalled.

I would suggest that both microcontrollers should implement a routine which tests whether the array voltage is below a well chosen threshold (say 50% to 60% of the open-circuit voltage). If that occurs once then either do a restart or inhibit the output to the motor and enter a wait routine of suitable length (for example a time-value between 30sec and 10min). A flowchart is shown in Figure 9.5. The program has to be placed into the timer-interrupt routine that obtains the array voltage from the ADC.

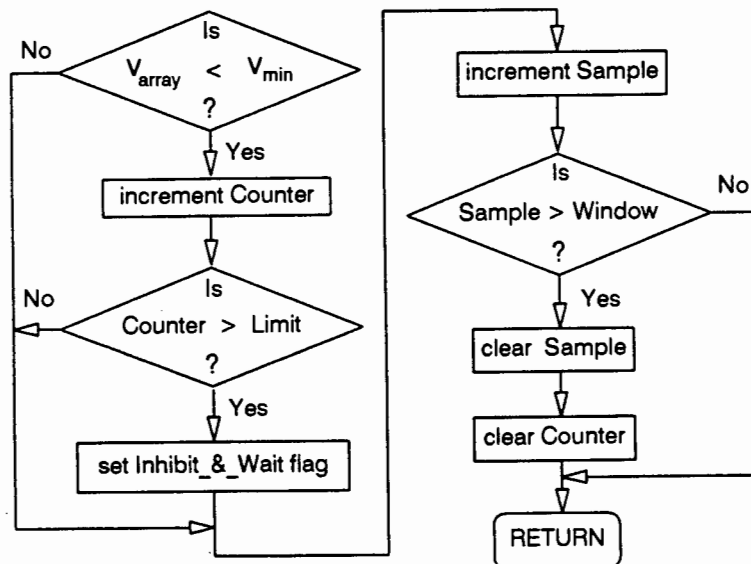


FIGURE 9.5 Flowchart for the monitoring of a low array voltage operating point

The flowchart shows a method of obtaining an average array voltage in software (assuming that the array voltage oscillations are still present). V_{min} is the minimum allowable average array voltage and V_{arr} is the instantaneous value from the analog-to-digital converter. One set of samples could be as many as 250 before resetting. This number would be stored in the 'Window' parameter. For the Solvo inverter this would cover array voltage samples over a time of 2.5sec (about eight array voltage oscillation cycles, at 3.5Hz). That is more than sufficient and could also be reduced. The 'Limit' parameter contains half the value held in 'Window'. Once the counter reaches the 'Limit' value a flag is set which is continuously scanned in the main program. The response may be a restart or wait routine. If the number of samples exceeds the value in the 'Window' parameter then the 'Sample' and 'Counter' parameter are cleared and the process is repeated. The program code for the Solvo inverter is listed in appendix A7.2.

The overall improvements from this addition to the program are as follows: The Solvo inverter will be able to exit from the situations of lost algorithm where the motor gets stuck. It will also avoid some of the non-essential states of operation (section 7.5). In case of a damaged power module this program addition will protect the drive circuit which usually overheats trying to drive the power module. The MLT inverter will be able to avoid most of its non-essential states of operation for both FVO mode (subsection 8.5.2) and MST mode (subsection 8.5.3).

9.2.2 Minimum power threshold

The idea behind this addition to the program is to use the pump as a form of power measurement. If the pump does not exceed a particular speed (detectable through the inverter frequency) within a particular time then inhibit the inverter output and enter a wait state for a set time period.

This additional algorithm should not be implemented too strictly as the states of operation and occurrence will change for different speed ratios (pulleys), different pump types and at different delivery heads. Hence the algorithm needs to incorporate sufficient tolerance to accommodate these factors.

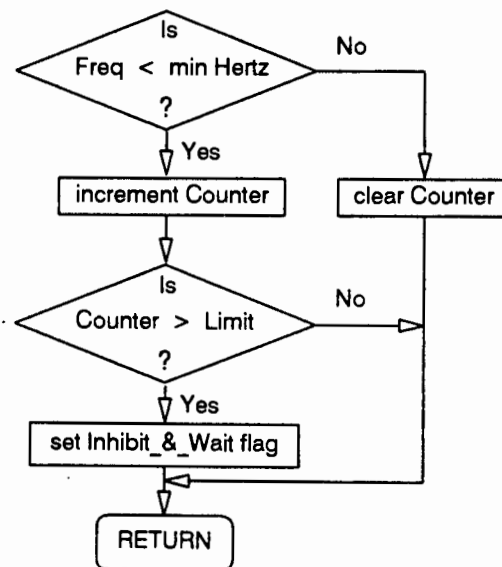


FIGURE 9.6 Flowchart for the detection of a minimum power threshold

Figure 9.6 contains a flowchart of this proposal for fixed voltage operated inverters. This routine has to be called from the subroutine which decides at what frequency the inverter will operate. The program code for the Solvo inverter is listed in appendix A7.3.

Each time the program cycles through the routine which decides whether to increase or decrease the frequency the actual frequency has to be compared to the 'min Hertz' parameter value which contains the lowest useful frequency for that application. For each time the actual frequency is below the 'min Hertz' frequency a counter is

incremented until it reaches a limit at which it will set the flag which will inhibit the inverter output and enter a wait routine. If the actual frequency exceeds the 'min Hertz' frequency then the counter is reset.

This program addition should prevent inverter damage in case of a blocked motor or pump and will avoid the remaining non-essential states of operation that occur for both the Solvo and MLT inverter.

During MST operation the MLT inverter can detect very easily whether sufficient power is available by evaluating the speed samples from the motor. If the value remains below a certain threshold then inhibit inverter output and enter a wait routine. One problem, however, that occurs in shake mode (subsection 8.5.3) is that it can mislead the microcomputer because the motor shakes (forward and backwards) but the speed pick-up still generates a signal. This is due to the possibility of the speed sensing sprocket oscillating through the magnetic pick-up. The microcomputer detects a speed-signal (although at low frequency) and the algorithm does not detect that the motor is shaking. As this state of operation is usually accompanied by a too low array voltage the routine in subsection 9.2.1 should guard against motor shake mode. Alternatively I would suggest to rather keep track of the inverter frequency and to establish from that whether the motor is in a non-essential state of operation as suggested above in the flowchart.

A criticism of the MLT inverter is its reset circuit. This is activated when the watchdog detects no speed-signal. It resets the microcomputer and the inverter performs a restart within one to two seconds. The inverter loses unnecessary control over the motor. It should rather use the watchdog circuit to set a flag and when detected the microcomputer should inhibit inverter output and enter a wait routine.

9.2.3 Monitoring overvoltage

The open-circuit voltage is easily measured before start-up. The maximum allowable open-circuit voltage should be scaled to 4.8V on the ADC and can be sampled once before start-up. If it exceeds the maximum allowable voltage then no start-up should occur.

This method does however assume that the maximum allowable voltage on the power module is lower than that of the power supply for the control electronics and that of the DC input capacitors. These components have to be protected by means of analog circuitry in the form of an overvoltage crowbar. This is discussed in section 9.5

9.3 Voltage to hertz relation

Three aspects compromise an optimum voltage to hertz (V/Hz) relation:

- one, the array voltage oscillations as discussed in section 9.1 which map directly onto the PWM line-to-line voltage and result in pulse height variations (PWM relies on a constant supply voltage and varies the pulse-width to change the voltage)
- two, the lack of resolution of the programmed line-to-line voltage, in particular for the Solvo inverter
- three, changes in the load over time

The first aspect can be resolved by an improved control algorithm as discussed and suggested in section 9.1. The second aspect can be improved by increasing the number of frequency intervals and thereby increasing the resolution of the V/Hz relation (discussed in more detail below). The third aspect however is not in the hand of the programmer. Theoretically the V/Hz relation can be adapted to any kind of load requirements, even the particularities of the pump as used in the tests (see Figure 6.15). Practically though, that is very tedious as the torque curve may be inaccurately specified or not available. In any case, changes in the load over time will result in a sub-optimal V/Hz relation. This raises the question of how much effort should be put into the derivation of an optimal V/Hz relation if the load requirements are not completely predictable (in parts of the torque versus speed curve of the S2M pump the torque requirements are not predictable as outlined in section 6.2.2). The conclusion is that the losses due to non-optimal V/Hz relations have to be evaluated and if found to be significant then software has to be written where the microcontroller goes through a process of finding the optimum V/Hz. This would involve complex evaluation routines as the controller has to evaluate two control variables (array voltage and speed) and has to generate two output signals (frequency and PWM voltage).

Increasing the resolution of the V/Hz relation can only improve the performance of the subsystem since the discontinuities in the PWM voltage are decreased (see Figure 7.13 which displays the V/Hz relation and shows the programmed amplitude for each major gear). The Solvo inverter has ten different amplitudes for a 78Hz frequency spectrum and the MLT inverter has 19 amplitudes for a 62Hz frequency spectrum. The MLT inverter voltage resolution is substantially better than that of the Solvo inverter. The Solvo inverter voltage resolution is good at low frequency operation but becomes poorer as the frequency increases (Figure 7.13). As a result the motor efficiency reduces during parts of a major gear as it is not driven optimally.

The Solvo inverter algorithm has 16 major gears (0 → 15) of which only the last eleven are being used. The frequency range in the first active gear (5) is 1.9Hz. The frequency range within the last major gear is 13.1Hz which is seven times as much as its first active gear. Inverter output voltage resolution becomes more important at

higher frequencies since the system pumps most water in this region. It is therefore suggested to assign voltages to a smaller frequency range once the frequency range per major gear exceeds 5Hz. This is shown in Table 9.1 below.

TABLE 9.1 Solvo frequency range per major gear

<i>Major gear</i>	<i>Frequency range [Hz]</i>	<i>number of amplitudes</i>
0 → 4	0	none
5	1.9	1
6	2.4	1
7	3.1	1
8	3.9	1
9	4.9	1
10	6.4	2
11	7.5	2
12	9.0	2
13	12.0	3
14	12.2	3
15	13.1	3

Major gears 5 to 9 remain as they are. Major gears 10 to 12 should receive two voltage amplitudes per major gear meaning their frequency per amplitude will be halved. Major gears 13 to 15 should receive three voltage amplitudes per major gear resulting in the frequency range being reduced to a third per amplitude.

The Solvo program is presently written in such a way as to only be able to assign one voltage amplitude per major gear. It is however not too difficult to change that. It would only require one additional program variable. The details are in appendix A7.4.

9.4 Solvo inverter switching frequency

The switching frequency of the Solvo inverter varies between 10.3kHz to 17.5kHz in the tested program. The losses for the inverter are therefore relatively high as was discussed. In my opinion it would be justified to run a series of tests based on two programs that have a different range of switching frequencies. The one program can use the existing frequency range and the other program could have a switching frequency range of 8kHz to 10kHz. The switching losses will decrease linearly and the motor will receive somewhat lower-frequency harmonics resulting in a lower efficiency. Which of the two effects will dominate has to be measured.

By monitoring the motor-speed to array-power ratio (which can be monitored most accurately) over a range of speeds a performance difference between the two programs may be measurable. Besides the system components remaining the same, the programs must contain the same algorithm and the same voltage to hertz relation.

A table in appendix A7.5 contains the switching frequency values for the new program. In addition it lists the hexadecimal values that have to be entered into the program and the equivalent fundamental frequency range.

9.5 Peculiarities of the MLT inverter

The aim of this section is to briefly list some of the MLT inverter peculiarities that will require some attention. It would go beyond the scope of this dissertation to analyse the source of these characteristics in detail.

In fixed voltage operating mode:

- The operating range is too narrow for the available power (in MST mode the system run at array powers where the FVO program would stall the motor). This gives the impression that the sampling time of the array voltage is too slow as it seems to drift past its set array operating point. In FVO mode, the inverter is neither efficient from a performance point of view nor from an economic point of view.
- The program uses the speed sensor input signal, which is substituted by a PWM signal (to avoid resetting the microcontroller), as a control variable (subsection 8.5.2). It should only use the array voltage as a control variable. This point is important as a speed sensor in terms of additional cable and equipment may be regarded as less reliable and unsuited for particular conditions. Therefore a FVO algorithm should only evaluate at the array voltage. The possibility that the narrow operating range and the PWM signal at the input to the speed sensing circuit are related problems should not be excluded.

One observation was made for the MLT inverter in MST mode: The potentiometer that is used to tune the maximum speed tracking set-point seemed to prevent the system from leaving its base speed (as explained in subsection 8.1.3 and section 8.6) if set to a particular value. This would get worse if turned in the one direction and better if turned into the other direction. This made it impossible to tune the set-point for MST operation as the greater concern was to have the inverter leave its base speed for as low input powers as possible.

9.6 Inverter protection

Once the inverter is in the field it can be subjected to many conditions that it may not have been designed for. This section discusses means of protecting the inverter against the most basic undesired conditions. Some of the proposals will require testing to establish their effectiveness.

Lightning protection

Depending on the site lightning protection may be a crucial feature since the array is a good receiver for lightning. A common approach is to use metal oxide varistors (MOV's). These devices are in a state of open-circuit if the voltage across them is below their rated voltage threshold. As the voltage exceeds the threshold voltage the MOV conducts. They are very fast responding and may well protect against a strike of lightning.

One MOV each should be connected from both the positive and negative lead to ground. This protects against voltage differences between the casing and the power leads. An additional MOV should be connected between the positive and the negative lead. The MOV's should be placed in close vicinity to the inverter but do not need to be inside it.

Polarity reversal

Polarity reversal is usually avoided by using a connector that can only be fitted into its socket in one way. Both inverters have these type of connectors fitted. Further protection is accomplished by the addition of a diode (see Figure 9.7) since it is still possible to reverse the leads of the array when the system is initially installed. This was not a standard feature in the tested prototype inverters.

Overvoltage

Overvoltage protection can be essential in cases where it is possible to connect strings of arrays in series instead of parallel (great care had to be taken during the test period since the array was either configured in parallel, 2×6, or in series, 1×12. Both the Miltek and the MLT controller would have been damaged if the array had been in series connection).

It is possible to protect the power module against overvoltage by monitoring the open-circuit voltage of the array. This is not the case for the power supply (since it provides the power to the microcontroller) and the input capacitors. These would have to be protected from overvoltage with analog circuitry.

The most effective method to avoid overvoltage damage is by use of an overvoltage crowbar. It consists of an overvoltage detector in the form of a zener diode which turns on a silicon controlled rectifier (SCR) device. When the voltage across it exceeds its zener voltage plus a diode drop the SCR conducts resulting in a short-circuit. Figure 9.7 shows a circuit diagram.

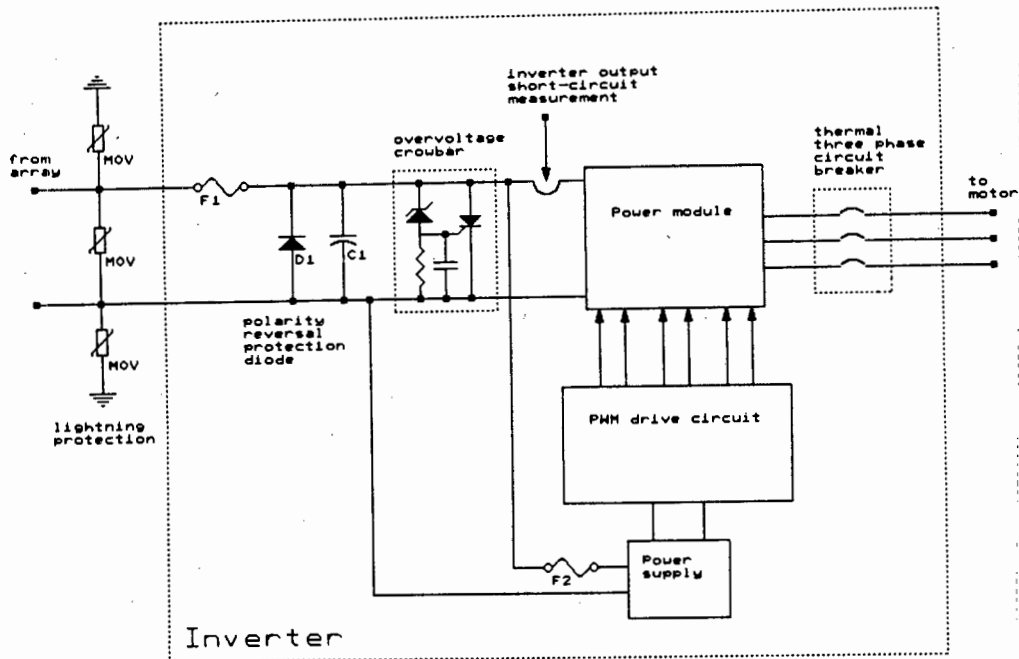


FIGURE 9.7 Proposed hardware protection features in an inverter

Another solution may be to use a special crowbar trigger IC (for example the MC3423-5 or the TL431). These are more adjustable and have a more predictable performance. Their power supply requirements and their response time (seeing that there will be no constant power supply) need to be investigated for feasibility.

Neither the Solvo nor the MLT inverter have an overvoltage crowbar at their input.

Fuses

There are two strategic places where fuses should be added in-line with the circuitry. All fuses should be of the 'slow-blow' type.

The first fuse (F_1) guards against overcurrent (refer to Figure 9.7). This fuse will only blow if the connected array can generate the threshold current that would exceed the power module specifications. It is therefore a question of design. F_1 should be sized to 95% of the continuous drain current of the power module at 80°C.

The second fuse (F_2) should be placed in the power supply circuit. Its current rating should exceed the worst case current requirements of the power supply by about 50%.

The Solvo inverter is fitted with F_1 but does not have a power supply fuse. It may however benefit from it. The drive circuit draws a lot of power when the power module is damaged and frequently leads to additional drive circuit component failure. A power supply fuse may prevent that.

The MLT inverter has a power supply fuse but not the proposed fuse F_1 .

Short-circuit on inverter output

Without protection, short-circuit on the inverter output will result in power module failure.

The Solvo inverter uses a toroid to measure the pulsed current that is generated out of the capacitors. The threshold can be tuned and the circuit has a very fast response time. In addition the circuit is connected to a flip-flop on the PWM IC which inhibits the PWM output of the IC if the flip-flop assumes a state of one. When a short-circuit occurs the toroid will pick up the surge current out of the capacitors and inhibit inverter output.

No reference was found in the MLT documentation about short-circuit protection.

A note on DC side short-circuit: A short-circuit on the DC side within the inverter can only be the result of a damaged DC capacitor that may either go into a state of short-circuit or open-circuit or a conducting diode due to phase reversal. None of the fuses as suggested above will or should respond to a short-circuit on the DC side. The inverter will not attempt to start operation (no voltage is available) and is therefore safe. The array will operate at its short-circuit current. This state of in-operation will prevail until noticed.

Overload protection

A thermal three phase circuit breaker (slow response) on the inverter output can be useful for situations like overload and a missing phase due to broken/disconnected lead. If tuned correctly the circuit breaker can also detect a blocked motor or pump. The difficulty is the tuning which will be different for each pump type and delivery head.

A second prototype Solvo inverter was fitted with a thermal three phase circuit breaker by Conrad Roedern at Solar Age Namibia. It proved to be a very reliable protection for the inverter but required a lot of tuning since the circuit breaker tripped when a lot of clouds were present due to multiple start-ups. (tuning takes so long because one has to let the system run under various conditions again to observe whether the new setting is now correct). The best situation would be where a thermal three phase circuit breaker would detect overload and a missing phase but where a blocked motor/pump could be detected by the software routine: for incorrect operating point and minimum power threshold as described in section 9.2.

Underload and no-load protection

Underload protection is required if the motor can over-speed in the case where the V-belt between the motor and the pump is torn. Since both inverters are limited in frequency an underload condition is stable.

The Solvo inverter is able to operate under no-load conditions (no motor connected). This was not tested for the MLT inverter.

Overheating

A temperature sensor should be installed on the heat sink in close vicinity to the power module. In case of overheating (which is power module specific) the inverter should stop driving the motor and wait for the power module to cool down by sampling the temperature signal in regular intervals.

The Solvo inverter activates an interrupt when the temperature increases beyond a set threshold. It is not clear whether the MLT inverter is protected against overheating. No reference was found in its documentation.

Galvanic isolation of driver stage

Galvanic isolation usually refers to input/output isolation. This is not the point of discussion here but rather isolation between the high power side and the driver circuit side. Galvanic isolation provides two advantages. Firstly the inverter drive circuitry (and all the other components) are protected if an error occurs on the high power side. Secondly no DC component can be present in the drive signal as it is AC coupled to the power module.

The Solvo inverter uses HF transformers on all six drive signals and is therefore completely isolated. The MLT inverter uses opto-couplers for driving the top three MOSFET's and drives the bottom ones directly as the drive circuit and the array share the same ground.

Pump dry-running

Some pumps provide a level switch which is activated if the water level in the borehole drops below a particular margin. This is essentially a pump protection scheme. The inverter would be required to provide a connection for this switch which would stop inverter operation altogether. An interrupt or a relay may be appropriate. This switch could also be used in a reservoir to avoid overflow.

None of the inverters presently offer this type of remote control.

9.7 General design considerations

This section discusses the 'user-friendliness' of the inverter. The points that are mentioned are not essential and should only be addressed once the inverter has reached a state of full reliability and good performance.

Main switch

A main switch/circuit-breaker is required, and should be incorporated into the inverter to avoid having to install another weather-proof box.

Status and error message LED's

Light emitting diodes (LED) are very useful for indicating the status of the inverter. They also provide users with analytical information about possible problems. For example, the case may arise where the motor bearings degenerate over a long period of time until the load becomes too large for the inverter. If an LED can indicate an overload condition it may save the time that would be spent seeking a fault in the inverter.

Possible error-message indicating LED's are:

- | | | |
|----------------------|---|--|
| <i>undervoltage</i> | ▷ | the inverter is operating at an incorrect (too low voltage) array operating point |
| <i>overvoltage</i> | ▷ | the input voltage exceeds the ratings of the inverter - the overvoltage crowbar is activated and is short-circuiting the array |
| <i>short-circuit</i> | ▷ | short-circuit at the inverter output |
| <i>overheating</i> | ▷ | the power module is too hot and the inverter inhibited the output to the motor, the inverter waits until the temperature decreases below a threshold |
| <i>overload</i> | ▷ | the motor draws too much current, pump may be blocked |

Possible status LED indicators are:

- | | | |
|------------------------|---|--|
| <i>power supply</i> | ▷ | microcontroller is operating |
| <i>array power low</i> | ▷ | the inverter is in a non-essential operating mode, the motor runs too slow |
| <i>wait routine</i> | ▷ | the microcontroller entered a wait routine because of too little array power or undervoltage |

- | | | |
|--------------------------|---|---|
| <i>array power</i> | ▷ | power from the array is available that is the array is not operating at short-circuit |
| <i>maximum frequency</i> | ▷ | the motor is receiving the maximum frequency |
| <i>remote switch</i> | ▷ | the pump is running dry or the reservoir is full |

These LED's would give the user a good insight into the system operation. However the effort and the additional hardware might not warrant so many LED's since the market for larger than $500W_{\text{peak}}$ PVP systems is not big enough. A selection of the most essential indicators may be justified.

The Solvo inverter is equipped with an over temperature LED and a short-circuit indicating LED. The MLT inverter does not have any LED indicators.

Physical layout

Both inverters were modular in that the driver circuit and the microcomputer circuit were on different printed circuit-boards (PCB) which is standard. The Solvo inverter had a very accessible design. Both PCB's are fully visible from the top and the power module can be replaced directly without removing any other parts of the inverter. This modularity (all FET's in one single package) is costly and wasteful during the development phase of the inverter but speeds up repairs. On the other hand the MLT inverter used six separate FET's which have to be de-soldered and unscrewed individually. These are only accessible once the microcomputer board has been removed. The layout is not as open as the one from the Solvo inverter but for that matter not all FET's have to be discarded in a case of breakdown. Nevertheless, developments are towards single package three phase full-bridge power modules and these should be placed for easy access.

The placement and orientation of the tuning potentiometers should be considered well. It is unnecessary to cause a short-circuit with a screwdriver on the microcomputer board just because the potentiometers are placed in an awkward position (for example the MLT inverter has its potentiometers in the same plane as the circuit board and facing towards the middle; rather use top adjust potentiometers in that case).

The EPROM placement may or may not be important. During the prototype phase it would have been useful to have zero insertion force sockets. One fault did occur when forcing an EPROM into its socket which was placed well in the middle of the PCB without any support at that point. This results in unnecessary bending of the PCB when the EPROM is exchanged. If the PCB is designed to cope with that then this point is not important.

Both inverters were contained in cast aluminium housings which are very rugged and weather-proof.

Chapter Ten

COMPARATIVE EVALUATION AND SIMULATIONS

This chapter compares the performance of the three systems tested. An additional comparison is performed with a simulation package which enables comparison with other photovoltaic pumps, such as the Grundfos three phase system. The chapter concludes with an assessment of other technical aspects and comparative costs following the evaluation criteria set out in chapter one.

Results are presented for the Miltek system, the Solvo system and the MLT system in maximum speed tracking mode. The MLT system operating in fixed voltage mode is not included since its operating range, as tested, was too narrow to be viable.

10.1 Performance of the Miltek, Solvo and MLT PVP systems

This section compares the tested instantaneous efficiencies and the derived daily energy efficiency of the three systems as well as the instantaneous flowrate and the volume flow.

10.1.1 Instantaneous performance

The controller and motor efficiencies are displayed in Figure 10.1a and 10.1b respectively.

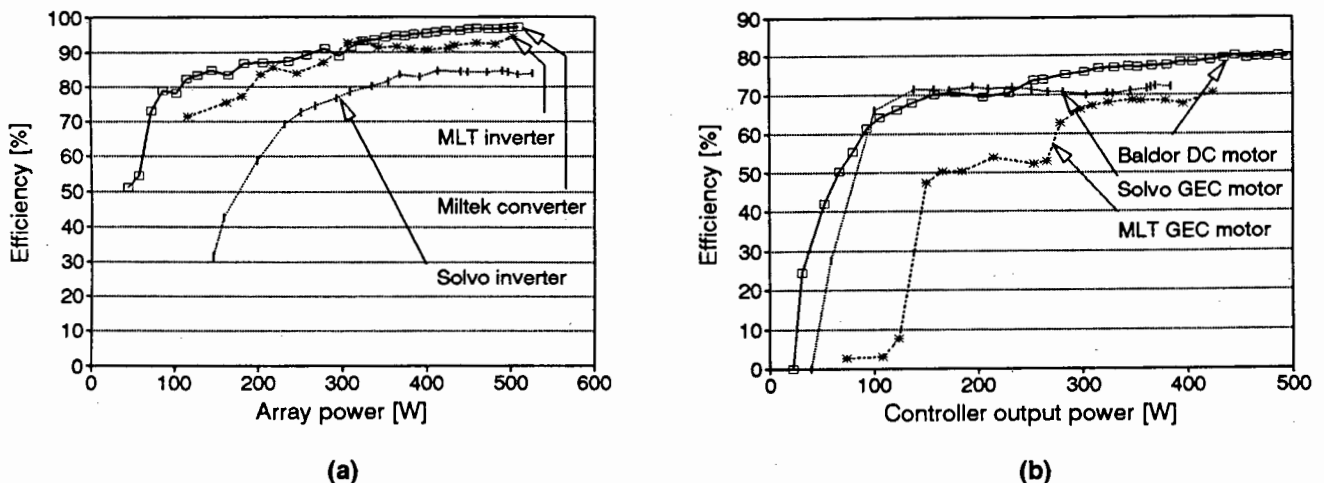


FIGURE 10.1 Efficiency of (a) the controllers and (b) the motors

The Miltek converter efficiency remains the highest over the complete operating range. The MLT inverter is on average 5% below the Miltek converter except for the low input power region. The Solvo inverter efficiency is less than 60% for an input power of less

than 200W. It remains about 14% on average below the Miltek converter efficiency over the input power range of 200W to 500W.

The Baldor DC motor reaches an efficiency of 80%. The Solvo-driven GEC motor reaches 70% at low input power and increases to 72% at high input power. The Baldor and Solvo-driven GEC motors have similar efficiency between 100W and 250W input power. Beyond that the Solvo-driven GEC motor efficiency is about 6% below the DC motor. The MLT-driven GEC motor has about 50% efficiency over half of its operating range and then increases to about 68% efficiency, being about 10% below the Baldor motor efficiency.

The different efficiency values measured for the GEC motor are most likely the result of higher harmonic content in the current waveform and higher torque production at low input power when being driven by the MLT inverter (the motor pulley used in the MLT system was larger). There is also a possibility that the voltage to hertz relation was not optimal for the MLT system as it was not known for which torque the voltage to hertz relation had been optimised. Finally, the relatively high uncertainty in the power measurement may have resulted in a measurement error.

The relative uncertainty in the presented data is listed in Table 10.1.

TABLE 10.1 Relative uncertainty in the controller and motor efficiency data

Uncertainty	Miltek [%]	Solvo [%]	MLT [%]
$U_{rel}(\eta_{con/inv})_{500W}$	1.7	5.3	4.8
$U_{rel}(\eta_{con/inv})_{250W}$	3.2	12.3	10.7
$U_{rel}(\eta_{mot})_{450W}$	3.6	6.6	6.1
$U_{rel}(\eta_{mot})_{250W}$	5.0	9.8	9.8

The combinations of the controllers and the motors are shown in the subset efficiency in Figure 10.2. The subset efficiency is the most realistic efficiency indicator for the performance of the inverter or the motor.

The Miltek subset efficiency curve follows the shape of a logarithmic curve reaching an efficiency of 77% at 500W input power. The Solvo subset efficiency has a similar shape to the Miltek subset curve with a difference of 10% at 230W input power and 17% at 500W input power. The MLT subset efficiency remains below the Solvo subset efficiency until 350W input power is reached where the MLT subset efficiency exceeds the Solvo subset efficiency. From that point onwards the MLT subset efficiency remains about 11% below the Miltek subset efficiency.

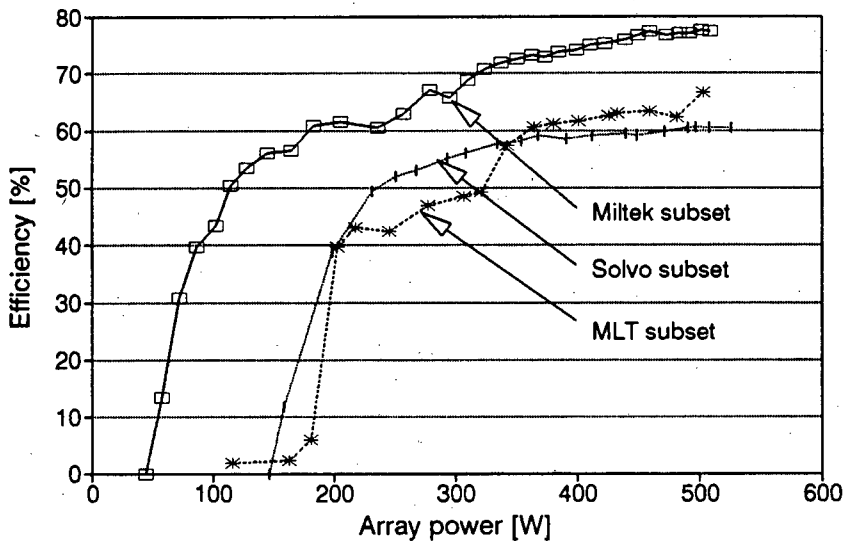


FIGURE 10.2 Subset efficiency of the PVP systems

The relative uncertainty in the presented subset efficiency data is listed in Table 10.2.

TABLE 10.2 Relative uncertainty in the subset efficiency data

Uncertainty	Miltek [%]	Solvo [%]	MLT [%]
$U_{rel}(\eta_{subset})_{500W}$	3.6	4.2	4.2
$U_{rel}(\eta_{subset})_{250W}$	5.4	4.9	4.9

Figure 10.3 shows the system efficiency as a function of the plane of array irradiance (graph a) and the subsystem efficiency as a function of array power (graph b). The Miltek system efficiency rises nearly linearly to 4.5%, remains constant at 4.5% between $700W/m^2$ to $900W/m^2$ and then decreases to 4.2% at $1050W/m^2$. The Solvo system efficiency reaches 3.9% at $700W/m^2$ and remains there. The MLT system efficiency reaches 3.6% to 3.7% at $700W/m^2$ but traces a lower efficiency path in the $450W/m^2$ to $700W/m^2$ region as it reaches 3.6% compared to the Solvo system.

The start-up irradiance values can be read from the graph. The Miltek system starts-up at $300W/m^2$, the Solvo system at $380W/m^2$ and the MLT system at $460W/m^2$. The Miltek system manages an earlier start-up due to superior efficiency and the Solvo system due to a very small motor pulley and closer tracking of the average fixed voltage point on the array.

The Miltek subsystem efficiency (Figure 10.3b) reaches a peak value of 42% from which it decreases to 39% at 500W array power. The Solvo subsystem efficiency is about 7% to 10% below the Miltek subsystem efficiency. The MLT subsystem efficiency is below the Solvo efficiency until 350W array power and exceeds it at that point to reach a subsystem efficiency of 35%. The Solvo and MLT subsystem efficiency curves are very similar to their subset efficiency curves. The Miltek

subsystem efficiency curve follows the shape of the pump efficiency curve since it delivers more power to the pump (see Figure 6.19). The Solvo and MLT systems deliver a maximum shaft power of 300W and 330W respectively to the pumping set. The pumping set efficiency curve has not decreased considerably at that power level.

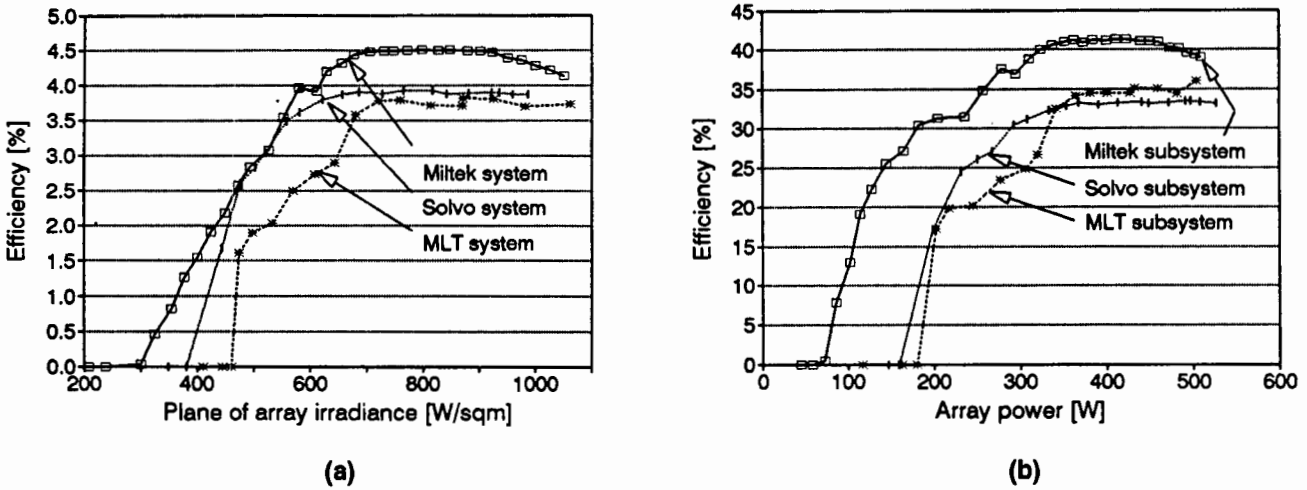


FIGURE 10.3 Performance of the PVP systems: (a) system efficiency and (b) subsystem efficiency

The relative uncertainty of the data for all three systems in Figure 10.3 is:

$$\begin{aligned}
 U_{rel}(\eta_{sys})_{1050W/sqm} &= 6.9\% \\
 U_{rel}(\eta_{sys})_{750W/sqm} &= 9.4\% \\
 U_{rel}(\eta_{subsys})_{500W} &= 2.5\% \\
 U_{rel}(\eta_{subsys})_{350W} &= 2.9\%
 \end{aligned}$$

The instantaneous flowrate for all three systems and subsystems is shown in Figure 10.4a and 10.4b. The Miltek subsystem (Figure 10.4b) delivers a maximum of 950l/h at an input power of 500W. The gradient of the flowrate curve decreases which is to be expected since the system and subsystem efficiency decrease. The flowrate curves for the Solvo and Miltek system and subsystems exhibit a similar trend to Figure 10.3. The Solvo flowrate as a function of irradiance is better than the MLT flowrate over the whole range but the MLT flowrate as a function of array power becomes better (>350W) than the Solvo flowrate. This indicates that the MLT inverter does not operate very efficiently on the array (see Figure 8.7; increasing irradiance). The module temperature range for Solvo data is 33°C to 37°C and for MLT data 22°C to 28°C. Therefore the MLT inverter only starts operating optimally on the array towards higher irradiance levels.

The relative uncertainty in the flowrate data as a function of irradiance and array power is the same as the uncertainty in the system and subsystem efficiency data. This is due to the low uncertainty in the static head measurement (0.2%) which does not affect the system efficiency uncertainties as their magnitudes are a factor of ten higher.

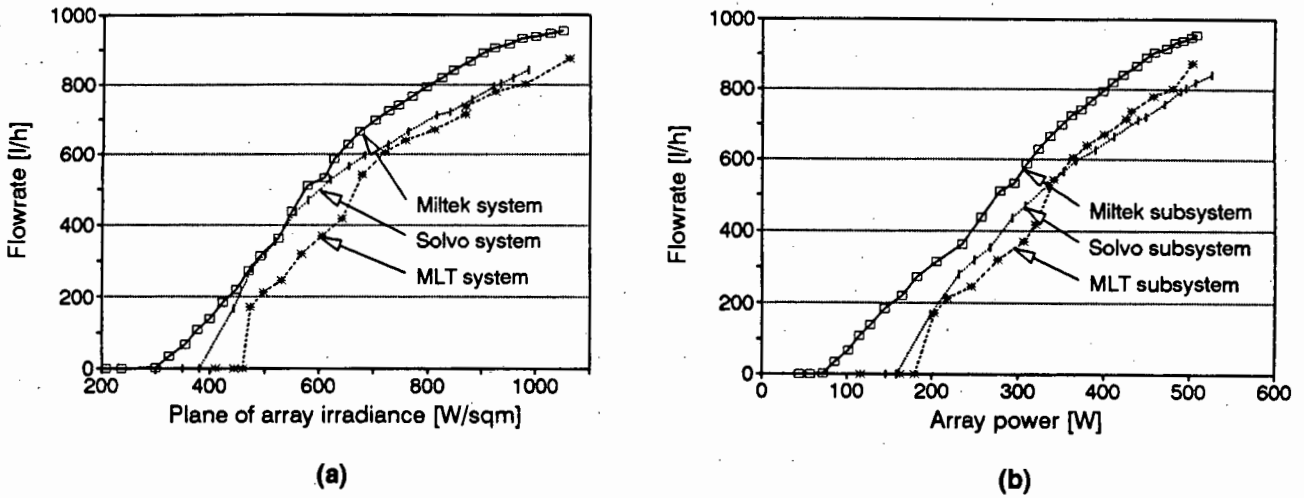


FIGURE 10.4 Performance of the PVP systems at a static head of 75m: (a) flowrate versus incident irradiance; (b) flowrate versus array power

10.1.2 Daily energy efficiency performance

The system daily energy efficiency (DEE) and the volume flow as a function of the standard solar day (SSD) are presented here for all three PVP's. In addition the percentage difference between a SSD and a tracking solar day (TSD) is shown for the complete system and the volume flow. The irradiance profiles for the SSD and the TSD and the method of DEE calculation are in appendix A5.

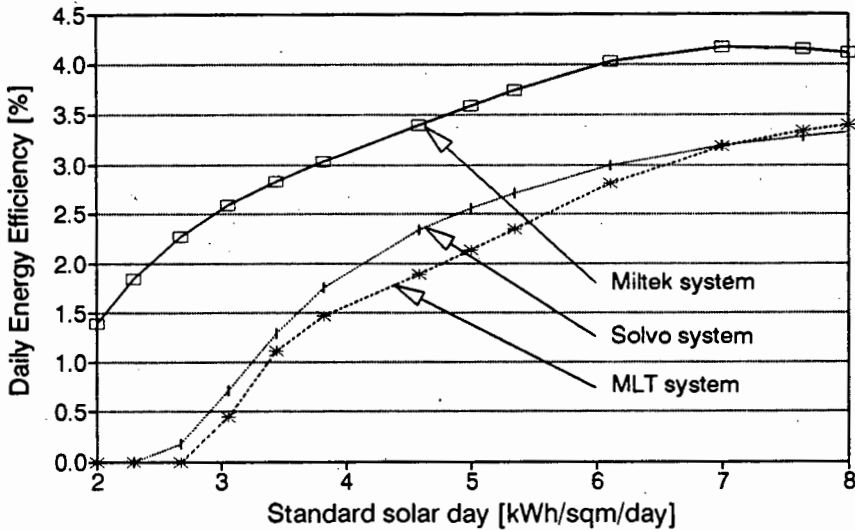


FIGURE 10.5 DEE of the PVP systems versus the standard solar day

Standard solar day

Figure 10.5 shows the DEE of the three systems. The Miltek system maintains a very good efficiency over the whole range of SSD's. At 3kWh/m²/day the DEE is 2.5%. The DEE peaks at 7kWh/m²/day and decreases slightly (due to a decrease in pumping set efficiency). The DEE curves of the Solvo and MLT systems lie fairly close together with the maximum difference being 0.5%. The DEE of the MLT system exceeds the DEE of the Solvo system at a SSD of 7kWh/m²/day.

The difference between the Miltek system and the Solvo system DEE is 1.8% at low irradiation content (3kWh/m²/day) which decreases to 1.0% for the middle range and finally decreases to 0.8% at 8kWh/m²/day. The difference between the Miltek system and the MLT system is 2.0% at 3kWh/m²/day, 1.5% in the middle range and decreases to 0.7% at 8kWh/m²/day.

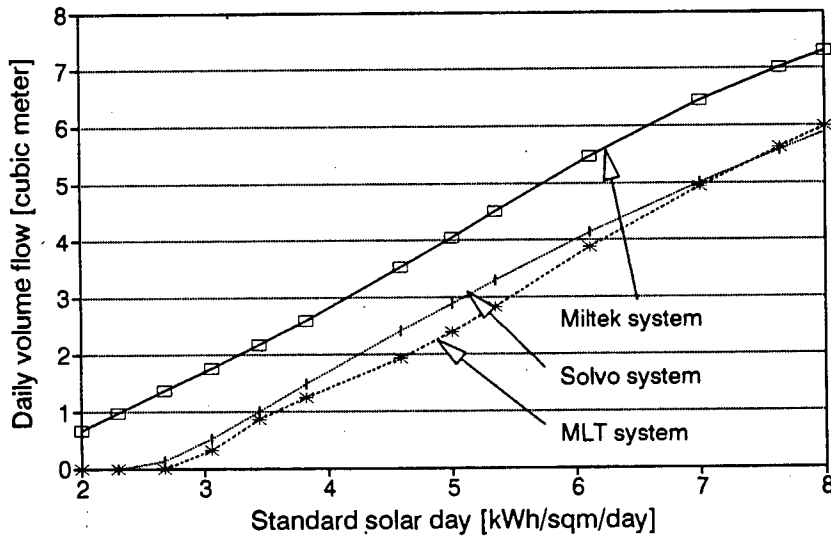


FIGURE 10.6 Daily volume flow of the PVP systems versus the standard solar day

The volume flow for all three systems is displayed in Figure 10.6 as a function of different SSD's. The average difference between the Miltek volume flow and the Solvo volume flow is about 1.3m³. Between the Miltek and the MLT this difference is about 1.4m³.

The DEE performance values for the components and sets of components at 5kWh/m²/day are shown in Table 10.3. As expected, the DEE of the Solvo inverter and the MLT driven GEC motor are relatively low. The main reasons for this are the high switching losses in the Solvo inverter and the high harmonic energy content in the MLT-driven GEC motor.

TABLE 10.3 Daily energy efficiency at 5kWh/m²/day

Component	Miltek	Solvo	MLT
Siemens array	10.8%	10.8%	10.8%
Converter/Inverter	88.6%	66.8%	83.9%
Motor	71.1%	68.0%	45.4%
Pumping set	52.9%	52.3%	52.1%
subset	63.0%	45.4%	38.1%
subsystem	33.3%	23.8%	19.9%
system	3.6%	2.6%	2.1%
volume-flow	4.1m ³	2.9m ³	2.4m ³

Tracking solar day versus standard solar day

The following two graphs display the percentage increase of the TSD performance over the SSD performance as a function of the noon peak irradiance (see appendix A5).

Figure 10.7 shows the percentage difference between the system DEE under TSD and SSD conditions with reference to the SSD condition. All three curves have a similar shape on the right-hand side. The Solvo and the MLT graph both peak towards low noon peak irradiance levels and then fall to zero as the system ceases to operate for both the SSD and the TSD. The percentage increase between the TSD and SSD for the Miltek system is the lowest. The MLT DEE has the highest efficiency improvements under TSD conditions compared to SSD conditions.

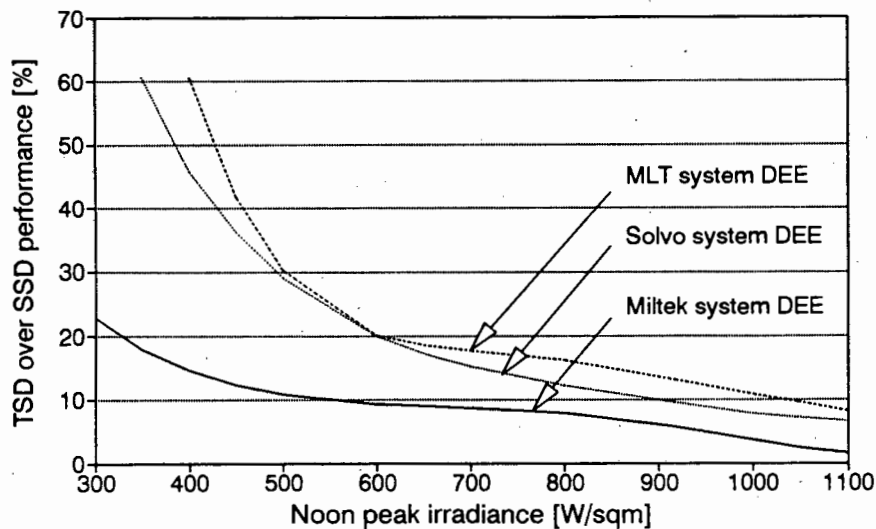


FIGURE 10.7 Percentage TSD over SSD PVP system performance versus the noon peak irradiance

Figure 10.8 displays the most important parameter: the volume flow. The volume flow increase from tracking is a minimum of 28% at $1100\text{W/m}^2_{\text{peak}}$ for the Miltek system. The gain for the Solvo system volume flow is 5% higher than the Miltek system over the range from 800W/m^2 to 1100W/m^2 noon peak irradiance. The MLT volume gains 9% more than the Miltek system over this range. The percentage difference between the TSD and the SSD for the three phase systems then increases substantially as the volume flow under SSD conditions decreases rapidly for decreasing noon peak irradiance levels.

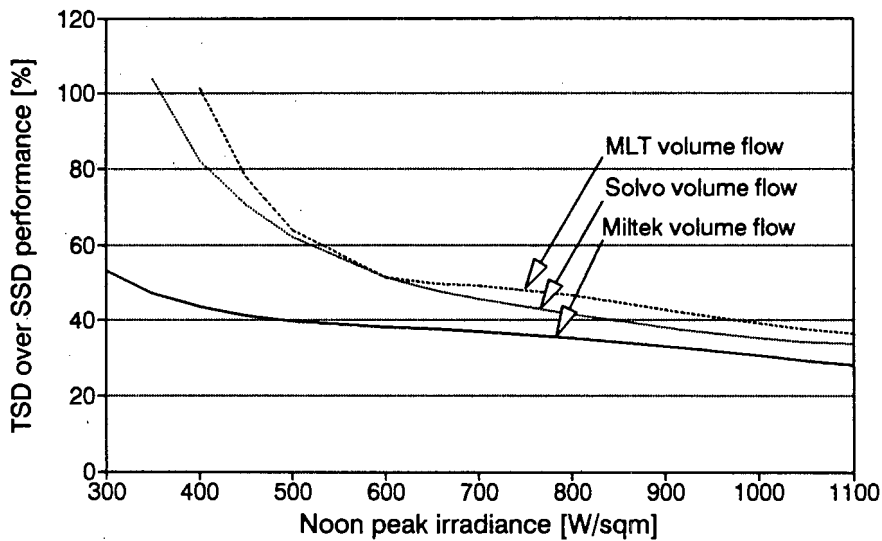


FIGURE 10.8 Percentage higher volume flow of TSD over SSD versus the noon peak irradiance

The MLT system stands to gain the most from a tracking array which is mainly due to its narrower operating range and due to its improving efficiency at higher input power levels. The Solvo system also gains at least 5% more than the Miltek system from a tracking array.

10.2 Simulated comparison with a Grundfos PVP system

The performance of the tested PVP systems is compared to a Grundfos PVP system by means of a simulation program. This program facilitates comparisons over the period of a year based on long-term meteorological data. The appendix A8 contains a brief description of the simulation package written by Davis (1994a; 1994b). These publications should be consulted for detailed information on the program features.

The Grundfos PVP system is a well established three phase water pumping system (the system has been available for over ten years). The three phase controller is capable of tracking the MPP on the array. The motor/pump set is submersible and uses a multi-stage centrifugal pump. Grundfos offers a range of PV pumps for different heads. The selected Grundfos PVP, the SP 2A - 15, can be installed over a head range of 50m to 120m. The most suitable number of series modules is eight (to achieve the optimum motor voltage) and the minimum W_{peak} array size is 800W. This resulted in a choice of 2×8 modules of $53W_{\text{peak}}$ each, being equivalent to 848W. The array output power is therefore 33% higher than the array size used in the tested systems. This difference is unfortunate but not avoidable as the simulation should model actual conditions as much as possible. The comparison is brought to the same level when the unit water cost is evaluated in section 10.4. The unit water cost combines the performance of the PVP system with its life cycle cost.

The simulation is performed with $53W_{\text{peak}}$ modules and the array is assumed to be a fixed array. The selected sites are Windhoek (latitude: $21^{\circ}34'$ and longitude: $17^{\circ}06'$) and Durban (latitude: $29^{\circ}58'$ and longitude: $30^{\circ}57'$). The angle of tilt is 20° at the Windhoek site and 35° at the Durban site. These angles have been selected with the aim of maximising the irradiation received in the worst month (Davis 1993a).

The simulation package also offers the option of a three position tilted array to accommodate seasonal changes. It does not however offer simulations with a tracking array. Only the results for the simulation with a fixed array are presented here.

Figure 10.9 shows the hourly results of a simulation. The irradiance profile has been disturbed by a cloud which has an impact on the flowrate of the PVP systems. The MLT PVP system has been omitted as it resembles the Solvo flowrate response closely. The Miltek and Solvo systems have similarly shaped responses. The Grundfos system has a narrower operating range but its output increases above that of the Miltek system as the irradiance levels increase. Over the particular day displayed the Miltek system pumps 8.5m^3 , the Solvo (MLT) system pumps 7.1m^3 and the Grundfos system pumps 6.7m^3 . This overall performance is to be expected from a centrifugal pump whose efficiency is better than that of a progressive cavity pump near and at its design operating input power but usually drops steeply to lower values when the input power reduces. The progressive cavity pumps have a flatter efficiency curve over their operating range (refer to Table 2.2 for a comparison).

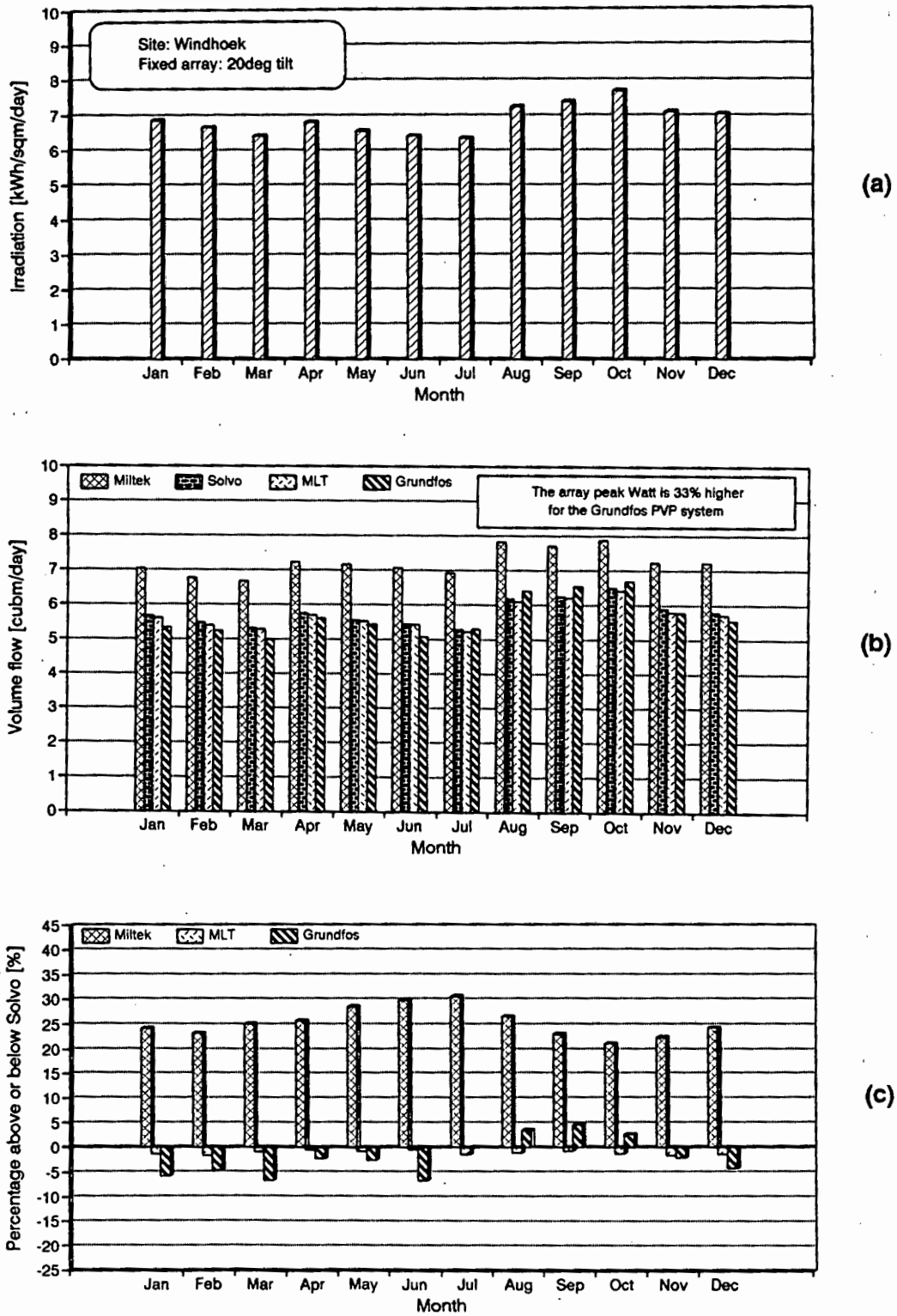


FIGURE 10.10 Monthly simulation results for the PVP's at 76m: Windhoek: (a) Daily irradiation; (b) Daily volume flow; (c) Percentage difference in volume flow compared to the Solvo PVP system

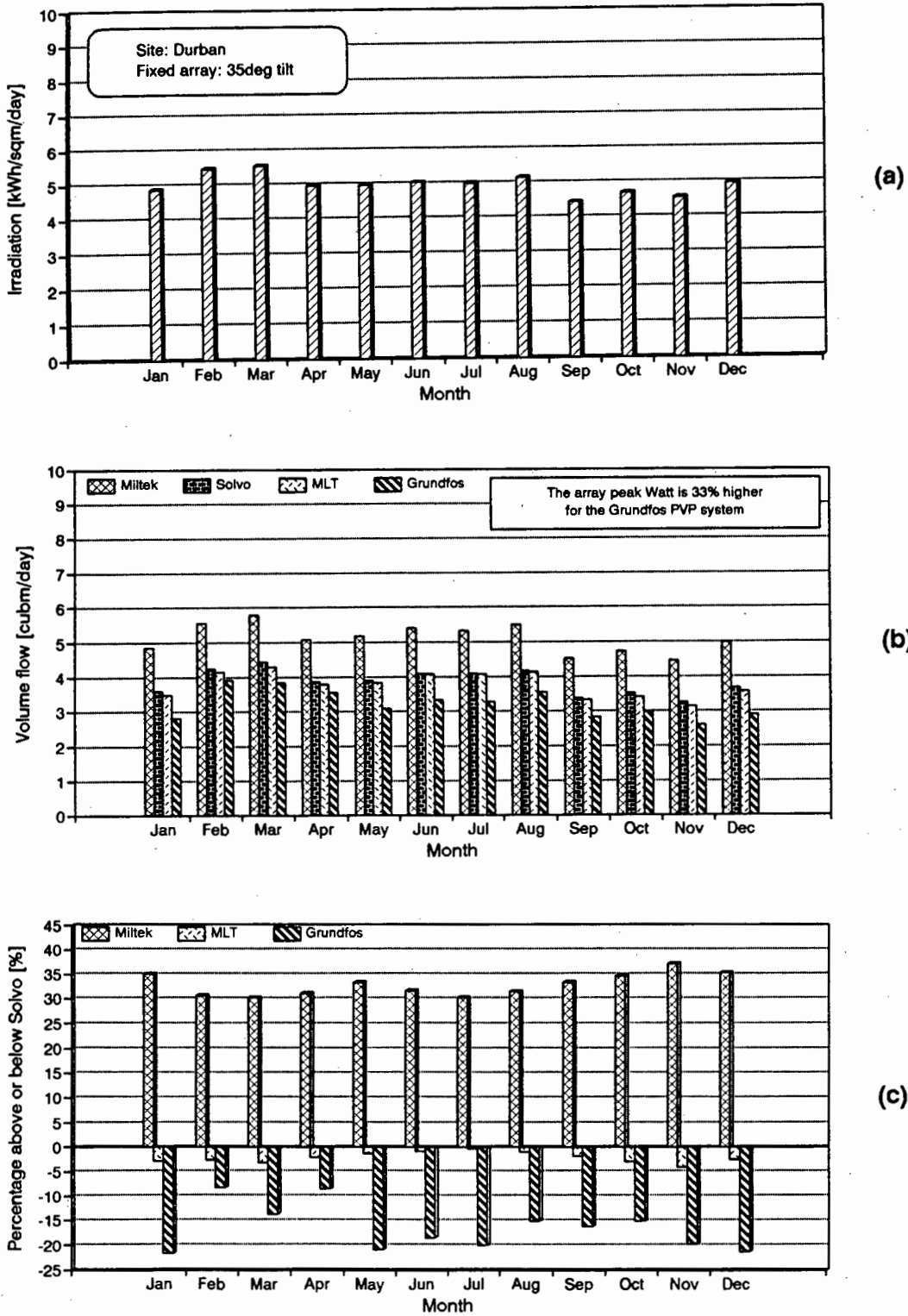


FIGURE 10.11 Monthly simulation results of the PVP's at 76m head: Durban: (a) Daily irradiation; (b) Daily volume flow; (c) Percentage difference in volume flow compared to the Solvo PVP system

10.3 Other technical aspects of the PVP systems

This section deals with other technical aspects of the PVP systems which are not directly related to the performance characterisation. System requirements include the availability of components, the maintenance needs of the system and the installation conditions. System attributes include component modularity, flexibility, protection and monitoring.

10.3.1 System requirements

Availability of components

The availability of the system components or parts of the individual components is an important consideration in terms of sustainable water supply from a PV pump.

The PV modules or at least the silicon cells are all imported to southern Africa. Since high quality crystalline modules have an expected service life of twenty years and have become the most reliable component of any type of PV system their future availability is not of major concern.

The Miltek and the MLT controllers have been built in South Africa. The Solvo controller was built in Germany but will in future be produced in Namibia. The electronic components in all the controllers are imported, but since there is a far greater general demand for such components, availability is probably secure.

The Baldor DC motor is imported from the USA. The three phase motor is produced in South Africa.

The progressive cavity Mono pump is produced in South Africa. In addition the company Orbit Pumps also produces progressive cavity pumps.

The Grundfos subsystem is imported from Denmark, through agents in southern Africa, and is presently readily available.

Disregarding the reliability and performance aspect of the four systems the most valuable aspect in terms of availability is to have the components manufactured locally (no hard currency loss and support of the local industry). Using that criterion the MLT subsystem is at present completely manufactured in South Africa. The Solvo inverter is intended for manufacture in Namibia.

Maintenance

A maintenance-free PVP system is attractive as it can be used for remote area pumping applications. In my opinion a system that does not require maintenance in a five year period can be considered to be maintenance-free.

The components of a PVP system that require maintenance are the motor and the pump. They are the only moving parts (except for a tracking array option). The Baldor permanent magnet DC motor requires new brushes every two years.

The three phase motors can be considered to be maintenance-free if the motor drive does not contain any low frequency harmonics or superimposed low frequency oscillations on the line-to-line voltage which can result in torque pulsations. This leads to a shorter motor life-span. The GEC motor could be considered to be maintenance-free if corrected algorithms are implemented in the Solvo and the MLT inverters. An overhaul (which includes a new set of bearings) is recommended every ten years.

The transmission between the motor and the pump is usually via a belt drive. This was the case for these tests. If the pulleys are correctly aligned and the belt tension is neither too low or too high then the belt should last over a ten year period without any breakdown (assuming the operating conditions are conducive, eg, no direct sun and no rain).

The pump will require maintenance or replacement at some stage as a progressive cavity pump has a considerable amount of wear and rotor axial movement. However the time-span is rather indeterminate as each pump element has its own characteristics. Water quality is also an important factor which will have an impact on the life-time of the pump element. The pumps are generally regarded as very durable and reliable with a service life of between five years and twenty years.

The Grundfos motor/pump set would require a service at least every ten years. It may involve motor bearing replacement, pump overhaul and replacements of seals.

All maintenance requirements can be met locally with spare parts being readily available.

Repair

In the case of PVP system break-down, it is most likely that this will occur in the controller (highest number of components, highest degree of complexity). The repair certainly requires skilled personnel.

The Solvo inverter, due to its modular design, is easily disassembled. The power module can be replaced without removing any other components (with a probability of 80% it can be assumed that the power module has broken down). However, the driver circuit has to be tested to ensure that no damage has resulted due to power module break-down. The Solvo inverter can be repaired within one hour assuming that the damage only occurred in the power module and driver stage (repair time based on my experience).

The MLT inverter uses separate power transistors (six) which are not accessible without the removal of the printed circuit boards. Repair from that point of view would require more time. The testing of the driver signals is obscured by the microcomputer

circuit board which would have to be removed. However, since this inverter is a prototype it is recommended for the next generation inverter to change the layout to allow for easier access.

No information was available on the repair time for a Grundfos inverter.

Installation

The installation for the progressive cavity borehole pump (Miltek, Solvo and MLT) requires a significant amount of labour and material since the motor is fitted to the discharge head assembly of the pump and transfers its shaft power via a transmission rod to the pump. The installation is therefore fixed and relatively rigid. It requires time to install the pump, connecting the rising main pipes and the rods (half a day to a full day, depending on borehole depth).

The Grundfos motor/pump set is submersible and can be lowered by means of a steel wire and a flexible plastic hose (it can also be attached to iron pipes as above). The time and construction requirements are therefore negligible. The Grundfos system is incomparably easy and quick to install.

10.3.2 System attributes

Modularity

Two levels of modularity are considered. The first level is whether components are separate or integrated and the second level is the modularity within the controller. The latter aspect was discussed in section 9.7 and is important with regard to upgrading and repairing the controller. In this respect, the Solvo inverter has realised a superior design compared to the Miltek converter and the MLT inverter. No details are available on modularity in the Grundfos inverter (SA 1500).

Component modularity has advantages and disadvantages. All three systems tested are completely modular. The most common combination is to match the motor and the pump into one unit, as with the Grundfos system.

A submersible pump is very easily installed, as noted above, and saves the cost of the cast iron pipes used in the tested systems. Another advantage is the motor cooling due to immersion in water. The disadvantages are the inability to change the speed ratio (the motor and pump are close coupled), the reduction in motor efficiency due to the reduced size and high speed (nominal 3000rpm) and the cost of replacing either the pump or the motor in case of break-down (since both are specialised components).

An advantage of a completely modular system is the ability to replace any one of its components provided the replacement adheres to the specifications. The components are substitutable and can be bought separately. In the case of the Grundfos system the whole subsystem has to be acquired. It might be the case however, that the Grundfos inverter could be used in the three phase systems that were tested (with

changes in the voltage to hertz relation - not possible without consultation with Grundfos, Denmark).

Flexibility

The tested systems are all quite flexible as they can be used for a range of array sizes and static heads. Adaption is possible by means of different pulley ratios. The frequency range and inverter/motor matching of the three phase systems can be altered in software.

However, these systems are less flexible in terms of re-installing at another site, since removal and installation are time-consuming.

The Grundfos range of PVP systems offers similar flexibility, in covering a fairly wide range (400W to 1800W). However, a particular system will operate best at its design input power and design head. The speed ratio cannot be changed. More sophisticated changes like the frequency range and voltage to hertz relation have to be done in Denmark. This last point requires the customer to buy modules in numbers of eight (as recommended by Grundfos) in order to operate the system at an optimum voltage to hertz relation.

The prototype inverters are more flexible in terms of software alterations by virtue of executing changes locally. The Grundfos system offers the greatest site flexibility since the pump subsystem is a portable unit.

Self-protection

This is an important aspect and has been discussed extensively in section 9.6. A well protected controller becomes more reliable and cost-saving. The protection for both three phase inverters could be improved.

The Grundfos inverter is very well protected. The features include protection against overheating, overload, underload, overvoltage, undervoltage, short-circuit, pump dry-running and earth leakage.

Monitoring capabilities

Monitoring capabilities are implemented with relative ease in microprocessor based inverters as opposed to analog controllers. However, none of the three tested controllers presently offer diagnostic capabilities or a PVP ↔ user interface.

The Grundfos inverter uses LED's to indicate the status of the system. The following conditions are indicated: Overload, underload, maximum frequency, DC power low, overheating, remote switch (pump dry-running or level switch), DC voltage high and DC voltage low.

10.4 Cost analysis

This section evaluates the cost of the Miltek, the Solvo, the MLT and the Grundfos system. This cost is calculated over a period of twenty years and therefore includes all anticipated future costs that will be incurred. In order to compare system costs, the unit water cost is calculated based on the total cost over twenty years and the yearly water delivered, based on results from the simulation package.

The initial capital cost of the systems

Table 10.4 contains the costs of all the components. The prices are specified in current rand (R) which is equivalent to the Namibia dollar (N\$).

TABLE 10.4 Costs of components in each PVP system

Component	Miltek [R]	Solvo [R]	MLT [R]	Grundfos [R]	
Array ¹⁾	12 × M55 (@ R1 399.-) Array structure ⁴⁾ (Tilt mechanism ⁵⁾ 10m cable (@ R10.-/m)	16 788.- 700.- 300.- 100.-	17 588.-	16 × M55 Array structure ⁴⁾ (Tilt mechanism ⁵⁾ 10m cable	22 384.- 700.- 300.- 100.-
	Total		17 588.-	Total	23 184.-
Controller	¹⁾ 1 404.-	¹⁾ 3 780.-	¹⁾ 2 808.-	SA 1500 ²⁾	4 764.-
Motor (brushes)	¹⁾ 3 672.- ¹⁾ 184.-	¹⁾	1 080.-	SP 2A - 15 ²⁾ Cable (90m) ²⁾ Piping (90m) ²⁾	3 916.- 1 170.- 630.-
Transmission ³⁾	Pulley Taperlock V-belt		63.- 24.- 17.-	Total	5 716.-
	Total		104.-		
Pump ³⁾	Discharge head 90m pipe 90m rod Bobbin bearings (60) S2M unit		1 302.- 2 235.- 893.- 1 646.- 1 188.-		
	Total		7 264.-		
Subsystem cost	12 444.-	12 228.-	11 256.-		10 480.-
Total system cost	30 032.-	29 816.-	28 844.-		33 664.-

¹⁾ Prices as per Solar Age Namibia, Windhoek, February 1994 price list
²⁾ Prices as per Namibian Engineering Corporation, Windhoek, February 1994 price list
³⁾ Prices as per Elwiwa, Windhoek, Namibia, February 1994 price list
⁴⁾ The cost of the Zomeworks tracker is R3 240.-
⁵⁾ The cost of this item has to be added to the life cycle cost if the simulation assumed a three position tilted array

The Zomeworks passive array tracker is not included as the simulation did not include a tracking array. However the prices of two array structures are listed, one fixed and one with the option of adjusting for seasonal changes (10°, 35° and 60°).

TABLE 10.5 Initial installation costs for all four PVP systems

Component	Miltek [R]	Solvo [R]	MLT [R]	Grundfos [R]
Initial installation cost: ³⁾	Basic 90m (R 6.74/m)		202.- 607.-	Basic 250.- n/a
Total			809.-	250.-

³⁾ Prices as per Elwiwa, Windhoek, Namibia, February 1994 price list

Table 10.5 lists the initial installation cost for a borehole pump (as for the Miltek, the Solvo and the MLT system) and a submersible pump (as for the Grundfos system). It does not include travel costs.

The future costs

The future costs are the maintenance and the replacement costs. The replacement costs will always have to include the removal and re-installation costs. The costs are listed in Table 10.6. They do not include travel costs.

TABLE 10.6 Maintenance and replacement costs for the four PVP systems

Description	Miltek [R]	Solvo [R]	MLT [R]	Grundfos [R]
Motor maintenance: Brushes Bearings	⁴⁾ 184.-/ 2yrs 300.-/10yrs	⁴⁾	n/a 180.-/10yrs	²⁾ n/a 500.-/10yrs
Pump maintenance: Discharge head V-belt Bobbin rubbers Total	³⁾ Bearing assembly 60 units (@ 5.69) Total		702.-/10yrs 17.-/10yrs 341.-/10yrs 1 060.-/10yrs	n/a n/a n/a
Replacement cost:	S2M unit ³⁾		1 188.-/10yrs	SP 2A -15 ²⁾ 1 500.-/10yrs
Removal and re-installation cost: ³⁾	Basic Removal 90m (R4.21/m) Re-installation 90m (6.74/m)		202.- 379.- 607.-	Basic 250.- n/a n/a
Total			1 188.-	250.-

²⁾ Prices as per Namibian Engineering Corporation, Windhoek, February 1994 price list

³⁾ Prices as per Elwiwa, Windhoek, Namibia, February 1994 price list

⁴⁾ Prices as per Rolf Rohe, Windhoek, Namibia, February 1994 price list

The assumptions in terms of the future costs are as follows: The maintenance requirements for the DC motor are a new set of brushes every two years. All other maintenance requirements and component replacements take place once in ten years.

Realistically the maintenance requirements and the possible component replacements may occur in shorter or longer intervals. This is highly dependent on the conditions under which the system operates. For example the delivery head, the water quality, torque pulsations, current ratings (DC motor brushes) are all factors which will affect the maintenance requirements of the system.

Life cycle cost

The life cycle cost (LCC) calculates all the anticipated costs that are incurred over a particular project lifetime. It includes the initial cost and all future expenditure. Appendix A9 gives a detailed description of the method of calculation and the equations used.

Table 10.7 lists the LCC for the four PVP's under discussion. The project lifetime is taken as twenty years (SL = 20), the real discount rate is 5%, the rate of escalation is assumed to be zero percent and the real interest rate is assumed to be 5%.

The initial cost for each system is taken from Table 10.4 and Table 10.5. The maintenance and the replacement costs are taken out of Table 10.6. For each replacement interval the pump or the motor/pump set have to be removed and re-installed. This cost is also listed in Table 10.6.

All amounts listed in Table 10.6 are reduced to their present value by incorporation of the discount rate and the time at which the cost occurs.

TABLE 10.7 Life cycle cost of the four PVP system with a project life of 20 years

<i>PVP system</i>	<i>Life cycle cost [R]</i>
<i>Miltek</i>	34 144.-
<i>Solvo</i>	32 739.-
<i>MLT</i>	31 767.-
<i>Grundfos</i>	35 230.-

¹⁾ The LCC of the Grundfos system includes the cost of sixteen modules where the other systems only use twelve modules

The Grundfos system has the highest LCC which is due to its larger array. The Miltek system has the second highest LCC which is mainly due to its motor maintenance requirements if compared to the Solvo and the MLT system. The Solvo system costs R1400.- less than the Miltek system. The MLT costs about R1000.- less than the Solvo system which is due to price difference in the inverters as all the other costs are the same.

Unit water cost

The unit water cost (UWC) is the most relevant costing parameter as it incorporates the system performance. The equation by which it is calculated is in appendix A9.

The unit water cost has been evaluated at two sites, namely Windhoek and Durban and for two types of array structures namely fixed and three position tilted array. The conditions under which the simulations took place are listed in appendix A8.2.

TABLE 10.8 Unit water cost for all four PVP systems

PVP system	Unit water cost [cents/m ³]			
	Windhoek		Durban	
	three position tilted array ¹⁾	fixed array	three position tilted array ¹⁾	fixed array
Miltek	100.1	103.8	140.4	146.7
Solvo	118.7	124.8	177.6	186.8
MLT	116.0	122.4	176.0	185.1
Grundfos	126.9	136.7	219.5	240.8

¹⁾ The three angles of tilt are: 10° for Nov - Feb; 35° for Mar - Apr and Sep - Oct; 60° for May - Aug

TABLE 10.9 Hydraulic unit water cost for all four PVP systems at 76m static head

PVP system	Unit water cost [cents/m ⁴]			
	Windhoek		Durban	
	three position tilted array ¹⁾	fixed array	three position tilted array ¹⁾	fixed array
Miltek	1.32	1.36	1.85	1.93
Solvo	1.56	1.64	2.34	2.46
MLT	1.53	1.61	2.32	2.44
Grundfos	1.67	1.80	2.89	3.17

¹⁾ The three angles of tilt are: 10° for Nov - Feb; 35° for Mar - Apr and Sep - Oct; 60° for May - Aug

Due to the higher performance of the Miltek system it manages to achieve the lowest UWC although the LCC is R2400.- higher than the cheapest PVP system, the MLT system. The Solvo and MLT systems have similar UWC. The UWC of the MLT system

is slightly lower than the Solvo UWC as it has a lower LCC which makes up for its slightly poorer performance compared to the Solvo system. The UWC of the Grundfos system is the highest as its performance did not meet up to the other three systems while its LCC is the highest. Compared to all the other systems the Grundfos UWC increases disproportionately when operating under Durban weather conditions. The UWC increases by over 70%. This is due to its drop in efficiency when it receives comparatively less power on average.

The UWC for all systems is likely to decrease when a tracking array is used. The LCC would increase by 7.2% to 8% (cost of the tracking array less the fixed array divided by the LCC) while the annual water output will increase by more than that percentage. A rough estimate for the Miltek system could be considered to be 20%. As shown earlier, the gain of a tracking array for the three phase prototype systems will be larger. It was also argued that the Grundfos PVP would benefit even more than the prototype three phase systems due to the sensitivity of the subsystem efficiency to the input power. The conclusion of this deliberation is that the relative gap between the UWC cost as it has been evaluated will decrease when a tracking array is used.

Further simulations show that the UWC of the Grundfos system drops substantially if the system is configured with 3×8 modules (equivalent to: 24 modules W_{peak} of 1271W and LCC of R46 721.-). Its UWC at the Windhoek and Durban site with a fixed array is 87.8c/m^3 and 133.4c/m^3 respectively. Unfortunately, data for the other three systems is not available at these array sizes. However, their UWC is likely to decrease as well since inverter efficiency and motor efficiency will improve (the efficiency of induction motors increases with higher power ratings; both increases are marginal though). In comparison, it is possible that the UWC of the Grundfos system would reach similar magnitudes to the UWC of the three phase prototype systems or perhaps even be lower. This is mainly due to the subsystem performance improvements as the Grundfos PVP moves towards its design power.

All considered, the Miltek PVP system, followed by the Solvo and MLT PVP systems perform superior to the Grundfos PVP in the sub-kilowatt region (fixed and three position array) at a static head range of 70m to 80m.

Chapter Eleven

CONCLUSIONS

Photovoltaic water pumping for remote deep wells can be efficiently implemented with a progressive cavity pump in the higher sub-kilowatt region. These pumps are widely used in southern Africa and are driven by wind, diesel, grid or PV power sources. Some of the advantages that PVP's offer over wind and diesel pumps are that they are virtually maintenance-free with zero operating costs, relatively modular, potentially better synchronised to the water supply in the borehole and able to operate autonomously. The major disadvantage is the high initial capital cost. The photovoltaic array makes up a large portion of initial costs, and there are limited economics of scale, with increasing power (unlike diesel pumps, which therefore become more competitive for larger pumping requirements).

Review

Two prototype three phase PV pump systems and a DC PV pump system were tested on a farm (Latitude: 21°6' and Longitude: 17°6') in Namibia, 100km north of Windhoek. The array consisted of twelve modules ($636W_{\text{peak}}$) mounted on a single-axis passive tracker. The depth of the water level was 75m and a progressive cavity pump with a self-compensating stator was used.

The field tests were conducted from February 1993 to June 1993. The time prior to testing was spent designing measurement circuitry for the primary data acquisition system and preparing test procedures. The primary data acquisition system was mainly used for the data collection of steady state PVP signals. A secondary data acquisition system was used to capture instantaneous samples of higher frequency signals.

The emphases of this study was to assess the performance of each system and its components under various operating conditions, to observe the response of the controller under transient conditions, to evaluate possible weaknesses in the systems which might lead to break-down and to make concrete suggestion towards the development of the Solvo inverter. In addition, the prototype systems, the DC system and a three phase Grundfos system were compared using a simulation program.

The collected data was presented instantaneously for each component or set thereof but was also processed to a more comparable level by looking at the daily performance and evaluating the daily energy efficiency over a standard solar day. The uncertainties for the collected data were reported in the main text and all the figures quoted here are subject to the uncertainty margins quoted earlier.

Overall performance and costs of the evaluated PVP systems

The DC PVP system tested in this study performed better than the three phase prototype systems. Under test conditions the subsystem efficiency of the Miltek system reaches a peak 42%. The MLT and Solvo subsystem efficiencies reach a peak of 35% and 33% respectively. Over the whole operating range, the Miltek subsystem efficiency remains approximately 7% above the three phase subsystems' efficiency. The operating range of the Miltek system is wider than that of the three phase systems, starting at 80W array power while the Solvo system and MLT system start operating at 160W and 180W respectively.

The system daily energy efficiency for a 5kWh/m²/day and a 7kWh/m²/day are listed below:

	Miltek [%]	Solvo [%]	MLT [%]
5kWh/m ² /day	3.6	2.6	2.1
7kWh/m ² /day	4.2	3.2	3.2

The difference between the Solvo and the MLT system at 5kWh/m²/day is due to higher subsystem efficiency of the Solvo system at lower array input power. The system DEE of the MLT PVP improves with respect to the Solvo system as the energy content of the standard solar day increases as can be seen for 7kWh/m²/day.

Simulations were conducted with the tested systems (636W_{peak array}) and a Grundfos PVP system (SP 2A-15, 848W_{peak array}) for a fixed and a three position tilted array at a static head of 76m. The simulation was performed at two sites, namely Windhoek and Durban. The annual average irradiation received in Windhoek is 6.9kWh/m²/day while Durban receives 5kWh/m²/day. It was found that the average performance of the Grundfos system was below that of the three tested systems at both sites. The difference was more marked at the Durban site where the Grundfos system performed poorest. It can be observed that the performance of the Grundfos system improves rapidly during days of high irradiance which is characteristic of centrifugal pumps.

The unit water costs were calculated from the amortised life cycle costs and the annual water flow. They are listed for the fixed array at Windhoek and Durban:

	Miltek [c/m³]	Solvo [c/m³]	MLT [c/m³]	Grundfos [c/m³]
Windhoek	103.8	124.8	122.4	136.7
Durban	146.7	186.8	185.1	240.8

(The poor performance of the Grundfos system is due to operating at non-optimal array peak power. Simulations where the array size was increased showed a marked improvement in the unit water cost of the Grundfos system.)

Array performance

The array performance was measured to be somewhat lower than the values specified in the module data sheets. Measured performance fell just outside of the $\pm 10\%$ range of the module specifications. As the performance of the array was based on the measurements of all modules combined it is expectable that the performance would be lower than the performance of a single module due to mismatch losses. In addition, the uncertainty in the measurements was higher than 13%, making an assessment of the array performance compared to the specifications impossible. However, this high uncertainty stems from the input measurement to the array. The array output can be assessed accurately and therefore does not compromise accurate evaluation of the subsystem.

The cell temperature has a marked effect on the performance of the array, and a PVP system operating at a fixed array voltage can lose substantial amounts of power if set to an inappropriate array operating point. Array measurements showed that if it was 47°C there would be losses of 7% if the system operated at $200V_{\text{arr}}$, 3% at $195V_{\text{arr}}$ and about 2% at $190V_{\text{arr}}$, relative to optimum power. The data demonstrated that it is more beneficial to operate at a lower array voltage set-point rather than a higher set-point as the losses incurred due to operation at relatively low array voltage are lower than at high array voltage assuming large variations in the cell temperature.

The benefits of the tracking array were evaluated for a particular time of year. It was found that the passive tracking array received 12% more solar energy than the fixed array. The difference is small due to the time required by the passive tracking array to move from a west-facing position to an east-facing position in the morning. An active tracking array was simulated (it faces east before the sun rises in the morning) and was found to receive about 23% more solar energy than a fixed array under test conditions.

Pump performance

The pump performance was as specified although the operating point at which the maximum efficiency occurred did not coincide with the specified operating point. The flowrate was about 5% lower than the specified flowrate. However the uncertainty in the flowrate measurement is 6.1%. The torque-speed characteristics were found to be non-linear with a pronounced discontinuity occurring at mid-operating range (500rpm to 600rpm). The torque rose exponentially at that point and then dropped steeply to a lower torque. This was found to be a known phenomena which is due to the self-compensating stator element of the pump. This characteristic did not affect the flowrate considerably. It does however demand a torque from the motor which may not always be generated efficiently over the complete operating range of the PVP system.

Compared to pumps from Orbit, the Mono S2M pump was the best choice considering the static head and the input power range.

Controller and motor subset performance

Since the switching frequency of the controller has an impact both on the controller efficiency and on AC motor efficiency it is more representative to either component to discuss the performance aspect from a combined efficiency point of view, that is the subset efficiency.

For an array output power range of 200W to 500W, the Miltek subset efficiency ranges from 60% to 78%, the Solvo subset efficiency ranges from 40% to 60% and the MLT subset efficiency ranges from 40% to 65%. The subset efficiency of the Miltek system exceeds the subset efficiency of the three phase systems over the whole range. The MLT subset efficiency is poor in the 200W to 350W array power region which is mainly due to poor motor efficiency. This may be the result of a high harmonic content in the current waveform. In addition, the voltage to hertz relation is disturbed by high variations in the array voltage operating point during maximum speed tracking mode which alters the reference voltage substantially. However, the MLT subset efficiency is slightly higher than the Solvo subset efficiency at array powers in excess of 350W.

Assessment criteria of the prototype three phase inverters

Although much emphasis was placed on the efficiency evaluation of the inverters, it was realised that the reliability aspect of the inverters was crucial. Efficiency is essential but system reliability is paramount as PVP's find good application in remote areas which thus requires reliability. It was therefore considered a priority to evaluate inverter reliability and suggest improvements in that respect. As a second priority the inverter efficiency was considered with suggestions made towards software alterations which would improve efficiency. Hardware alterations for that purpose were not considered.

Assessment of the Solvo prototype three phase inverter

The main findings were in the areas of inverter algorithm capabilities, inverter output waveform quality, inverter efficiency losses, inverter protection and inverter diagnostic capabilities.

Control algorithm

The control algorithm which decides whether the motor speed is increased or decreased was found to be incapable of operating at a fixed voltage. Instead the array voltage oscillated around a mean value. The system was therefore stable but did experience array power losses due to voltage swings in the order of $\pm 10V$ to $\pm 15V$. This behaviour also had an impact on the line-to-line voltage applied to the motor resulting in a non-optimal voltage to hertz relation and torque pulsations. In addition, the monitoring of system operating states (for example, a low array operating voltage point) would be made difficult as a simple threshold value would not suffice. A mean of the particular parameter would have to be sampled. Suggestions towards an improved control algorithm are in section 9.1.

Operating states algorithms

The operating states algorithms were found to be incomplete. The system would therefore get into operating states that were either unproductive (eg, no water pumped) or could possibly result in inverter breakdown. The most basic operating state algorithm which was not implemented was an algorithm monitoring a bottom threshold of the array voltage. It was therefore possible to find a system operating at half its set operating voltage. Instead of performing a restart the system was stuck in this state. Algorithms which avoid unproductive operating states are presented in section 9.2.

Quality of the output waveforms

The inverter generated a sinusoidal PWM signal at high switching frequency. Due to the array voltage oscillations, the rms voltage had a superimposed low frequency ripple which resulted in 4 - 8% amplitude variations. In terms of variable voltage control, the resolution of the rms voltage was poor in that only ten different amplitudes were programmed for the frequency range from 6Hz to 85Hz.

The inverter produced a high quality current waveform in the windings of the motor due to its sinusoidal PWM switching scheme and its high switching frequency. The waveform quality did not degenerate at low operating frequencies due to these switching characteristics.

Efficiency improvements

It was found that the voltage applied to the motor over the full operating range was changed in a series of large steps. This undermined efforts at an optimal voltage to hertz relation. Improving the resolution would improve the subset efficiency (section 9.3), assuming that the optimal voltage to hertz relation is known. It was also suggested to perform tests on the subset efficiency of a Solvo inverter, with a lower switching frequency range which could reduce switching losses (section 9.4).

Inverter protection

The inverter was protected against short-circuit on the inverter output, overload, no-load and overheating. Further protection would involve protection against lightning, polarity reversal, overvoltage and pump dry-running.

General assessment

In general the reliability and possibly the efficiency of the Solvo inverter will improve with the implementation of the suggestions made in chapter nine. The dedicated PWM IC used by the Solvo inverter proved to be somewhat inflexible as it could not overmodulate the output voltage to generate a higher line-to-line voltage. On the other hand, this particular IC protects the power module as bus shoot-through (both switches on at the same time) is not possible with this type of digital drive circuit hardware.

The power for the drive circuitry and the microcomputer was supplied from a switched-mode power supply which is more efficient than a linear voltage regulator.

No user interface was offered in this prototype inverter. As these are relatively inexpensive, a user interface should be considered once the software requirements and development time have been assessed. However, this may not be a viable option if the potential market is not big enough to justify this type of addition to the inverter.

The physical layout of Solvo inverter is to be recommended as it proved to be extremely modular thus making hardware and software upgrades simple and fast.

Assessment of the MLT prototype three phase inverter

The main findings for this inverter were in the area of fixed voltage operation (FVO) and maximum speed tracking (MST) algorithm capabilities, inverter output signal waveform, inverter protection and inverter diagnostic capabilities.

Control algorithm

The basic control algorithm for both FVO and MST operation was implemented in exactly the same way as the algorithm in the Solvo inverter. The conclusions regarding the basic decision making of the inverter were therefore the same. However, it was also observed that the MLT inverter in FVO mode had a very narrow operating range. This point requires further investigation as the system cannot be operated economically in this operating mode.

The MST program presented tuning difficulties as the maximum speed set-point interfered with the start-up threshold of the system. A particular set-point might for example prevent the system from leaving its base speed (a low speed operation with no water delivery) until a 600W/m^2 solar irradiance level was received. Another setting might result in start-up at 450W/m^2 . The maximum speed was therefore never optimised but the start-up threshold was lowered as much as possible.

Operating states algorithms

This inverter was unable to distinguish between useful states of operation and unproductive states of operation. Both programs (FVO and MST) exhibited similar characteristics in that respect. Like the Solvo inverter, the MLT inverter could lose its operating point and 'operate' at less than half the array voltage set-point. As the line-to-line voltage applied to the motor under these conditions was far too low, the motor stalled since it could not draw sufficient current (from the capacitors and the array) to maintain the torque at such low array voltage and inverter output voltage. Suggestions to avoid this behaviour are in section 9.2.

The reset circuit which is activated in MST mode resets the controller when the motor does not turn. In principle the idea is good but the problem is that the microcontroller restarts immediately. Instead of losing control over its state of operation the

microcontroller should rather inhibit its output and enter a wait state. This essentially involves a change from a hardware implementation to a software implementation.

The inverter progresses through a number of non-essential operating stages as it starts up and as it comes to halt. These states are unproductive and can be avoided with proper monitoring as suggested in section 9.2.

Quality of the output waveforms

The inverter generated two types of PWM switching schemes namely sinusoidal and harmonic elimination PWM. The sinusoidal PWM scheme is suitable for low speed operation and the harmonic elimination PWM scheme improves the inverter efficiency due to a reduction in required switching while still applying a PWM waveform to the motor that is free of undesired low frequency harmonics. Both schemes were implemented, with sinusoidal PWM at low operating frequency and harmonic elimination at higher operating frequency.

The inverter is capable of overmodulating its output voltage signal which has the benefit of generating higher voltages from the available DC voltage than a strictly sinusoidal PWM signal. However, overmodulation has a negative impact on the harmonic spectrum.

The resolution of the variable voltage signal was good being nineteen amplitudes over an operating range of 3Hz to 65Hz.

Due to the array voltage oscillations, the rms voltage had a superimposed low frequency ripple which resulted in 8 - 13% amplitude variations.

The inverter produced a current waveform in the windings of the motor which was of reasonable quality. However, due to its low overall switching frequency, the current waveform was slightly distorted indicating the presence of large amplitude and low frequency harmonics, apparently leading to reduced motor efficiency.

Inverter protection

The MLT inverter offers hardly any protection except for a power supply fuse. It is therefore recommended that the inverter be protected against lightning, polarity reversal, overvoltage, phase short-circuit, overload, overheating and pump dry-running.

General assessment

The inverter achieves a comparatively good efficiency due to its sophisticated PWM switching scheme which is generated directly out of the ports of the microcontroller. Efficiency could be improved with a more efficient power supply (that is a switched-mode power supply). The general algorithm implementation is too simplistic and requires a more complex controller. These aspects are discussed in sections 9.1 and 9.2.

The principle of maximum speed tracking could possibly be changed to maximum power point tracking using the same algorithm. It may however be advisable to perform analog multiplication as this provides a continuous signal to the ADC and does not have any phase-shift problems as may be the case with software multiplication. This would avoid the use of an external sensor like the speed sensor. However, this option requires detailed investigation.

A user interface was not available for this prototype inverter. It would be recommended if the demand for such PV pump inverters is high enough to justify this type of development. Should it be found that a user interface is not justifiable then a panel of status LED's should be integrated into the design.

The physical layout of the inverter poses accessibility problems and the structures holding the PCB's are clumsy. Replacing a MOSFET took about an hour as all circuit boards had to be removed. The potentiometers for array voltage and speed adjustments were placed in the plane of the PCB. They should be top adjustment-type potentiometers.

Concluding comment

This study evaluated two prototype AC pumping systems and compared them with an established DC system, in a subkW deep borehole application ($636W_{\text{peak}}$, static head of 75m and about $0.069\text{m}^4/\text{day}$ to $0.083\text{m}^4/\text{day}$).

With switching schemes like those implemented in the MLT inverter, low power drive circuits, single chip microprocessor boards, higher power supply efficiency due to switched-mode power supplies and improved motor design, a three phase system could become an attractive alternative to the DC system. In addition, the three phase systems could be offered at a better price since the motors can be produced locally. Monitoring capabilities and some form of interaction with the user can be standard features. However, it is unlikely that the performance of the three phase systems will improve beyond that of a DC system due to higher drive circuitry requirements and generally lower subset efficiencies in this power range. If the switching frequency and the voltage to hertz relation have been optimised with a particular motor and if the motor itself has been optimised for efficiency then a three phase system could achieve a peak performance that is possibly within 3% of the current peak subsystem efficiency (42%) of the Miltek DC system. Cost factors, maintenance requirements and potential local production could then favour a three phase system.

For larger PV pumping systems (in the kW range), the AC systems have a more established place, mainly due to the cost, size and limited availability of suitable high-power DC motors. Grundfos submersible AC pumpsets (using centrifugal pumps) extend into the kW range. However, simulation comparisons with a Grundfos PV pump system (SP 2A-15, $848W_{\text{peak}}$, centrifugal pump) indicated that the three tested system, using progressive cavity pumps, had a superior performance in the subkW region.

Chapter Twelve

REFERENCES

- Anand, D K (1974). *Introduction to control systems*. New York: Pergamon.
- Baltas, P & Russell, P E (1987). *The dynamics of PV water pumping*. Nineteenth IEEE Photovoltaic Specialists Conference, 1031-5.
- Borchers, M L (1992). *Considerations in assessing the economic viability of stand-alone photovoltaic systems relative to other supply options*. Engineering Professions Association Conference on Solar Energy, Windhoek, Namibia.
- Bose, B K (1986). *Power electronics and AC drives*. New Jersey: Prentice Hall.
- Burton R (1992). *PV water pumping - The Botswana experience*. Engineering Professions Association Conference on Solar Energy, Windhoek, Namibia.
- Cowan, W D (Ed) (1992). *RAPS design manual*, Volume 1. Energy for Development Research Centre, University of Cape Town, Cape Town.
- Davies J L (1992). *The design and optimisation of a system using an induction motor driven pump, powered by solar panels*. MSc. Dissertation, Elec Eng, University of Cape Town.
- Davis M (1993a). *Photovoltaic pump handbook*. RTU Report Series 1, Energy for Development Research Centre, University of Cape Town.
- Davis M (1993b). *Directory of PV pumping equipment*. RTU Report Series 2, Energy for Development Research Centre, University of Cape Town.
- Davis M (1994a). *PVPump - A user's manual*. Energy for Development Research Centre, University of Cape Town.
- Davis M (1994b). *Simulation of PV pumping systems*. Energy for Development Research Centre, University of Cape Town.
- Gosnell R J (1991). *Photovoltaic water pumping - A case study in KwaZulu*. MSc. dissertation, Energy for Development Research Centre, University of Cape Town.
- Halcrow W (1983). *Small scale solar powered pumping systems: The technology, its economics and advancement*. Intermediate Technology Power, Sir William Halcrow & Partners, UNDP Project GLO/80/003, Executed by the World Bank, London: Swindon and Reading.

- Herrmann B, Karl H, Kopf E & Lehner G (1987). *Realistic indoor testing of photovoltaic water pumping systems*. Solar Energy, Vol. 38, No 4: 275-9.
- Hexfet Power MOSFET Designers Manual (1987). 4th edition, International Rectifier, California.
- Hirschmann G (1989a). *Leistungshalbbrücke für Drehstrommotoren mit IGBT BUP 304*. Der Elektroniker, No 12: 27-30.
- Hirschmann G (1989b). *Sinustabellenprogramm 'Sinus' mit Turbo-Pascal für das PWM-Konzept*. Internal report, Siemens Bericht No 8902 PD11.
- Holman J P (1978). *Experimental methods for engineers*. 3rd edition, New York: McGraw-Hill.
- Horowitz P & Hill W (1989). *The art of electronics*. Second edition, New York: Cambridge University Press.
- Iliceto A, Piazza V & Guastella S (1987). *Long-term comparison between two-axis and single axis tracking PV systems and a fixed PV array*. Nineteenth IEEE Photovoltaic Specialists Conference, 238-42.
- Kitchin C & Counts L (1986). *RMS to DC conversion application guide*. Second edition, Analog Devices, USA.
- Lasnier F, Gan Ang T, Lwin K S & Hemasuk T (1988). *Photovoltaic tests and instrumentation - Pumping system*. Energy Technology Division, Asian Institute of Technology, Bangkok, Thailand.
- Lasnier F & Gan Ang T (1990). *Photovoltaic engineering handbook*. Bristol: Adam Hilger.
- Mohan N, Undeland T M & Robbins W P (1989). *Power electronics: Converters, applications and design*. Singapore: John Wiley & Sons.
- Murphy J M D & Turnbull F G (1988). *Power electronic control of AC motors*. Oxford: Pergamon.
- Payne S A E (1986). *The design and production of solar powered positive displacement pumping systems*. Unnumbered conference paper, Renewable Energy Potential in Southern Africa Conference, Energy Research Institute, University of Cape Town, 8-10 Sept.
- Schaefer J F (1985). *Results of a survey of 111 photovoltaic water pumping systems in New Mexico*. New Mexico Solar Energy Institute, Las Cruces, New Mexico.

-
- Scholey D (1982). *Induction motors for variable frequency power supplies*. IEEE Transactions on Industry Applications, Vol 1A-18, No 4, July/August.
- Schmalschläger T, Piernavieja G & Kranz G (1993). *Sonnenstandsnachführung - Theorie und Praxis bei kleinen PV-Anlagen*. Sonnenenergie, No 3: 8-11.
- Schmid J (1987). *Recommendations for measurements on inverters*. European PV Plant Monitoring Newsletter, Commission of the European Community, Number 2, July 1987.
- Vetter G & Wirth W (1992). *Exzentrerschneckenpumpe - Einsatz in der Photovoltaic*. Sonnenenergie, No 3: 12-9.
- Vetter G & Wirth W (1993). *Suitability of eccentric helical pumps for turbid water deep well pumping in photovoltaic systems*. Solar Energy, Vol 51, No 3: 205-14.
- Whitfield G R & Bentley R W (1988). *The efficiency of small scale solar photovoltaic water pumping systems*. International PV Conference, 1123-6.

Appendix A1

PV PUMP COMPONENT SPECIFICATION SHEETS

A1.1 Siemens M55S module

Installation advice

The following minimum distances must be observed in order to ensure sufficient rear ventilation of the module:

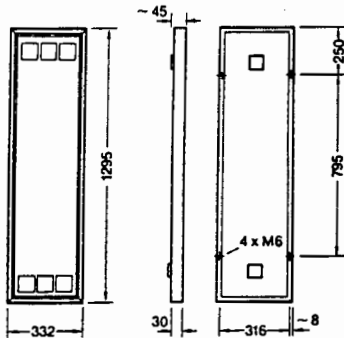
- from the rear walls > 50 mm
- from the neighboring modules > 5 mm

Recommended minimum slope 15°

Installation from the rear is facilitated by M6 nuts pressed into the frame.

The wiring of the modules is accomplished via plastic cable bushings in two plastic terminal boxes attached to the back; one positive, one negative. One of the boxes is clearly marked with a "+" to designate the polarity.

Measurements



Internal Circuitry

Bypass diodes (in the terminal box) protect from "hot spot effects" preventing possible destruction if the module is partly shaded.

Limit values	Storage temperature	-40°C ... +90°C
	Ambient temperature (operational)	-40°C ... +50°C
	Surface pressure	2400 N/m ²
	Frame deformation (diagonal lifting of the module plane)	max. 1.2°

Electrical parameters:	Short circuit current $I_{sc}^{(1)}$	3.27 A
	Maximum output $P_{max}^{(1)}$	53 W _p ⁽²⁾
	Open circuit voltage U_L	21.8 V

Weights:	M 55 S	6.3 kg
----------	--------	--------

Thermal parameters:	NOCT ⁽³⁾	47°C
	Temperature coefficient of the short circuit current	+4 x 10 ⁻⁴ /K
	Temperature coefficient of the open circuit voltage	-3.4 x 10 ⁻³ /K

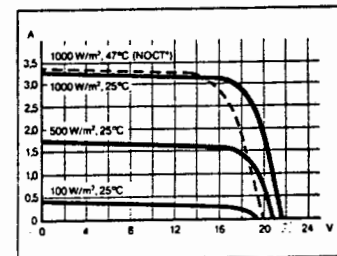
Qualifications	The modules meet and surpass CEC specifications	
	Temperature range	-40°C ... +95°C
	Humidity at 90°C	95% relative humidity
	Hailstorm	dia. = 25 mm vel. = 100 km/h
	Ice, salt fog	
	UV, SO ₂ and O ₃ loads	
	Surface pressure and torsion	

¹⁾ These values are subject to a manufacturing deviation of plus/minus 10%.

²⁾ W_p
Watt peak = peak output under standard testing conditions:
Air mass AM = 1.5
Insolation E = 1000 W/m²
Cell temperature T_c = 25°C

³⁾ Normal cell operating temperature at:
Insolation E = 800 W/m²
Ambient temperature T_a = 20°C
Wind speed V_w = 1 m/s

Current voltage characteristics



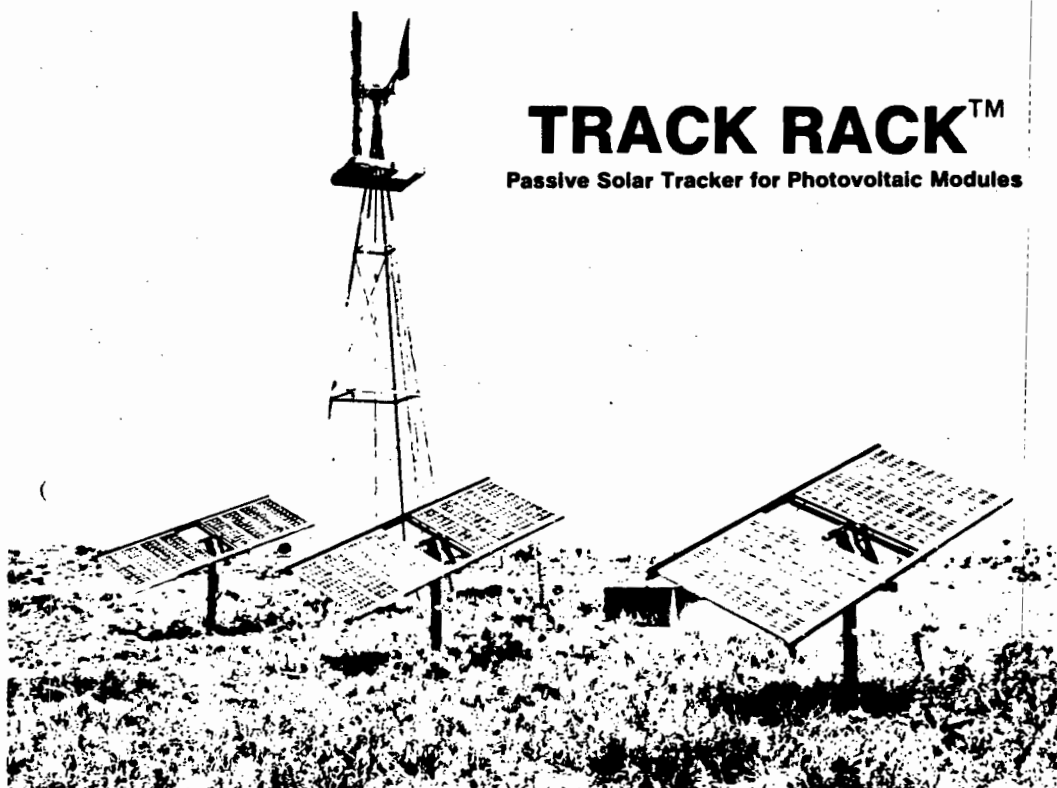
Subject to technical alterations

Siemens Solar GmbH
A joint venture of
Siemens AG and Bayernwerk AG

Frankfurter Ring 152
8000 Munich 40
Tel. (0 89) 35 00-24 11
Fax (0 89) 35 00-25 73

1:55 1090 GB02 DAT

A1.2 Zomeworks TRPM12/AR passive solar tracker



TRACK RACK™ Passive Solar Tracker for Photovoltaic Modules

Three 8408 TRACK RACKS™ pumping water to a stock tank at Los Ojos Ranch, Santa Rosa, New Mexico. Installation by Tom Volek.

Our Passive Solar TRACK RACKS™ operate by liquid flowing between sealed frame members. There are no drive motors, gears or pistons; there is little to wear out. The Zomeworks Passive Solar TRACK RACKS™ are as dependable as gravity and the heat of the sun.

TESTS CONDUCTED OVER A 12-MONTH PERIOD BY NEW MEXICO STATE UNIVERSITY AT 34° N LATITUDE SHOWED AN IMPROVEMENT IN ELECTRICAL OUTPUT BY TRACKING AROUND AN ADJUSTABLE N-S AXIS OF 29% OVER A FIXED LATITUDE MOUNT. THE IMPROVEMENT RANGED FROM 19% IN NOVEMBER TO 42% IN JUNE AND JULY. THIS MEANS THAT USING AN EIGHT-MODULE TRACK RACK™ IS LIKE HAVING 1.6 EXTRA MODULES IN THE WINTER AND 3.2 IN THE SUMMER, OR AN AVERAGE OF 2.3 EXTRA MODULES FOR THE YEAR.

The Zomeworks TRACK RACK™ is ideal for stock watering or irrigation. On a clear summer day, photovoltaic modules mounted on our tracker will deliver 55% more energy than modules on a fixed latitude mount. The solar electric power comes in a smooth dawn-to-dusk flow rather than a noon peak. This enables 55% more water to be pumped on the hottest days of the year without purchasing additional modules or a larger pump.

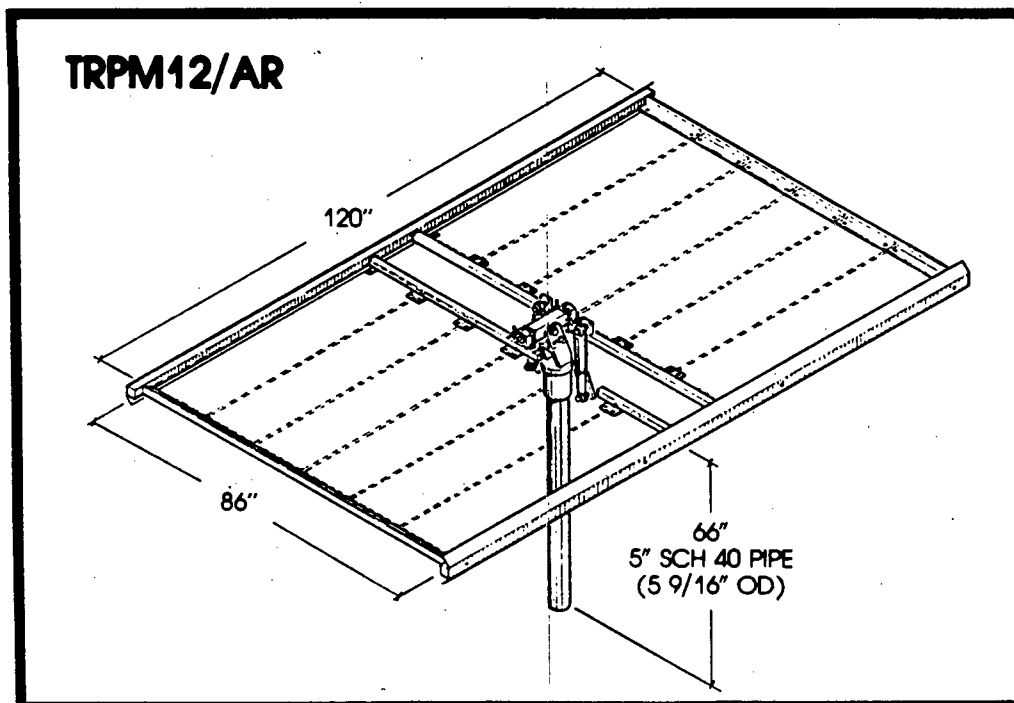
The Zomeworks TRACK RACK™ is constructed of painted mild steel. Stainless steel racks are available. The TRACK RACK™ is designed to withstand 30 lbs/sq ft wind loading. Specially-made shock absorbers dampen motion in high winds.

The TRACK RACK™ is easy to install. It slips over a pipe most set in concrete and is locked into place by tightening one bolt.

The N-S axis is seasonally adjustable for top performance all year long.

US Patent # 4,275,712

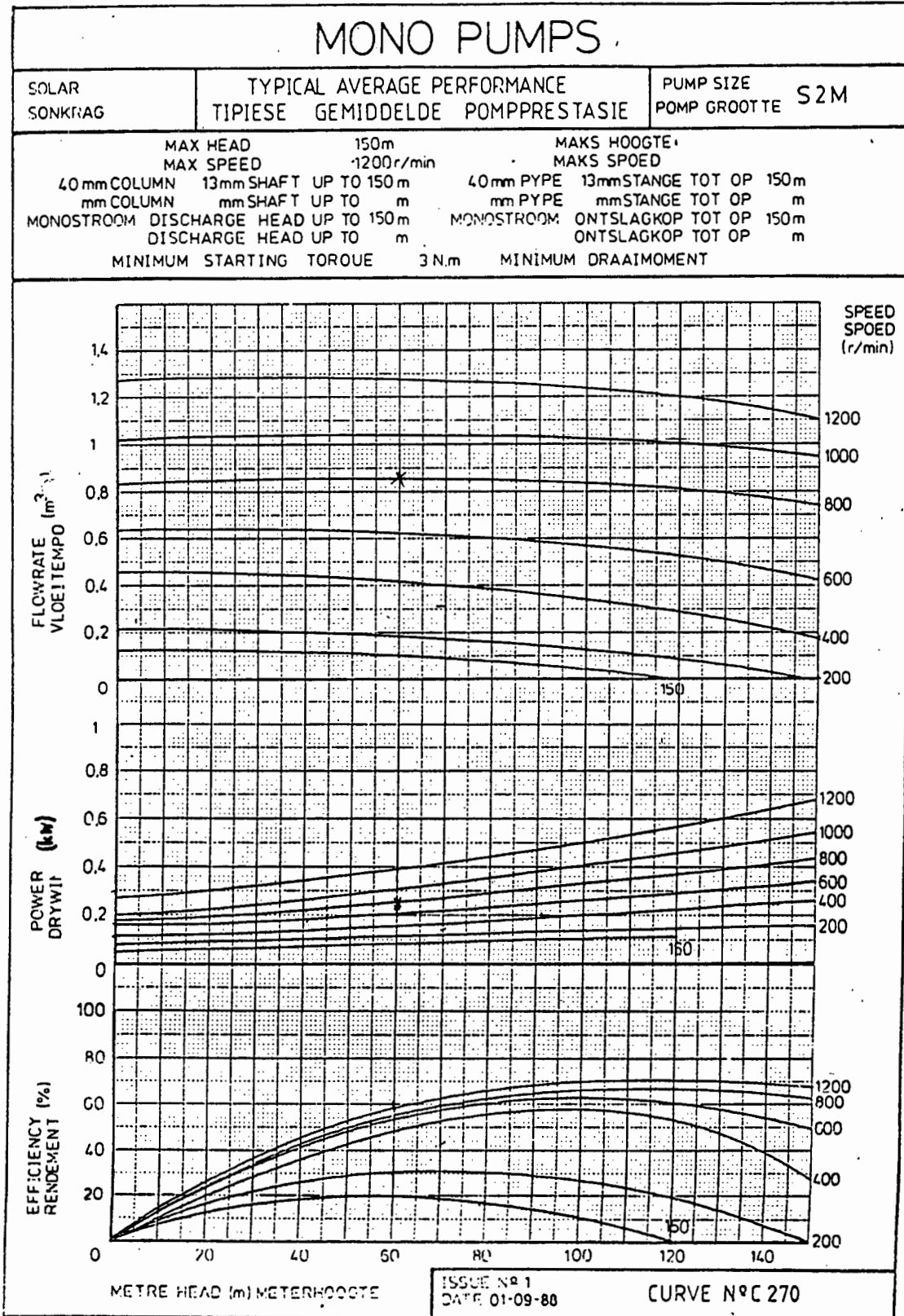
ZOMEWORKS
Passive Solar Energy Products



TECHNICAL DATA

Model	TRPM02/AR	TRPM04/AR	TRPM08/AR	TRPM12/AR	TRPM14/AR
Number of Modules	1 or 2	4	8	12	14
Maximum Module Area (sq ft)	9.5	18.5	37	55.5	64.5
Rack Dimensions (inches)	28 X 52	51.5 X 68	59 X 117	86.5 X 115	100 X 121
Mounting Mast (height from ground)	30"	40"	56"	66"	74"
Pipe Size (Sch 40) steel	2"	2.5"	4"	5"	6"
Actual Pipe OD	2.375"	2.875"	4.5"	5.563"	6.625"
Shipping Weight (lbs)	50	80	130	180	210
Angles Axis Adjustment	5-45°	5-45°	5-45°	5-45°	5-45°
Tracker Groves Max N-S Spacing (approx) Max E-W Spacing	NA NA	15' 20'	20' 20'	30' 30'	30' 35'
Price					

A1.3 Mono S2M borehole pump



A1.4 Solvo circuit breaker and power module

A1.4.1 Thermal three phase circuit breaker Mbs 25

Motor Protective Switch

Type Mbs 25

Specification

Motor protective switch complies with »Agreement for Low Voltage Switchgear« to DIN 57 660/VDE 0660 and the IEC Publication 292-1 and 157-1. When incorporated in the insulated enclosure, front plate, and with the emergency stop mushroom pushbutton it also complies with VDE 0113 for Main, and emergency disconnect switches.

Operating mechanism

Manually operated by pushbuttons, with a positive trip free feature. Clearly visible switch position indication, and positive contact separation. Available with padlocking facility in the »Off« position, accommodating up to 3 padlocks, with bow thickness of 6-8 mm, when used in insulated enclosure type i, or frontplate type it.

Trip device

Thermal overload trip »b«
Triple pole, adjustable, motor protection characteristic (trip characteristic T II). Single phase fault sensitivity, and ambient

temperature compensation (-5°C up to +40°C) to VDE 0660 and IEC 292-1. Frequency range 40 - 60 Hz.

Magnetic short circuit trip »s«

The response current value is fixed. Once the response current value is attained, the magnetic trip instantaneously releases the latch mechanism. The response current value is approx. $12 \times I_b \cdot I_e$ = the highest setting value on the adjustable thermal trip.

Auxiliary trip block

Units are suitable for subsequent fitting within the equipment. It is possible to fit either an a- or r-trip.

Shunt trip »a«

For remote tripping function. Rated for short time energisation its control circuit should be via its N.O. auxiliary switch. voltage tolerance 0.7 ... x 1.2U_c

Undervoltage trip »r«

Can be used without an auxiliary switch (100% ED). Where auxiliary switch control is required, this should be via an auxiliary switch block, type HS 9V.20 with 2 early make contacts.

Voltage tolerance - closing - 0.85...1.1 x U₂
- opening - 0.7 ... 0.35 x U_c

Power consumption: 2.2/1 VA/W

Auxiliary switch block type HS 9

Up to 2 auxiliary switches, can be subsequently fitted, either on the LHS or RHS of main switch unit.

Versions available: 1N.O.1N.C., 2N.O. or 1N.O.+1N.C., 2N.O. with early make feature I_b 6 A AC 11, U_e ~ 500 V
I_b 6 A DC 11, U_e ~ 220 V

For a wide range of additional accessories see pages 7/4, 7/5.

Enclosure

Moulded enclosure, and moulded front plate for flush mounting are of flame retardant material, offering IP41 and IP55 protection. Four cable entry »knockouts« - Pg 16 are provided, along with earthing connection. The switch module snap fits into the enclosure. Accessories include an indicator lamp, and a neutral N conductor, which can be self fitted.

General

Integral snap fitting to DIN rail - DIN EN 50 022 feature, or screw mounting, as required. For d.c. applications, use all 3 poles connected in series.

Technical values

Rated insulation voltage U_i	~ 660 V, IGr. C	
Rated voltage U_c	a.c. voltage 3- 660 V	d.c. voltage earthed or unearthed ... 220 V (with all three poles series connected)
Rated current I_{th}	25 A up to 40° with unenclosed switch	
Rated short circuit breaking capacity I_{cn} to VDE 0660, IEC 157-1, P-1; 0-1-C0 Effective values for unenclosed breaker, with incoming supply on upper terminals	a.c. 3-	d.c. time constant T = 15 ms ... 220 V
≤ 6.3 A	∞ kA -	∞ kA
10 A	∞ kA -	∞ kA
16 A	6 kA 0.7	4 kA 0.8
25 A	6 kA 0.7	4 kA 0.8
	380 V cos φ	415 V cos φ
	∞ kA -	∞ kA -
	6 kA 0.7	6 kA 0.7
	4 kA 0.8	3.5 kA 0.8
	6 kA 0.7	2.5 kA 0.9
	500 V cos φ	660 V cos φ
	3 kA 0.9	1.5 kA 0.95
	3 kA 0.9	1.5 kA 0.95
	3 kA 0.9	1.5 kA 0.95
	1.5 kA 0.95	1 kA 0.95
	∞ kA	∞ kA
	∞ kA	∞ kA
	6 kA	6 kA
Increased short circuit breaking capacity I_{cn} when using type id current limiting module.	∞ kA -	∞ kA -
≤ 6.3A	∞ kA -	∞ kA -
≤ 25A	100 kA 0.7	50 kA 0.7
	50 kA 0.7	50 kA 0.7
Motor switching capacity	AC-3, DC-4	
Mechanical/Electrical lifespan	10 ⁵ ops/10 ⁵ ops (at AC-3 duty)	
Switching frequency	40 ops/hour	
Total opening time	approx. 7 ms	
Total power loss	6 W (with rated current - warm condition)	
Fuses Highest permissible rating, only necessary if the short circuit current could be greater than the rated breaking capacity	b-trip adjustable range A	D-fuse - slow, or NH-fuse type NT 3- 220 V ∞ 220 V A
		3- 380 V 3- 415 A A
		3- 500 V A
		3- 660V A
	0.1 ... 0.16 0.16 ... 0.25 0.25 ... 0.4 0.4 ... 0.63 0.63 ... 1 1 ... 1.6 1.6 ... 2.5 2.5 ... 4 4 ... 6.3 6.3 ... 10 10 ... 16 16 ... 20 20 ... 25	No back up fuse necessary, even with higher fault current installations.
		25 35 50 50 50 63 63 63 63 63 63 63 63
		20 25 35 35 35 35 50 50 50

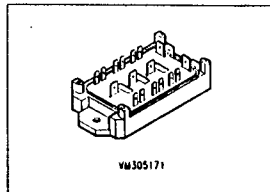
SIEMENS

IGBT Module Preliminary Data

$V_{CE} = 1000\text{ V}$
 $I_C = 6 \times 15\text{ A}$

- Power module
- 3-phase full-bridge
- Including fast free-wheel diodes
- Package with insulated metal base plate
- Package outline / Circuit diagram: 3b¹⁾

BSM 15 GD 100 D



Type	Ordering Code
BSM 15 GD 100 D	C67076-A2500-A2

Maximum Ratings

Parameter	Symbol	Values	Unit
Collector-emitter voltage	V_{CE}	1000	V
Collector-gate voltage, $R_{GE} = 20\text{ k}\Omega$	V_{CGR}	1000	
Gate-emitter voltage	V_{GE}	± 20	
Continuous collector current, $T_C = 80\text{ }^\circ\text{C}$	I_C	15	A
Pulsed collector current, $T_C = 80\text{ }^\circ\text{C}$	$I_{C\text{ pulsed}}$	30	
Operating and storage temperature range	T_J T_{sto}	$-55 \dots +150$	$^\circ\text{C}$
Power dissipation, $T_C = 25\text{ }^\circ\text{C}$	P_{tot}	150	W
Thermal resistance Chip - case	$R_{th\text{ JC}}$	≤ 0.8	K/W
Insulation test voltage ²⁾ , $t = 1\text{ min.}$	V_{is}	2500	V _{ac}
Creepage distance	-	16	mm
Clearance	-	11	
DIN humidity category, DIN 40 040	-	F	-
IEC climatic category, DIN IEC 68-1	-	55/150/56	-

¹⁾ See chapter Package Outlines and Circuit Diagrams

²⁾ Insulating test voltage between collector and base plate referred to standard climate 23/50 in acc. with DIN 50 014, IEC 146, para. 492.1.

BSM 15 GD 100 D

Electrical Characteristics at $T_J = 25\text{ }^\circ\text{C}$, unless otherwise specified.

Parameter	Symbol	Values			Unit
		min.	typ.	max.	

Static characteristics

Collector-emitter breakdown voltage $V_{GE} = 0, I_C = 0.5\text{ mA}$	$V_{(BR)CES}$	1000	-	-	V
Gate threshold voltage $V_{GE} = V_{CE}, I_C = 1\text{ mA}$	$V_{GE(th)}$	4.5	5.5	6.5	
Collector-emitter saturation voltage $V_{GE} = 15\text{ V}, I_C = 15\text{ A}$ $T_J = 25\text{ }^\circ\text{C}$ $T_J = 150\text{ }^\circ\text{C}$	$V_{CE(sat)}$	-	2.8 4.0	3.3 4.5	
Zero gate voltage collector current $V_{CE} = 1000\text{ V}, V_{GE} = 0$ $T_J = 25\text{ }^\circ\text{C}$ $T_J = 125\text{ }^\circ\text{C}$	I_{CES}	-	-	500 2000	μA
Gate-emitter leakage current $V_{GE} = 20\text{ V}, V_{CE} = 0$	I_{GES}	-	-	100	nA

AC characteristics

Forward transconductance $V_{CE} = 20\text{ V}, I_C = 15\text{ A}$	g_{fs}	4.5	8	-	S
Input capacitance $V_{CE} = 25\text{ V}, V_{GE} = 0, f = 1\text{ MHz}$	C_{iss}	-	2000	2700	pF
Output capacitance, $V_{GS} = 0$, $V_{CE} = 25\text{ V}, V_{GE} = 0, f = 1\text{ MHz}$	C_{oss}	-	160	-	
Reverse transfer capacitance $V_{CE} = 25\text{ V}, V_{GE} = 0, f = 1\text{ MHz}$	C_{rss}	-	65	-	

A1.5 GEC 750W DZ90L three phase motor

MOTOR TEST CERTIFICATE

CUSTOMER SOLAR AGE NAMIBIA

SERIAL NUMBER

X012640/1A

FRAME SIZE DZ90L OUTPUT 0.75 kw 3 PHASES

VOLTAGE 110 v SPEED 1435 R/MIN

ENCLOSURE IP44 RATING S1 CONNECTION DELTA

ROTATION ON D.E. CLOCKWISE F.L. CURRENT 6.4 AMP.

FREQUENCY 50 Hz. CLASS OF INSULATION F ALTITUDE 0 m.

CUSTOMERS REF. K093

WORKS REF. X012640/1A

LOAD TEST ON THIS / AN IDENTICAL MACHINE						
VOLTAGE	SATOR AMP	R/MIN	INPUT kw	OUTPUT kw	P.F.	EFF. %
110	4.62	1472	.510	.372	.579	72.97
110	5.70	1453	.765	.593	.704	77.54
110	6.70	1430	1.020	.803	.799	78.80
HOT * COLD - NO LOAD TEST			CALCULATED START CONDITIONS AS FULL VOLTAGE			
VOLTAGE	AMP	INPUT kw	VOLTAGE	AMP	TORQUE Nm.	
110	3.725	.115	110	37.50	15.79	
SHORT CIRCUIT TEST				WINDING RESISTANCE		
VOLTAGE	AMP	TORQUE Nm.	INPUT kw.	PHASE TERM	TEMP. °C	
110	37.50	15.794	5.900	1.69500	18.00	
MAXIMUM TEMPERATURE RISE AS OBTAINED ON THIS / AN IDENTICAL MACHINE						
MACHINE	70.98 °C.	PHASE TERM RESISTANCE				
STATOR COLD	1.69500 OHMS	AMB.	18.00 °C			
STATOR HOT	1.85600 OHMS	AMB.	21.00 °C			
VIBRATION VEL. mm/s - MICRONS			SHAFT FITTED WITH HALF KEY			
D.E. V.	D.E. H.	AXIAL	N.D.E. V.	N.D.E. H.		

REMARKS:

H.V. TEST AT 2000 V FOR 1 min

MEGGER AT 500 v STATOR 100+ M.OHMS

ROTOR BALANCE AND BEARINGS OK

DATE OF TEST 18/05/92

DATE 27/05/92 SIGNED *msv.*

Appendix A2

TEST METHODOLOGY DETAILS

This chapter presents all the necessary and most important information on how data was acquired. This includes the test purpose, the test set-up, the test procedure and the data logger details (the parameters, their channel configuration, the log interval and the settling time for the test system and the data acquisition system). Finally the assumptions are stated where appropriate.

Most tests were at least repeated three times either because of measurement problems or to verify the consistency and repeatability in the data sets.

The main tests areas were:

- the array characterisation
- the pump characterisation
- the Miltek system characterisation which included the converter and motor characteristics and a component matching evaluation
- the Solvo and MLT system characterisation which also consisted of the inverter and motor characteristics, a component matching evaluation and a hardware and a software algorithm evaluation

The structure of this chapter aims to follow the information flow of the main text where possible.

A2.1 The array

The array consisted of twelve Siemens modules mounted on a Zomeworks tracker which was a single-axis, passive tracking mechanism.

Array tests consisted of the acquisition of IV curves for a number of irradiance levels and cell temperatures as well as a series of tests to compare a fixed array to a tracking array for a particular day.

A2.1.1 IV curves

TABLE A2.1 Test methodology for IV curves

	Test, procedure and logging details
<i>Purpose</i>	<ul style="list-style-type: none"> • array characteristics • comparison to specifications • MPP's as a function of G_{POA} and t_{mod}
<i>Apparatus</i>	System: array and tracker DAS: interface, data logger, computer
<i>Aux. equipment¹⁾</i>	15W, 30W, 60W, 120W, 240W, 480W, 1300W and 2100W loads (bulbs and a heater) as well as a variable resistor (2A maximum) and a short circuit plug; each load was fitted with a switch; the loads were all connected in parallel
<i>Procedure</i>	<ul style="list-style-type: none"> • moved array to approximate position to receive required irradiance; waited for correct t_{mod}; synchronised logger and stopwatch; started from short circuit current, switching loads every 5sec until the open circuit voltage was reached; an effort was made to switch small loads in 15W steps near the MPP; • repeated for G_{POA} of 200, 400, 600, 800 & 1000 W/m^2 and for t_{mod} of 25, 35, 47 and 55°C
<i>Parameter: Analog</i>	G_{POA} , t_{mod} , t_{amb} , I_{arr} & V_{arr} (all instantaneous)
<i>Constants</i>	G_{POA} , t_{mod} , t_{amb} during one set of test
<i>Log interval</i>	5sec
<i>Settling time</i>	3sec
<i>Assumptions</i>	<ul style="list-style-type: none"> • that all modules were at the same temperature • that the plane of array irradiance and the temperature did not vary
<i>Results in section</i>	6.1.1, 2 & 3

¹⁾ Auxiliary equipment

A2.1.2 Tracking versus fixed array

TABLE A2.2 Test methodology for tracking and fixed array

	Test, procedure and logging details
<i>Purpose</i>	<ul style="list-style-type: none"> to assess the difference in performance between a tracking and a fixed array for one particular day to find the difference to the standard solar day
<i>Apparatus</i>	System: array, tracker (tracking and fixed), Miltek converter, Baldor motor and pump DAS: interface, data logger and computer
<i>Conditions</i>	clear blue sky, no clouds
<i>Procedure</i>	<ul style="list-style-type: none"> fixed array: tracking mechanism was inhibited and the array was fixed in a north-facing direction passive tracking array: no interference 'active' tracking array: moved the array to an east-facing position the evening before the test
<i>Parameter:</i> Analog Digital	G_{POA} , t_{mod} , t_{amb} , I_{arr} , V_{arr} , T_{mot} (instantaneous), time & day S_{mot} (event)
<i>Log interval</i>	30sec ¹⁾
<i>Settling time</i>	not applicable - no disturbances
<i>Assumptions</i>	<ul style="list-style-type: none"> that the spectral conditions have not changed within the three days of testing that the 'active' tracking array simulation does not lag behind the sun
<i>Results in section</i>	6.1.5

¹⁾ Every 40th data set was eventually used.

A2.2 The pump

The pump that was used was a S2M Mono borehole pump with a self-compensating stator.

The tests constituted correlations, torque and efficiency characteristics and higher head simulations.

A2.2.1 Correlations

The correlations included the flowrate to pump speed correlation and the drawdown to pump speed correlation.

Flowrate

It was too tedious to read the differential flow through the volume-flowmeter for each steady state test manually (the flowrate transducer did not operate successfully as discussed later). A correlation therefore simplified the data collection and avoided mistakes. Errors in the correlation would be applicable for all three systems and would therefore carry little weight in the comparison amongst the systems but carry more weight in comparison to other systems.

The installed Kent volume-flowmeter was calibrated using a bucket of known volume. The flowrate at a particular pump speed (which was logged) was found by noting the start and stop readings of the volume-flowmeter in a 20 or 40 second interval timed with a stopwatch. This was repeated for various pump speeds and at a head of about 75 and 82m.

Drawdown

This correlation simplified the measurement procedure considerably since it was often the case that a test had to be performed under virtually constant condition. Having to measure the water level drawdown was simply too time consuming.

The correlation took place as follows: The borehole water-level was at rest. The pump was started at a slow speed and left for about three minutes to settle without a change in pump speed. Then the static head was measured while the pump speed was logged. This was repeated for different pump speeds until the maximum pump speed was reached.

A2.2.2 Torque and efficiency characteristics

TABLE A2.3 Test methodology for the main pump characteristics

	<i>Test, procedure and logging details</i>
<i>Purpose</i>	<ul style="list-style-type: none"> to obtain the steady state torque versus speed characteristics as well as the efficiency curve to obtain the starting torque & power requirements
<i>Apparatus</i>	System: array, Miltek converter, Baldor motor and pump DAS: interface, data logger, computer
<i>Procedure</i>	moved the array from a low irradiance position to a high irradiance position in incremental steps so that the system received sufficient time to settle
<i>Parameter:</i> Analog Digital	T _{mot} (mean) S _{mot} (event)
<i>Log interval</i>	5sec ¹⁾
<i>Settling time</i>	25sec (used every sixth data set)
<i>Assumptions</i>	none
<i>Results in section</i>	6.2.2/3 (at standard head)

¹⁾ A short log-interval was selected to ensure that the mean of the torque was logged during a steady state period. Non-settled data sets were discarded as a standard procedure.

A2.2.3 Pump characteristics at higher heads

Higher heads were simulated using a constant pressure valve attached to the output of the pump. The problem was however that the pressure varied if the flowrate varied unless it is readjusted whenever the flowrate changed. This was not done since the adjustment on the valve was very crude. The pressure (mean) was therefore recorded for each data-point and the additional simulated head plus its variation could be calculated. The remaining test details were as in Table A2.3 above.

A2.3 The Miltek DC system

The Miltek DC system consisted of the PV array, a Miltek controller (MEI 400), a Baldor DC motor and the pump.

The tests were aimed at the characterisation of the converter and motor as well as the system and subsystem. Other tests included matching between the array and the controller, the system start-up conditions and the dynamic conditions.

A2.3.1 The main system and component performance tests

TABLE A2.4 Test methodology for the main Miltek DC PVP system characteristics

	<i>Test, procedure and logging details</i>
<i>Purpose</i>	<ul style="list-style-type: none"> to obtain the efficiency curves of the converter and motor at standard and higher heads to obtain the characteristic curves of the converter and the motor to assess the fixed array voltage operation capabilities to obtain the system start-up values to obtain the instantaneous system and subsystem performance characteristics
<i>Apparatus</i>	System: array, Miltek converter, Baldor motor and pump DAS: interface, data logger, computer
<i>Procedure</i>	<ul style="list-style-type: none"> moved the array from a low irradiance position (noticed start-up conditions) to a high irradiance position in incremental steps so that the system received sufficient settling time; repeated for higher simulated heads as explained in subsection A2.2.3 above
<i>Parameter: Analog Digital</i>	G_{POA} , t_{mod} , t_{amb} , I_{arr} , V_{arr} , I_{con} , V_{con} & T_{mot} (mean) S_{mot} (event)
<i>Log interval</i>	5sec ¹⁾
<i>Settling time</i>	25sec (used every sixth data set) ¹⁾
<i>Assumptions</i>	none
<i>Results in section</i>	6.3.1, 6.3.2 (in part), 6.3.3 (in part) and 6.3.4

¹⁾ A short log-interval was selected to ensure that the mean of the parameters were logged during a steady state period. Non-settled data sets were discarded as a standard procedure.

A2.3.2 Dynamic array operating point with the Miltek converter

The purpose was to assess the array losses due to the switching of the converter.

The instantaneous array voltage was measured with a hand-held oscilloscope (described in section 5.4) at a few system operating points which were registered manually by measuring the array current. The data was downloaded from the device to the computer. The result is shown in subsection 6.3.2.

A2.3.3 Dynamic conditions

TABLE A2.5 Methodology for testing dynamic conditions

	<i>Test, procedure and logging details</i>
<i>Purpose</i> ¹⁾	<ul style="list-style-type: none"> to evaluate the system response capabilities to disturbances (that is, does the converter loose its operating point and perform a restart or can it cope with the disturbance like for instance a cloud)
<i>Apparatus</i>	System: array, Miltek converter, Baldor motor and pump DAS: interface, data logger, computer
<i>Conditions</i>	thick isolated clouds are ideal
<i>Procedure</i>	<ul style="list-style-type: none"> if clouds were present then it was a matter of starting the logger at least a few seconds before the shade of the cloud fell on the array; if no clouds were present then one of the parallel strings of modules was disconnected and once the system had settled it was reconnected; in this way it was possible to generate a step-down and a step-up
<i>Parameter: Analog Digital</i>	G_{POA} , t_{mod} , t_{amb} , I_{arr} , V_{arr} , I_{con} , V_{con} & T_{mot} (instantaneous) S_{mot} (event)
<i>Log interval</i>	1sec
<i>Assumptions</i>	the settling time of each channel in the interface signal conditioning unit is the same (not true)
<i>Results in section</i>	6.3.3 (Dynamic conditions)

¹⁾ This test cannot be used to make deductions on the system settling time requirements due to the measured parameters having different settling times. The main function of this test was to establish whether the system would loose time due to frequent restarts during cloudy weather or whether the controller would respond fast enough.

A2.4 The Solvo and MLT three phase systems

The Solvo and MLT systems consisted of the array, an inverter, a three phase GEC motor and the pump. The Solvo inverter only operates in FVO mode and the MLT inverter operates in FVO and MST mode.

The tests for the three phase systems were similar in most respect. They are therefore discussed in the same section. Some of the tests conducted with the prototype systems were more detailed than the Miltek system tests.

The tests were aimed at the characterisation of the inverter and motor as well as the system and subsystem. Other tests included matching between the array and the controller, a detailed analysis of the control algorithm capabilities, the system start-up conditions and the dynamic conditions.

A2.4.1 The main system and component performance tests

TABLE A2.6 Test methodology for the prototype system characteristics

	<i>Test, procedure and logging details</i>
<i>Purpose</i> ¹⁾	<ul style="list-style-type: none"> • to obtain the efficiency curves of the inverter and the motor at standard and higher heads • to obtain the characteristic curves of the inverter and the motor • to evaluate the steady state array operating point characteristics for all modes of operation • to verify the programmed voltage to hertz relation • to obtain the system start-up values • to obtain the instantaneous system and subsystem performance characteristics
<i>Apparatus</i>	<p>System: array, Solvo or MLT inverter, GEC three phase motor and pump</p> <p>DAS: interface, power meter, data logger, computer</p>
<i>Proceduse</i>	<ul style="list-style-type: none"> • moved the array from a low irradiance position (noticed start-up conditions) to a high irradiance position in incremental steps so that the system received sufficient time to settle; done for Solvo (FVO) system; • repeated for MLT with FVO and MST; • repeated for higher simulated heads as explained in subsection A2.2.3 above

<i>continued</i>	<i>Test, procedure and logging details</i>
<i>Parameter: Analog Digital</i>	G_{POA} , t_{mod} , I_{arr} , V_{arr} , I_{line} , V_{LN} , P_{inv} , T_{mot} (mean) f_{fund} , S_{mot} (all event)
<i>Log interval</i>	5sec ²⁾
<i>Settling time</i>	25sec (used every sixth data set) ¹⁾
<i>Assumptions</i>	all three phases were balanced
<i>Results in section</i>	7.1.1/2/3, 7.2, 7.4, 7.6 (in part), 7.7.1 for Solvo system 8.1.1/2/3, 8.2, 8.4, 8.6 (in part), 8.7.1 for MLT system

¹⁾ Three principle test series were conducted: the Solvo system in FVO and the MLT system in FVO and MST mode.

²⁾ The mean of all the measured parameters was taken. That mean should however be taken over a steady state period and not the full 30sec. Therefore data was logged in 5sec intervals and the data set that was chosen was the one just before the array was moved. This represented steady state.

A2.4.2 Dynamic array operating point tests

The purpose of this test was the assessment of the array losses due to particular inverter operating characteristics.

The measurements were conducted with a hand-held oscilloscope (described in section 5.4). Data was downloaded to the computer via an optical link.

The following data was captured:

- the instantaneous array voltage (data presented in subsection 7.3.1 and 8.3.1)
- the envelope curve of the PWM line-to-line voltage on the inverter output (data in subsection 7.3.3 and 8.3.3)
- the instantaneous array voltage for an increased input capacitance at the inverter input which was connected in parallel to the existing capacitance (data in subsection 7.3.4 and 8.3.4)

This test was done for the Solvo inverter in FVO mode and for the MLT inverter in MST mode.

A2.4.3 Dynamic operating conditions test

TABLE A2.7 Methodology for testing dynamic conditions

	Test, procedure and logging details
<i>Purpose</i> ¹⁾	<ul style="list-style-type: none"> to assess the ability of the systems to deal with dynamic conditions
<i>Apparatus</i>	System: array, Solvo or MLT inverter, GEC three phase motor and pump DAS: interface, power meter, data logger, computer
<i>Conditions</i>	thick isolated clouds were ideal
<i>Procedure</i>	<ul style="list-style-type: none"> if clouds were present then it was a matter of starting the logger at least a few seconds before the shade of the cloud fell on the array; if no clouds were present: <ul style="list-style-type: none"> MLT: disconnected one of the parallel strings of modules and once the system had settled reconnected it; in this way it was possible to generate a step-down and a step-up Solvo: two modules were covered with a sheet of cardboard²⁾
<i>Parameter: Analog</i> <i>Digital</i>	G_{POA} , t_{mod} , I_{arr} , V_{arr} , I_{line} , V_{LN} , P_{inv} , T_{mot} (instantaneous) f_{fund} , S_{mot} (event)
<i>Log interval</i>	1sec ¹⁾
<i>Assumptions</i>	the same settling time for each channel in the data acquisition system
<i>Results in section</i>	7.6 (in part) for the Solvo system 8.6 (in part) for the MLT system

¹⁾ No conclusion on the actual system settling time can be deduced from this test.

²⁾ This particular procedure was not an actual current step but a voltage step. This may certainly model realistic conditions closer.

Appendix A3

SPECIFICATIONS FOR THE DATA ACQUISITION SYSTEMS

A3.1 Transducers and data logger specification sheets

A3.1.1 LI-COR pyranometer LI-200SZ

A pyranometer is an instrument for measuring solar radiation received from a whole hemisphere. It is suitable for measuring global sun plus sky radiation.

Solar radiation varies significantly among regions. Season and time of day are major considerations, but surrounding terrain elevation, man-made obstructions, and surrounding trees can also cause large variations in locations of a small area. Often, the most required measurement is the energy flux density of both direct beam and diffuse sky radiation passing through a horizontal plane of known unit area (i.e. global sun plus sky radiation).

The silicon photodiode has made possible the construction of simple pyranometers of reasonable accuracy where the photodiode is stable. The response of the silicon photodiode sensor (Figure 3) is not ideal, (equal spectral response from 280-2800nm) but does not cause serious error provided the photodiode is used only for solar radiation and not under conditions of altered spectral distribution. **IMPORTANT:** For this reason, we do not recommend its use under artificial lighting or within plant canopies. Also, reflected radiation can be erroneously measured.

The LI-COR pyranometer may be handheld or mounted at any required angle, provided that reflected radiation is not a significant portion of the total. In its most frequent application, the pyranometer sensor is set on a level surface free from any obstruction to either direct or diffuse radiation. The sensor may be most conveniently leveled by using the 2003S Mounting and Leveling Fixture.

SPECIFICATIONS

Calibration: Calibrated against an Eppley Precision Spectral Pyranometer (PSP) under natural daylight conditions. Absolute error under these conditions is $\pm 5\%$ maximum, typically $\pm 3\%$.

Sensitivity: Typically $80 \mu\text{A}$ per 1000 W m^{-2} .

Linearity: Maximum deviation of 1% up to 3000 W m^{-2} .

Stability: $< \pm 2\%$ change over a 1 year period.

Response Time: $10 \mu\text{s}$.

Temperature Dependence: $\pm 0.15\%$ per $^{\circ}\text{C}$ maximum.

Cosine Correction: Cosine corrected up to 80° angle of incidence.

Azimuth: $< \pm 1\%$ error over 360° at 45° elevation.

Tilt: No error induced from orientation.

Detector: High stability silicon photovoltaic detector (blue enhanced).

Sensor Housing: Weatherproof anodized aluminum case with acrylic diffuser and stainless steel hardware.

Size: 2.38 Dia. x 2.54 cm H (0.94" x 1.0").

Weight: 28 g (1 oz.).

Accessories: 2003S Mounting and Leveling Fixture.

Cable Length: 3 meters (10 ft) standard. LI-200SZ-50: 50 ft.

A3.1.2 Temperature sensor LM35D

General Description

The LM35 series are precision integrated-circuit temperature sensors, whose output voltage is linearly proportional to the Celsius (Centigrade) temperature. The LM35 thus has an advantage over linear temperature sensors calibrated in ° Kelvin, as the user is not required to subtract a large constant voltage from its output to obtain convenient Centigrade scaling. The LM35 does not require any external calibration or trimming to provide typical accuracies of $\pm 1/4^\circ\text{C}$ at room temperature and $\pm 3/4^\circ\text{C}$ over a full -55 to $+150^\circ\text{C}$ temperature range. Low cost is assured by trimming and calibration at the wafer level. The LM35's low output impedance, linear output, and precise inherent calibration make interfacing to readout or control circuitry especially easy. It can be used with single power supplies, or with plus and minus supplies. As it draws only $60\ \mu\text{A}$ from its supply, it has very low self-heating, less than 0.1°C in still air. The LM35 is rated to operate over a -55° to $+150^\circ\text{C}$ temperature range, while the LM35C is rated for a -40° to $+110^\circ\text{C}$ range (-10° with improved accuracy). The LM35 series is

available packaged in hermetic TO-46 transistor packages, while the LM35C is also available in the plastic TO-92 transistor package.

Features

- Calibrated directly in ° Celsius (Centigrade)
- Linear + 10.0 mV/°C scale factor
- 0.5°C accuracy guaranteeable (at +25°C)
- Rated for full -55° to $+150^\circ\text{C}$ range
- Suitable for remote applications
- Low cost due to wafer-level trimming
- Operates from 4 to 30 volts
- Less than $60\ \mu\text{A}$ current drain
- Low self-heating, 0.08°C in still air
- Nonlinearity only $\pm 1/4^\circ\text{C}$ typical
- Low impedance output, $0.1\ \Omega$ for 1 mA load

Connection Diagrams

TO-46
Metal Can Package*

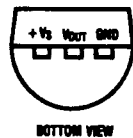


TL/H/5516-1

*Case is connected to negative pin

Order Number LM35H, LM35AH,
LM35CH, LM35CAH or LM35DH
See NS Package Number H03H

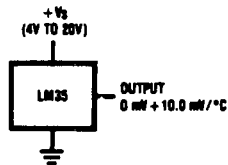
TO-92
Plastic Package



TL/H/5516-2

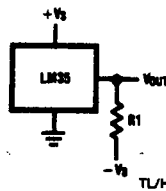
Order Number LM35CZ or LM35DZ
See NS Package Number Z03A

Typical Applications



TL/H/5516-3

FIGURE 1. Basic Centigrade Temperature Sensor ($+2^\circ\text{C}$ to $+150^\circ\text{C}$)



Choose $R_1 = -V_S/50\ \mu\text{A}$

$V_{OUT} = +1,500\ \text{mV}$ at $+150^\circ\text{C}$
 $= +250\ \text{mV}$ at $+25^\circ\text{C}$
 $= -550\ \text{mV}$ at -55°C

TL/H/5516-4

FIGURE 2. Full-Range Centigrade Temperature Sensor

A3.1.3 LEM current probe LA 50-P

Definition-Principle

The "LEM Module LA 50-P" is a current sensor for electronic measuring of currents : DC, CA, IMPL, etc., with galvanic isolation between the primary (high current) and the secondary (electronic) circuit. Based on the principle of compensation of the magnetic field, the LEM sensors supply a measuring current proportional to the primary current.

Electrical Data

Nominal Current I_N	: 50 A rms
Measuring range	: 0 to +/- 70 A (supply voltage + and - 15 V, R. meas. = 100 ohms)
Turn ratio	: 1 : 1000
Measuring currents	: - nom. 50 mA for 50 A - max. 70 mA for 70 A
Accuracy	: +/- 0.5 % of I_N at 25°C including offset current at $I_{prim.} = 0$ max. +/- 0.2 mA
Drift with temperature	: of the offset current between 0° and 70°C typical: +/- 0.35 mA max.: +/- 0.50 mA
Linearity	: 0.1 %
Response time	: better than 1 us
dI/dt accurately followed	: better than 50 A/us
Test voltage	: between primary and secondary circuit : 2 kV rms./50 Hz/1 mn.

Secondary circuit

Connection	: on 3 pins, section 0.63 x 0.56 mm
Internal resistance	: 90 ohm at 70°C (internal voltage drop 4.5 V/50 A primary)
Supply voltage	: + and - 15 V (+/- 5 %)
Current drain	: 10 mA (no-load current) + I_m (measuring current)

General Data

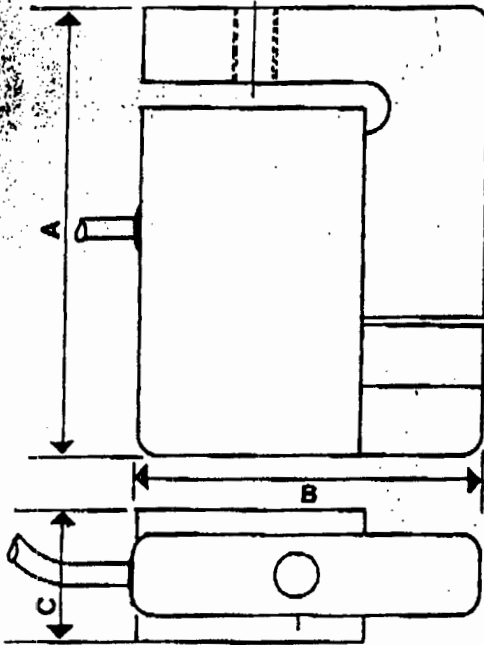
Execution	: insulated plastic injected case
Mounting	: mounting on printed circuit by 3 pins hole size 0.9 mm
Dimensions	: see drawings overleaf - Weight : 25 g
Operating temperature	: 0°C to + 70°C
Storage temperature	: - 25°C to + 85°C
"In-Out" signal sense	: to obtain a positive measuring current on terminal M, the primary current has to flow in the direction of the arrow on the LEM Module

Particularity

: minimum measuring resistance 100 ohms

A3.1.4 Loadcell UBG 10

DIMENSIONAL SPECIFICATIONS



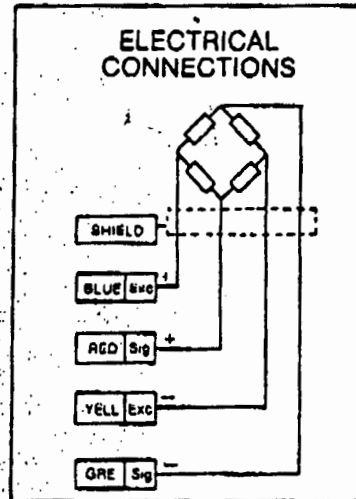
ALL DIMENSIONS
IN mm

CAP. (kg)	A	B	C
5, 10, 20	65	60	17.5

M8

SPECIFICATIONS

		UB-8
RATED OUTPUT (NOMINAL)	mV/V	3
TEMPERATURE EFFECT ON RATED OUTPUT/°C	% RO	0.003
TEMPERATURE EFFECT ON ZERO SIGNAL/°C	% RO	0.003
COMBINED ERROR: LINEARITY + HYSTERESIS	% RO	0.05
REPEATABILITY	% RO	0.02
CREEP AFTER 20 MIN AT 23°C	% RO	0.03
INPUT RESISTANCE ±1%	Ω	350
OUTPUT RESISTANCE	Ω	350
INSULATION RESISTANCE AT 50 VDC	MΩ	1k
RECOMMENDED EXCITATION AC/DC	V	8
MAXIMUM EXCITATION AC/DC	V	15
SAFE OVERLOAD	% RO	120
ULTIMATE OVERLOAD	% RO	180
BREAKING LOAD	% RO	300
CABLE	m	3



ORDERING INFORMATION

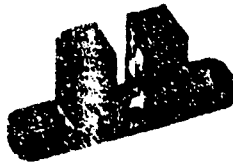
Loadcell Type UB / 8 / 20
 Accuracy Class _____
 Capacity in kg _____

from:

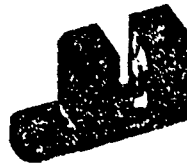
A3.1.5 Optical switch TCST 2000



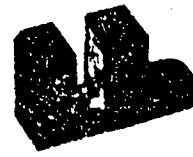
Package 1



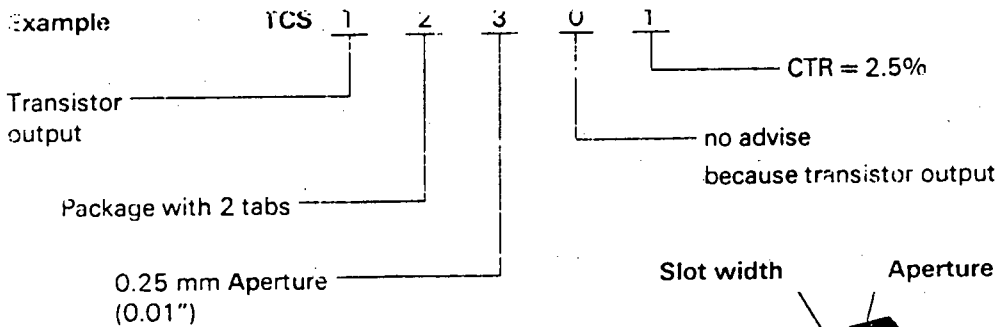
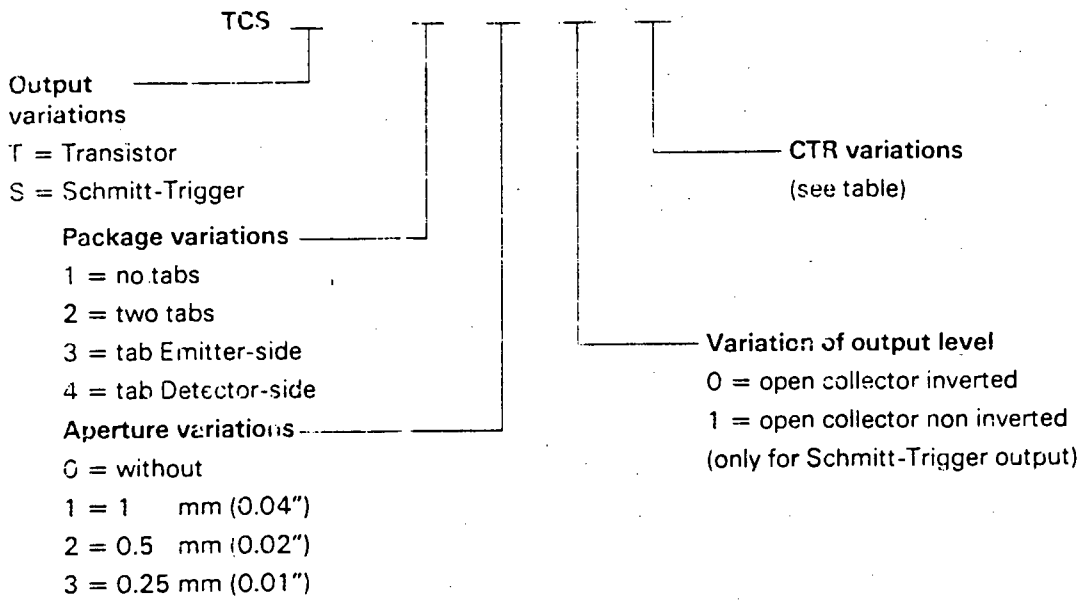
Package 2



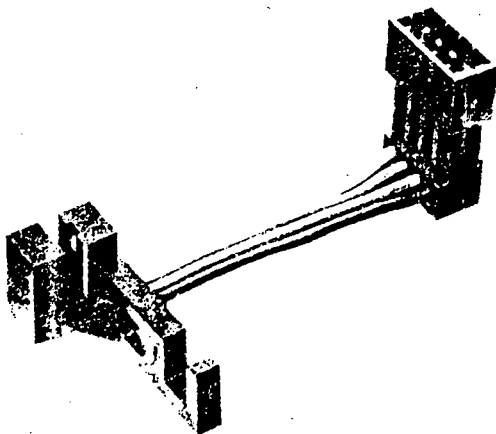
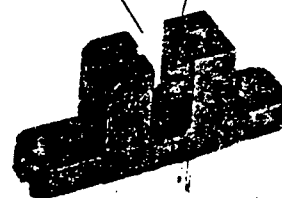
Package 3



Package 4



Slot width Aperture



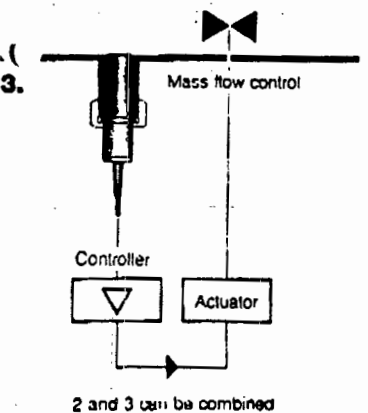
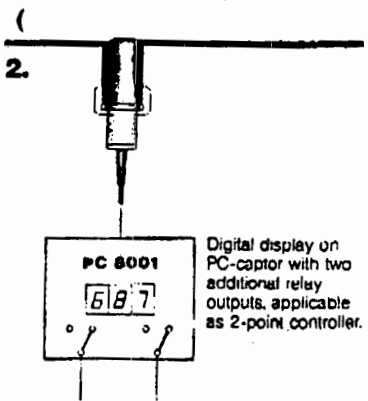
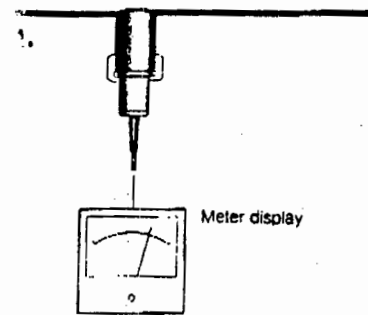
We have the facilities to provide your special custom design, included wires and connectors

A3.1.6 Flow-captor Type 4113.30

flow-captor

Application examples:

Compact Flow Meter
Type 4113.30



Electrical Data:

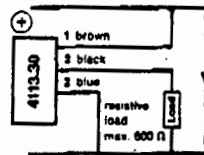
Voltage supply	24 V DC	Current consumption max. 100 mA
Output current	4 to 20 mA	
Resistive load	0-600 Ohm	

Measurement range adjustment:

The two potentiometers protected by covering hubs, allow for the zero balancing and the adjustment of the measuring range by means of a small screwdriver. A color changing LED signalizes flow within the adjusted measuring range (green) or overflow (red).

Connection diagram

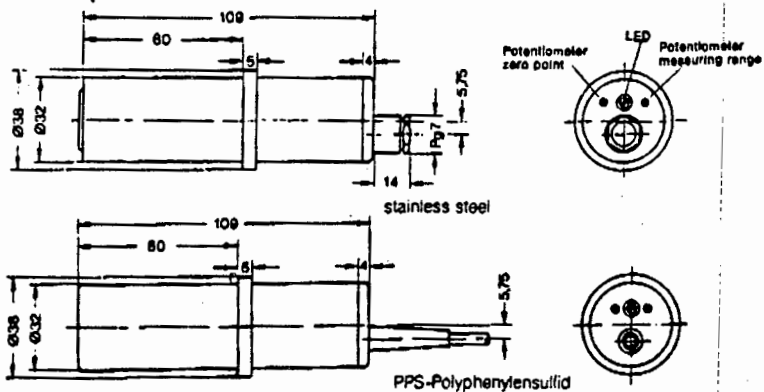
4-20 mA current output



Mechanical Data:

Material	Sensorhead	Housing
	Ceramic KER 221	stainless steel WN 4305 PPS-Polyphenylensulfid
Operating pressure	max. 30 bar, attention! not applicable under vacuum conditions	
Medium temperature range	-10° C to +80° C (14° F to 175° F)	
Ambient temperature	-10° C to +60° C (14° F to 160° F)	
Union fitting	R 1 1/4" SW 50 DIN 259 ISO 328	
Electrical connection	2 m moulded difflex cable	
Protection standard	IP 65	
Weight	plastic approx. 230 g, stainless steel approx. 410 g	

Dimensions in mm



This flow-captor is also available in 25 mm Ø housing. (Type 4111.30)

weber

Sensortechnik GmbH · D-2201 Kollmar · Strohdiech 32 · Telefon: 0 41 28 / 591 · Telex: 218 326

A3.1.7 PSM water meter Size 3

Technical Specifications

Classification		Size 3	Size 5	Size 7	
Nominal Bore	mm	15	20	25	32
PERFORMANCE					
Starts to register at about	ℓ/h	4	4	6	14
Minimum accurate registration ±2%	ℓ/h	24	24	32	68
Flows at 30 kPa pressure drop	kℓ/h	2	3	4,1	5,8
Flows at 100 kPa pressure drop	kℓ/h	3,7	5,6	7,5	11
Maximum recommended continuous flow	kℓ/h	2,8	3	4,6	6,8
Test pressure	MPa	2	2	2	2
Maximum water temperature	°C	50	50	50	50
Counter resets to zero at	kℓ	9 999	9 999	99 999	99 999

The group of white numbers in the counter (register) represent kilolitres and are used for periodic meter reading. The orange numbers represent litres and are intended to be used when checking the meter accuracy against a calibrated measure.

NET MASS

Meter only	kg	1	1,3	2,4	3,6
Meter with connectors	kg	1,2	1,7	3	4,6

DIMENSIONS

Length over body	A	mm	114	165	198	198
	B	mm	44	44	57	60
Length over connectors	C	mm	200	267	311	327
Meter body screwed ISO-R7 thread		mm	20	25	32	40
Connectors screwed ISO-R7 thread		mm	15	20	25	32

MATERIALS

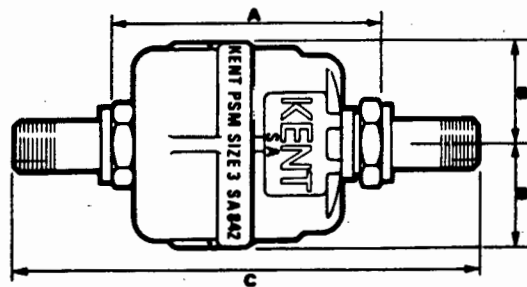
Body – brass SABS 200 1972 Code 9A.
 Chamber – graphited styrene
 Counter – diakon
 Number wheels – delrin
 Gear wheels – nylon
 Spindles – nickel

The PSM, designed for the measurement of potable water, has a specially developed thermoplastic working chamber to ensure an exceptionally long working life. It is also highly resistant to chemically aggressive water whilst still retaining its high accuracy and reliability.

Standard Features

Semi-positive rotary piston of latest design which commences to register at extremely low flows and is accurate within plus or minus 2% throughout a wide range.

Counters and working chambers interchangeable between 15 mm and 20 mm meters.



Optional Features

Disc-type non-return, valve.

Normally supplied with connectors for iron pipe comprising union nuts and tailpieces screwed BSP.

Connectors for copper pipe by means of flared-type reducing pillar cock adaptor can also be supplied.

Approved in terms of Section 21 of the Trade Metrology Act and Regulations.

A3.1.8 Pressure transmitter Model 891.14.525



TRONIC LINE

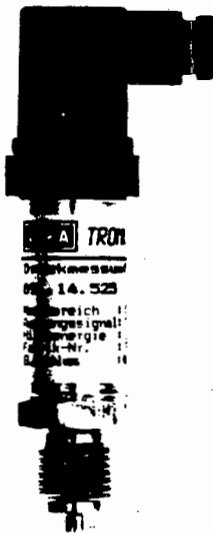
Application

- Measurement of positive and negative pressure
- of liquid and gaseous media
- in fluid power and pneumatic systems
- process plant and machine control
- General pressure instrumentation

Pressure Transmitter · Model 891.14.525

Accuracy 0.5%

Piezoresistive



FEATURES

Pressure transmitter with piezoresistive sensor and temperature compensation.
Stainless steel body with padded electronics

Output signal rising proportional with rising pressure applied

STANDARD FEATURES

Wetted parts of stainless steel 1.4571

Body of stainless steel

Pressure connection G 1/2 A seating per DIN 16 288

Electric outlet with L-plug per DIN 43 650

Internal transmitting liquid silicon oil

Gauge pressure measurement

Output signal 4 ... 20 mA
2-wire system

RANGES

0 ... 400 mbar	0 ... 4 bar
0 ... 600 mbar	0 ... 6 bar
0 ... 1 bar	0 ... 10 bar
0 ... 1,6 bar	0 ... 16 bar
0 ... 2.5 bar	0 ... 25 bar

Other pressure ranges feasible

OPTIONAL EXTRAS

Other materials upon request, see also Wika S.A.P.-System

Other connections feasible

Outlet 1.5 m shielded cable
Outlet 5-pin jack

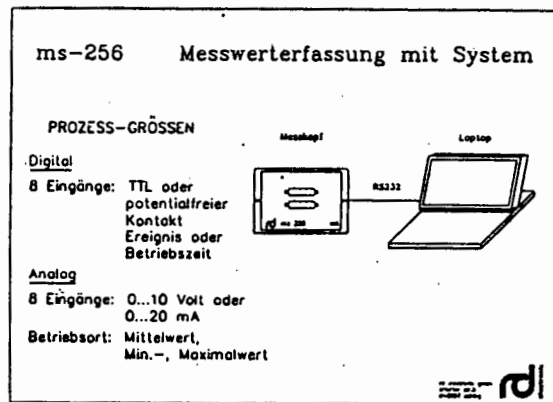
Other liquids upon request

Absolute pressure measurement

3-wire system 0 ... 20 mA
0 ... 5 V
0 ... 10 V

MS-256 Messwerterfassungssystem

Das System MS256 ist ein Mikroprozessor gesteuertes Meßsystem, das für den Einsatz in der Langzeitsmesstechnik entwickelt wurde. Es besteht aus modularen Komponenten, die autonom vor Ort Meßdaten erfassen können.



In der Abbildung sind die Komponenten eines einzelnen Messkopfes dargestellt. Jeder Messkopf ist mit einem Netzteil und einem Akku-Puffer ausgerüstet. Ein Messbetrieb über 24 Stunden bei ausfallender Versorgungsspannung kann garantiert werden. Der Datenspeicher, die Konfiguration und die laufende Zeit/Datum, werden über eine Lithiumbatterie für 5 Jahre versorgt

Analog

Jeder Meßkopf des Systems MS256 hat acht analoge Eingangskanäle für Strom- oder Spannungsmessung. Die Meßrate des A/D-Wandlers beträgt 700 Messungen/Sekunde/Kanal. Alle Meßwerte eines Abspeicher Intervalls können zu einem Mittelwert verdichtet werden. Durch dieses Verfahren wird eine Auflösung von 16 Bit erzielt.

Jeder Analogeingang kann wahlweise eine der folgenden Aktivierungen einnehmen:

Mittelwert	(2Byte)
Mittelwert & Minimum	(4Byte)
Mittelwert & Maximum	(4Byte)
Mittelwert & Minimum & Maximum	(6Byte)
Momentanwert	(2Byte)

Der in Klammern angegebene Wert zeigt den benötigten Speicherbedarf pro Intervall und Kanal. Eine gemischte Belegung aller Kanäle ist jederzeit möglich.

Digital

Die acht digitalen Eingangskanäle werden für die Messung von Betriebszeiten oder Ereignissen eingesetzt. Jeder Digital-eingang kann dabei wie folgt aktiviert werden:

Betriebszeit	(2Byte)
Ereignis	(2Byte)

Auch hier beziehen sich die Werte in den Klammern auf den Speicherplatzbedarf pro Intervall und Kanal. Die digitalen Eingänge sind für den Anschluß von TTL-Signalen oder nicht entprellten Einzelschaltkontakten eingerichtet. Werden Zählerstände mit mehr als 16-Bit (65535) benötigt, so können alle Digitaleingänge z.B. zu 32-Bit Zählern kaskadiert werden. Eine Anzeige des Schaltzustandes ist jederzeit möglich (H=offen / L=geschlossen). Die Entprellung der Eingänge kann auf 3Hz...3KHz erfolgen. Die maximale Zählfrequenz beträgt 2 MHz.

A3.2 Interface circuits and description

The purpose of the interface is to process the signals from the transducers to meet the signal input requirements of the data acquisition system (DAS). As the DAS has an instantaneous sampling frequency of 1Hz, signals from the transducers should be processed to near DC quantities. Additionally the signals to the logger must be limited to the zero to 10V range.

This section discusses the design of the interface signal conditioning circuits, their transfer functions and their settling time as for the parameters listed in Table 5.1 (except the inverter current, frequency, voltage and power - section A3.3). Additional information is supplied where necessary (like present settings, trimming procedure hints and where applicable possible improvements).

Horowitz and Hill (1989) was used as the main reference for the design of the electronic circuitry.

The settling time (t_s) is the time that it takes the output to settle to within 1% of its final value after a change in input signal. It is calculated as follows:

$$V(t) = V_{\text{final}} \times (1 - e^{-t/RC})$$

$$0.99 = 1 - e^{-t/RC}$$

$$t = 4.6 \times RC$$

When a few RC time constants are in a circuit then the overall settling time is calculated as follows:

$$t_s = 4.6 \times \sqrt{\tau_1^2 + \tau_2^2 + \dots + \tau_n^2}$$

The settling time is important as it indicates the time required for DAS to settle to steady state values after a change of input to the system under test. The settling time for instance should guide the logging interval. Under dynamic conditions the parameters can be brought to the same time instance with the use of software filters. This is not required here since the main emphasis is on steady state operation. Dynamic conditions are only investigated in terms of system stability.

App. A3.4 contains the introductory data sheet for each IC mentioned in this section.

The circuit diagrams use the following conventions: The transducers are shown on the left. Each IC is numbered with ICx where 'x' is a particular number. Where appropriate the output of an IC is named with Sx (signal number). The gain is usually stated above the component with Gx. Px are multi-turn potentiometers. A resistor value like 12k + 5k~ means a fixed resistor of 12k Ω in series with a 5k Ω potentiometer. R_i is an input

resistor to an op-amp and R_f is a feedback resistor of an op-amp. The roll-off and cutoff frequency refer to the -3dB point. RC is the time-constant and is referred to as τ . V_{out} is the output signal which is sent to the data logger.

A3.2.1 Irradiance

The LI-COR pyranometer requires a termination resistor whose value will result in a voltage of less than 10mV at 1000W/m². A resistor value that is too large can result in a non-linear response. A 147 Ω resistor or less is recommended in the specifications.

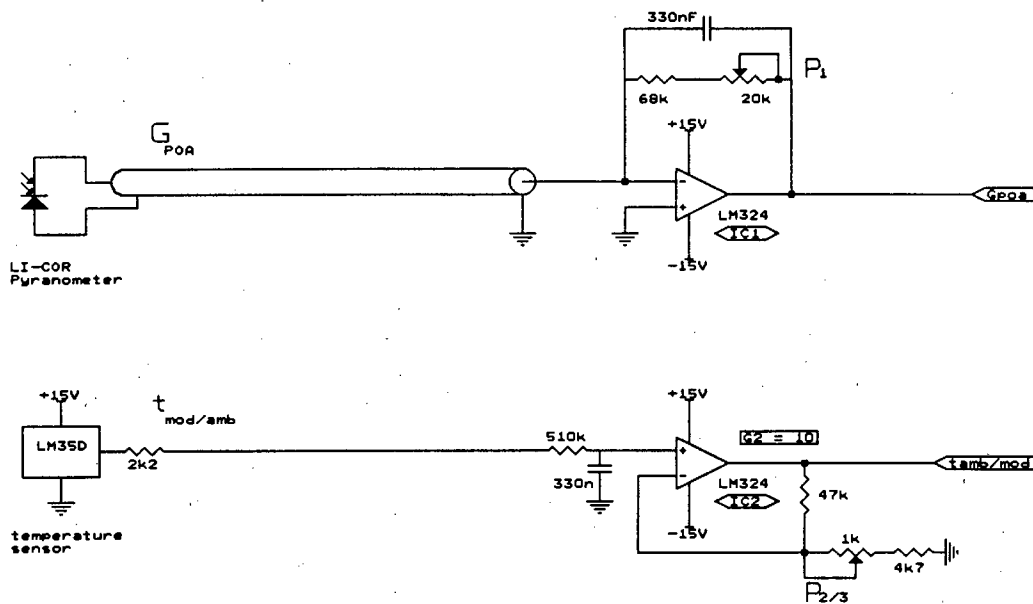


FIGURE A3.1 Circuit diagram of the irradiance and temperature parameters

It was decided to choose a trans-impedance op-amp configuration as shown in Figure A3.1. This results in an input impedance of 0.27 Ω meaning the LI-COR is virtually operating at short-circuit.

$$Z_{in} = \frac{R_f}{(1 + A)}$$

where A is the open loop gain of the op-amp (here 110dB).

The LI-Cor is calibrated at 94 μ A/1000W/m². A maximum irradiance level of 1250W/m² will result in a photocurrent of 117.5 μ A. A feedback resistor of 85k Ω will set the full-scale signal to 10V. The input bias current of the LM324 is typically 45nA and the input offset voltage is typically 2mV. At 200W/m² (which is the lowest value of interest) the LI-COR generates a photocurrent of 19 μ A and the op-amp output is about 1.6V. Neither the bias current nor the offset voltage will cause a serious error (0.24% and

0.01% respectively).

The roll-off frequency of the LPF is 5.7Hz with a settling time of 130msec. The output is adjusted with P_1 .

The transfer function is:

$$G_{\text{POA}} = 125 \times i_{\text{photo}} \times R_f \quad [\text{W/m}^2]$$

A3.2.2 Temperature

The LM35D produces an output of 10mV/°C. It is amplified by ten with a non-inverting op-amp configuration (Figure A3.1). The gain is set with P_2 and P_3 for the ambient and module temperature circuit respectively.

The 2k2Ω resistor is added to decouple the capacitive load of the long cable (about 10m) else a high frequency ripple occurs on the output of the LM35D. The $f_{-3\text{dB}}$ point of the LPF is at 0.9Hz with t_s being 0.77sec.

The transfer function is:

$$t_{\text{amb/mod}} = G_2 \times V_{\text{out}} \quad [^\circ\text{C}]$$

A3.2.3 Array voltage

The array voltage is processed by IC1 and IC2 in Figure A3.2. IC1 is a differential op-amp which has a gain of 1/30. Care has been taken to match the resistors although the amount of common-mode signal is small. The inverting op-amp configuration (IC2) is used to fine-tune the gain to 1/30 with P_1 , and to roll off the signal at 0.48Hz with $t_s = 1.52\text{sec}$.

The LT1097 is used for both op-amp's. It has a very low input offset voltage (50μV max) and bias current (250pA max). The array voltage is usually fixed at either 90V or 180V and is therefore scaled to 3V or 6V in Figure A3.2 respectively. The offsets are consequently negligible and no trimming was required.

Transfer Function:

$$V_{\text{arr}} = V_{\text{out}} \div (G_1 \times G_2) \quad [\text{V}]$$

A3.2.4 Array current

The voltage drop across the shunt is fed into a differential op-amp (IC3) with a gain of 4.7. The output is sent into a two pole Butterworth LPF with $f_{-3dB} = 0.48\text{Hz}$ and $t_s = 1.78\text{sec}$ which removes the ripple caused by the switching of the inverter or converter. The output of IC4 is sent to two non-inverting op-amps with different gain. The one branch has an overall gain of ten and is used for the array current when the array is in the parallel configuration (higher array current: Miltek and MLT system). The other branch is used when the array is in the series configuration (Solvo system). Only the gain of IC6 can be adjusted. The output of IC5 has to have a calibration factor.

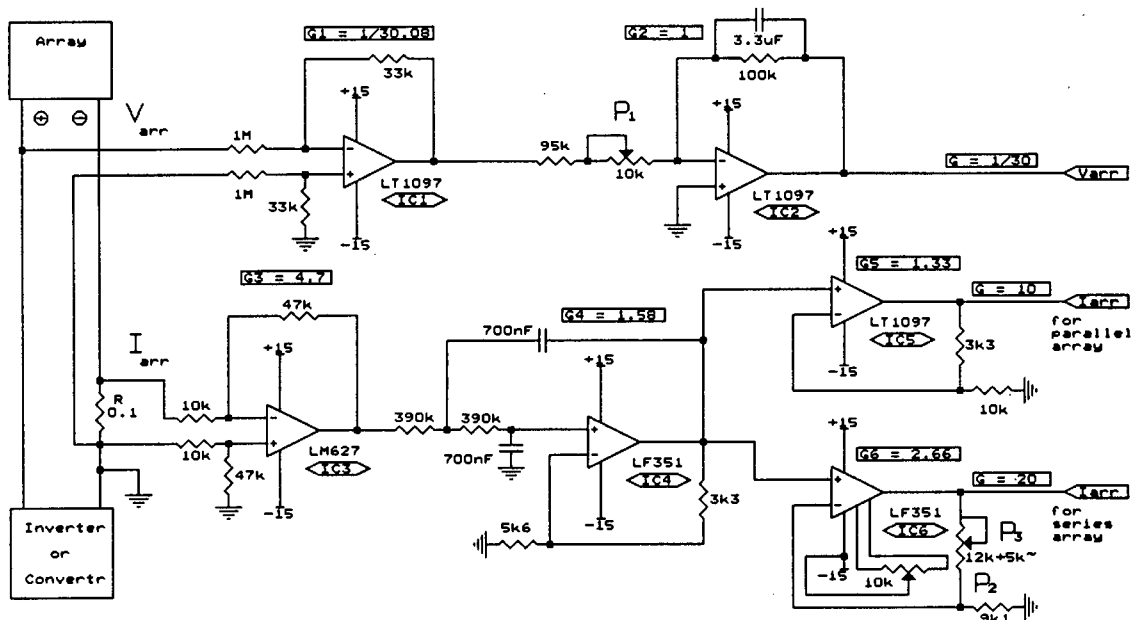


FIGURE A3.2 Circuit diagram of array voltage and array current parameter

The IC3 op-amp uses an LM627 which has a gain-bandwidth product in excess of 10MHz and a negligible input offset voltage. It does however have an input offset current of 50nA_{max} . This becomes problematic if the op-amp sees a large input resistance on one op-amp input as it will result in a voltage drop across the resistor. A LM627 was used for IC4 but exactly that problem occurred. Instead of adding a resistor of similar value to the other input (to reduce the offset current) a LF351 which is also a wide-band op-amp was used. It does not have the precision of the LM627 but its input bias current is a factor 1000 lower. The offset voltage in the array current measurement branch for the parallel array configuration cannot be trimmed to zero as no trimming potentiometers were added. However the maximum recorded offset was 0.5mV. The series array current measurement can be trimmed to zero with potentiometer P₂.

Transfer Function:

$$I_{\text{arr}} = V_{\text{out}} \div (R_{\text{shunt}} \times G_{\text{total}}) \text{ [A]}$$

A3.2.5 Converter voltage

The converter voltage (Figure A3.3) has in principle the same circuit as the array voltage except that it uses a two pole Chebychev LPF in an inverting op-amp configuration. The cutoff frequency is at 0.48Hz and t_s is 1.76sec.

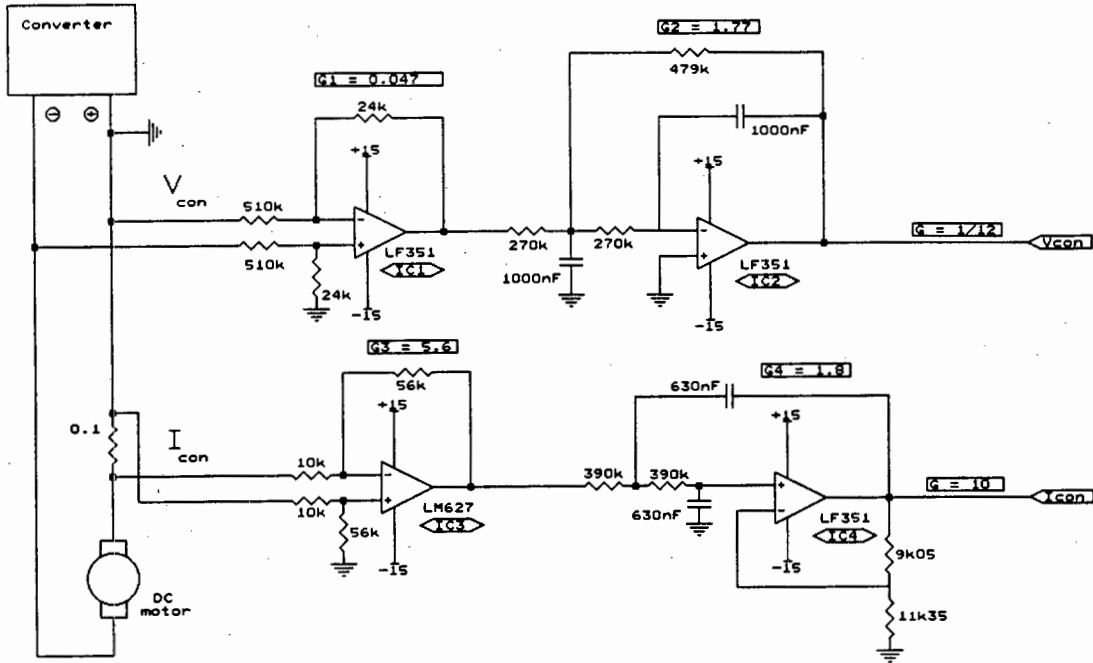


FIGURE A3.3 Circuit diagram for the converter voltage and converter current parameter

No provision has been added to trim the input offset voltage zero. The maximum recorded offset voltage was -3.4mV.

The transfer function is:

$$V_{con} = V_{out} + (G_1 \times G_2) [V]$$

A3.2.6 Converter current

The voltage drop across the shunt is fed into a differential amplifier with a gain of 5.6 (Figure A3.3). The LPF is a Chebychev type filter with a cutoff frequency at 0.53Hz and a t_s of 1.6sec. The overall gain is set to ten.

Note that the shunt is in the positive line to the motor. During measurements on the Miltek system the positive lead is tied to ground and the array current is also

measured in the positive lead to the converter (the converter switches the negative lead to the motor, see Figure 3.2 in main text).

The transfer function is:

$$I_{\text{con}} = V_{\text{out}} \div (R_{\text{shunt}} \times G_3 \times G_4) \text{ [A]}$$

A3.2.7 Motor torque

The circuit for the torque measurement is shown in Figure A3.4. The sensitivity of the loadcell is 3mV/V. With a 10V_{DC} excitation this will result in a 30mV full-scale signal riding on about 5V. The common-mode rejection requirements of the op-amp has to be 90dB if an error of 0.5% is tolerated ($20 \log (5000/[0.005 \times 30])$). The LT1097 has a CMRR of minimum 115dB and maintains it above 90dB for frequencies up to 5kHz. The resistors have been well matched. IC2 provides for scaling, zero adjust and offset adjust. Its output is instantaneous and can be used for a fast sampling device. IC3 is a unity gain amplifier with a two pole Sallen and Key LPF which has a $f_{-3\text{dB}}$ point at 0.25Hz with τ being equal to 640msec. This is a long time-constant and to reach 1% of its final value (from a step input) requires $4.6 \times \tau$ seconds which is 2.9sec.

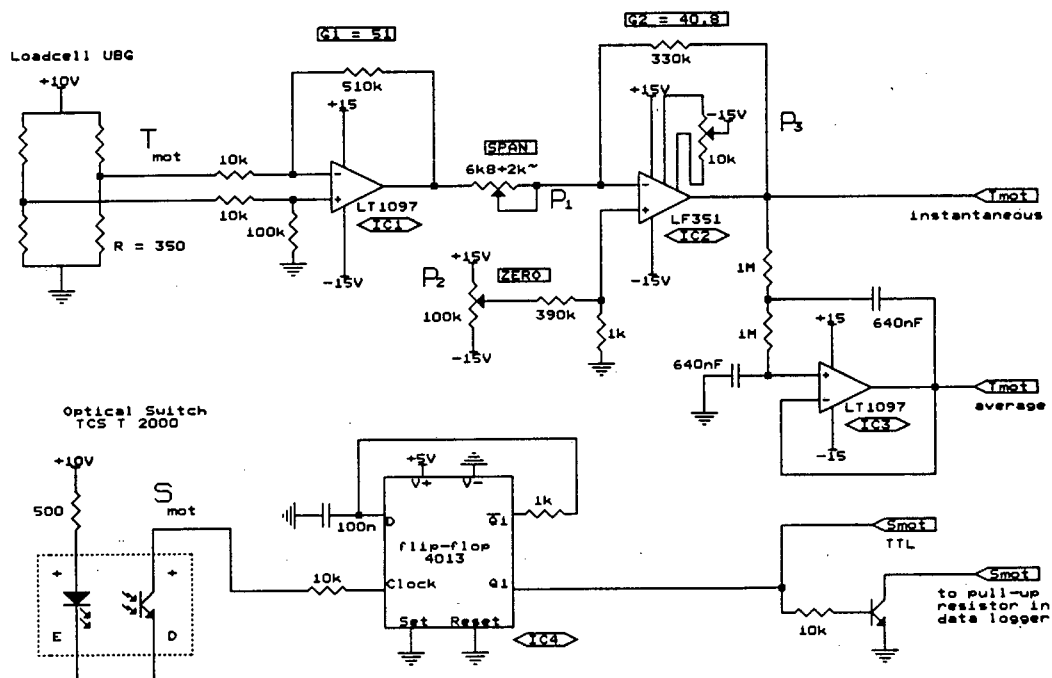


FIGURE A3.4 Circuit diagram for the motor torque and motor speed parameters

The motor torque is calculated by multiplying the force F on an arm of length L . The gain was adjusted so that 1kg would result in 2V output. Consequently the transfer function is:

$$\begin{aligned}
 T_{\text{mot}} &= F \times L \\
 &= \text{mass} \times g \times \\
 &\quad 0.25\text{m} \\
 &= 2.45 \times \text{mass} \\
 &= 1.225 V_{\text{out}} [\text{N.m}]
 \end{aligned}$$

A3.2.8 Motor speed

An optical switch is used to count the revolutions per log-interval (Figure A3.4). A disc which is mounted on the motor pulley has eight flags (or in some cases two or three flags) to interrupt the light barrier. At very high motor speeds (larger than 1310rpm) the interruption frequency of the light barrier exceeds 175Hz (data logger maximum). A divide by two circuit is therefore added. The flip-flop halves the frequency from the optical switch.

The output of the flip-flop drives the base of a transistor. The open collector is fed into the data logger where it is pulled up to 5V via a 5k6Ω resistor when no base signal is present.

The transfer function below uses the variable count C as the one recorded by the data logger. The number of flags F and the log-interval i relate C to the motor speed in units of rpm.

The transfer function is:

$$S_{\text{mot}} = 2 \times C \div (T \times i) [\text{rev/min}]$$

A3.2.9 Flowrate

The flow-captor is directly connected to the data logger as can be seen in Figure A3.5. The flow-captor allows for zero and span adjust on the device itself. The flowrate can be calculated from the flow speed but it is far more accurate to calibrate the flowrate with a bucket of known volume.

A3.2.10 Static and pressure head

The pressure transmitter is directly connected to the data logger. Due to its large pressure range it is not the most suitable to measure a pressure of half a meter.

Transfer Function:

$$Pr = 2 \times (V_{\text{out}} - 2) [\text{bar}]$$

The depth probe is used to measure the water level in the borehole. It has markings on the cable indicating the depth.

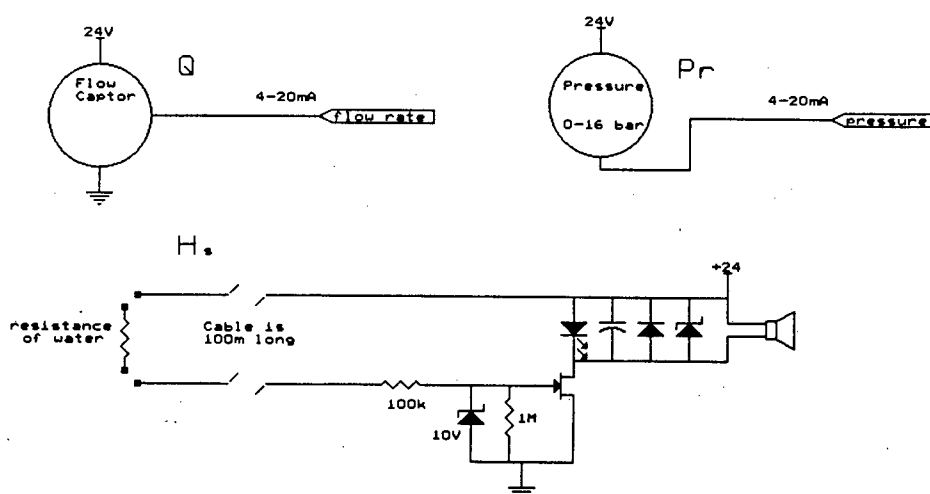


FIGURE A3.5 Circuit diagram for the flowrate, pressure and static head parameter

A FET is used to activate an LED or a speaker when the probe makes contact with the water. The resistance of the water provides a gate drive signal to the FET.

A3.2.11 Power Supply

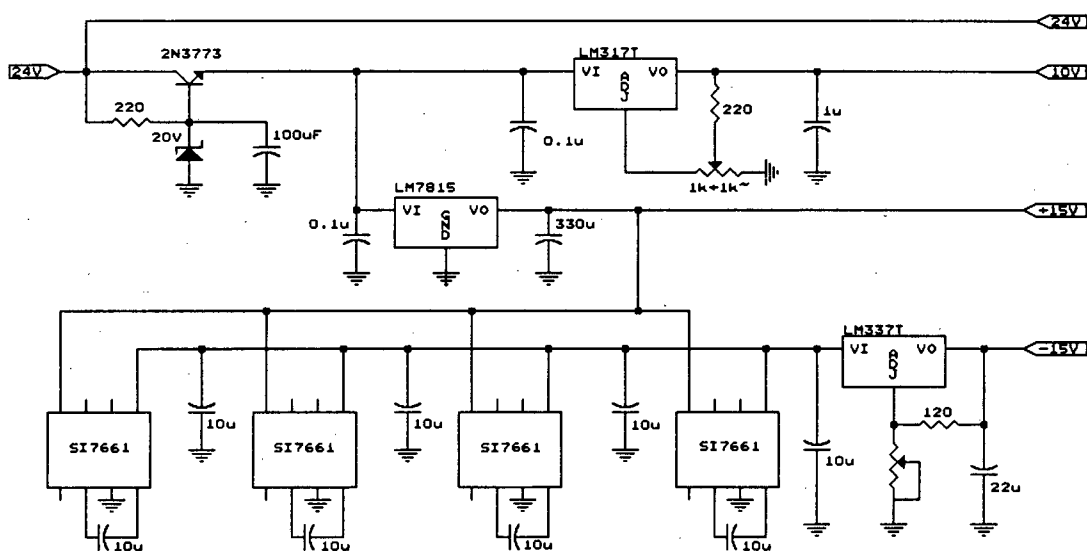


FIGURE A3.6 Circuit diagram of the interface power supply

The power supply must provide power to the transducers and the interface. Most transducers only require a single voltage supply (loadcell = 10V; flow-captor = 24V). As some signals can be very small (for example G_{POA} in the morning and afternoon) it is quite appropriate to use a split supply to avoid non-linearities.

Power is obtained from two batteries in series, that is 24V. That supplies the flow captor, the pressure transmitter and the depth probe directly. The battery voltage is fed to a active zener clamp which reduces the voltage to 20V plus a diode drop. This was done because a few regulators were having to dissipate a substantial amount of power. The 20V is fed to an adjustable regulator (set to 10V for the loadcell and the optical switch) and to a 15V regulator (LM7815). Minus 15V are generated from the +15V by means of voltage converters (Si7661). Four of these were used in order to provide the current that was required. The negative voltage is regulated with an adjustable regulator to generate about -11V.

A3.3 Power meter circuits and description

The power meter is a stand-alone unit which converts the current and the voltage to rms DC quantities. The inverter frequency is derived from the current and the active power is derived from the instantaneous multiplication of the current and the voltage. The device has its own power supply and requires a 24V power source. Figure 3.7 shows the general layout of the power meter with respect to circuit distribution on the printed circuit boards (PCB).

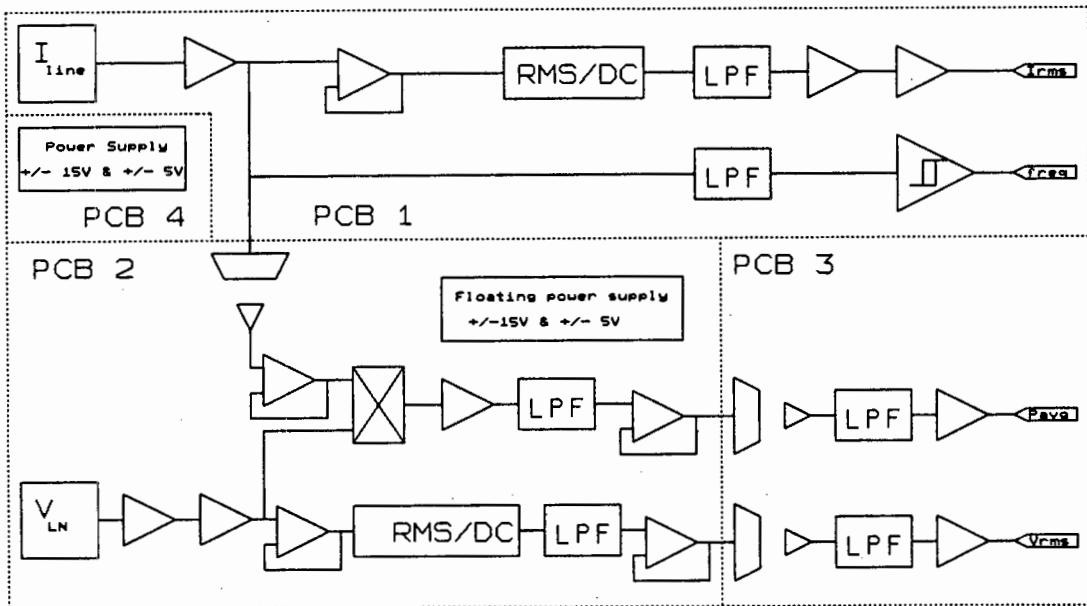


FIGURE A3.7 Block-diagram of the PCB layout of the power meter

The distribution is as follows:

- PCB1 contains the line current and the frequency processing circuitry.
- PCB2 consists of the voltage and the multiplication circuitry. Signals on this PCB are floating with respect to signal ground.
- PCB3 contains the circuitry that couples the floating voltage and power reference signals to the signal ground side.
- PCB4 contains the power supply for the power meter.

What follows is an explanation of the circuitry with additional information on the choice of components, the transfer functions and the settling time of the parameters. If applicable additional information is supplied.

Refer to the introductory paragraphs of section A3.2 for information on conventions.

A3.3.1 Inverter current

The LEM module (bandwidth: DC to 100kHz) generates a proportional current (1:1000) for the primary current and returns it through its ground lead as shown in Figure A3.8. A measurement resistor (R_m) converts this current to a voltage. Accuracy is increased by increasing the number of turns through the LEM provided one does not exceed 50 A (that is number of loops times line current ≤ 50) and provided there is more than 60mA available from the power supply to drive the LEM. The loops through the LEM and the size of the measurement resistor (not less than 100 Ω) must be chosen such that the maximum rms voltage at S_1 is 2V.

IC1 is a unity gain inverting op-amp, the LT1097 (low input offset voltage, 700kHz bandwidth). The non-inverting input can be tuned at P_6 to null the LEM offset current (due to drift caused by temperature variations) of up to 350 μ A and maximum 500 μ A. This current would be converted to a voltage at the measurement resistor and would result in an undesired voltage offset. The output of IC1 is distributed for multiplication, RMS to DC conversion and frequency measurement.

IC2 (LT1097) is configured as a voltage follower and acts as a buffer into the RMS to DC converter as it has a fairly low input impedance.

IC3 is an RMS to DC converter, the AD637 (high accuracy, maximum nonlinearity at $2V_{rms}$ is 0.04%, 3dB bandwidth at $2V_{rms}$ is 8MHz). Depending on the frequency range of the signal, an averaging capacitor is chosen. The fundamental frequency varies from 6 to 85 Hz. Highest accuracy is required in the 40Hz to 85Hz range. When choosing an averaging capacitor (Kitchin & Counts 1986) there is a trade-off between the averaging error and settling time. Presently a 680nF averaging capacitor (C_{av}) has been selected. All the higher harmonics that are part of the current spectrum will be converted with negligible DC error. The peak ripple (or AC error) can be reduced by

post filtering. A one pole filter at the output has been selected with C_2 equal to $2.2\mu\text{F}$ and R equal to $24\text{k}\Omega$. Error and settling time can be read off from a graph in Kitchin and Counts (1986: Figure 24). The scale factor of the AD637 can be trimmed but is internally laser trimmed to $2V_{\text{rms}}$. There is consequently no need for scale factor adjustment in this application as the signal processing pre-AD637 has been designed for $2V_{\text{rms}}$ maximum input signal. There is however provision for this potentiometer. P_2 (50k) trims the output offset voltage to zero.

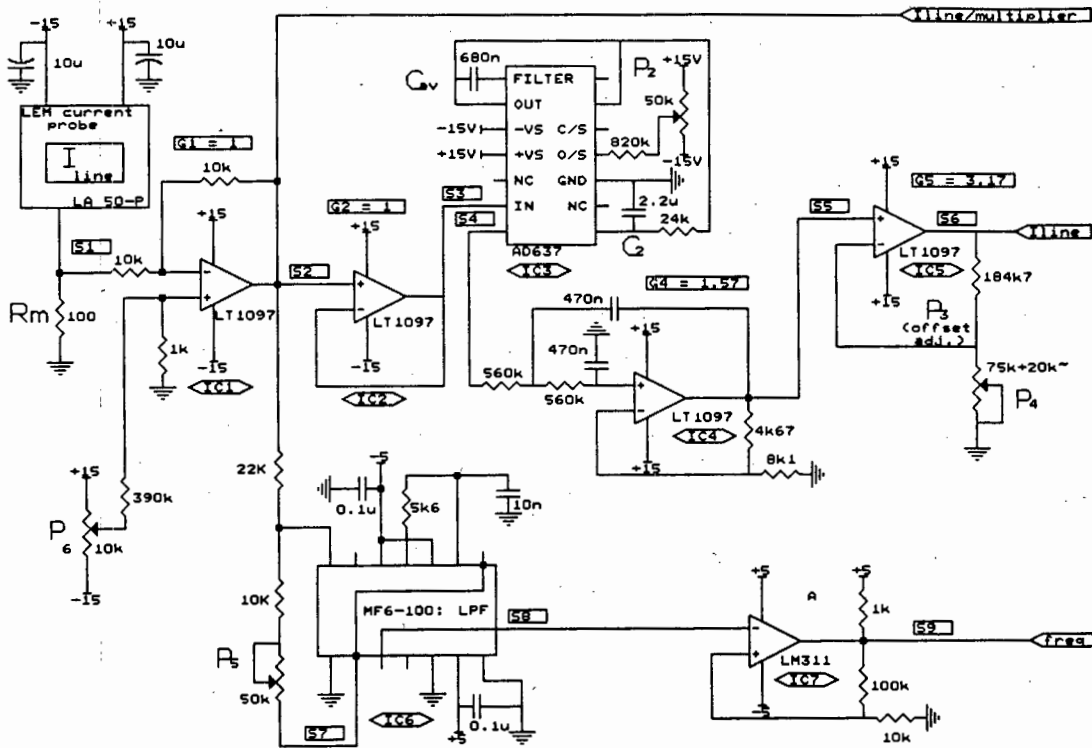


FIGURE A3.8 Circuit diagram of the inverter current and the frequency parameter

IC4 (LT1097) is an active two pole Butterworth LPF (Gain = 1.57, $f_{-3\text{dB}} = 0.604\text{Hz}$, $\tau = \sqrt{(RC^2+RC^2)} = 372\text{ms}$) to smooth any ripple that may remain on the signal from the AD637.

IC5 is a gain stage which is adjusted with P_4 . Due to the low offset op-amp, P_3 has been removed (Offset trimming is provided on the PCB but is only compatible to LF351 pin configurations {Pin 1 & 5 for offset trim}).

The transfer function is as follows:

$$I_{\text{line}} = 1000 \times V_{\text{out}} \div (N \times R_m \times G_1 \times G_4 \times G_5) [A_{\text{rms}}]$$

where V_{out} is the output signal at S_6 , N are the number of turns through the LEM probe, R_m is the measurement resistor that converts the current out of the LEM probe and G_x are the respective gain stages.

The settling time (t_s) has to be calculated for the whole I_{line} circuit. Delays occur only at IC3 and IC4.

$$t_s = 4.6 \times \sqrt{(0.68 \times 0.025)^2 + (2.2 \times 0.025)^2 + 2 \times (0.47 \times 0.56)^2} = 1.73 \text{ sec}$$

where the first value in brackets is always the capacitor in μF and the second value is the resistor in $\text{M}\Omega$. The AD637 has an internal $1\text{k}\Omega$ resistor in series with the $24\text{k}\Omega$ external resistor.

A3.3.2 Inverter frequency

The circuit which processes the fundamental frequency is also shown in Figure A3.8. IC6 (MF6-100) is a six pole switched capacitor lowpass filter with two on-board op-amps where one is used to scale the voltage to between 4V to 5V using P_s . The cutoff frequency is set to 105Hz (clock frequency = $1/1.69RC = 10.5\text{kHz}$) with an RC network on the Schmitt trigger input to retrieve the fundamental frequency.

IC7 is a comparator for zero-crossing detection. The resulting square wave (0V or 5V) has the same frequency as the fundamental frequency and can be logged by a digital channel that has a counter. The threshold voltage V_{thresh} is set to 0.45V (that is $V_{\text{thresh}} = [R_i / [R_i + R_f]] \times 5\text{V} = [10\text{k} / [10\text{k} + 100\text{k}]] \times 5\text{V} = 0.45\text{V}$). Hysteresis is determined by the resistor divider ratio which is one to eleven. It can be increased by decreasing the size of the feedback resistor. This could be required in cases where the switching frequency has a low value since the harmonics will then appear closer to the fundamental frequency resulting in a ripple on the current waveform which can cause multiple triggering. However it can be expected that the six pole filter will remove those harmonics.

The transfer function is:

$$f_{\text{fund}} = \text{count} \div \text{log-interval [Hz]}$$

A3.3.3 Inverter voltage

The inverter voltage has to be isolated from the signal ground since it does not have a neutral which is or could be on the same signal level. Even a fictitious neutral (as created by a star termination of three resistors) will have a fluctuating neutral with respect to signal ground. Isolation also provides a form of protection for the circuitry on the reference side should a fault occur on the floating side.

The line-to-neutral voltage (V_{LN}) is obtained by star termination of three $100\text{k}\Omega$ precision resistors. The circuit is displayed in Figure A3.9. The voltage is reduced by

ground reference and the output ground symbol (IC1 right) designates the floating ground.

The floating signal is coupled across with the AD202 (IC13) in Figure A3.10. A LPF at the output of the AD202 reduces the 25kHz ripple as introduced by the AD202. The non-inverting op-amp (IC14) is the final gain stage where the offset voltage of the AD637, the AD202 and the LF351 can be trimmed to zero with P₃. The input offset voltage of the AD202 can be as large as 10mV. It therefore makes sense to use a low-cost op-amp whose trimming range is large enough to null all the offsets. The gain of the LF351 can be adjusted with P₄.

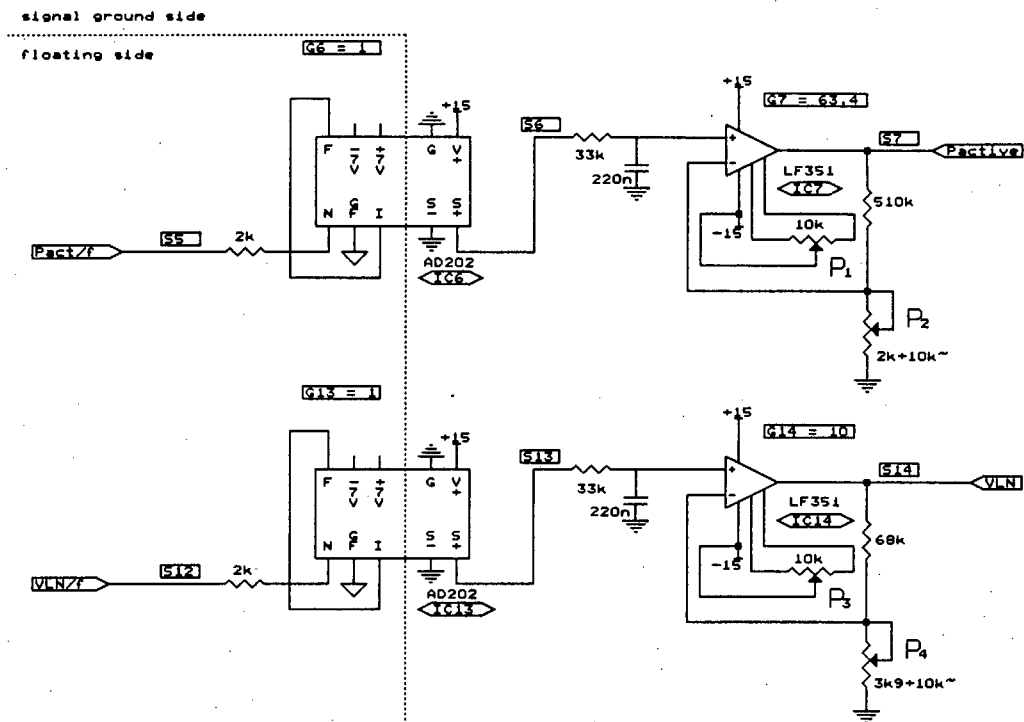


FIGURE A3.10 Circuit diagram of the inverter voltage and active power parameters referenced to signal ground

The transfer function for the line-to-line voltage is:

$$V_{LL} = \sqrt{3} \times V_{out} \div (G_8 \times G_9 \times G_{14}) [V_{rms}]$$

where V_{out} is the output signal at S₁₄ and G_x are the respective gains in Figure A3.8 and A3.9 which form part of the V_{LL} circuit.

The settling time is:

$$t_s = 4.6 \times \sqrt{(0.68 \times 0.025)^2 + (2.2 \times 0.025)^2 + 2 \times (0.47 \times 0.075)^2} = 0.35 \text{ sec}$$

where the first value in brackets is always the capacitor in μF and the second value is the resistor in $\text{M}\Omega$.

The reason for this comparatively short settling time has purely logistic reasons. Since a lot of alterations took place at the test site the case occurred where a particular component was not available. In this case no op-amp with a low bias current was available and therefore the input resistors chosen had to be smaller to avoid significant voltage drops at the input of the op-amp. Larger capacitors were also not available.

A3.3.4 Inverter active power

The circuits for P_{active} are shown in Figure A3.9 and A3.10. The current reference signal ($I_{\text{line/multiplier}}$) from Figure A3.8 is coupled across to the floating side with the isolator AD202 (IC1, 2kHz bandwidth, output resistance = $7\text{k}\Omega$) for multiplication purposes. The gain of the isolator is $1/(2 \times \sqrt{2})$ to reduce signal magnitude to $\pm 1V_{\text{pp}}$ (the current is a sine-wave and square-root of 2 is therefore valid). The AD202 receives its power from the floating power supply.

Due to a relatively large bias current (typically $45\mu\text{A}$) from the multiplier AD834 and a large output resistance of the AD202 (about $7\text{k}\Omega$) the output signal from the AD202 has to be buffered. The LT1097 (IC2) acts as a buffer and therefore avoids voltage offsets due to bias current. The magnitude of the input offset current of the AD834 is not mentioned in the data sheet.

The AD834 (IC3) is a 500MHz wide-band four-quadrant multiplier. This is far in excess of the bandwidth required but was the best option available at the time of design. The multiplier has a current output which is converted to a voltage and then amplified by IC4 to produce an output of $\pm 1V$ FS for $\pm 1V$ into the multiplier inputs (this circuit has been copied from the specifications sheet of the AD834). A potentiometer P_3 (100Ω) has been added to one of the potential divider legs in the circuit to trim the op-amp output to zero.

IC5 (LM627) is configured as a voltage follower. In addition, the input is configured as a two pole Sallen & Key with $f_{-3\text{dB}} = 0.6\text{Hz}$ and $\tau = 372\text{msec}$.

Isolated power is supplied to the circuit as explained in the subsection on the inverter voltage above.

The floating power signal is coupled across to the signal ground reference in the AD202 (as shown in Figure A3.10). The circuit for the rms voltage and the active power are virtually identical. The gains of the LF351's are different though. The input

offset voltage can be trimmed to zero as explained before.

The transfer function is as follows:

$$P_{\text{active}} = 1000 \times V_{\text{out}} \div (N \times R_m \times G_1 \times G_8 \times G_9 \times G_{2\&3} \times G_7) \text{ [W]}$$

where V_{out} is the signal at S_7 , N is the number of turns through the LEM probe, R_m is the magnitude of the measurement resistor of the LEM, and G_x are the respective gains in Figure A3.9 and A3.10.

The settling time for the active power circuitry is:

$$t_s = 4.6 \times \sqrt{2 \times (0.48 \times 0.56)^2} = 1.71 \text{ sec}$$

A few alterations can be suggested.

- Replace the AD202 with a higher bandwidth isolator to couple across currents with harmonic content in excess of 2kHz.
- Replace the AD834 with the AD734. It has a full-power bandwidth of 10MHz (which is more appropriate), a full-scale differential input range of $\pm 12.5\text{V}$, a lower power consumption, a wide power supply range. It is very accurate and generally more versatile.
- Move the DC to DC converters off the printed circuit board that it now shares with the circuitry in Figure A3.9. It may have caused interference with the rms voltage signal due to poor layout. Rather have it on a PCB by itself.

A3.3.5 Power Supply

The input voltage to the power supply can be between 24V to 28V (Figure A3.11). The transistor circuitry at the input 'regulates' the voltage to about 20V. This circuit is implemented to reduce the strain on the other regulators which were getting excessively hot. Power dissipation was sometimes in the order of $12V \times 120mA = 1.44$ Watt. A high watt resistor (39Ω) was inserted in line before the LM7812 which supplies the DC to DC converters as it was still getting too hot.

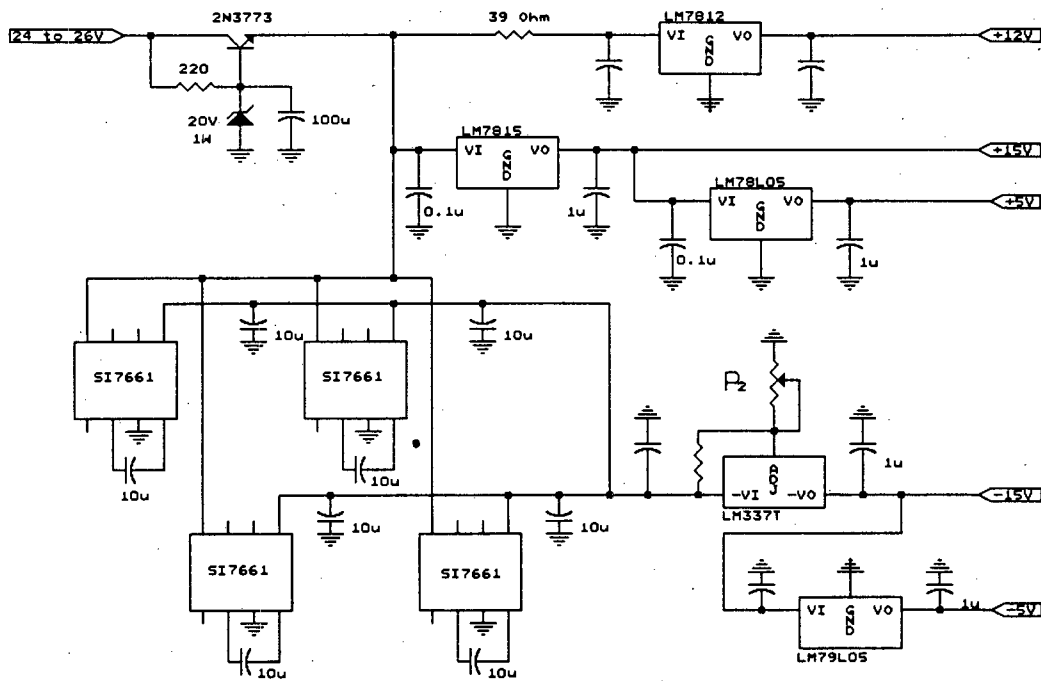


FIGURE A3.11 Circuit diagram of the power meter power supply

Minus 20V is generated from the Si7661 voltage inverters. Their output is regulated to -15V.

The power supply could be improved by increasing the negative supply current capabilities so that the LEM module can generate $\pm 50mA$ at full-scale signal on the primary side. Currently the power supply is limiting the LEM current probe to 20mA on the negative supply rail. This is therefore a loss in resolution since the turns through the LEM can not be increased until it reaches 50mA on the secondary side.

A3.4 Data sheets for electronic components

The data sheets (the first page only) for the components are listed in the sequence in which they occur in the previous two sections.

Op-amp LM324

General Description

The LM124 series consists of four independent, high gain, internally frequency compensated operational amplifiers which were designed specifically to operate from a single power supply over a wide range of voltages. Operation from split power supplies is also possible and the low power supply current drain is independent of the magnitude of the power supply voltage.

Application areas include transducer amplifiers, DC gain blocks and all the conventional op amp circuits which now can be more easily implemented in single power supply systems. For example, the LM124 series can be directly operated off of the standard +5 V_{DC} power supply voltage which is used in digital systems and will easily provide the required interface electronics without requiring the additional ± 15 V_{DC} power supplies.

Unique Characteristics

- In the linear mode the input common-mode voltage range includes ground and the output voltage can also swing to ground, even though operated from only a single power supply voltage.
- The unity gain cross frequency is temperature compensated.
- The input bias current is also temperature compensated.

Advantages

- Eliminates need for dual supplies
- Four internally compensated op amps in a single package
- Allows directly sensing near GND and V_{OUT} also goes to GND
- Compatible with all forms of logic
- Power drain suitable for battery operation

Features

- Internally frequency compensated for unity gain
- Large DC voltage gain 100 dB
- Wide bandwidth (unity gain) 1 MHz (temperature compensated)
- Wide power supply range:
 - Single supply 3 V_{DC} to 32 V_{DC}
 - or dual supplies ± 1.5 V_{DC} to ± 16 V_{DC}
- Very low supply current drain (700 μ A)—essentially independent of supply voltage
- Low input biasing current 45 nA_{DC} (temperature compensated)
- Low input offset voltage 2 mV_{DC} and offset current 5 nA_{DC}
- Input common-mode voltage range includes ground
- Differential input voltage range equal to the power supply voltage
- Large output voltage swing 0 V_{DC} to V⁺ - 1.5 V_{DC}

Low power, precision op-amp LT1097

FEATURES

- Offset Voltage 50 μ V Max
- Offset Voltage Drift 1.0 μ V/ $^{\circ}$ C Max
- Bias Current 250pA Max
- Offset Current 250pA Max
- Bias and Offset Current Drift 4pA/ $^{\circ}$ C Max
- Supply Current 560 μ A Max
- 0.1Hz to 10Hz Noise 0.5 μ Vp-p, 2.2pAp-p
- CMRR 115dB Min
- Voltage Gain 117dB Min
- PSRR 114dB Min
- *Guaranteed Operation on Two NiCad Batteries*

APPLICATIONS

- Replaces OP-07/OP-77/OP-97/OP-177/AD707/LT1001 with Improved Price/Performance
- High Impedance Difference Amplifiers
- Logarithmic Amplifiers (Wide Dynamic Range)
- Thermocouple Amplifiers
- Precision Instrumentation
- Active Filters (with Small Capacitors)

DESCRIPTION

The LT1097 achieves a new standard in combining low price and outstanding precision performance.

On all operational amplifier datasheets, the specifications listed on the front page are for highly selected, expensive grades, while the specs for the low cost grades are buried deep in the datasheet.

The LT1097 does not have any selected grades, the outstanding specifications shown in the features section are for its only grade

The design effort of the LT1097 concentrated on optimizing the performance of all precision specs — at only 350 μ A of supply current. Typical values are 10 μ V offset voltage, 40pA bias and offset currents, 0.2 μ V/ $^{\circ}$ C and 0.4pA/ $^{\circ}$ C drift. Common mode and power supply rejections, voltage gain are typically in excess of 128dB.

All parameters that are important for precision, low power op amps have been optimized. Consequently, using the LT1097, error budget calculations in most applications are unnecessary.

Protected by U.S. patents 4,575,685; 4,775,884 and 4,837,496

Precision wideband op-amp LM627

General Description

The LM627/LM637 series feature extremely low noise and excellent precision along with high speed. Voltage noise is a low $3 \text{ nV}/\sqrt{\text{Hz}}$ in the flat band and rises to only $3.5 \text{ nV}/\sqrt{\text{Hz}}$ at 10 Hz. The A grades offer guaranteed specifications of $25 \mu\text{V}$ offset voltage and $0.3 \mu\text{V}/^\circ\text{C}$ drift, and their *guaranteed* 126 dB CMRR, 120 dB PSRR and voltage gain of 5 Million ensure an ultra-low V_{OS} under all conditions.

The unity-gain stable LM627 is nearly twice as fast as the OP-27 with a slew rate of $4.5 \text{ V}/\mu\text{s}$ and a 14 MHz gain-bandwidth product. Stable at gains of 5 or more, the decompensated LM637 is considerably faster.

Other enhancements of the LM627/LM637 include a guaranteed 600Ω load drive capability over temperature: $\pm 10\text{V}$ output swing at voltage gains over one million. Bias current has been reduced to 10 nA for the A and B grades and 25 nA for the C grade. Furthermore the LM627 may be overcompensated to allow it to drive capacitive loads up to 2000 pF while maintaining its superb dc specs.

Features

- Low Noise $3 \text{ nV}/\sqrt{\text{Hz}}@1 \text{ kHz}$
 $3.5 \text{ nV}/\sqrt{\text{Hz}}@10 \text{ Hz}$
- Low V_{OS} $25 \mu\text{V}$ Max
- Low Drift $0.3 \mu\text{V}/^\circ\text{C}$ Max
- Offset Drift 100% Tested (A and B grades)
- Noise Voltage 100% Tested (A and B grades)
- High Gain 5 Million Min
- High CMRR 126 dB Min
- High PSRR 120 dB Min
- High Speed
- LM627: 14 MHz Gain-Bandwidth
 $4.5 \text{ V}/\mu\text{s}$ Slew Rate
- LM637: 65 MHz Gain-Bandwidth
 $14 \text{ V}/\mu\text{s}$ Slew Rate
- *Guaranteed* 600Ω drive over temperature
- Wide Power Supply Range $\pm 3.5\text{V}$ to $\pm 18\text{V}$
- Overcompensation Pin Allows driving high C_L

Wide bandwidth JFET op-amp LF351

General Description

The LF351 is a low cost high speed JFET input operational amplifier with an internally trimmed input offset voltage (BI-FET IITM technology). The device requires a low supply current and yet maintains a large gain bandwidth product and a fast slew rate. In addition, well matched high voltage JFET input devices provide very low input bias and offset currents. The LF351 is pin compatible with the standard LM741 and uses the same offset voltage adjustment circuitry. This feature allows designers to immediately upgrade the overall performance of existing LM741 designs.

The LF351 may be used in applications such as high speed integrators, fast D/A converters, sample-and-hold circuits and many other circuits requiring low input offset voltage, low input bias current, high input impedance, high slew rate and wide bandwidth. The device has low noise and offset voltage drift, but for applications where these requirements are critical, the LF356 is recommended. If maximum supply

current is important, however, the LF351 is the better choice.

Features

- Internally trimmed offset voltage 10 mV
- Low input bias current 50 pA
- Low input noise voltage $25 \text{ nV}/\sqrt{\text{Hz}}$
- Low input noise current $0.01 \text{ pA}/\sqrt{\text{Hz}}$
- Wide gain bandwidth 4 MHz
- High slew rate $13 \text{ V}/\mu\text{s}$
- Low supply current 1.8 mA
- High input impedance $10^{12}\Omega$
- Low total harmonic distortion $A_V=10$, $R_L=10\text{k}$, $V_O=20 \text{ Vp-p}$, $\text{BW}=20 \text{ Hz}-20 \text{ kHz}$ $<0.02\%$
- Low 1/f noise corner 50 Hz
- Fast settling time to 0.01% $2 \mu\text{s}$

High precision, wideband RMS-to-DC converter AD637

FEATURES

High Accuracy

- 0.02% Max Nonlinearity, 0 to 2V RMS Input
- 0.10% Additional Error to Crest Factor of 3

Wide Bandwidth

- 8MHz at 1V RMS Input
- 600kHz at 100mV RMS

Computes:

- True RMS
- Square
- Mean Square
- Absolute Value

dB Output (60dB Range)

Chip Select-Power Down Feature Allows:

- Analog "3-State" Operation
- Quiescent Current Reduction from 2.2mA to 350 μ A

PRODUCT DESCRIPTION

The AD637 is a complete high accuracy monolithic rms to dc converter that computes the true rms value of any complex waveform. It offers performance that is unprecedented in integrated circuit rms to dc converters and comparable to discrete and modular techniques in accuracy, bandwidth and dynamic range. A crest factor compensation scheme in the AD637 permits measurements of signals with crest factors of up to 10 with less than 1% additional error. The circuit's wide bandwidth permits the measurement of signals up to 600kHz with inputs of 200mV rms and up to 8MHz when the input levels are above 1V rms.

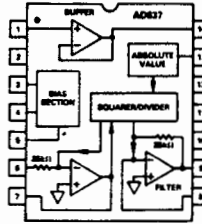
As with previous monolithic rms converters from Analog Devices, the AD637 has an auxiliary dB output available to the user. The logarithm of the rms output signal is brought out to a separate pin allowing direct dB measurement with a useful range of 60dB. An externally programmed reference current allows the user to select the 0dB reference voltage to correspond to any level between 0.1V and 2.0V rms.

A chip select connection on the AD637 permits the user to decrease the supply current from 2.2mA to 350 μ A during periods when the rms function is not in use. This feature facilitates the addition of precision rms measurement to remote or hand-held applications where minimum power consumption is critical. In addition when the AD637 is powered down the output goes to a high impedance state. This allows several AD637s to be tied together to form a wide-band true rms multiplexer.

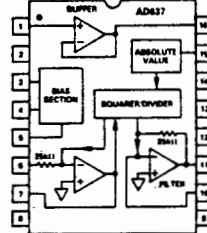
The input circuitry of the AD637 is protected from overload voltages that are in excess of the supply levels. The inputs will not be damaged by input signals if the supply voltages are lost.

AD637 FUNCTIONAL BLOCK DIAGRAMS

Ceramic DIP (D) and
Cerdip (Q) Package



SOIC (R) Package



The AD637 is available in two accuracy grades (J, K) for commercial (0 to +70°C) temperature range applications and one (S) rated over the -55°C to +125°C temperature range. All versions are available in hermetically-sealed, 14-pin side-brazed ceramic DIPs as well as low-cost cerdip packages. A 16-pin SOIC package is also available.

PRODUCT HIGHLIGHTS

1. The AD637 computes the true root-mean-square, mean square, or absolute value of any complex ac (or ac plus dc) input waveform and gives an equivalent dc output voltage. The true rms value of a waveform is more useful than an average rectified signal since it relates directly to the power of the signal. The rms value of a statistical signal is also related to the standard deviation of the signal.
2. The AD637 is laser wafer trimmed to achieve rated performance without external trimming. The only external component required is a capacitor which sets the averaging time period. The value of this capacitor also determines low frequency accuracy, ripple level and settling time.
3. The chip select feature of the AD637 permits the user to power down the device during periods of nonuse, thereby, decreasing battery drain in remote or hand-held applications.
4. The on-chip buffer amplifier can be used as either an input buffer or in an active filter configuration. The filter can be used to reduce the amount of ac ripple, thereby, increasing the accuracy of the measurement.

Sixth order switched capacitor Butterworth lowpass filter MF6

General Description

The MF6 is a versatile easy to use, precision 6th order Butterworth lowpass active filter. Switched capacitor techniques eliminate external component requirements and allow a clock tunable cutoff frequency. The ratio of the clock frequency to the lowpass cutoff frequency is internally set to 50 to 1 (MF6-50) or 100 to 1 (MF6-100). A Schmitt trigger clock input stage allows two clocking options, either self-clocking (via an external resistor and capacitor) for stand-alone applications, or an external TTL or CMOS logic compatible clock can be used for tighter cutoff frequency control. The maximally flat passband frequency response together with a DC gain of 1 V/V allows cascading MF6 sections for higher order filtering. In addition to the filter, two independent CMOS op amps are included on the die and are useful for any general signal conditioning applications.

Features

- No external components
- 14-pin DIP or 14-pin wide-body S.O. package
- Cutoff frequency accuracy of $\pm 0.3\%$ typical
- Cutoff frequency range of 0.1 Hz to 20 kHz
- Two uncommitted op amps available
- 5V to 14V total supply voltage
- Cutoff frequency set by external or internal clock

Isolation amplifier AD202

FEATURES

Small Size: 4 Channels/Inch
Low Power: 35mW (AD204)
High Accuracy: $\pm 0.025\%$ max Nonlinearity (K Grade)
High CMR: 130dB (Gain = 100V/V)
Wide Bandwidth: 5kHz Full-Power (AD204)
High CMV Isolation: $\pm 2000\text{V}$ pk Continuous (K Grade)
 (Signal and Power)
Isolated Power Outputs
Uncommitted Input Amplifier

APPLICATIONS

Multichannel Data Acquisition
Current Shunt Measurements
Motor Controls
Process Signal Isolation
High Voltage Instrumentation Amplifier

GENERAL DESCRIPTION

The AD202 and AD204 are members of a new generation of low cost, high performance isolation amplifiers. A new circuit design, novel transformer construction, and the use of surface-mounted components in an automated assembly process result in remarkably compact, economical isolators whose performance in many ways exceeds that previously available from very expensive devices. The primary distinction between the AD202 and AD204 is that the AD202 is powered directly from +15V dc while the AD204 is powered by an externally supplied clock (AD246).

The AD202 and AD204 employ transformer coupling and do not require the design compromises that must be made when optical isolators are used: each provides a complete isolation function, with both signal and power isolation internal to the module, and they exhibit no long-term parameter shifts under sustained common-mode stress. Power consumption, nonlinearity, and drift are each an order of magnitude lower than can be obtained from other isolation techniques, and these advantages are obtained without sacrifice of bandwidth or noise performance.

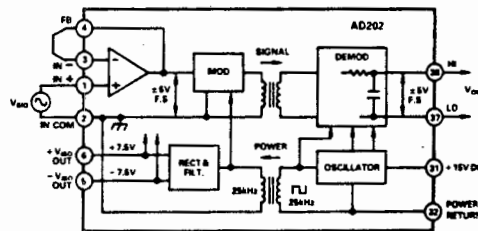
The design of the AD202 and AD204 emphasizes ease of use in a broad range of applications where signals must be measured or transmitted without a galvanic connection. In addition, the low cost and small size of these isolators makes component-level circuit applications of isolation practical for the first time.

PRODUCT HIGHLIGHTS

The AD202 and AD204 are full-featured isolators offering numerous benefits to the user:

Small Size: The AD202 and AD204 are available in SIP and DIP form packages. The SIP package is just 0.25" wide, giving the user a channel density of four channels per inch. The isolation barrier is positioned to maximize input to output spacing. For applications requiring a low profile, the DIP package provides a height of just 0.350".

AD202 FUNCTIONAL BLOCK DIAGRAM



High Accuracy: With a maximum nonlinearity of $\pm 0.025\%$ for the AD202K/AD204K ($\pm 0.05\%$ for the AD202J/AD204J) and low drift over temperature, the AD202 and AD204 provide high isolation without loss of signal integrity.

Low Power: Power consumption of 35mW (AD204) and 75mW (AD202) over the full signal range makes these isolators ideal for use in applications with large channel counts or tight power budgets.

Wide Bandwidth: The AD204's full-power bandwidth of 5kHz makes it useful for wideband signals. It is also effective in applications like control loops, where limited bandwidth could result in instability.

Excellent Common-Mode Performance: The AD202K/AD204K provide $\pm 2000\text{V}$ pk continuous common-mode isolation, while the AD202J/AD204J provide $\pm 1000\text{V}$ pk continuous common-mode isolation. All models have a total common-mode input capacitance of less than 5pF inclusive of power isolation. This results in CMR ranging from 130dB at a gain of 100 to 104dB (minimum at unity gain) and very low leakage current (2 μA maximum).

Flexible Input: An uncommitted op amp is provided at the input of all models. This provides buffering and gain as required, and facilitates many alternative input functions including filtering, summing, high-voltage ranges, and current (transimpedance) input.

Isolated Power: The AD204 can supply isolated power of $\pm 7.5\text{V}$ at 2mA. This is sufficient to operate a low-drift input preamp, provide excitation to a semiconductor strain gage, or to power any of a wide range of user-supplied ancillary circuits. The AD202 can supply $\pm 7.5\text{V}$ at 0.4mA which is sufficient to operate adjustment networks or low-power references and op amps, or to provide an open-input alarm.

Wideband four-quadrant multiplier AD834

FEATURES

DC to >500MHz Operation
 Differential $\pm 1V$ Full Scale Inputs
 Differential $\pm 4mA$ Full Scale Output Current
 Low Distortion ($\leq 0.05\%$ for 0dBm Input)
 Supply Voltages from $\pm 4V$ to $\pm 9V$
 Low Power (280mW typical at $V_G = \pm 5V$)

APPLICATIONS

High Speed Real Time Computation
 Wideband Modulation and Gain Control
 Signal Correlation and RF Power Measurement
 Voltage Controlled Filters and Oscillators
 Linear Keyers for High Resolution Television
 Wideband True RMS

PRODUCT DESCRIPTION

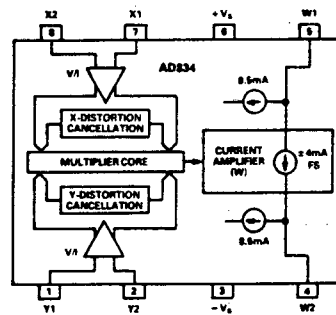
The AD834 is a monolithic laser-trimmed four-quadrant analog multiplier intended for use in high frequency applications, having a transconductance bandwidth ($R_L = 50\Omega$) in excess of 500MHz from either of the differential voltage inputs. In multiplier modes, the typical total full scale error is 0.5%, dependent on the application mode and the external circuitry. Performance is relatively insensitive to temperature and supply variations, due to the use of stable biasing based on a bandgap reference generator and other design features.

To preserve the full bandwidth potential of the high speed bipolar process used to fabricate the AD834, the outputs appear as a differential pair of currents at open collectors. To provide a single ended ground referenced voltage output, some form of external current to voltage conversion is needed. This may take the form of a wideband transformer, balun, or active circuitry such as an op amp. In some applications (such as power measurement) the subsequent signal processing may not need to have high bandwidth.

The transfer function is accurately trimmed such that when $X=Y = \pm 1V$, the differential output is $\pm 4mA$. This absolute calibration allows the outputs of two or more AD834s to be summed with precisely equal weighting, independent of the accuracy of the load circuit.

The AD834 is specified for use over the commercial temperature range of 0 to $+70^\circ C$ and is available in an 8-pin cerdip package, an 8-pin plastic DIP package, and an 8-pin plastic SOIC package. AD834A is available in cerdip for operation over the industrial temperature range of $-40^\circ C$ to $+85^\circ C$. The AD834S/883B is specified for operation over the military temperature range of $-55^\circ C$ to $+125^\circ C$ and is available in the 8-pin cerdip package. S-Grade chips are also available.

AD834 FUNCTIONAL BLOCK DIAGRAM



PRODUCT HIGHLIGHTS

1. The AD834 combines high static accuracy (low input and output offsets and accurate scale factor) with very high bandwidth. As a four-quadrant multiplier or squarer, the response extends from dc to an upper frequency limited mainly by packaging and external board layout considerations. A large signal bandwidth of over 500MHz is attainable under optimum conditions.
2. The AD834 can be used in many high speed nonlinear operations, such as square rooting, analog division, vector addition and rms-to-dc conversion. In these modes, the bandwidth is limited by the external active components.
3. Special design techniques result in low distortion levels (better than $-60dB$ on either input) at high frequencies and low signal feedthrough (typically $-65dB$ up to 20MHz).
4. The AD834 exhibits low differential phase error over the input range—typically 0.08° at 5MHz and 0.8° at 50MHz. The large signal transient response is free from overshoot, and has an intrinsic rise time of 500ps, typically settling to within 1% in under 5ns.
5. The nonloading, high impedance, differential inputs simplify the application of the AD834.

Voltage Converter Si7661

FEATURES

- Conversion of +4.5 V to +20 V Logic Supply to -4.5 V to -20 V Supplies
- Voltage Multiplication ($V_{out} = (-) nV_{in}$)
- 99.7% Typical Open Circuit Voltage Conversion Efficiency
- 95% Typical Power Efficiency

BENEFITS

- Inexpensive Negative Supply Generation
- Easy to Use, Requires Only 2 External Capacitors
- Minimum Parts Count
- Small Size

APPLICATIONS

- On board Negative Supply for Dynamic RAMs
- Localized μ -Processor (8080 Type) Negative Supplies
- Inexpensive Negative Supplies for Analog Switches
- Data Acquisition Systems
- Up to -20 V for Op Amps, and other Linear Circuits

DC to DC converters NMA 1205 and 1215

- ★ Pcb mountable
- ★ Input/Output isolated 500 VDC
- ★ No derating
- ★ 100% burned-in
- ★ Triple tested
- ★ Low profile
- ★ High efficiency up to 80%
- ★ DIP and SIP packages
- ★ 5, 12, 24 and 48 volt input

DESCRIPTION

The NMA051/12/24/48 Series is a range of miniature high efficiency isolated DC-DC converters available in both DIP and SIP packages. The DIP requires only 0.32 square inches of board space and the SIP only 0.18 square inches. The units operate from 5, 12, 24 or 48 volts input and the range provides isolated output voltages of $\pm 5V$, $\pm 12V$ and $\pm 15V$. The delivered power is 750 mWatts total, all of which may be drawn from one output pin, with an input to output isolation of 500 VDC. Both types of package are fully epoxy encapsulated with the plastic SIP and DIP casing having UL94-V0 rating. No heatsinks are needed for the rated performance and the operating temperature range is $-25^{\circ}C$ to $80^{\circ}C$.

PART NUMBER	INPUT VOLTAGE	OUTPUT VOLTAGE	CURRENT (mA) EACH OUTPUT	PACKAGE
NMA0505D	5	± 5	75	DIP14
NMA0512D	5	± 12	30	DIP14
NMA0515D	5	± 15	25	DIP14
NMA0505S	5	± 5	75	SIP6
NMA0512S	5	± 12	30	SIP6
NMA0515S	5	± 15	25	SIP6
NMA1205L	12	± 5	75	DIP14
NMA1212D	12	± 12	30	DIP14
NMA1215D	12	± 15	25	DIP14
NMA1205S	12	± 5	75	SIP6
NMA1212S	12	± 12	30	SIP6
NMA1215S	12	± 15	25	SIP6
NMA2405C	24	± 5	75	DIP14
NMA2412D	24	± 12	30	DIP14
NMA2415D	24	± 15	25	DIP14
NMA2405S	24	± 5	75	SIP6
NMA2412S	24	± 12	30	SIP6
NMA2415S	24	± 15	25	SIP6
NMA4805D	48	± 5	75	DIP14
NMA4812D	48	± 12	30	DIP14
NMA4815D	48	± 15	25	DIP14
NMA4805S	48	± 5	75	SIP6
NMA4812S	48	± 12	30	SIP6
NMA4815S	48	± 15	25	SIP6

Absolute maximum ratings over operating free-air temperature range

Input voltage V_{in} NMA05 types	7V
Input voltage V_{in} NMA12 types	15V
Input voltage V_{in} NMA24 types	28V
Input voltage V_{in} NMA48 types	54V
Output power total	750mW
Short-circuit duration	1.0 second
Isolation voltage	500VDC
Operating temperature range	$-25^{\circ}C$ to $80^{\circ}C$
Storage temperature range	$-55^{\circ}C$ to $110^{\circ}C$

Electrical specifications over operating free-air temperature range

Input voltage range NMA05	$5V \pm 10\%$
Input voltage range NMA12	$12V \pm 10\%$
Input voltage range NMA24	$24V \pm 10\%$
Input voltage range NMA48	$48V \pm 10\%$
Load voltage regulation (min. load of 1 mA)	$\pm 10\%$
Line voltage regulation	1% / 1% of V_{in}
Output voltage accuracy	$\pm 5\%$
Input reflected noise (20 MHz Band limited)	75mV p-p max
Output ripple and noise (20 MHz Band limited)	50mV p-p max
Input output isolation	500 VDC min.
Insulation resistance at 500 VDC	1000 Megohms min
Efficiency at full load, 12V and 15V output types	80% typical 75% min
Efficiency at full load, 5V output types	75% typical 70% min
Temperature drift	0.03% per $^{\circ}C$ max.
Temperature rise above ambient at full load	$8^{\circ}C$ max.
Weight SIP	2.1 grams
Weight DIP	2.3 grams

A3.5 Specifications of calibration devices

A3.5.1 LI-COR Calibration certificate

CERTIFICATE OF CALIBRATION

Model Number: **LI-200SZ PYRANOMETER SENSOR**

Serial Number: **PY12909**

Calibration Constant: **94.0** LI-1000 Multiplier: **-10.64**

Units: microamps per 1000 watts m⁻² Units: watts m⁻² per microamp

Please consult the instruction manual for further information on the calibration constant and LI-1000 Multiplier. Recalibration recommended every two years.

Date of Calibration: **June 13, 1990**

By: BH

LI-COR, inc. / LI-COR, Ltd.
Box 4425 / Lincoln, Nebraska 68504 USA
 Phone (402) 467-3576 / TWX. 910-621-8116
 FAX NO. 402-467-2819

A3.5.2 Fluke 83 DVM

FUNCTION	RANGE	RESOLUTION	ACCURACY*		
			50 Hz - 60 Hz	45 Hz - 5 kHz	
\tilde{V} (Fluke 83)	400.0 mV	0.1 mV	$\pm(1.0\% + 4)$	$\pm(1.5\% + 4)$	
	4.000V	0.001V	$\pm(1.0\% + 3)$	$\pm(1.5\% + 3)$	
	40.00V	0.01V	$\pm(1.0\% + 3)$	$\pm(1.5\% + 3)$	
	400.0V	0.1V	$\pm(1.0\% + 3)$	$\pm(1.5\% + 3)$	
	1000V	1V	$\pm(1.0\% + 3)$	$\pm(2.5\% + 3)$	
\tilde{V} (Fluke 85)			50 Hz-60 Hz	45 Hz-5 kHz	5 kHz-20 kHz
	400.0 mV	0.1 mV	$\pm(0.5\% + 4)$	$\pm(1.0\% + 4)$	$\pm(2.0\% + 4)$
	4.000V	0.001V	$\pm(0.5\% + 2)$	$\pm(1.0\% + 2)$	$\pm(4.0\% + 4)$
	40.00V	0.01V	$\pm(0.5\% + 2)$	$\pm(1.0\% + 2)$	$\pm(4.0\% + 4)$
	400.0V	0.1V	$\pm(0.5\% + 2)$	$\pm(1.0\% + 2)$	$\pm(4.0\% + 4)$
	1000V	1V	$\pm(0.5\% + 2)$	$\pm(2.0\% + 2)$	Unspecified

* Accuracy is given as $\pm([\% \text{ of reading}] + [\text{number of least significant digits}])$ at 18°C to 28°C with relative humidity up to 90%, for a period of one year after calibration. AC conversions are ac-coupled, average responding, and calibrated to the rms value of a sine wave input.

FUNCTION	RANGE	RESOLUTION	ACCURACY	
			Fluke 83	Fluke 85
\overline{V}	4.000V	0.001V	$\pm(0.3\% + 1)$	$\pm(0.1\% + 1)$
	40.00V	0.01V	$\pm(0.3\% + 1)$	$\pm(0.1\% + 1)$
	400.0V	0.1V	$\pm(0.3\% + 1)$	$\pm(0.1\% + 1)$
	1000V	1V	$\pm(0.3\% + 1)$	$\pm(0.1\% + 1)$
\overline{mV}	400.0 mV	0.1 mV	$\pm(0.3\% + 1)$	$\pm(0.1\% + 1)$
Ω	400.0 Ω	0.1 Ω	$\pm(0.4\% + 1)$	$\pm(0.2\% + 1)$
	4.000 k Ω	0.001 k Ω	$\pm(0.4\% + 1)$	$\pm(0.2\% + 1)$
	40.00 k Ω	0.01 k Ω	$\pm(0.4\% + 1)$	$\pm(0.2\% + 1)$
	400.0 k Ω	0.1 k Ω	$\pm(0.4\% + 1)$	$\pm(0.2\% + 1)$
	4.000 M Ω	0.001 M Ω	$\pm(0.4\% + 1)$	$\pm(0.2\% + 1)$
	40.00 M Ω	0.01 M Ω	$\pm(1\% + 3)$	$\pm(1\% + 3)$
(nS)	40.00 nS	0.01 nS	$\pm(1\% + 10)$	$\pm(1\% + 10)$

FUNCTION	RANGE	RESOLUTION	ACCURACY**	
Capacitance	5.00 nF	0.01 nF	±(1% + 35)***	
	0.0500 µF	0.0001 µF	±(1% + 2)	
	0.500 µF	0.001 µF	±(1% + 2)	
	5.00 µF	0.01 µF	±(1% + 2)	
Diode Test	3.000V	0.001V	±(2% + 1)	

FUNCTION	RANGE	RESOLUTION	ACCURACY		BURDEN VOLTAGE
			Fluke 83	Fluke 85	
mA A ~ (45 Hz to 2 kHz)	40.00 mA	0.01 mA	±(1.2% + 2)	±(0.6% + 2)	1.5 mV/mA
	400.0 mA	0.1 mA	±(1.2% + 2)	±(0.6% + 2)	1.5 mV/mA
	4000 mA	1 mA	±(1.2% + 2)	±(0.6% + 2)	0.03 V/A
	10.00A†	0.01A	±(1.2% + 2)	±(0.6% + 2)	0.03 V/A
mA A ---	40.00 mA	0.01 mA	±(0.4% + 2)	±(0.2% + 2)	1.5 mV/mA
	400.0 mA	0.1 mA	±(0.4% + 2)	±(0.2% + 2)	1.5 mV/mA
	4000 mA	1 mA	±(0.4% + 2)	±(0.2% + 2)	0.03 V/A
	10.00A†	0.01A	±(0.4% + 2)	±(0.2% + 2)	0.03 V/A

** With film capacitor or better
 *** ±(1% + 2) if Relative mode is used to zero residual
 † 10A continuous, 20A for 30 seconds maximum

A3.5.3 Soar DVM

Anmerkung:
 Technische Daten sind spezifiziert für einen Temperaturbereich von 18°C bis 28°C bei einer relativen Luftfeuchtigkeit von 80% max.
 Die Genauigkeit der nachfolgend im Einzelnen aufgeführten Betriebsarten ist jeweils wie folgt angegeben: ±% des angezeigten Wertes (kurz d.A. genannt) bezüglich der Anzahl der Stellen (+ ... digits letzte Stelle der Anzeige)

TECHNISCHE DATEN

DC-SPANNUNG			
Bereich	Anflöwing	Genauigkeit	Eingangsleistung
250 mV	10 µV	±0,04% d.A. ±2 digits ±0,05% d.A. ±2 digits (3450)	1 GΩ
2500 mV	1000 µV	±0,04% d.A. ±2 digits ±0,07% d.A. ±2 digits (3450)	11 MΩ <50 pF
25 V	1 mV	±0,04% d.A. ±2 digits ±0,07% d.A. ±2 digits (3450)	10 MΩ <50 pF
250 V	10 mV	±0,05% d.A. ±2 digits ±0,07% d.A. ±2 digits (3450)	10 MΩ <50 pF
1000 V	100 mV	±0,05% d.A. ±2 digits ±0,07% d.A. ±2 digits (3450)	10 MΩ <50 pF

NMRR >60 dB (50/60 Hz)
 CMRR >100 dB (50/60 Hz); R_s = 1 kΩ
 Einschwingzeit max. 1 s auf die spezifizierte Genauigkeit im gewählten Bereich
 Eingangsspannung max. zulässig: 1200 VDC oder 900 VACrms
 im 250 mV Bereich 500 VDC oder ACrms

AC-SPANNUNG 3430				
Bereich	Anflöwing	Frequenz		Eingangsleistung
		20 Hz - 10 kHz	10 kHz - 20 kHz	
250 mV	10 µV	±1% d.A. ±10 digits	±1% d.A. ±40 digits	1000 MΩ <110 pF
2500 mV	100 µV	±0,5% d.A. ±10 digits	±1% d.A. ±40 digits	11 MΩ <50 pF
25 mV	1 mV	±0,5% d.A. ±10 digits	±1% d.A. ±40 digits	10 MΩ <50 pF
250 mV	10 mV	±0,5% d.A. ±10 digits	±1% d.A. ±40 digits	10 MΩ <50 pF
750 mV	100 mV	±1% d.A. ±10 digits	400 Hz	10 MΩ <50 pF

Einschwingzeit max. 3 s auf die spez. Genauigkeit im gewählten Bereich
 Eingangsspannung max. zulässig: 1200 VDC oder 900 VACrms
 250 mV Bereich DC und ACrms 500 V
 Crest Faktor <3

AC-SPANNUNG 3450				
Bereich	Anflöwing	Frequenz	Genauigkeit	Eingangsleistung
250 mV	10 µV	40 Hz - 1 kHz	±0,5% d.A. ±10 digits	>1000 MΩ <100 pF
2500 V	0.1 mV	40 Hz - 1 kHz	±0,5% d.A. ±10 digits	11 MΩ <50 pF
25 V	1 mV	40 Hz - 1 kHz	±0,5% d.A. ±10 digits	10 MΩ <50 pF
250 V	10 mV	40 Hz - 400 Hz	±1% d.A. ±10 digits	10 MΩ <50 pF
750 V	0.1 V	40 Hz - 400 Hz	±1% d.A. ±10 digits	10 MΩ <50 pF

Einschwingzeit max. 3 s auf die spez. Genauigkeit im angewählten Bereich
 Eingangsspannung max. zulässig: 1200 VDC oder 900 Vrms AC
 250 mV Bereich DC und AD 500 Vrms

DC-STROM			
Bereich	Anflöwing	Genauigkeit	Überlastspannung
250 mA	10 µA	±0,25% d.A. ±2 digits	0.6 V max.
10 A	1 mA	±1% d.A. ±2 digits	0.2 V max.

Einschwingzeit max. 1 s im vorgewählten Bereich
 Überlastgrenze 250 mA Bereich 500 mA Sicherung
 (500 mA flink/250 V Sicherung) und
 4 A/600 V zweiter Sicherungsschutz
 10 A; nicht abgesichert, ca. 15 s mit 20 A überlastbar

AC-STROM				
Bereich	Anflöwing	Frequenz	Genauigkeit	Überlastspannung
10 A	1 mA	20 Hz - 1 kHz (40 Hz - 1 kHz)	±2% d.A. ±10 digits	0.2 Vrms max.

Einschwingzeit max. 3 s im vorgewählten Bereich

A3.6 Uncertainty analysis of acquired data

In this section of the appendix the uncertainty of the acquired data for each parameter is evaluated.

Definition of terms (based on Holman (1978))

Error: The error is the deviation from a known value.

Accuracy: The accuracy of an instrument indicates the deviation of the reading from a known input. Accuracy is usually expressed as a percentage of the full-scale reading. This deviation causes a larger error at smaller readings.

Precision: The precision of an instrument indicates its ability to reproduce a certain reading with a given accuracy. It is usually expressed as a \pm percentage. The accuracy of an instrument can be improved by calibration but it cannot be improved beyond the precision of an instrument.

Uncertainty: In cases where no true value is known for comparison the results have to be expressed with a particular uncertainty (\pm a smaller value with units or \pm a percentage). In an experiment one can speak of an experimental uncertainty which would refer to the possible value the error may have. It is often more appropriate to speak of experimental uncertainty rather than experimental error because the magnitude of an error is often uncertain.

Accuracy or uncertainty of data

From the above definitions, it would be appropriate to talk of the accuracy of the data acquisition system (transducers, interface, power meter and logger) because the accuracy for the transducers and the error sources in the components of the signal conditioning are available from data sheets. The collected data though, should be expressed on the basis of uncertainty. The reason for this is that the calibration of the data acquisition system is not based on the comparison to known values but is compared to other measuring devices that have a particular accuracy. The calibration thus introduces an uncertainty.

Method of calculation

Error sources that are specified as a value plus units (rather than a percentage) are converted to percentages by dividing that value by the full-scale (FS) output signal of that component.

The accuracy of the DAS is calculated by taking the square-root of the sum of all errors/accuracies squared. The equation runs as follows:

$$\text{Accuracy} = \sqrt{\theta_1^2 + \theta_2^2 + \theta_3^2 + \dots + \theta_n^2}$$

This assumes that all error sources are independent of each other and are symmetrical about zero (which may not be true). It does not matter that some accuracies are specified for different FS reading as all errors can be amplified.

Most errors are chosen as typical values rather than choosing the maximum specified value (for example as found in op-amp specification sheets). If other assumptions are made they are usually pointed out.

The uncertainty here cannot be calculated as stipulated in the standard uncertainty analysis method as the random and bias component of each elemental error source are not known. Therefore the uncertainty in the data has to be calculated from the accuracy of the data acquisition system (DAS) as shown and the accuracies of the calibration devices used to calibrate the DAS.

The best method is to use the above equation for combining these two accuracies. Unfortunately it will not give a percentage range in which one is 90% or 95% certain that the collected data will fall in that range but rather just a \pm percentage of the full-scale signal.

Structure of subsections

Each parameter that has been logged is treated in a subsection where the errors and the uncertainty are evaluated. The errors for each parameter are listed in a table which has the following structure: transducer error or accuracy, signal conditioning error, data logger error (which is always the same), calibration uncertainty and the resulting uncertainty. The main focus is on the dominant errors since these result in the highest uncertainty component. The composition of a small magnitude accuracy (for example a precision op-amp) is not shown since this would absorb too much space with too little meaning. Those errors have nevertheless been calculated.

The table will also reflect which errors are fixed and which are variable. Fixed errors do not change due to different operating conditions like for example the stability error of the pyranometer which slowly changes during a year. These types of errors are therefore assumed to have remained unchanged during the field tests. Variable errors vary as the operating conditions change. For example, the cosine response of the pyranometer is a variable error since the error changes in magnitude as the incidence angle of the sun (zenith angle) to the pyranometer changes. Similarly op-amps have variable errors that vary for example with frequency. Nevertheless, a fixed value is assigned to variable errors since the uncertainty evaluation would become too complex. These variable values are usually a reflection of the maximum deviation that can occur due to the particular error source. The function according to which the errors vary is indicated in the Table.

Two categories of uncertainties are specified at the end of the table, namely the absolute and the relative uncertainty. The absolute (or total) uncertainty includes all error components. The relative uncertainty is a subset of the absolute uncertainty and excludes all error components that will not have changed during the field tests and also those variable error components that are repeatable. The relative uncertainty therefore is a reflection of the random error component (this is not entirely true in terms of the standard uncertainty analysis method). It points to a change in conditions that has not been measured, is not measurable, was not noted (for example spectral variations) or is too complex to evaluate (for example the variation of the averaging error in the RMS to DC converter is frequency dependent). It is in this way that the relative uncertainty reflects the random component of the total uncertainty. The aim of this separation is to use the relative uncertainty for comparison among the three PVP's tested here and the absolute uncertainty for comparison of this data to other PVP data (for example Grundfos system data, Halcrow (1983), Gosnell (1991) etc).

The signal path can be traced in the circuit diagrams in section A3.2 and A3.3. References to the circuit diagrams are provided in the tables. The abbreviations used are:

var	-	variable error
rel	-	relative error component
neg	-	negligible
f ⁿ (...)	-	function of
V _{os}	-	input offset voltage
I _B	-	input bias current
I _{os}	-	input offset current
FSR	-	full-scale reading

A3.6.1 Plane of array irradiance data

TABLE A3.1 Uncertainty in the irradiance measurement

Type of error	[%]	Comments
Transducer: LI-COR LA-200SZ		
Calibration	3.0	fixed
Stability (over 3 years)	3.0	fixed
Azimuth response	1.0	fixed
Tilt	0.0	fixed
Mounting ($\pm 8^\circ$)	1.0	fixed
Linearity	1.0	var, f^n (G_{POA})
Temperature (25-40°C)	2.3	var, f^n (t_{amb} & u_{wind}), rel
Cosine response	5.0	var, f^n (θ)
Spectral response	5.0	var, f^n (spectrum), rel
Signal conditioning (Figure A3.1)	neg	V_{os} max error: 0.05%
Data Logger	0.2	var, f^n (quant), rel
Relative uncertainty	5.5	of 1250W/m ²
Absolute uncertainty	8.7	FSR

Assumptions:

LI-COR errors have been taken from the specification sheets
 LI-COR temperature variations are assumed 15°C

A3.6.2 Ambient and module temperature

TABLE A3.2 Uncertainty in the temperature measurement

Type of error	t_{amb} [%]	t_{mod} [%]	Comments
Transducer: LM35D			
Accuracy (0.9°C)	2.3	1.5	var, rel
Nonlinearity (0.2°C)	0.5	0.3	var
Difference to cell temperature (4°C)	n/a	6.7	fixed
Signal conditioning (Figure A3.1)	0.5	0.4	var, f^n (I_B), rel
Data Logger	0.2	0.2	var, f^n (quant), rel
Calibration (2°C)	5.0	3.3	fixed
Relative uncertainty	2.3	1.5	
Absolute uncertainty	5.5	7.6	

Assumptions & conditions:

t_{amb} : FSR is 40°C
 t_{mod} : FSR is 60°C
 input impedance to LM324 is 510k Ω with $I_B = 50nA$

A3.6.3 Array voltage

TABLE A3.3 Uncertainty in the array voltage measurement

Type of error	[%]	Comments
Differential resistors	0.2	var, f ⁿ (temp, moisture), rel
Signal conditioning (Fig. A3.2)		
IC1: LT1097	neg	I _{os} is max error: 0.0025%
IC2: LT1097	neg	I _B is max error: 0.0003%
Data Logger	0.2	var, f ⁿ (quant), rel
Calibration	0.9	Fluke DVM: ±(0.3% + 1)
Relative uncertainty	0.3	of 180V
<i>Absolute uncertainty</i>	<i>1.1</i>	FSR

Assumptions & conditions:

IC1 input impedance is 32kΩ
 IC1 differential input impedance is zero
 IC2 input impedance is about 50kΩ

A3.6.4 Array current

TABLE A3.4 Uncertainty in the array current measurement

Type of error	[%]	Comments
Transducer: Dale shunt	1.0	var, f ⁿ (temp), rel
Signal conditioning (Fig A3.2):		
IC3: LM627	0.01	var, f ⁿ (I _{os}), rel
IC4: LF351	0.13	var, f ⁿ (V _{os}), rel
IC5: LT1097	neg	
IC6: LF351	0.05	var, f ⁿ (V _{os}), rel
Data Logger	0.2	var, f ⁿ (quant), rel
Calibration	0.5	Fluke DVM ± (0.4% + 2)
Relative uncertainty	1.1	of 3A
<i>Absolute uncertainty</i>	<i>1.2</i>	FSR

Assumptions & conditions:

IC3 has an input resistance of 10kΩ
 IC4 and IC6 have an input offset voltage of 5mV maximum

A3.6.5 Converter voltage

TABLE A3.5 Uncertainty in the converter voltage measurement

Type of error	[%]	Comments
Differential resistors:	0.2	var, f ⁿ (temp, moisture),rel
Signal conditioning (Fig. A3.3)		
IC1: LF351	0.12	var, f ⁿ (V _{os}), rel
IC2: LF351	0.07	var, f ⁿ (V _{os}), rel
Data Logger	0.2	var, f ⁿ (quant), rel
Calibration	1.0	Fluke DVM: ±(0.3% + 1)
Relative uncertainty	0.3	of 90V
Absolute uncertainty	1.1	FSR

Assumptions & conditions:

Input offset voltage V_{os} is 5mV

A3.6.6 Converter current

TABLE A3.6 Uncertainty in the converter current measurement

Type of error	[%]	Comments
Transducer: Dale shunt	1.0	var, f ⁿ (temp),rel
Signal conditioning (Figure A3.3)		
diff. resistor	0.2	var, f ⁿ (temp, moist),rel
LM627	0.01	var, f ⁿ (I _{os}), rel
LF351	0.08	var, f ⁿ (V _{os}), rel
Data Logger	0.2	var, f ⁿ (quant), rel
Calibration	1.0	Fluke DVM: ±(0.4% + 1)
Relative uncertainty	1.0	of 6A
Absolute uncertainty	1.3	FSR

Assumptions & conditions:

LM627 input impedance is 8.5kΩ

Its differential input impedance is zero: I_B has no effect

LF351 has V_{os} = 5mV

A3.6.7 Motor torque

TABLE A3.7 Uncertainty in the motor torque measurement

Type of error	[%]	Comments
Transducer: Loadcell	0.05	specifications
Signal conditioning (Fig. A3.4)		
LT1097	0.83	var, f ⁿ (V _{cc}), rel
LF351	0.67	var, f ⁿ (V _{cc}), rel
LT1097	neg	
Data Logger	0.2	var, f ⁿ (quant), rel
Calibration: Inaccuracy of weights	1.0	fixed
Spring measurement	3.1	var, f ⁿ (resolution), rel
Calibration drift: shock	1.0	var, f ⁿ (starting torque), rel
Relative uncertainty	3.4	of 2N.m
Absolute uncertainty	3.6	FSR

Assumptions:

- The inaccuracy in the known weights has been estimated
- The inaccuracy in measurements with the spring has been calculated in terms of readability
- The drift in calibration of the loadcell due to shock as the motor starts has been estimated

A3.6.8 Motor speed

The accuracy of the motor speed has been calculated at 800rpm which is a fairly low speed. The log-interval of the signal was usually chosen to be 5sec. The flag wheel (which cuts through the light barrier) had two, three or eight flags. Worst case error is therefore for a two flag set-up and it was calculated to be 0.8% with the following equation:

$$e = \left(\frac{\text{speed} \times \text{loginterval} \times \text{flags}}{60} \right)^{-1} \times 100 \text{ [%]}$$

A3.6.9 Flowrate

As explained in the main text, the flow measurement with the flow-captor was not successful. This error analysis is therefore for the correlation of flowrate to the motor speed.

TABLE A3.8 Uncertainty in the flowrate measurement

<i>Type of error</i>	<i>[%]</i>	<i>Comments</i>
Transducer: Kent PSM meter	2.0	fixed
Calibration: Jug	2.0	fixed, used to calibrate bucket
Bucket	5.0	fixed
Correlation to speed	2.0	var
Relative uncertainty	2.2	over full
<i>Absolute uncertainty</i>	6.1	range

Assumptions & conditions:

The relative uncertainty includes the 0.8% uncertainty in the motor speed measurement

The calibration errors of the jug and the bucket are estimates

A3.6.10 Static head

This error is estimated to be about 15cm due to cable stretching and inaccurate markings. Over 75m the error evaluates to 0.2%.

A3.6.11 Inverter current

TABLE A3.9 Uncertainty in the inverter current measurement

Type of error	[%]	Comments
Transducer: LEM probe		
Accuracy	1.56	var, rel
tempco	1.25	var, rel
BW error	1.0	fixed
Signal conditioning (Fig. A3.8):		
meas. resistor	0.24	var, f ⁿ (temp, moist); rel
LT1097's	neg	all less than 0.01%
AD637:		
tempco	0.14	var, rel
DC reversal	0.25	var, rel
Averaging	0.20	var, f ⁿ (f), rel
Data Logger	0.2	var, f ⁿ (quant), rel
Calibration: Fluke DVM	1.3	± (1.5% + 3)
Unbalanced phases	2.0	
Relative uncertainty	3.0	of 5A _{line}
Absolute uncertainty	3.3	FSR

Assumptions & conditions:

temperature variations are assumed to be 30°C
 The following errors have been estimated:
 Bandwidth (BW) error
 Unbalanced phases

A3.6.12 Inverter frequency

The error is calculated to be 0.4% at 50Hz and a log-interval of 5sec. The error increases at lower operating frequencies but decreases for longer log-intervals. It is calculated as follows:

$$e = (f \times \loginterval)^{-1} \times 100 \text{ [%]}$$

A3.6.13 Inverter voltage

TABLE A3.10 Uncertainty in the inverter voltage measurement

Type of error	[%]	Comments
Transducer: star termination	0.34	var, f ⁿ (load-cycling, moist.), rel
Signal conditioning (Fig. A3.9/10)		
diff. resistors	0.23	var, f ⁿ (temp, moist.), rel
LM627's	0.14	var, f ⁿ (PSRR), rel
AD637		
tempco	0.27	var, rel, 30°C variation
bandwidth	1.0	var, f ⁿ ($f_{\text{harmonics}}$)
DC reversal	0.25	var, rel at 2V _{rms}
Averaging	0.2	var, f ⁿ (f), rel
Crest factor	1.0	var, f ⁿ (PWM, f_c), rel
AD202	0.1	var, f ⁿ (tempco), rel
LF351	neg	less than 0.005%
Data Logger	0.2	var, f ⁿ (quant), rel
Calibration	5.0	
Relative uncertainty	2.8	of 110V _{LL}
Absolute uncertainty	5.8	FSR

Assumptions & conditions:

The LM627 error comes from the power supply rejection ratio being relatively low at 10kHz (45dB). The voltage converters have a ±30mV ripple on the supply voltage.

The AD637 has a BW error of 1% over 200kHz

The calibration error is estimated at 5% since there was no calibration standard for PWM signals

A3.6.14 Inverter power

TABLE A3.11 Uncertainty in the inverter power measurement

Type of error	[%]	Comments
Signal conditioning (Fig. A3.9/10)		
Current pre-multiplier	3.78	var, rel
Voltage pre-multiplier	0.41	var, rel
AD834	2.22	var, f ⁿ (nonlinearity), rel
LM627's	0.01	var, f ⁿ (V_{os}), rel
AD202	0.16	var, f ⁿ (tempco, nonlinearity), rel
LF351	neg	
Data Logger	0.2	var, f ⁿ (quant), rel
Calibration	2.0	
Unrealistic calibration	5.0	
Relative uncertainty	4.4	of 500W
Absolute uncertainty	6.9	FSR

Assumptions & conditions:

The current and voltage pre-multiplier errors are a subset of their respective errors
Both value for calibration have been estimated

A3.7 Calculation of the uncertainty in the efficiency data

This section presents how the uncertainty in the efficiency data was calculated from the uncertainties in the parameters (previous section). Since the uncertainties have a lower value at full-scale reading (FSR), the uncertainty has to be scaled up if the uncertainty is evaluated at less than FSR. This may not be strictly correct since the errors might not rise linearly as the signal magnitude is reduced from FSR.

The method of calculation is shown by means of an example: Evaluation of the absolute (abs) uncertainty in the Solvo subset efficiency data at 250W input power from the array. The uncertainty data is drawn out of the previous section or from the table in section 5.3 in the main text.

The subset efficiency (η_{subset}) is calculated by the following formula:

$$\eta_{subset} = \frac{60}{2\pi} \times \frac{S_{mot} \times T_{mot}}{I_{arr} \times V_{arr}}$$

The magnitudes of the four parameters have to be assessed at the operating point, here 250W array power. The array voltage is fixed at 180V but the array current is about half the FSR at that operating point (op). From the characteristic curves of the inverter one can calculate the motor torque at an input power of 250W by dividing the pump torque (Figure 7.2 a) through the speed ratio (pulley speed ratio = 247/97 = 2.546). The motor speed can be taken to be half of the worst case uncertainty due to an eight flag sprocket (higher resolution). Therefore:

$$U_{abs}(I_{arr})_{250W} = (I_{FSR} \div I_{op}) \times U_{abs}(I_{arr})_{FSR} = (3A \div 1.5A) \times 1.2\% = 2.4\%$$

$$U_{abs}(V_{arr})_{250W} = U_{abs}(V_{arr})_{500W} = 1.1\%$$

$$U_{abs}(T_{mot})_{130W} = (T_{FSR} \div T_{op}) \times U_{abs}(T_{mot})_{FSR} = (2N.m \div 1.7N.m) \times 3.6\% = 4.2\%$$

$$U_{abs}(S_{mot})_{8flag} = 0.4\%$$

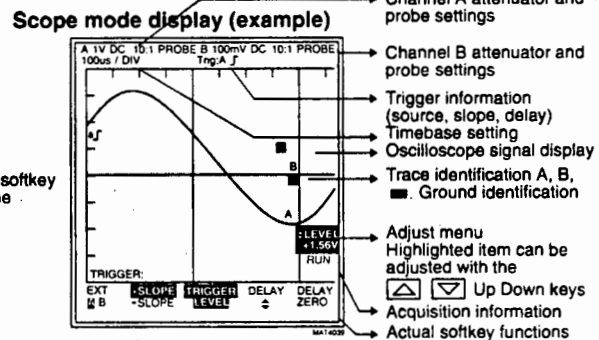
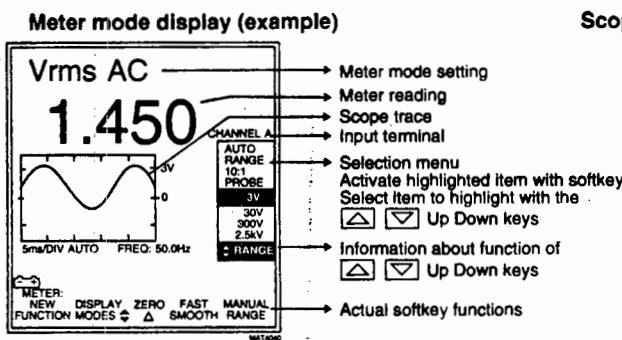
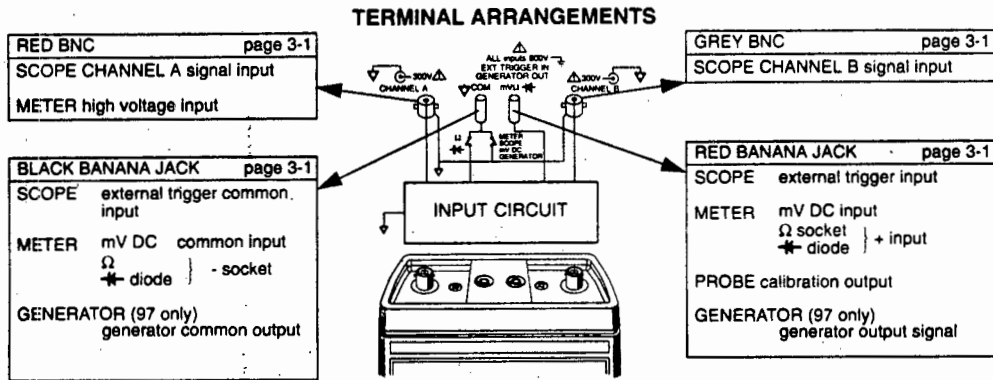
The absolute uncertainty (U_{abs}) in the subset efficiency (with all the parameter uncertainties being absolute) is calculated by:

$$U_{abs}(\eta_{subset})_{250W} = \sqrt{U^2(I_{arr})_{250W} + U^2(V_{arr})_{250W} + U^2(T_{mot})_{130W} + U^2(S_{mot})_{8flag}}$$

The same calculation was performed for the relative uncertainty. The method remains but the relative instead of the absolute uncertainty values are extracted from the table in section 5.3. This calculation was performed for all the uncertainty values stated in the main text.

A3.8 Specifications of the secondary data acquisition system

Philips PM97 specifications



1 INTRODUCTION

The PM9080/001 is an optical RS-232-C interface cable to obtain computer communication facilities with the ScopeMeter model 97.

It offers two applications:

1. Hard copy on Epson FX or HP ThinkJet or compatibles.
2. Remote control and programming of the PM97.

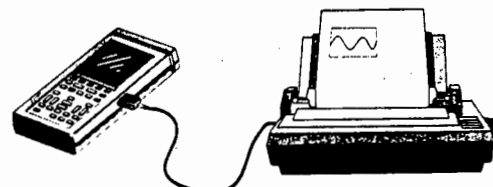


Figure 1 PM97 in hardcopy configuration

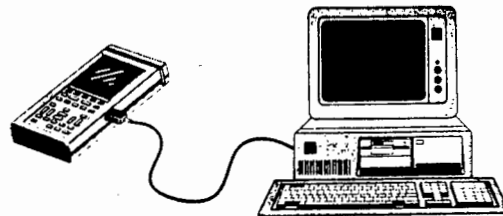


Figure 2 PM97 in remote control configuration

The communication port of the ScopeMeter is optically linked by means of an infrared transmitter (TxD line) and a photo-transistor (RxD line). Because the TxD and RxD lines are the only two implemented lines in the ScopeMeter, handshaking is possible only when using the software Xon/Xoff protocol.

The cable wiring diagram is shown in Figure 3.

The power necessary for the transmitter and receiver is generated internally from the voltages on the RTS and/or DTR line.

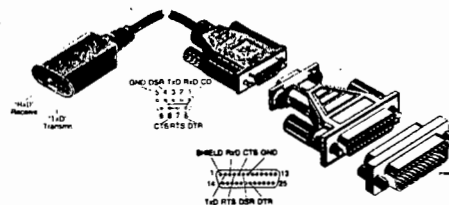


Figure 3 Cable wiring

10.1 Introduction

A. Performance Characteristics

- PHILIPS and FLUKE guarantee the properties expressed in numerical values with stated tolerance. Specified non-tolerance numerical values indicate those that could be nominal expected from the mean of a range of identical instruments.
- For definitions of terms, reference is made to IEC Publication 351-1.

B. Safety Characteristics

This instrument has been designed and tested in accordance with IEC Publication 348, Safety Requirements for Electronic Measuring Apparatus, and has been supplied in a safe condition. This manual contains information and warnings that must be followed by the user to ensure safe operation and to keep the instrument in a safe condition.

Contents:

1	Introduction	4	Multimeter
2	Display	5	Generator
3	Oscilloscope	6	Undo
	Vertical system	7	Input terminals
	Horizontal system	8	External power requirements
	Trigger	9	Internal batteries
	Setup memories	10	Environmental data
	Waveform memories	11	Mechanical data
	Mathematics	12	Accessories
	Cursors		
	Autoset		

Nonlinearity

$\pm(2\% \pm 1 \text{ digit})$ including Analog to Digital Converter, which will have no missing codes and is monotonic.

Move Control Range

+4 divisions and -4 divisions

DC Balance

The base line is automatically readjusted after switching the attenuator or ac/dc/ground.

Min/Max (Models 95 and 97 only)

Acquisition mode at 1 μ s per division or slower on Channel A only.

Pulse width for 100% probability of detection is 40 ns.

Average (Models 95 and 97 only)

The running average can be set to 256 maximum.

In Roll this is 10 fixed.

Zoom (Models 95 and 97 only)

Zoom offers the possibility to zoom in or out around the 4th division, within the limits of the timebase and the maximum delay.

Horizontal system

Range

5s per div up to 10 ns per division with triggered start.

The ROLL mode is active from 60s per division up to 10s per division.

Single shots are possible from 5s per division up to 100 ns per div; for timebase settings faster than 1 μ s per division an automatic interpolation takes place. The useful bandwidth is about 6 MHz.

For timebase settings of 50 μ s or slower, the Channels are chopped; for settings of 20 μ s or faster, the Channels are alternated, so Channel A is displayed first and, after a second trigger pulse, Channel B is displayed.

10.2 Display

The display used is of the LCD type Super Twisted Nematic. The rectangular active area of 240x240 pixels has a diagonal of 4.7 inches (12 cm). The trace area is 200x240 pixels. A graticule with 25 pixels per division can be chosen with softkey control.

- Model 97 has an Electro Luminescence backlight.
- The CONTRAST ratio is adjustable in the LCD menu.

10.3 OSCILLOSCOPE

Vertical system

Deflection Factor

Models 95 and 97: 1 mV per division to 100V per division in 1-2-5 sequence, for timebase 60s to 1 μ s/division.

Model 93: 5 mV per division to 100V per division in 1-2-5 sequence.

This can be expanded a factor of 10 with the delivered 10 to 1 safety designed probe.

Vertical Resolution

8 bits, 25 levels per division.

DC Accuracy

$\pm 2\%$

Rise Time

Vertical amplifier response limits the rise time to 7 ns. For time base settings slower than 200 ns the rise time is smaller than the sample distance, so the measured rise time is unreliable if it is smaller than $\frac{2 \times s/div}{25}$

Bandwidth

> 50 MHz (-3 dB)

Accuracy

$\pm 0.1\% \pm 1 \text{ LSB}$

Sample Frequency

Dependent on timebase: $\frac{25}{s/div} \text{ Hz}$ (maximum 25 MHz)

In Min/Max mode (Models 95 and 97 only): 25 MHz

Record Length

512 samples calibrated for 25 samples per division

CAPTURE gives the possibility to select a record length of 10 divisions or 20 divisions.

Move Control

+4 divisions up to -16.5 divisions

A versus B

Channel A is displayed along the vertical axis, and Channel B along the horizontal axis. The timebase is set manually.

TRIGGER

Internal Sensitivity

<0.5 div for frequencies lower than 10 MHz.

Models 95 and 97 have an extra amplification in the vertical system to create 2 mV and 1 mV per division. That is not valid for the trigger, so the sensitivity decreases in 2 mV and 1 mV with a factor of 5.

Level Range

+4 divisions and -4 divisions

External

TTL compatible. Selectable for use with or without 10:1 probe.

Trigger level is indicated in the screen.

Delay Range

-20 up to 640 divisions in delay time mode.

1 up to 1023 in EVENTS delay mode (Models 95 and 97 only).

In N_CYCLE mode, the trigger frequency is divided by a number N, ranging 2 to 255 (Models 95 and 97 only).

Appendix A4

PROCESSING METHOD OF MODULE SPECIFICATIONS

Calculation method for processing specification data

The MPP data from the specifications are processed to the level of the acquired data by taking into account the number of modules, the effect of cell temperature variation and the logarithmic reduction of the MPP voltage as a result of a decrease in solar irradiance.

It is assumed that the specified temperature coefficients for the open circuit voltage and the short circuit current are the same as for the MPP voltage and the MPP current respectively. The reduction in MPP voltage (due to a decrease in irradiance) is probably overestimated resulting in a slightly lower efficiency than might be specified under the particular conditions. This reduction of MPP voltage as a function of irradiance is shown in Figure A4.1 below.

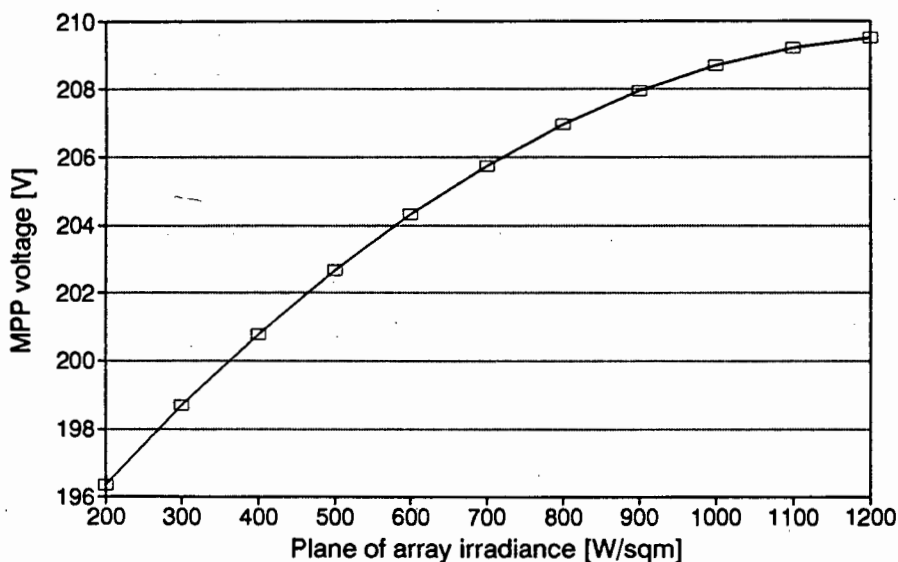


FIGURE A4.1 Logarithmic increase of array voltage as a function of irradiance

The array efficiency is calculated by dividing the array power (which is a function of irradiance and cell temperature) by the plane of array irradiance and the array area. The array power is calculated by multiplying the MPP voltage and the MPP current.

$$P_{MPP} = V_{MPP} (f^n : t, G) \times I_{MPP} (f^n : G, t) \quad (\text{A4.1})$$

where f^n means function of, t is the cell temperature and G is the plane of array irradiance. The most dominant variable in the brackets is mentioned first.

The MPP voltage, as a function of irradiance (as displayed in Figure A4.1), has been fitted with the following curve:

$$V_{MPP} = (190 - V_{\text{temperature}}) + 0.29 \times G - 1.31 \times 10^{-5} \times G^2 \quad (\text{A4.2})$$

where $V_{\text{temperature}}$ is the voltage drop due to a cell temperature in excess of 25°C. The equation for $V_{\text{temperature}}$ is shown below:

$$V_{\text{temperature}} = 17.4 \times \frac{0.34}{100} \times \Delta C \quad (\text{A4.3})$$

where 0.34 is the temperature coefficient [Units: %/°C] of the module open circuit voltage and ΔC is the difference temperature between 25°C and the actual cell temperature.

The equation for the MPP current runs as follows:

$$I_{MPP} = \frac{G}{1000} \times (3.05 + 3.05 \times \frac{0.04}{100} \times \Delta C) \quad (\text{A4.4})$$

where 3.05A is the MPP current at 1000W/m² and 25°C and 0.04 is the temperature coefficient of the module short circuit current [Units: %/°C].

Using these equations the efficiency of the array was calculated in a Quattro Pro spreadsheet. The first column contained the plane of array irradiance, the second column contained equation A4.3, the third column contained equation A4.2 and the fourth column contained equation A4.1 and A4.4 combined. The fifth column contained the efficiency of the array. The efficiency was calculated from 200W/m² to 1100W/m² in 100W/m² steps.

Appendix A5

CALCULATION OF DAILY ENERGY EFFICIENCY

A5.1 Definitions

Daily Energy Efficiency

The daily energy efficiency (DEE) is the total energy flow out of a component (or a string of components) over the total energy into a component (or a string of components) over the course of a whole day (usually a 12 hour day, following a sine-wave irradiance profile). Mathematically, the DEE is expressed as follows:

$$DEE = \frac{\int_6^{18} P_{out} \times dt}{\int_6^{18} P_{in} \times dt} \times 100 \quad (A5.1)$$

where: t is time and
integral interval is 6hours to 18hours

Standard Solar Day

The standard solar day (SSD) is a defined daily solar irradiance profile which has the shape of a sine-wave. The length of a SSD is usually 12hours. The energy content of the profiles can therefore only be changed by varying the peak irradiance of the sine-wave. The graph below shows the profile of a SSD with a peak irradiance of 1000W/m². It has an energy content of 7.64kWh/m²/day.

The primary purpose of a standard solar day is the comparison amongst photovoltaic systems. For photovoltaic pumps (PVP) the most common daily energy content used is 5kWh/m²/day which has a peak irradiance of 654.5W/m².

The equation for the standard solar day is written as follows:

$$G(t) = G_{peak} \times \sin \frac{\pi}{12} (t - 6) \quad (A5.2)$$

where: $6 \leq t \leq 18$
 $G_{peak} = E_{incident} \times m$ [W/m²]
 $m = 1000 \times \pi + 24 = 130.9$
and $E_{incident}$ has the units [kWh/m²/day]

Tracking Solar Day

The tracking solar day (TSD) has only been defined for this work. The shape of the curve is based on the data collected for the array (see Figure 6.10). It is quite certain however that every make of tracking array will track a different solar irradiance profile due to their different physical constructions (unless of course similar) which will result in different tracking paths.

The main aim of defining a TSD is to observe whether a tracking array will bring the DEE of the three phase systems relatively closer to the DC system. A SSD does not give a good reflection of PVP systems that are meant to use a tracking array (like many three phase systems) due to poor efficiencies at low irradiance levels. In addition a TSD gives a good indication of how the average efficiency of a PVP system improves from a fixed array to a tracking array. After all, the data is based on a realistic data set.

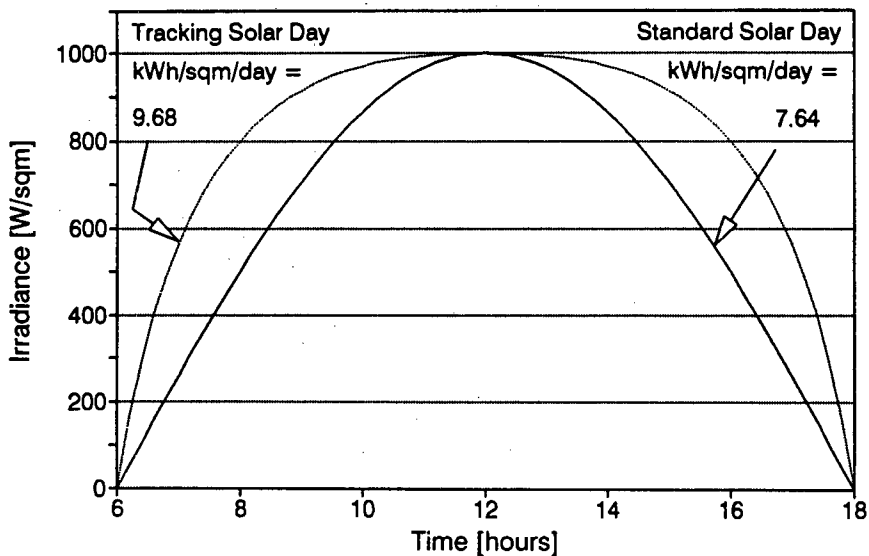


FIGURE A5.1 Standard solar day and tracking solar day irradiance profiles

The TSD also has a length of 12 hours. The profile is shown in the graph above. For a peak irradiance of 1000W/m² the energy content is 9.68kWh/m²/day which contains 26.1% more energy than a SSD with the same peak irradiance.

The equation for this tracking solar day is:

$$G(t) = k \times G_{peak} \times \frac{\log(t-5)}{(t + \frac{\pi}{2})} \tag{A5.3}$$

for: $6 \leq t \leq 12$

$$G(t) = G(-t' + 24) \tag{A5.4}$$

for: $12 \leq t \leq 18$ while
 $12 \leq t' \leq 6$

For equation A5.3 & A5.4: $k = 16.058$
 $G_{\text{peak}} = E_{\text{incident}} \times 103.08 \text{ [W/m}^2\text{]}$
 and E_{incident} has the units $[\text{kWh/m}^2/\text{day}]$

Basis of comparison for SSD and TSD

The means of comparison between a SSD and a TSD is through the peak plane of array irradiance at noon. The assumption is that both arrays have the same angle of tilt at noon (as defined here the TSD always receives 26.1% more energy than a SSD). The table below shows the energy content of the SSD and the TSD at a range of peak irradiancies.

TABLE A5.1 Energy content of a SSD and a TSD for different peak irradiance levels

G_{peak} [W/m ²]	SSD [kWh/m ² /day]	TSD [kWh/m ² /day]
300	2.29	2.91
400	3.06	3.87
500	3.82	4.84
600	4.58	5.81
700	5.35	6.78
800	6.11	7.75
900	6.88	8.72
1000	7.64	9.68
1100	8.40	10.65

A5.2 Method of calculation

The DEE was calculated discretely (as opposed to continuously) in a Quattro Pro spreadsheet. The spreadsheet had three areas. One contained the solar irradiance profiles of the SSD or the TSD. The second section contained the equations of the component efficiencies which map the output power of the component to its input power. The equations were fitted to the real data of each component. The third section contained the calculations to obtain the daily energy efficiencies.

Spreadsheet area one

The standard solar day or the tracking solar day profiles were calculated every 3min from 6⁰⁰ to 12⁰⁰. The peak irradiance values were changed in the calculation to obtain different SSD or TSD energy contents.

Spreadsheet area two

The instantaneous component efficiency was calculated in the adjacent columns next to the irradiance profile columns. For example, the array efficiency column would contain the array efficiency equation as a function of the irradiance. This column would therefore contain the instantaneous efficiency of the array at the particular irradiance level. The next column would contain the power out of the array at each 3min instance. That power is calculated by multiplying the irradiance times the array efficiency times the array area and would serve as the input power to the next component. This is the procedure for all four components resulting in eight columns all together. A column for the flowrate is also included.

Spreadsheet area three

Each of the four columns containing the instantaneous power of a component were summed with the following equation to yield the energy out of the component:

$$E_{out} = \frac{2 \times \left(\sum_{r=0}^{119} + \frac{r=120}{2} \right)}{1000 \times 20} \quad (\text{A5.5})$$

where r is one interval of 3minutes ($120 \times 3\text{min} = 6\text{hours}$) and where r could mean 'row' in spreadsheet

The equation is taken times two since only half a day is calculated and is divided by 1000 to obtain kilo units and by 20 since the power was calculated every 3minutes and not every hour. The last value in the column is at 12^{00} ($r = 120$) and has to be halved to be very correct.

The DEE of a component (or a string of components) is calculated by dividing the energy out of the component (or the string of components) by the energy into the component (or string thereof). This ratio is multiplied by 100 to obtain the efficiency. In this way the DEE can be calculated for components, subset, subsystem and system. The instantaneous flow column is calculated with equation A5.5 above with the result being in m^3/day . It was found that a 3min interval has sufficient resolution and that the estimated error would not exceed 0.3%.

The DEE calculations were performed for SSD's of $2\text{kWh}/\text{m}^2/\text{day}$ to $8\text{kWh}/\text{m}^2/\text{day}$ and the comparative data for SSD and TSD was calculated for noon peak irradiance levels of $300\text{W}/\text{m}^2$ to $1100\text{W}/\text{m}^2$.

A5.3 List of fitted curves

The collected data for the component efficiency was fitted with curves by using the Quattro Pro regression tool. In some cases two curves were fitted per component. The equations would be exchanged at a particular power threshold due to discontinuities at that point. The equations for the component efficiencies and the flowrate as a function of their respective input powers are listed in the tables below (E1 is equation one, T is the threshold power, E2 is equation two, η is the instantaneous efficiency and P is the input power to the particular component or indicates the threshold power when adjacent to T):

TABLE A5.2 Fitted equations for the array and the pump

Component	Equations and threshold specifications
Array:	$\eta = 9.8 + 0.002753 \times G - 1.5569 \times 10^{-6} \times G^2$
Pump: E1:	$\eta = -33.82 + 2.1 \times P - 0.018 \times P^2 + 5.216 \times 10^{-5} \times P^3$
T:	P = 150W
E2:	$\eta = 42.9556 + 0.114 \times P - 2.42 \times 10^{-4} \times P^2$
Flowrate:	$Q = -60.63 + 2.77 \times P + 0.0032 \times P^2 - 9.36 \times 10^{-6} \times P^3$

TABLE A5.3 Fitted equations for the Miltek subset components

Component	Equations and threshold specifications
Converter: E1:	$\eta = -108.74 + 4.1328 \times P - 0.022574 \times P^2$
T:	P = 100W
E2:	$\eta = 72.3 + 0.0863 \times P - 7.3337 \times 10^{-4} \times P^2$
Motor:	$\eta = -29.087 + 1.89 \times P - 0.01376 \times P^2 + 4.73 \times 10^{-5} \times P^3 - 7.6 \times 10^{-8} \times P^4 + 4.6 \times 10^{-11} \times P^5$

TABLE A5.4 Fitted equations for the Solvo subset components

Component	Equations
Inverter:	$\eta = -65.7 + 0.99 \times P - 0.00217 P^2 + 1.573 \times 10^{-6} \times P^3$
Motor:	$\eta = -133.57 + 3.8 \times P - 0.029 \times P^2 + 0.00011 \times P^3 - 1.87 \times 10^{-7} \times P^4 + 1.27 \times 10^{-10} \times P^5$

TABLE A5.5 Fitted equations for the MLT subset components: MST

Component	Equations and threshold specifications
<i>Inverter:</i>	$\eta = - 19.8 + 1.15 \times P - 0.0045 \times P^2 + 7.9 \times 10^{-6} \times P^3 - 5.01 \times 10^{-9} \times P^4$
<i>Motor:</i> E1:	$\eta = - 35.6833 + 2.048477 \times P - 0.01103 \times P^2$
T:	P = 90W
E2:	$\eta = 55.2142 + 0.0959475 \times P - 9.3312 \times 10^{-5} \times P^2$

TABLE A5.6 Fitted equations for the MLT subset components: FVO

Component	Equations and threshold specifications
<i>Inverter:</i> E1:	$\eta = 0$
T:	P = 350W
E2:	$\eta = 148.28 - 0.465 \times P + 0.001176 \times P^2 - 9.441 \times 10^{-7} \times P^3$
<i>Motor:</i> E1:	$\eta = 0$
T:	P = 280W
E2:	$\eta = 65.72 + 0.0022 \times P$

Validity of regression models

The statistic that measures the validity of the model is R squared (R^2). The closer R^2 is to unity the more valid the model. R^2 was always in excess of 0.96 and mostly above 0.985 for all regressions except for MLT FVO subset components (to be discussed below). The standard error in the Y estimation was in the range of 0.01% to 7.7% and the standard error of the X coefficient(s) was in the range of 1.8% to 18.8% for the first coefficient. The error in the second coefficient is usually higher. The smaller error of the Y estimation would usually go with the larger error of the X coefficient or vice versa.

Figure A5.1 displays the MLT motor (MST) efficiency curve with the fitted data. R squared is 0.96 for equation 2 and the standard error in the x-coefficient is 18.0%. R squared is 0.99 for equation 1 and the x-coefficient error is 4.3%. The standard error in the Y-estimate is less than 0.2% for both equations.

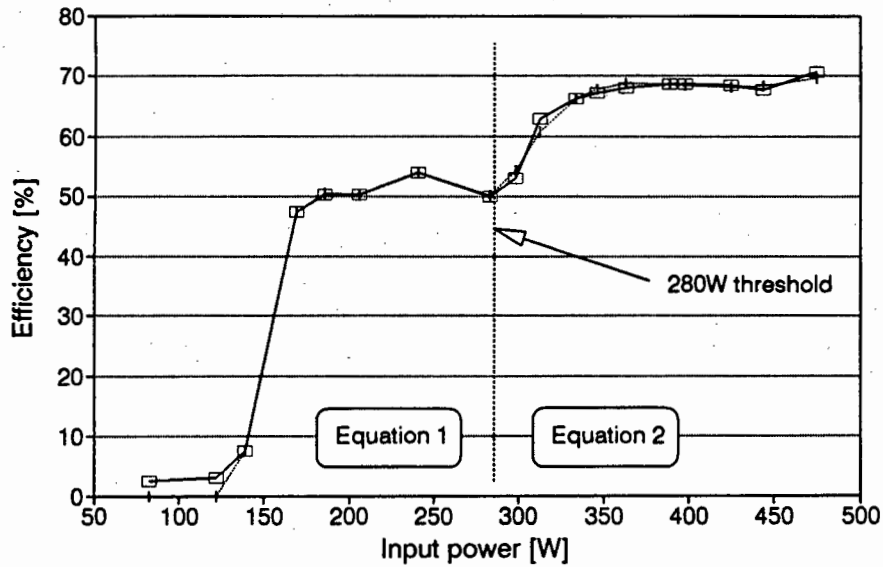


FIGURE A5.2 Acquired and fitted data for the GEC motor (driven by MLT inverter)

The regression for the MLT FVO subset component curves had different values to the ones from above. R^2 was as low as 0.58 for the inverter regression and 0.05 for the motor regression curve. To the eye the fitted curve superimposed well on the actual data. This is most probably due to these curves being of nearly constant values (see Figure 8.17). Under these conditions the standard error in the Y estimate becomes most important. These errors were 0.6% for the inverter and 1.1% for the motor respectively.

Appendix A6

CALCULATION OF ARRAY LOSSES DUE TO ARRAY VOLTAGE OSCILLATIONS

The aim of this method is to use realistic data to assess the losses due to array voltage oscillations. Therefore all data used here is based on acquired data that has been obtained during the filed test period. Figure A6.1 shows graphically what is being attempted here.

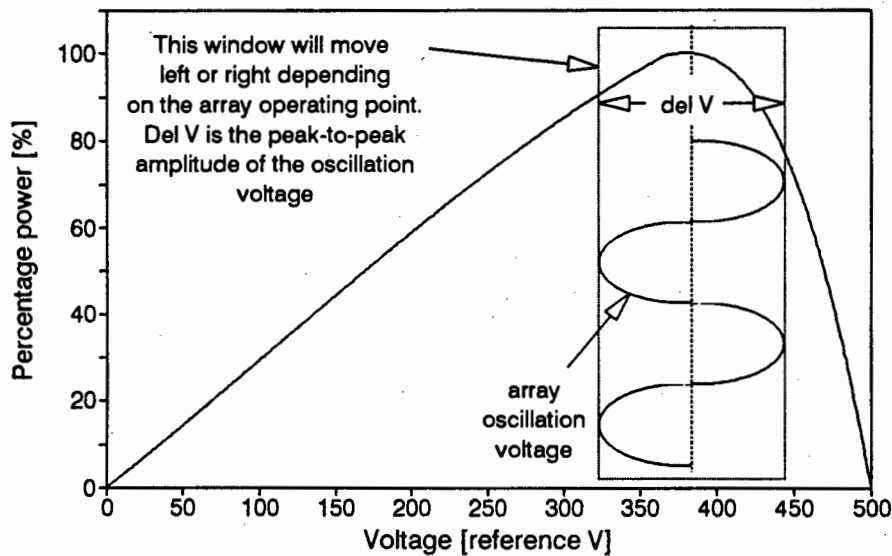


FIGURE A6.1 Array oscillation voltage superimposed on steady state array power versus voltage characteristics

Characteristic curves

A characteristic curve of the array power versus the array voltage at 1000W/m^2 and 55°C was used (in retrospect, a curve at lower module temperature would have been more suitable rather than a curve acquired at an extreme operating condition). The peak power was scaled to hundred to serve as a percentage power reference and the voltage was scaled to 500 at open-circuit (five-hundred due to not realising that the Fill function in Quattro Pro can also handle numericals smaller than one).

The curve that was fitted to this graph is shown in Figure A6.2a. It consists of two equations where equation A6.1 is used in region zero to 350refV and equation A6.2 for region 350refV to 500refV .

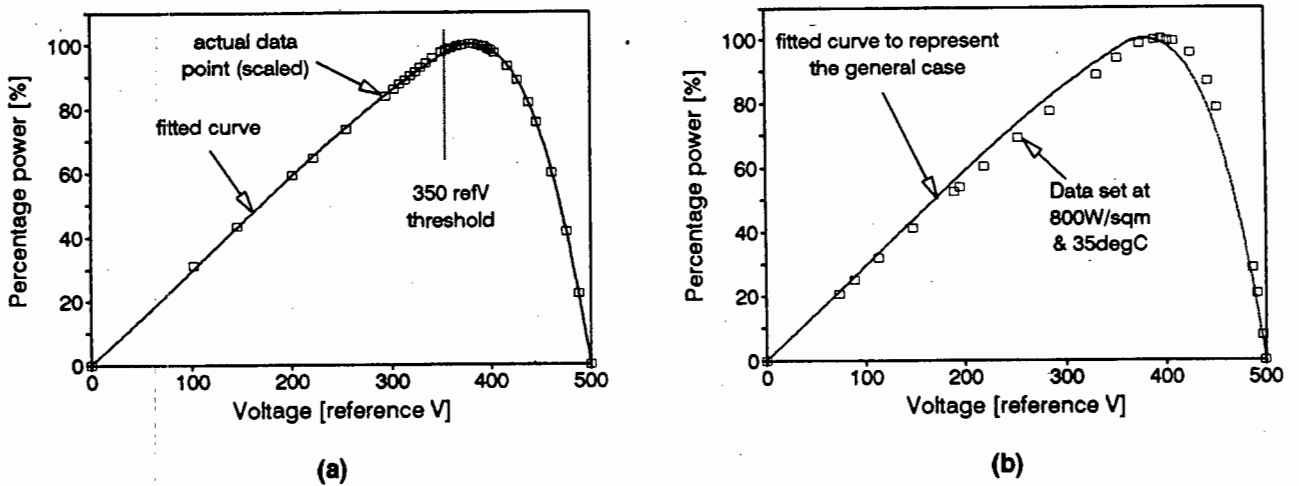


FIGURE A6.2 Fitted power curve with (a) actual data and (b) confirmation of fitted curve on a different data set

(A6.1)

$$P = 0.28 \times V + (1.9 \times 10^{-4}) V^2 - (5.77 \times 10^{-7}) V^3$$

(A6.2)

$$P = 1256.5 - 11.14 \times V + 0.036 \times V^2 - (4.28 \times 10^{-5}) \times V^3 + (1.03 \times 10^{-8}) \times V^4$$

The shape of the curve was verified by scaling another curve that was sampled at 800W/m^2 with a module temperature of 35°C . The curves differ slightly but the area under both curves is nearly the same. This is shown in Figure A6.2b.

The oscillation waveform was used as it was sampled.

Method of calculation

The method of calculation is based on discrete frequency distribution analysis and is performed in a Quattro Pro spreadsheet. The spreadsheet consists of one main area of calculation and another area containing the sampled oscillation waveform which serves as the values block.

The main area is arranged as follows: The first column contains the reference voltage from zero to five-hundred. The next column contains the reference power. The reference voltage is scaled ($\times V_{oc} / 500$) to the open circuit voltage of the test array

in the third column. The fixed voltage point (FVP) that the inverter is operating at (around 180V for the series array and around 90V for the parallel configured array) is subtracted from the scaled voltage and entered into the fourth column. This is now referred to as the level shifted voltage. The level shifted voltage has zero volts at the FVP with reference to the horizontal voltage axis, has a negative voltage below the FVP and a positive voltage above the FVP. It now serves as a look-up table (or in Quattro Pro as the bin block).

The oscillation waveform is the column of values (Quattro Pro: values block) that is analysed for occurrences. The interval of the oscillation waveform has to be chosen such that a multiple of periods is selected.

The frequency distribution table is generated in the fifth column by listing the number of times that a particular amplitude range occurs in the oscillation waveform. This column is generated next to the look-up table. This column is multiplied row-for-row by the reference power (in column 2) and entered into column six. Column six is then summed and divided by the total number of occurrences (summed in column 5). This will result in a value equal or less than 100 (equal to 100 only if the oscillation amplitude is zero). The minimum voltage range that will occur in the look-up table is 0.48V for a 240V_{oc} array and 0.24V for a 120V_{oc} array.

Manipulations

The FVP can be moved to observe the mismatch losses as the oscillation waveform operates around different points on the power curve. This method also gives the opportunity to calculate the losses in array output due to operation away from the MPP. This is done by changing the array operating point to a value other than V_{MPP} and by decreasing the oscillation voltage amplitude to zero.

Evaluation of this calculation method

The accuracy is limited due the limited amount of voltage steps. If the oscillation peak amplitude is too small the error will get too large unless the resolution of the voltage range is increased (a voltage step is equal to $V_{oc} / 500$). Accuracy can be increased by dividing the voltage into more steps. Ultimately the accuracy is limited to the resolution of the device that captures the oscillation waveform.

The time base of the oscillation is irrelevant. Only shape/symmetry and amplitude are important.

Oscillation waveform polarity should not be reversed if the signal is asymmetrical with respect to the time axis.

For most reliable results it should be known where the MPP voltage is relative to the actual operating voltage during the sampling of the oscillation waveform in case the oscillation waveform shape is sensitive to its operating point position with respect to the MPP. This was not observed though.

Appendix A7

SOLVO INVERTER IMPROVEMENTS

A7.1 Controller with regions and deadband

The flowchart shows the implementation of this type of controller. The actual error at each sample interval is stored in $e(z)$. The constants $errorE$ to $errorB$ contain the range of values that the error may have to fall in to one of the five regions (from the graph in Figure 9.5, $errorE = 0$ to 1 , $errorD = 1$ to 3 , $errorC = 3$ to 6 and $errorB = 6$ to 12). $CountD$, $CountC$ and $CountB$ count the consecutive number of times that the error $e(z)$ falls in to a region. If constants $TimeD$, $TimeC$ and $TimeB$ are exceeded then a change of frequency will occur. $TimeD$, $TimeC$ and $TimeB$ are multiples of the sampling time and $TimeD > TimeC > TimeB$.

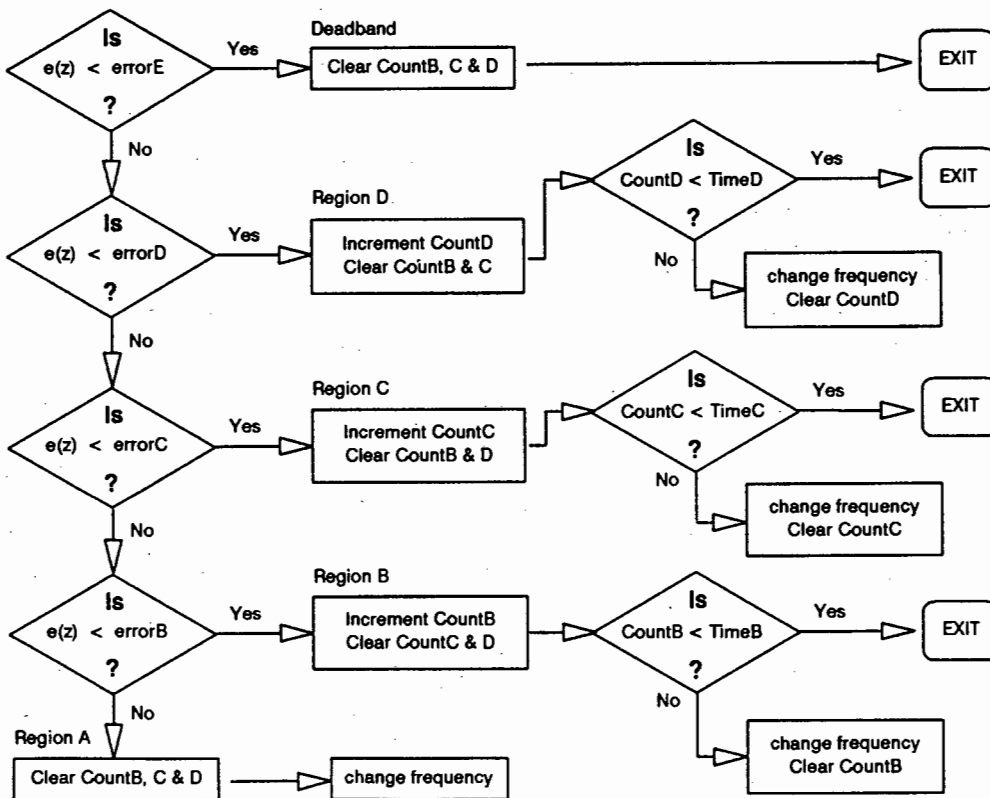


FIGURE A7.1 Flowchart for the regions-and-deadband algorithm

The program code to implement this controller is listed below. The constants $errorB$ to $errorE$ and $TimeB$ to $TimeD$ and the variables $CountB$ to $CountD$ have to be defined and initialised at the beginning of the program. The $errorX$ and $TimeX$ constants have to be chosen by trial and error. The best approach is to start with small values. The variables $CountX$ have to be reset.

The program code below (*italics*) must be added to the Timer1 interrupt-routine. It replaces four program code lines.

```

GREATER:
MOV     A,SWNEU
CLR     C
SUBB   A,SWALT
SETB   HOCHFL

MOV     error,A
CJNE   A,errorE,AUX_E
JMP     EXIT

AUX_E:  JC     REG_E
        JMP   AUX_D
REG_E:  MOV   CountB,#0
        MOV   CountC,#0
        MOV   CountD,#0
        JMP   EXIT

AUX_D:  CJNE  A,errorD,AUX_DD
        JMP   REG_D
AUX_DD: JC     REG_D
        JMP   AUX_C
REG_D:  INC   CountD
        MOV   CountB,#0
        MOV   CountC,#0
        MOV   A,CountD
        CJNE  A,TimeD,POST_D
POST_D: JC     EXIT
        MOV   CountD,#0
        JMP   CHANGE_FREQUENCY

AUX_C:  MOV   A,error
        CJNE  A,errorC,AUX_CC
        JMP   REG_C
AUX_CC: JC     REG_C
        JMP   AUX_B
REG_C:  INC   CountC
        MOV   CountB,#0
        MOV   CountD,#0
        MOV   A,CountC
        CJNE  A,TimeC,POST_C
POST_C: JC     EXIT
        MOV   CountC,#0
        JMP   CHANGE_FREQUENCY

```

```
AUX_B:      MOV      A,error
            CJNE     A,errorB,AUX_BB
            JMP      REG_B
AUX_BB:     JC       REG_B
            JMP      AUX_A
REG_B:      INC      CountB
            MOV      CountC,#0
            MOV      CountD,#0
            MOV      A,CountB
            CJNE     A,TimeB,POST_B
POST_B:     JC       EXIT
            MOV      CountB,#0
            JMP      CHANGE_FREQUENCY

AUX_A:      MOV      CountB,#0
            MOV      CountC,#0
            MOV      CountD,#0
            JMP      CHANGE_FREQUENCY
```

Note: The original program uses the address 'HILF' instead of 'EXIT' and 'AKTST' instead of 'CHANGE_FREQUENCY'. The original addresses should be used. The first four lines of program code after the five original lines at the top have to be deleted to fit into the existing program.

This controller would handle installations which have a faster settling time (smaller RC) without any problem. If an installation has a longer settling time then the array voltage oscillations would start occurring and the algorithm requires retuning.

A7.2 Incorrect array operating point

Figure A7.2 shows the same flowchart as in the main text but more specific for the Solvo program. The explanations are therefore the same.

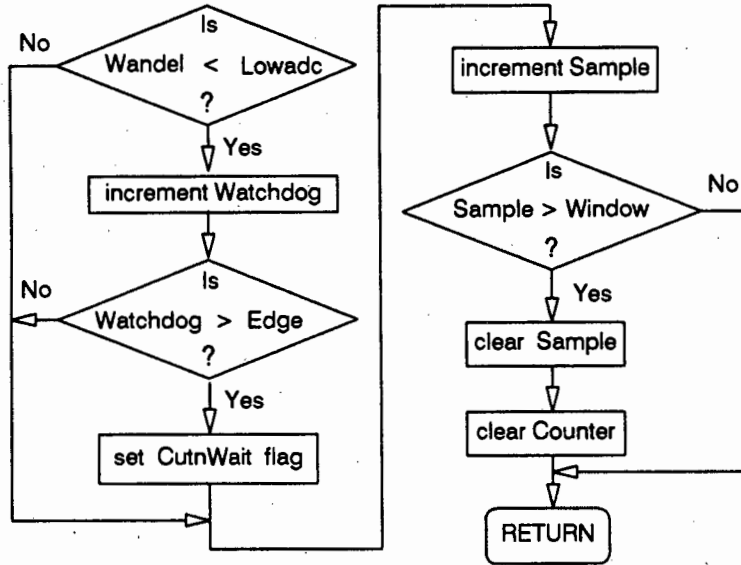


FIGURE A7.2 Flowchart for avoiding incorrect array operating points

The program code for the subroutine is listed below. Lowadc, Window, Sample, Edge, Watchdog and CutnWait have to be defined and initialised.

```

LOUSY:      MOV      A,STALT
            CJNE    A,STNEU,ROSES
            JMP     ARE
ROSES:      JC      ARE
            MOV     A,STNEU
ARE:        CJNE    A,#2,DARK
            JMP     RED
DARK:       JC      MOTION

RED:        MOV     A,WANDEL
            CJNE    A,LOWADC,ZAP1
            JMP     NOTLOW
ZAP1:       JC      ZAP2
            JMP     NOTLOW
ZAP2:       INC     WATCHDOG
            MOV     A,WATCHDOG
            CJNE    A,EDGE,CASE1
            JMP     NOTLOW
CASE1:      JC      NOTLOW
            SETB   CUTNWAIT
NOTLOW:     INC     SAMPLE
  
```

```

                                MOV     A,SAMPLE
                                CJNE   A,WINDOW,CASE2
                                JMP     ENDLY
CASE2:                          JC      ENDLY
MOTION:                          MOV     SAMPLE,#0
                                MOV     WATCHDOG,#0
ENDLY:                            RET

```

This subroutine is called in the Timer1 interrupt routine after the array voltage has been read in at the ADC. Lowadc should be chosen to be about 50% to 60% of the open-circuit voltage. Window should not be less than 100 and Edge should always be half of the Window value. If the Watchdog counts more occurrences of low voltage than the value held in Edge then the CutnWait flag is set. This flag is continuously scanned in the main program. When the flag is true then the inverter output is inhibited and the program enters a waitstate of a set time.

This routine would reduce considerably if the controller was implemented correctly so that the array voltage oscillations would reduce to about $\pm 1V$. Then there would be no need to take an average of the array voltage.

A7.3 Minimum power threshold

The flowchart in Figure A7.3 shows the program flow for the Solvo inverter. First the lowest major gear is detected (Stalt/Stneu) and then whether the program has entered the active gears (major gear 5 to 15; major gear 0 to 4 do not generate an output but the program still runs through them. As long as the program remains between Actgear and Lowgear (largest unwanted gear) the Ticker variable will be incremented until it reaches a value larger than Prevail.

The program code for the subroutine is listed below. The routine is called from Timer1. Actgear, Lowgear, Ticker, Prevail and CutnWait have to be defined and initialised. Actgear always takes the value of the first active gear. This is presently gear 5. The program changes as suggested in section A7.5 would have Actgear equal to zero. Lowgear should be set to gear 6 or 7 for the present program. The following has to hold true for the constant 'Prevail': $Prevail > (Lowgear - Actgear + 1) \times 16$.

```

TOOSLOW:  MOV     A,STALT
                                CJNE   A,STNEU,SOHO
                                JMP     GETON
SOHO:     JC      GETON
                                MOV     A,STNEU
GETON:    CJNE   A,ACTGEAR,VERIFY
                                JMP     MOVEON
VERIFY:   JC      NAUGHT
MOVEON:   CJNE   A,LOWGEAR,TESTFO
                                JMP     GROW

```

```

TESTFO:    JC      GROW
NAUGHT:    MOV     TICKER,#0
           JMP     ENDSLOW

GROW:      INC     TICKER
           MOV     A,TICKER
           CJNE   A,PREVAIL,OUTRO
           JMP     ENDSLOW

OUTRO:     JNC     SETF
           JMP     ENDSLOW

SETF:      SETB   CUTNWAIT

ENDSLOW:   RET

```

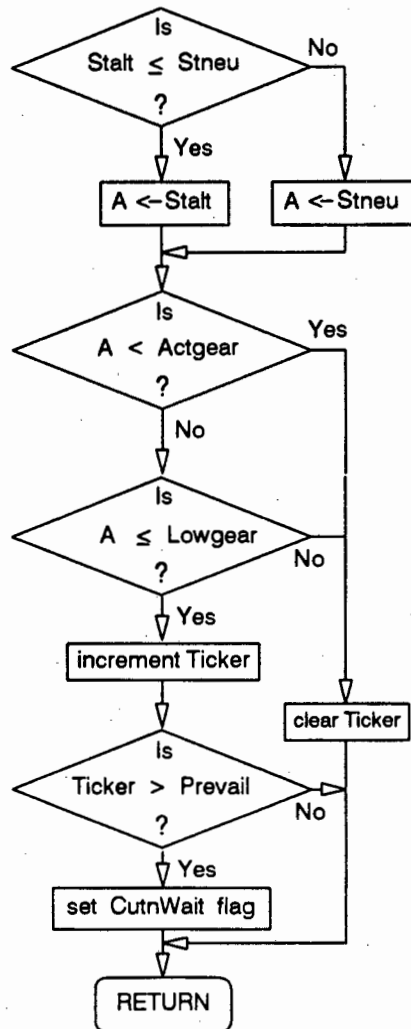


FIGURE A7.3 Flowchart for the detection of a minimum power threshold

This program code cannot be implemented before the algorithm has not been improved since the array voltage oscillations also result in frequency oscillations (see Figure 9.2).

A7.4 Higher resolution voltage to hertz relation

The increase in resolution for the voltage to hertz relation requires one additional variable. This variable must continuously update itself to hold the value of the minor gear in which the inverter program presently resides (the program has 16 major gears and within each major gear it has 16 minor gears). The variable (Minorgear) can therefore only hold values between zero and fifteen.

The variable has to follow the minor gear while the inverter remains in a major gear and has to assume either zero or fifteen when the program changes to another major gear. The flowchart in Figure A7.4 shows how the variable (Minorgear) keeps track of the actual minor gear.

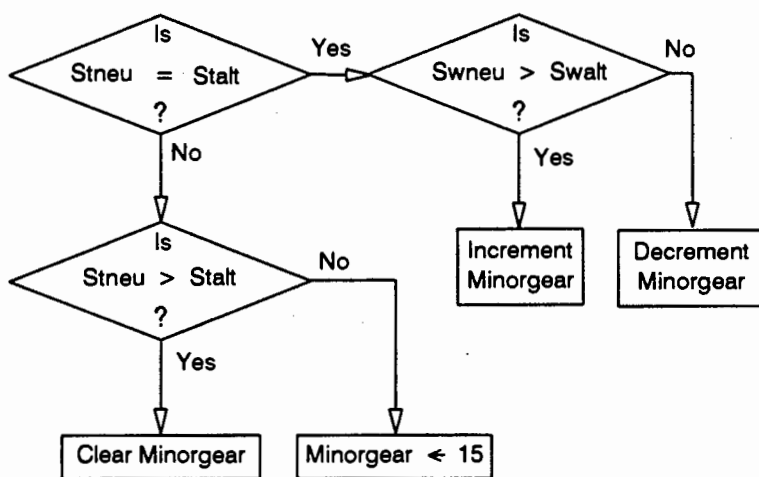


FIGURE A7.4 Flowchart for keeping track of the minor gear

'Stneu' (new major gear), 'Stalt' (old major gear), 'Swneu' (array voltage) and 'Swalt' (reference voltage) are present variables in the program. The routine in the flowchart is executed every time the program decides how to drive the motor. It has to find whether there is a change between major gears (is Stneu = Stalt ?) and if so if the gears are decreasing or increasing. If there was no change in major gears it has to find out whether the frequency is increasing or decreasing which it can do by comparing the array voltage to the reference voltage.

Since the program does this process as well only a few appropriate codes have to be added. The variable Minorgear has to be defined and initialised (to zero). In the Timer1 interrupt routine the following line (italics) has to be added after the existing code line:

```

INC          SCHFREQ
INC          MINORGEAR

DEC          SCHFREQ
DEC          MINORGEAR
    
```

```

INC      STALT
MOV      MINORGEAR , #0

DEC      STALT
MOV      MINORGEAR , 15
    
```

The variable Minorgear is used in a subroutine called from Timer1 which assigns the required values to the IC that generates the PWM signals. The routine is called 'Wertzu'. Where necessary the following flowchart can be implemented to increase the resolution of the voltage to hertz relation.

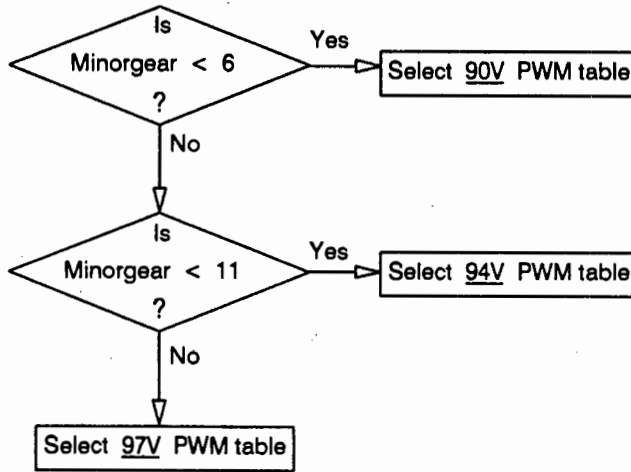


FIGURE A7.5 Flowchart for the assigning of a higher resolution voltage to hertz relation

In this example the sixteen minor gears are divided into three submajor-gear categories. Each of the three can now be assigned a different voltage. As a further example, say major gear 14 should be divided into three sub-major frequency ranges. The program would have the following additions (in italics):

```

ST14:      MOV      A,MINORGEAR
           CJNE     A,#6,ST14A
ST14A:     JNC      ST14B
           MOV      LOWTAB,#LOW TAB90
           MOV      HIGHTAB,#HIGH TAB90
           JMP      REST14
ST14B:     CJNE     A,#11,ST14BB
ST14BB:    JNC      ST14C
           MOV      LOWTAB,#LOW TAB94
           MOV      HIGHTAB,#HIGH TAB94
           JMP      REST14
ST14C:     MOV      LOWTAB,#LOW TAB97
           MOV      HIGHTAB,#HIGH TAB97
    
```

```

REST14:  MOV    STSTNEU,#48
          MOV    PH1NEU,#16
          MOV    PH2NEU,#32
          MOV    ZANEU,#4
          MOV    TMIN,#0B7H
          MOV    TMAX,#0A8H
          JMP    EXIT
    
```

TAB90, TAB94 and TAB97 are addresses of voltage look-up tables which contain PWM ratios for different voltage amplitudes.

This program code can be added to any of the sixteen major gears. It was suggested in the main text that major gears 10 to 12 should be divided into two sub-major gears and major gears 13 to 15 into three sub-major gears. The program code above can be added at the appropriate place in the program.

A7.5 Solvo inverter switching frequency

The table below contains the values for a program that will have a generally lower switching frequency.

TABLE A7.1 Program values for a lower switching frequency

Major gear	T_{max} [μ s]	T_{min} [μ s]	T_{max} [hex]	T_{min} [hex]	f_{s-min} [kHz]	f_{s-max} [kHz]	f_{min} [Hz]	f_{max} [Hz]	m'_f	N
0	60	45	C4	D3	16.7	22.2	5.0	6.6	48	70
1	68	53	BC	CB	14.7	18.9	6.7	8.7	48	45
2	76	61	B4	C3	13.2	16.4	8.8	11.0	48	31
3	75	60	B5	C4	13.3	16.7	11.1	13.9	48	25
4	99	84	9D	AC	10.1	11.9	14.0	16.5	48	15
5	103	88	99	A8	9.7	11.4	16.9	19.7	48	12
6	116	101	BC	9B	8.6	9.9	20.0	22.9	48	9
7	112	97	90	9F	8.9	10.3	23.3	26.8	48	8
8	110	95	92	A1	9.1	10.5	27.1	31.3	48	7
9	110	95	92	A1	9.1	10.5	31.6	36.5	48	6
10	112	97	90	9F	8.9	10.3	37.2	43.0	48	5
11	120	105	88	97	8.3	9.5	43.4	49.6	48	4
12	112	97	90	9F	8.9	10.3	49.6	57.3	36	5
13	121	106	87	96	8.3	9.4	57.4	65.6	36	4
14	127	112	81	90	7.9	8.9	65.6	74.4	30	4
15	124	109	84	93	8.1	9.2	74.7	84.9	36	3

T is the period of the switching frequency. The hexadecimal values are used as down counters in the program. f_s is the switching frequency and f is the inverter output frequency. m'_f is the scaled frequency modulation index and N is number of times that the equal width-pulses are repeated. The actual frequency modulation index is $m'_f \times N$.

The fundamental frequency is calculated with the following equation:

$$f = \frac{1}{m_f \times N \times T} \quad (\text{A7.1})$$

The assigning of frequency ranges to the major gear is slightly tedious and lacks some flexibility. The aim was to stay below a 10kHz switching frequency but that is not possible at lower fundamental frequency else the frequency range becomes so narrow that more major gears would be required (but are not available) to span a frequency range from 5Hz to 85Hz.

The switching frequency therefore increases above 10.5kHz in the frequency range from 20Hz to 5Hz. That is fine since the inverter will operate most of the time above 40Hz. The switching frequency range for the main operating range is therefore 7.9kHz to 10.5kHz. All sixteen major gears are now used which is not as such essential since the frequency resolution is good. Using more major gears does not improve the voltage to hertz resolution.

Appendix A8

PV PUMP SIMULATION PROGRAM

The information in this appendix is based on 'PVPUMP - A user's manual' by Davis (1994a) and 'Report on RAPS water pumping project' also by Davis (1994b). For detailed information on the PV pump simulation program, both the manual and the report should be consulted.

A8.1 Overview

The PV pump simulation program can be used to predict the water delivery of photovoltaic water pumps at different sites on an hourly, daily and monthly basis. This program has been written by Mark Davis for the Energy for Development Research Centre at the University of Cape Town. The following is a brief description of the program, the simulation conditions, the equations used by the program for the subsystem performance data and the assumptions and limitations of the program.

The program relies on a database of different types of PV modules and on a database of long-term meteorological weather data which consists of hourly records of the horizontal global irradiance, the horizontal diffuse irradiance, the ambient temperature and the wind speed. The program uses a set of yearly data that has been selected from the long term data to represent typical irradiation patterns. In addition, an extensive database provides the subsystem performance data for various available PV pumps at different heads and for different array configurations. Subsystem data for other PV pumps can be added if the necessary information is available.

A simulation requires the user to specify the site conditions (such as static head, locality etc) as well as the selection of the PV pump system and the PV array configuration.

The program calculates the plane of array irradiance using the enhanced Perez model and the cell temperature using an algorithm developed by Fuentes. The array output is calculated using an analytical model developed by Rauschenbach. These methods are discussed in detail by Davis (1994b). The array operating point is calculated as the intersection of the array supply function and the load curve. The latter is a function of the generic type of system, for example AC with MPPT, DC with linear current booster etc. The calculation produces flowrate results on an hourly basis.

Depending on the program settings the data is presented either hourly (irradiance, short-circuit current, operating current, operating voltage, efficiency and flowrate) or in terms of daily and monthly averages (daily irradiation, daily volume flow from which the monthly and annual averages are processed).

The program offers a supply versus demand analysis of the water-reservoir tank levels

after the simulation has been completed. This provides a good insight into the reservoir capacity requirements.

Finally the program evaluates the life cycle cost over a desired period of time, taking into account the project life time, the discount rate, the installation cost, the maintenance costs and the replacement costs. The unit water cost is calculated from the annual volume flow and the amortised life cycle cost. However the costing evaluation in this dissertation was performed in a Quattro Pro spreadsheet.

A8.2 Simulation conditions

During the simulation of the four systems (Miltek, Solvo, MLT and Grundfos PVP's) the following variables were held constant:

Albedo:	0.2; reflective coefficient for dry grassland
Array peak Watt:	636W _{peak} for the Miltek, Solvo and MLT PVP system 848W _{peak} for the Grundfos SP 2A - 15 PVP system ¹⁾
Module type:	AEG MQ36K 53W (in place of the Siemens 53W module)
Configuration:	2 × 6 in series: Miltek and MLT PVP system 12 in series: Solvo PVP system 2 × 8 in series: Grundfos system
Operating voltage:	91V: Miltek and MLT PVP system 182V: Solvo PVP system 120V: Grundfos - variable reference voltage due to MPPT
Static head:	76m

The following variables were changed:

Meteorological data:	Windhoek (Namibia) or Durban (Natal, South Africa)
Array position:	fixed (Angle of tilt: Windhoek: 20° and Durban: 35°) three tilts: 10° (Nov - Feb) 35° (Mar - Apr, Sep - Oct) 60° (May - Aug)

This resulted in four sets of data namely Windhoek for a fixed and a three position tilted array and Durban for a fixed and a three position tilted array. As can be seen above, the MLT inverter is assumed to be operating in FVO mode rather than MST.

¹⁾ The Grundfos SP2A - 15 system requires a minimum of 800W_{peak} to operate.

A8.3 Fitted equations used by simulation program

The simulation program requires the subsystem efficiency curves of a PV pump over its input power range. These curves are specified as two second order polynomials. The threshold power from one polynomial to the other is usually chosen to be the point of largest discontinuity in the curve.

The table below specifies the subsystem equations for the four PVP systems that are used in the simulations. The minimum (min) and the maximum (max) subsystem input power values are specified. Two equations for subsystem efficiency (E1 and E2) are listed where equation E1 is valid between min and the threshold T and equation E2 is valid between T and max.

TABLE A8.1 List of fitted subsystem equations with threshold specifications

PVP subsystem	Equations and threshold specifications		
Miltek:	Min:	81	[W]
	T:	240	[W]
	Max:	550	[W]
	E1:	$- 39.27 + 0.685 \times P - 0.00165 \times P^2$	[%]
	E2:	$- 4.48 + 0.225 \times P - 0.00027 \times P^2$	[%]
	¹⁾ Load-line:	$0.05 \times I_0 + 0.4$	[A]
Solvo:	Min:	140	[W]
	T:	270	[W]
	Max:	550	[W]
	E1:	$- 147.38 + 1.336 \times P - 0.00256 \times P^2$	[%]
	E2:	$- 0.37 + 0.154 \times P - 0.00017 \times P^2$	[%]
MLT:	Min:	190	[W]
	T:	250	[W]
	Max:	550	[W]
	E1:	$- 458.42 + 4.196 \times P - 0.00915 \times P^2$	[%]
	E2:	$- 52.22 + 0.389 \times P - 0.00043 \times P^2$	[%]
Grundfos: ²⁾	Min:	480	[W]
	T:	850	[W]
	Max:	1800	[W]
	E1:	$- 98.77 + 0.286 \times P - 0.00016 \times P^2$	[%]
	E2:	$17.72 + 0.023 \times P - 0.0000082 \times P^2$	[%]

¹⁾ The load-line is used by the simulation program to evaluate the array operating point once the Miltek converter enters into direct mode.

²⁾ The Grundfos data (amongst others) is provided with the PVP simulation package and has been derived from manufacturers specifications.

A8.4 Assumptions contained in the simulation

The error sources and the limitations of the simulation procedure are discussed in detail by Davis (1994b). Error sources are found in the weather data, the array output model and the pump subsystem performance models. Limitations are mainly experienced in the consideration of the past weather data as being representative and in the partly random components of some of the system characteristics.

Most of these errors and limitations are not applicable to the category of simulations performed since the simulation results are used mainly for comparative purposes and not for the performance prediction of a single PVP system. Therefore the limitations of the weather data in terms of potentially low sequential irradiation intervals are not of serious concern. Nor are the inaccuracies in the array output model.

The errors that will have the largest impact on the comparison are the errors in the determination of the subsystem efficiency characteristics. Variations have occurred during the acquisition of data for the three tested systems especially in terms of the start-up conditions. If incorrectly assessed this might favour or disfavour a particular PVP system in the comparison. Another factor is that the subsystem efficiency characteristics, no matter how accurate, represents one system only and not the characteristics of a number of same model PVP systems.

The simulation introduces an error by assuming that the head is constant. In the case of the tested PVP systems a head variation of 2m was measured due to drawdown. The head loss variations due to flowrate changes were measured to be negligible. The error due to drawdown is about 1.3% but as all four systems have been assumed to operate at constant head the error is reduced in the comparison.

Appendix A9

COSTING EQUATIONS

The method with which the cost has been calculated is presented here. The information has been extracted from Cowan (1992).

Life cycle cost

The life cycle cost (LCC) includes all the costs incurred over the project lifetime (SL) of the photovoltaic pump, which is usually taken as twenty years. The LCC includes the initial capital cost, the installation cost, the annual maintenance cost and replacement costs. The operation costs are zero since a PV system does not require any fuel.

All the future costs are reduced to their present value by a rate which is equivalent to the opportunity cost of the capital investment (which is the cost of holding capital rather than investing it). This rate is referred to as the real discount rate (dr) which can be taken to be the difference between the interest rate and the inflation rate. The present value ($PVal$) is calculated as follows:

$$PVal = C \times \left[\frac{1}{1 + dr} \right]^n \quad (A9.1)$$

C is the cost in terms of today's money which is being incurred n years from the present.

The LCC is calculated as follows:

$$LCC = C_{initial} + C_{install} + \sum_{n=1}^{SL} M + \sum_{n=1}^{SL} R \quad (A9.2)$$

where $C_{initial}$ and $C_{install}$ are the total initial and installation cost respectively. M and R are the annual maintenance and replacement costs respectively. Both have been reduced to their present yearly value with equation A9.1 over a period of one to 20 (SL) years. The replacement cost must incorporate the salvage value of the replaced part or component.

The assumptions for the LCC are that the interest and the inflation rate remain constant, that the rate of escalation (which is the price escalation above the inflation rate) is zero and that the maintenance and replacement costs have been correctly assessed.

Unit water cost

The unit water cost is useful when a few PVP's are compared in terms of cost. The unit water cost takes the cost of the system and the water delivered into account. The units are in cents/m³. In order to evaluate the unit water cost the life cycle cost has to be amortised into annual amounts first.

$$P = LCC \times \left[\frac{(1+i)^{SL} \times i}{(1+i)^{SL} - 1} \right] \quad (\text{A9.3})$$

P is the amortised annual amount, SL is the project lifetime (20 years) and i is the interest rate. The real interest rate is taken to be the same as the real discount rate used in equation A9.1.

The unit water cost [cents/m³] is calculated by:

$$\text{unit water cost} = \frac{P}{Q_{\text{vol: annual}}} \quad (\text{A9.4})$$

where $Q_{\text{vol: annual}}$ is the total amount of water pumped per year [m³].

In cases where the PVP's that are being compared are not delivering the water at the same static head the unit water cost can be stated as cents/m⁴ where the unit water cost as calculated in equation A9.4 is divided by the static head.